Fragment-Based Drug Design of Bromodomain Ligands

Dissertation

zur

Erlangung der naturwissenschaftlichen Doktorwürde
(Dr. sc. nat.)

vorgelegt der

Mathematisch-naturwissenschaftlichen Fakultät

der

Universität Zürich

von
Jian Zhu
aus
P.R. China

Promotionskommission

Prof. Dr. **Amedeo Caflisch** (Vorsitz)

Prof. Dr. **Raimund Dutzler**

Prof. Dr. **Martin Jinek**

Zürich, 2018

Summary

Epigenetic mechnisms are essential for normal development and alterations of epigenetic processe are correlated with many human diseases, e.g., cancer. One of the important epigenetic modifications, acetylation of lysine, is mainly recognized by structurally conserved protein module bromodomains. Targeting bromodomains by small molecules is an emerging therapeutic strategy for cancer treatment. In this thesis, we invetigated the protein-ligand interactions for bromodomains that belong to different subfamilies, in the context of the application of fragment-based drug discovery appoach.

In this thesis, fragment-based high throughput screening was employed to identify diverse novel chemotypes binding to BRPF1 bromodomain. A multidisciplinary approach combining in silico docking, protein X-ray crystallography and calorimetry was used for further hit optimization. Two series of potent and selective BRPF1 bromodomain inhibitors, 2,3-dioxo-quinoxaline and 2,4-dimethyl-oxazole derivatives were characterized eventually. The selectity was measured experimentally by biochemical assay and isothermal titration calorimetry, and analyzed by explicit-solvent molecular dynamics simulations. Another virtual screening campaign in conjunction with ligand-observed NMR spectroscopy was used to discover highly ligand-efficient fragments targeting the CREBBP bromodomain and ligand binding mode was validated by X-ray crystallography. By application of a de novo developed virtual sysnthesis method, an initial fragment hit was evolved into low nanomolar CREBBP inhibitor with excellent selectivity against BRD4(1) bromodomain. In another study, using a combined scaffold hopping and ligand docking approach, acetyl indoles were discovered as binders of the bromodomains of CREBBP, BAZ2B and BRPF1. A comparative crystal structure analysis revealed the importance of the gatekeeper residue in bromodomains with respect to the binding of ligands.

In summary, by means of fragment-based drug design approach, a couple of fragment hits and potent inhibitors for brodomains were identified, and they are promising starting points to generate therapeutic agents and chemical probes to interrogate bromodomain biology. Similar fragment-based drug design approaches can be applied to lead discovery projects for less studied bromodomains and other drug targets.

Zusammenfassung

Epigenetische Mechanismen sind für eine normale Entwicklung wesentlich und Veränderungen epigenetischer Prozesse sind mit vielen menschlichen Erkrankungen, z.B. Krebs, korreliert. Eine der wichtigen epigenetischen Modifikationen, die Acetylierung von Lysin, wird hauptsächlich von strukturell konservierten Proteinmodul-Bromodomänen erkannt. Die gezielte Bekämpfung von Bromodomänen durch kleine Moleküle ist eine neue therapeutische Strategie für die Krebsbehandlung. In dieser Arbeit untersuchten wir die Protein-Ligand-Interaktionen für Bromodomänen, die zu verschiedenen Unterfamilien gehören, im Rahmen der Anwendung von Fragmenten-basierten Medikamentenentdeckungen.

In dieser Arbeit wurde das Fragment-basierte Hochdurchsatzscreening eingesetzt, um diverse neuartige Chemotypen zu identifizieren, die an BRPF1-Bromodomäne binden. Ein multidisziplinärer Ansatz, der In-Silico-Docking, Protein-Röntgenkristallographie und Kalorimetrie kombiniert, wurde für die weitere Optimierung der Treffer verwendet. Zwei Serien von potenten und selektiven BRPF1-Bromodomäneninhibitoren, 2,3-Dioxochinoxalin und 2,4-Dimethyloxazolderivaten wurden schließlich charakterisiert. Die Selektivität wurde experimentell mittels biochemischer Analyse und isothermer Titrationskalorimetrie gemessen und durch explizite Solvens-Moleküldynamiksimulationen analysiert. Eine weitere virtuelle Screening-Kampagne in Verbindung mit Liganden-beobachteter NMR-Spektroskopie wurde verwendet, um hoch ligandeneffiziente Fragmente zu entdecken, die auf die CREBBP-Bromodomäne abzielen, und der Ligandenbindungsmodus wurde durch Röntgenkristallographie validiert. Unter Verwendung einer de novo entwickelten virtuellen Methode wurde ein anfänglicher Fragmentschlag in einen niedrig nanomolaren CREBBP Inhibitor mit ausgezeichneter Selektivität gegen BRD4(1) Bromodomäne entwickelt. In einer weiteren Studie, bei der ein kombinierter Scaffold-Hopping und Liganden-Docking-Ansatz verwendet wurde, wurden Acetylindole als Binder der Bromodomänen von CREBBP, BAZ2B und BRPF1 entdeckt. Eine vergleichende Kristallstrukturanalyse zeigte die Bedeutung des Gatekeeper-Restes in Bromodomänen in Bezug auf die Bindung von Liganden.

Zusammengefasst wurden mittels Fragment-based Drug Design Ansatz einige Fragment-Hits und potente Inhibitoren für Brodomänen identifiziert, die vielversprechende Ansatzpunkte für die Entwicklung von Therapeutika und chemischen Sonden zur Untersuchung der Bromodomänenbiologie darstellen. Ähnliche, auf Fragmenten basierende Ansätze zur Wirkstoffentwicklung können auf Forschungsprojekte für weniger erforschte Bromodomänen und andere Wirkstoffziele angewendet werden.

Contents

Chapter 1

Introduction

Epigenetic post-translational modifications are crucial for controlling chromatin state and thus influence gene expression. In recent years, bromodomains, protein module that recognize the acetylated lysine histone mark, have emerged as promising therapeutic targets for the treatment of cancer and other diseases.

Drug discovey is a constanly changing field. Nowadays fragment-based drug design (FBDD) gradually becomes a mainstream in lead discovery taking advantage of the high quality interactions of the small-size fragments with therapeutic protein target. In this thesis, we will focus on the application of the fragment-based drug discovery approach on a series of bromodomains, mainly BRPF1, CREBBP, BAZ2B and BRD4(1).

In the following, a brief intruduction of bromodomain protein family and a more detailed description of BRPF1 bromodomain and its implication in leukemia are given in Section 1.1 and 1.2, respectively. In Section 1.3, we introduce the fragment-based drug discovery and its application in discovering bromodomain inhibitors, and particularly, the use of X-ray protein crystallography in FBDD is described in Section 1.4.

1.1 Bromodomains

Contemporary epigenetics is defined as heritable gene expression that is not associated with any alteration of DNA sequence, but with chemical modification of DNA, i.e., DNA methylation, or of the covalent modification of histone bound to it [1]. A histone modification is a post-translational modification (PTM) to histone proteins which mainly include phosphorylation, acetylation, methylation, ubiquitylation and sumoylation [2]. A number of protein families are involved in epigenetic regulation through writing, erasing and reading specific post-translational modifications, referred to as writers (histone acetyltransferases (HATs), histone methyltransferases), erasers (histone deacetylases (HDACs), histone

demethylases) and readers (bromodomains, chromodomains, plant homeodomains, etc.). Aberrant regulation of epigenetic proteins are hallmarks of many diseases including cancer [3].

Lysine acetylation (Kac) is one of the important and main PTMs. Acetylation of chromatin is generally related with the structure and function of chromatin, and transcriptional activation [2]. It is also found to be involved in regulating metabolism [4] and protein stability [5]. The acetylation of lysine residue on histone is catalyzed by histone acetyltransferases (HATs) and removed by histone deacetylases (HDACs). Bromodomains (BRDs) are evolutionarily conserved protein-protein interaction modules that specifically recognize acetylation marks on histone tails.

Human proteome analysis reveals in total 61 bromodomains found in 46 diverse proteins, which can be clustered into eight sub-families. The bromodomain-containing proteins play an essential role in regulating gene transcriptions through different ways. First, they can act as scaffold to recruit trans chromation factors to assemble large complex. Second, some bromodomain-containing proteins are themselves transcriptional factors or regulators. Last, BRD-containing proteins can act as methyltransferases, acetyltransferases and helicases, thereby they are engaged in various chromation modifications [6]. Proteins contain bromodomains have been implicated in several disease process, including inflammation, neugological disease, as well as cancer [6,7].

Bromodomains contain approximately 110 residues folded into a bundle of four left-handed α helices (αZ, αA, αB and αC), linked by two variable loop regions known as ZA loop and BC loop. The four helices form the hydrophobic acetyl binding site to accommodate the side chain of the neutralized acetylated lysine, which is flanked by the two loops. Reported crystal strucures of bromodomain in complex with acetylated histone tail have revealed details of a conserved binding motif for recognition of kac: a conserved asparagine at the N-terminal BC loop is responsible for the recognition of acetyl-lysine via a specific hydrogen bond; structurally conserved water molecules locating at the bottom of the binding site are also involved in the ineractions with the acetyl-lysine. The hydrophic nature of the binding pocket of bromodomains as well as the variation of the residues surrounding the kac pocket make them as druggable target for developing therapeutic inhibitors. Notably, some inhibitors targeting the bromodomain ans extraterminal (BET) subfamily have been advanced into clinical trials for the treatment of acute myeloid leukemia (AML) [8].

1.2 BRPF1 bromodomain

The bromodomain and plant homeodomain (PHD) finger containing proteins (BRPF1/2/3) are members of subfamily IV bromodomains, other members of this subfamily are BRD7, BRD9, ATAD2A and ATAD2B bromodomains. BRPF bromodomains contain multiple epigenetic reader domains, including a unique double PHD and zinc finger assembly (PZP), a bromodomain and a C-terminal PWWP domain. In BRPF1, it's bromodomain can specifically recognize multiple acetyl lysine marks in histone tails including H2AK5ac, H3K14ac, H4K5ac, H4K8ac, and H4K12ac [9]. BRPF1 is a scaffolding subunit of the monocytic leukemic zinc finger (MOZ) histone acetyltransferase, in which BRPF1 connects the MOZ catalytic subunit to ING5 and hFaf6, thereby enhancing the acetylation acrivity of MOZ.

The MOZ acetyltransferase is involved in chromosomal translocations process found in a subtype of acute myeloid leukemia (AML) with poor prognosis [10]. Such chromosomal translocation in AML are believed to cause aberrant expression profile of HOX genes mediated by the acetylation activity of MOZ during hematopoiesis, which is found to be critical for leukemogenesis [11]. In AML with MOZ-TIF2 translocation pattern, the MOZ-TIF2 forms a stable complex with BRPF1 and deregulate the expression of HOX genes. The depletion of BRPF1 decreases the MOZ localization to HOX genes and mutant MOZ-TIF2 lacking HAT activity was incapable of deregulating HOX expression as well as inducing leukemia [12]. MOZ complex is also found to be able to associate with the trithorax group protein MLL (mixed-lineage leukemia) to coordinately activate HOX gene expression [13]. Apart from the important role in leukemic translocations, BRPF1 is essentially involved in maintaining the HOX gene expression and hematopoiesis in development [14,15]. Togethor, the emerging body of evidence suggests the potential of BRPF1 as a therapeutic target in leukemia. The architecture of the MOZ complex and its role in leukemogenesis is depicted in Figure 1.

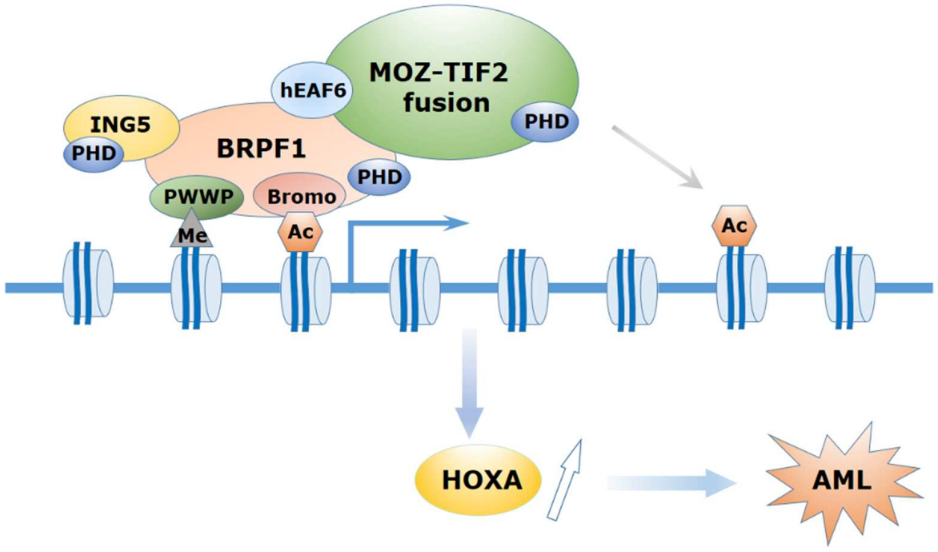

Figurge 1. MOZ complex structure and the mechnism of MOZ-TIF2 fusion in leukemogenesis. BRPF1 recognizes the acetylation and methylation histone modifications by its bromodomain and PWWP domain, respectively. MOZ-fusion/BRPF1 complex promotes histone acetylation resulting in upregulation of downstream HOX genes expression, which lead to the development of leukemia. The figure is adapted and modified from Ref [12].

A few nubmer of chemical probes of BRPF1 bromodomain have been developed by both industry and academic groups. In general, these compounds bear a 1,3-dimethyl benzimidazolone or a N-methylquinolin-2-one scaffold as acetyl-lysine mimetics to target BRPF1. Chemical probes are used to interrogate the target-phenotype relationship and this is strengthened by development of the chemically diverse inhibitors, since different chemical entities may have distinct physiocochemical properties and off-target profiles [16].To explore chemically distinct small molecules to target BRPF1, we performed a fragment-based high throughput virtual sceening using over 10000 fragments, which led to the discovery of six different novel chemotypes (Chapter 2). In a follow up study, two series of potent and selective BRPF1 inhibitors were identified and characterized by hit optimization, which is presented in Chapter 3. These newly discovered chemotypes are promising starting points for the development of novel BRPF1 chemical probes.

1.3 Fragment-based drug design (FBDD)

With nearly 20 years development, FBDD is increasingly implemented as an alternative for high through screening (HTS) in target-based lead discovey. Dozens of molecuels derived from

this approach have beedn advanced to clinical trials [17]. In recent years, FBDD is also widely applied in the development of bromodomains inhibitors throughout industry and academia [18].

A fragment-based drug design project usually starts with the construction of a fragment library for screening, fragments binding is then experimentally validated and finally the promising hits are grown into larger and more potent inhibitors. The process and methodology of FBDD is shown in Figure 2. In the Caflisch group, screening is performed by high throughput docking [19] which is usually carried out with the in house developed program called SEED [20,21]. The process and methodology of FBDD is shown in Figure 2.

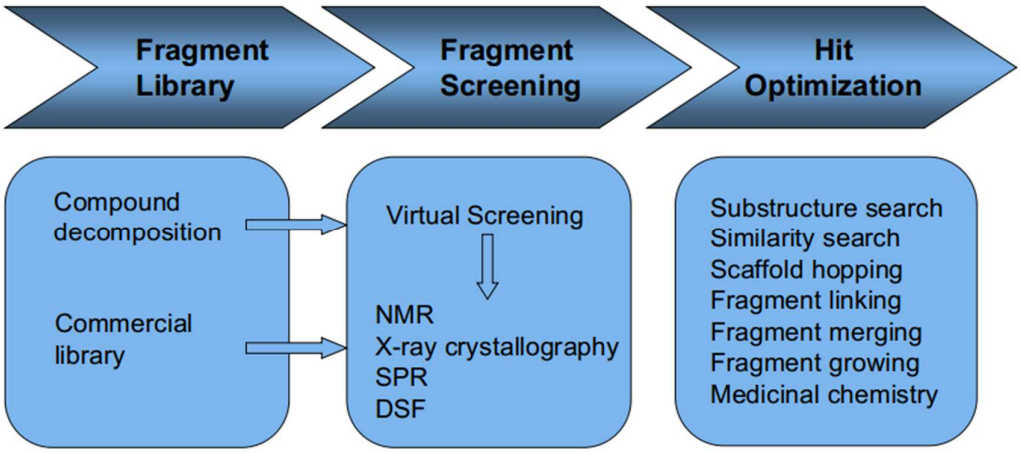

Figurge 2. General process of fragmet-based drug design.

In contrast to the large collection of drug-sized compound library that are used in high through screening, FBDD adopts a smaller library of low molecular weight (MW < 250 Da) compounds for screening on a target protein of interest. Typically, a fragment library comprises thousands of chemically diversed scaffolds which can sample chemical space similar to a million of 'drug-like' molecules. Thus fragment-based screening can achieve higher hit rates than conventional high throughput screening. On the other hand, in many cases, a fragment is adequate to form favorable interactions with target protein and mismatches between larger molecules and target can be avoided, so that screening hits with desirable ligand efficiency (LE) can be obtained from a FBDD campaign.

Since the fragments bind to target protein weakly (100 μM – 10 mM affinity range), sensitive and efficient binding detection methods are required and in fact, this is the key issue in FBDD. In practice, biophysical techniques such as Nuclear Magnetic Resonance Spectroscopy (NMR), X-ray crystallography, Surface Plasmon Resonance (SPR), Differential Scanning Fluorimetry (DSF) are widely used to detect fragment binding. Other methods like

microscale thermophoresis and weak affinity chromatography hold the potential to be useful tools in fragment screening [17]. As listed above, there are a variety of methods available for fragment-finding, however, the limitaiton is whether the target protein is amenable to the screening method, which should be carefully considered. Sometimes, combination of some screening method are needed. In chapter 4, we report on the discovery of several ligand-efficient fragments targeting BAZ2A bromodomain by using a ligand-observed NMR fragment screening strategy [22].

A challenging task after finding of the initial hits is how to evolve them into lead compounds. By means of some cheminformatics applications, e.g., substructure and similarity search around screening hits on commercial available compound database often yield more potent analogues. An example of hit optimization of BRPF1 inhibitor is described in Chapter 3. In chapter 6, we show an application of fragment-based scaffold hopping in the discovery of inhibitors targeting BAZ2B and CREBBP bromodomains [23].

From the medicinal chemistry view, hit optimisation are accomplished by either linking two fragments that occupy adjacent sub-pockets, or merging structural portions of overlapped molecules into one fragment, or growing the fragment by adding funtional groups [24]. In a recent work, a virtual synthesis method developed in the Caflisch group to grow a previously identified fragment instucted rational medicinal chemistry optimization resulting in the identification of very potent and selective CREBBP inhibitos (Chapter 5).

As mentioned above, in silico screening is an alternative way to screen fragments in a high-throuput manner. In the past few years, by using an in-house developed docking tool SEED [20,21], our group had performed several fragment-based virtual screening campaigns on a few number of bromodomains, including BRPF1 [25], BRD4(1) [26], BAZ2A [27], BAZ2B [28] and CREBBP [29]. Some of thees campaigns are described throughout this thesis.

1.4 X-ray crystallography in FBDD

X-ray crystallography is a well-establised method for structural determination of proteins and other biomolecules, which is also widely used in the drug discovery scenarios as it can produce atomic resolution structures of protein complexes with various ligands. For FBDD an important advantage of X-ray crystallography is the validation of fragment hits which are then structurally modified to improve potency by cycles of chemical synthesis and acquisition of activity data under the guidance of structural information of binding mode primarily derived from X-ray crystallography [30]. Both X-ray crystallography and NMR can map the interactions between the protein target and ligands, and ideally these two techniques can complement one another.

However, NMR takes longer time for determining the three-dimentional structures and it generally cannot deal with large proteins. Along with the recent development of high speed detectors for rapid X-ray data collection and in situ co-crystallization screening [31], X-ray crystallography can even serve as a primariy screening tool in drug discovery.

The protein/ligand complex structures are commonly obtained by two ways: soaking and co-crystallization. In the soaking appoach, a single ligand or a cocktail ligands in solution will be incubated with a crystallized target protein without any ligand or substrate (apo crystal). Co-crystallization are performed by mixing ligand and target protein prior to crystallization and the complex is crystallized.

Owing to the relatively weak affinity of fragments, in soaking or co-crystallization expriments, fragments should be prepared at high concentrations, even up to 100 mM. This requires fragments have good aqueous solubility in the mother liquor used for ligand soaking or co-crystallization.

Well-established and robust preformed crystals are suitable for compound soaking as batches of crystals can be reproduced. In this approach, importantly, apo crystals should be compatible with ligand binding. Because bound ligands may induce protein conformational change or disrupt crystal lattice contacts, then soaked crystals may crack or dissolve [32].

Another limitation of soaking is that lattice contacts in apo crystal may inhibit ligand from accessing to the binding site of target protein, resuting in false negatives upon ligand binding. This issue could be circumvented by performing co-crystallization of protein in the presence of ligands. However, it always requires experimentalists to rescreen crystal growth conditions for a specific ligand. In the hit optimization stage of a FBDD project, such problems can be encountered. Figure 3 shows an example in which crystal contacts occlude ligand binding. The apo BRPF1 crystal and a co-crystal of BRPF1 with a fragment are grown from the same condition. An attempt of soaking apo BRPF1 with a derivative of the fragment failed. Subsequent crystallization optimization yielded the complex structure of BRPF1 with this larger ligand. Structural alignment shows an N-terminal glutamic acid residue from another symmetry related protein molecule in the space group of the apo crystal that causes steric collision with this ligand, while it does not interfer with the smaller fragment. Thus, different packings are sometimes required for the fragment and large derivatives of it.

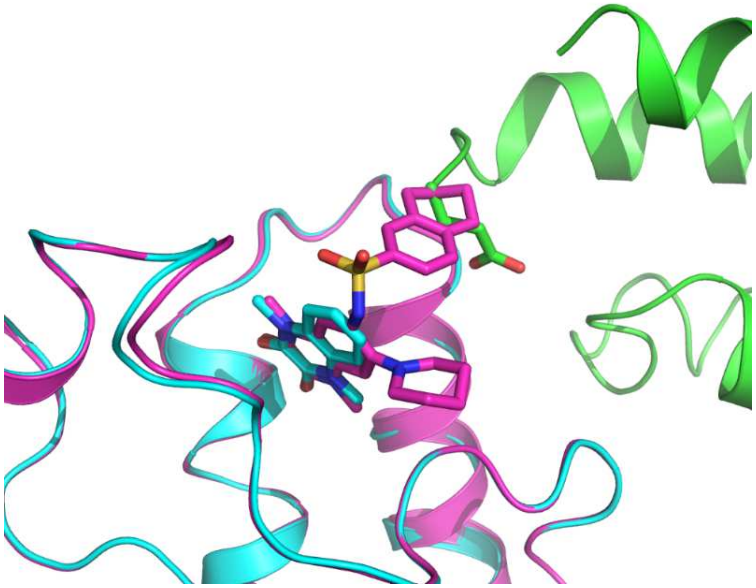

Figure 3. Different space groups (packing arrangement in the crystal) for fragment and derivative with large substituents. The structure of BRPF1 in complex with a fragment (PDB ID 5O4T; in cyan) belongs to space group $P3_221$ and contains one protein molecule in the asymmetric unit. One of the symmetry related protein molecule is shown in green. The structure of BRPF1 complexed with a larger ligand (PDB ID 5MWG; in magenta) belongs to space group $P2_12_12_1$ which was overlapped to the structure of 5O4T. The side chain of a glutamate residue in the neibouring protein molecule prevents binding of the derivative in the same space group as the parent fragment.

In this thesis, x-ray crystallography play a central role in many bromodomain FBDD projects. Complex crystal structures of bromodomains with ligands are used to validate the predicted binding mode in all of the chapters, to guide hit optimization (Chapters 3, 5 and 6) and to validate fragment hits identified in silico (Chapters 2 and 7).

References

1. Felsenfeld, G., A brief history of epigenetics. *Cold Spring Harb Perspect Biol* **2014,** *6* (1).

2. Bannister, A. J.; Kouzarides, T., Regulation of chromatin by histone modifications. *Cell Res* **2011,** *21* (3), 381-95.

3. Esteller, M., Epigenetics in cancer. *N Engl J Med* **2008,** *358* (11), 1148-59.

4. Choudhary, C.; Weinert, B. T.; Nishida, Y.; Verdin, E.; Mann, M., The growing landscape of lysine acetylation links metabolism and cell signalling. *Nat Rev Mol Cell Biol* **2014,** *15* (8), 536-50.

5. Kouzarides, T., Chromatin modifications and their function. *Cell* **2007,** *128* (4), 693-705.

6. Fujisawa, T.; Filippakopoulos, P., Functions of bromodomain-containing proteins and their roles in homeostasis and cancer. *Nat Rev Mol Cell Biol* **2017,** *18* (4), 246-262.

7. Muller, S.; Filippakopoulos, P.; Knapp, S., Bromodomains as therapeutic targets. *Expert Rev Mol Med* **2011,** *13*, e29.

8. Braun, T.; Gardin, C., Investigational BET bromodomain protein inhibitors in early stage clinical trials for acute myelogenous leukemia (AML). *Expert Opin Investig Drugs* **2017,** *26* (7), 803-811.

9. Poplawski, A.; Hu, K.; Lee, W.; Natesan, S.; Peng, D.; Carlson, S.; Shi, X.; Balaz, S.; Markley, J. L.; Glass, K. C., Molecular insights into the recognition of N-terminal histone modifications by the BRPF1 bromodomain. *J Mol Biol* **2014,** *426* (8), 1661-76.

10. Brown, T.; Swansbury, J.; Taj, M. M., Prognosis of patients with t(8;16)(p11;p13) acute myeloid leukemia. *Leuk Lymphoma* **2012,** *53* (2), 338-41.

11. Troke, P. J.; Kindle, K. B.; Collins, H. M.; Heery, D. M., MOZ fusion proteins in acute myeloid leukaemia. *Biochemical Society symposium* **2006,** (73), 23-39.

12. Shima, H.; Yamagata, K.; Aikawa, Y.; Shino, M.; Koseki, H.; Shimada, H.; Kitabayashi, I., Bromodomain-PHD finger protein 1 is critical for leukemogenesis associated with MOZ-TIF2 fusion. *International journal of hematology* **2014,** *99* (1), 21-31.

13. Paggetti, J.; Largeot, A.; Aucagne, R.; Jacquel, A.; Lagrange, B.; Yang, X. J.; Solary, E.; Bastie, J. N.; Delva, L., Crosstalk between leukemia-associated proteins MOZ and MLL regulates HOX gene expression in human cord blood CD34+ cells. *Oncogene* **2010,** *29* (36), 5019-31.

14. Katsumoto, T.; Aikawa, Y.; Iwama, A.; Ueda, S.; Ichikawa, H.; Ochiya, T.; Kitabayashi, I., MOZ is essential for maintenance of hematopoietic stem cells. *Genes & development* **2006,** *20* (10), 1321-30.
15. Laue, K.; Daujat, S.; Crump, J. G.; Plaster, N.; Roehl, H. H.; Tubingen Screen, C.; Kimmel, C. B.; Schneider, R.; Hammerschmidt, M., The multidomain protein Brpf1 binds histones and is required for Hox gene expression and segmental identity. *Development* **2008,** *135* (11), 1935-46.
16. Shortt, J.; Ott, C. J.; Johnstone, R. W.; Bradner, J. E., A chemical probe toolbox for dissecting the cancer epigenome. *Nat Rev Cancer* **2017,** *17* (3), 160-183.
17. Erlanson, D. A.; Fesik, S. W.; Hubbard, R. E.; Jahnke, W.; Jhoti, H., Twenty years on: the impact of fragments on drug discovery. *Nat Rev Drug Discov* **2016,** *15* (9), 605-19.
18. Radwan, M.; Serya, R., Fragment-Based Drug Discovery in the Bromodomain and Extra-Terminal Domain Family. *Arch Pharm (Weinheim)* **2017,** *350* (8).
19. Sledz, P.; Caflisch, A., Protein structure-based drug design: from docking to molecular dynamics. *Curr Opin Struct Biol* **2017,** *48*, 93-102.
20. Majeux, N.; Scarsi, M.; Apostolakis, J.; Ehrhardt, C.; Caflisch, A., Exhaustive docking of molecular fragments with electrostatic solvation. *Proteins* **1999,** *37* (1), 88-105.
21. Majeux, N.; Scarsi, M.; Caflisch, A., Efficient electrostatic solvation model for protein-fragment docking. *Proteins* **2001,** *42* (2), 256-68.
22. Spiliotopoulos, D.; Zhu, J.; Wamhoff, E. C.; Deerain, N.; Marchand, J. R.; Aretz, J.; Rademacher, C.; Caflisch, A., Virtual screen to NMR (VS2NMR): Discovery of fragment hits for the CBP bromodomain. *Bioorg Med Chem Lett* **2017,** *27* (11), 2472-2478.
23. Unzue, A.; Zhao, H.; Lolli, G.; Dong, J.; Zhu, J.; Zechner, M.; Dolbois, A.; Caflisch, A.; Nevado, C., The "Gatekeeper" Residue Influences the Mode of Binding of Acetyl Indoles to Bromodomains. *J Med Chem* **2016,** *59* (7), 3087-97.
24. de Kloe, G. E.; Bailey, D.; Leurs, R.; de Esch, I. J., Transforming fragments into candidates: small becomes big in medicinal chemistry. *Drug Discov Today* **2009,** *14* (13-14), 630-46.
25. Zhu, J.; Caflisch, A., Twenty Crystal Structures of Bromodomain and PHD Finger Containing Protein 1 (BRPF1)/Ligand Complexes Reveal Conserved Binding Motifs and Rare Interactions. J Med Chem 2016, 59 (11), 5555-61.
26. Zhao, H.; Gartenmann, L.; Dong, J.; Spiliotopoulos, D.; Caflisch, A., Discovery of BRD4 bromodomain inhibitors by fragment-based high-throughput docking. Bioorg Med Chem Lett 2014, 24 (11), 2493-6.

27. Spiliotopoulos, D.; Wamhoff, E. C.; Lolli, G.; Rademacher, C.; Caflisch, A., Discovery of BAZ2A bromodomain ligands. Eur J Med Chem 2017, 139, 564-572.
28. Lolli, G.; Caflisch, A., High-Throughput Fragment Docking into the BAZ2B Bromodomain: Efficient in Silico Screening for X-Ray Crystallography. ACS Chem Biol 2016, 11 (3), 800-7.
29. Xu, M.; Unzue, A.; Dong, J.; Spiliotopoulos, D.; Nevado, C.; Caflisch, A., Discovery of CREBBP Bromodomain Inhibitors by High-Throughput Docking and Hit Optimization Guided by Molecular Dynamics. J Med Chem 2016, 59 (4), 1340-9.
30. Scott, D. E.; Coyne, A. G.; Hudson, S. A.; Abell, C., Fragment-based approaches in drug discovery and chemical biology. *Biochemistry* **2012,** *51* (25), 4990-5003.
31. Yin, X.; Scalia, A.; Leroy, L.; Cuttitta, C. M.; Polizzo, G. M.; Ericson, D. L.; Roessler, C. G.; Campos, O.; Ma, M. Y.; Agarwal, R.; Jackimowicz, R.; Allaire, M.; Orville, A. M.; Sweet, R. M.; Soares, A. S., Hitting the target: fragment screening with acoustic in situ co-crystallization of proteins plus fragment libraries on pin-mounted data-collection micromeshes. *Acta Crystallogr D Biol Crystallogr* **2014,** *70* (Pt 5), 1177-89.
32. Danley, D. E., Crystallization to obtain protein-ligand complexes for structure-aided drug design. *Acta Crystallogr D Biol Crystallogr* **2006,** *62* (Pt 6), 569-75.

Chapter 2

Twenty Crystal Structures of Bromodomain and PHD Finger Containing Protein 1 (BRPF1)/Ligand Complexes Reveal Conserved Binding Motifs and Rare Interactions

Zhu J, Caflisch A., Journal of Medicinal Chemistry 2016; 59(11): 5555–5561.

Journal of Medicinal Chemistry

Brief Article

pubs.acs.org/jmc

Twenty Crystal Structures of Bromodomain and PHD Finger Containing Protein 1 (BRPF1)/Ligand Complexes Reveal Conserved Binding Motifs and Rare Interactions

Jian Zhu and Amedeo Caflisch*

Department of Biochemistry, University of Zürich, Winterthurerstrasse 190, CH-8057 Zürich, Switzerland

Supporting Information

ABSTRACT: BRPF1 plays a scaffolding role in transcription. We report on fragment screening by high-throughput docking to the BRPF1 bromodomain which resulted in six chemotypes with very favorable ligand efficiency (0.45−0.50 kcal/mol per non-hydrogen atom). Twenty crystal structures of BRPF1/ligand complexes show structural conservation in the acetyllysine binding site, common binding motifs, and unusual interactions (e.g., the replacement of a conserved water molecule). The structural information is useful for the design of chemical probes.

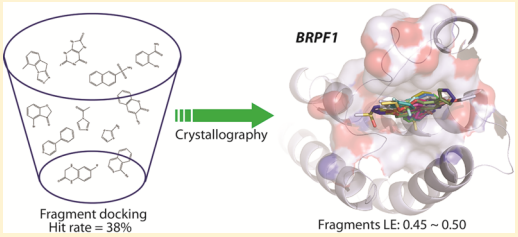

INTRODUCTION

Genetic analysis on zebrafish has shown that the bromodomain and PHD finger (BRPF) containing protein BRPF1 is a member of the Trithorax group with a central role during development in vertebrates.[1] BRPF1 associates with the histone acetyltransferase monocytic leukemia zinc finger protein (MOZ) and recruits it to distinct sites of chromatin. The bromodomain of BRPF1 binds to acetylated histone tails.[2]

In contrast to the bromodomain and extra terminal (BET) subfamily of bromodomains, e.g., bromodomain-containing protein 4 (BRD4), very few crystal structures of complexes of the BRPF1 bromodomain with ligands (holo) are available. Lubula et al.[3] reported the crystal structure of the BRPF1 bromodomain in complex with acetylated histone peptides H4K12ac and H2AK5ac. Demont et al.[4] identified 1,3-dimethyl benzimidazolones as potent BRPF1 bromodomain inhibitors and have disclosed the structures of two of these ligands in the complex with BRPF1.

Experimental approaches to fragment-based screening have been used to identify ligands of bromodomains of the BET subfamily, viz., bromodomain-containing protein 2 (BRD2)[5] and BRD4,[6] and also for non-BET bromodomains, viz., ATPase family, AAA domain containing 2 (ATAD2),[7] bromodomain adjacent to zinc-finger domain 2B (BAZ2B),[8] and binding protein of the cAMP response element-binding protein (CREBBP).[9]

Here, we have screened a library of 24133 molecules by docking into the BRPF1 bromodomain followed by experimental validation of the in silico top ranking hits by X-ray crystallography. We could solve the crystal structures of BRPF1 (see Experimental Section for details) in the complex with 20 ligands at resolutions between 1.33 and 1.75 Å (Table 1). Six new chemotypes have been identified: tricyclazole, phenylpyridine, mercaptopurine, hydroxyisoquinoline, quinoxalin-2-one, and acetylindole. Common binding motifs and infrequent interactions emerge from the analysis of the 20 crystal structures. The acetyl lysine binding site of BRPF1 is conserved except for a slight displacement of the ZA loop. Only one of the 20 ligands displaces a conserved water molecule that is present in most crystal structures of bromodomain/ligand complexes.

RESULTS AND DISCUSSION

We screened in silico the 24133 molecules devoid of rotatable bonds and with molecular weight smaller than 550 g/mol (called fragments in the following) that were present in the 2014 version of the ZINC library.[13] The screening was carried out by high-throughput fragment docking into the structure of apo BRPF1 (PDB code 4LC2) using the program SEED[14] (see Experimental Section for details). Virtual screening required about 24 h; the preparation of the library of fragments took less than 1 h, and the docking of the 24133 fragments required less than a day on a commodity desktop. An initial set of 13 molecules among the top 30 ranking fragments was selected according to predicted binding energy (SEED energy) and availability and tested by experiments of soaking into crystals of the apo form of the BRPF1 bromodomain. The crystal structures of the complexes of BRPF1 with five of these fragments (**1**, **2**, **3**, **5**, and **8** in Table 1 and Supporting Information (SI), Figure S1) were solved. Electron densities were not observed for the other eight fragments (SI, Figure S2). The predicted binding mode of fragments **1**, **2**, and **8** was confirmed by the crystal structures (SI, Figure S1). Fragment **3** shows a different orientation in the crystal with respect to the docked pose, which is probably due to the lack of reorientation of the structural water molecules during docking. The oxygen atom of fragment **5** (1-isoquinolinone) replaces the buried water molecule that bridges to the side chain of the conserved Tyr665 (see below) and was present during docking. Thus, the

Received: February 11, 2016
Published: May 11, 2016

DOI: 10.1021/acs.jmedchem.6b00215
J. Med. Chem. 2016, 59, 5555−5561

Table 1. Structures, K_D Values for BRPF1, and Ligand Efficiencies (LE) of in Silico Hits[a]

Cpd PDB ID	Structure	K_D (μM)	LE	Cpd PDB ID	Structure	K_D (μM)	LE
1 5EQ1	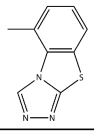	21	0.49	**11** 5EPS	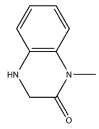	38	0.50
2 5EWD	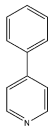	>200		**12** 5EPR	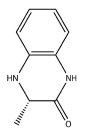	91	0.46
3 5E3G	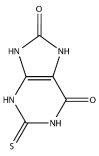	>50		**13** 5EWC	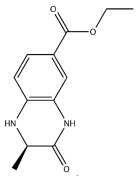	N.D.	
4 5E3D	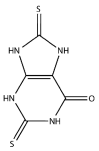	95	0.46	**14** 5DYA	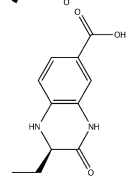	>200	
5 5C87	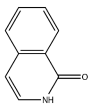	>200		**15** 5ETB	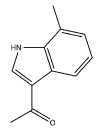	29	0.48
6 5EM3	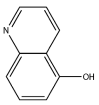	>200		**16** 5ETD	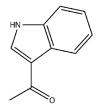	N.D.	
7 5EWH	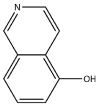	170	0.47	**17** 5D7X	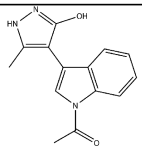	15	0.35
8 5C85	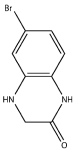	105	0.45	**18** 5EV9	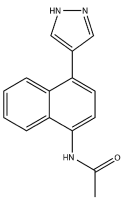	N.D.	
9 5DYC	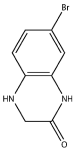	N.D.		**19** 5EVA	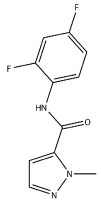	>200	
10 5DY7	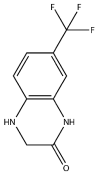	>200		**20** 5C7N	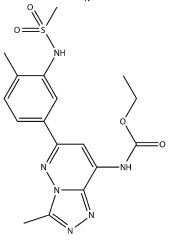	0.27	0.32

[a]Molecules **1**–**16** can be clustered (SI, Figure S3) in six chemotypes (horizontal lines). The K_D values were determined by a competition binding assay BROMOscan[10] in duplicate (SI, Figure S4). For compound **20**, an IC_{50} value of 0.65 μM was determined by AlphaScreen[11] (SI, Figure S5). Ligand efficiency[12] is calculated as LE = (1.37/HA) × pK_D, in the units of kcal/mol per non-hydrogen atom.

hit rate, i.e., ratio of binders versus purchased fragments, is 38% (or 23% if one considers only the poses correctly predicted by docking).

An additional set of 15 molecules were tested in a second round of soaking experiments. This set consists of nine purchasable analogues (according to the definition in the ZINC database with a similarity threshold of 70%) of the five original hits, the acetylindole derivative **17** (which binds to another bromodomain of subfamily IV, the BRD9 bromodomain),[15] four molecules similar to **17** (compounds **15**, **16**, **18**, and **19**), and the pan-bromodomain inhibitor bromosporine (**20**).[16] In total, five ligands show a value of the equilibrium dissociation constant (K_D) for the BRPF1 bromodomain smaller than 100 μM while bromosporine has a K_D of 0.27 μM (Table 1). Importantly, the seven ligands with K_D < 200 μM (compounds **1**, **4**, **7**, **8**, **11**, **12**, and **15**) have very favorable ligand efficiency (LE) in the range 0.45–0.50 kcal/mol per non-hydrogen atom. Of these, fragments **1** and **8** are two of the five original docking hits.

For the analysis of the 20 crystal structures of the BRPF1 bromodomain/ligand complexes (Table 1), it is useful to describe first the binding site and common binding motifs. The acetyl lysine binding site has a parallelepiped-like shape in which the ligands are sandwiched by van der Waals contacts with the ZA-loop side chains Val657, Pro658, and Val662 on one of the two largest sides of the pocket and Ile652, Asn708, and Phe714 (the so-called gatekeeper) on the opposite side of the pocket (Figure 1). The bottom of the binding site is occupied by conserved water molecules and the phenyl ring of the conserved Phe653 (SI, Figures S6–S8). The structural overlap of the 20 complexes shows that the backbone and most side chains in the acetyl lysine binding site are conserved (Figure 1A). This finding is congruent with the similar size of the compounds, which consist of two or three (fused) ring systems. Furthermore, all crystals belong to the same space group and there are no crystal contacts in the acetyl lysine binding site. The structural similarity in the binding site is very high for the BC loop (residues 707–712) and the N-terminal segment of the ZA-loop (residues 650–656). The latter includes the Asn651-Ile652-Phe653 segment that corresponds to the Trp-Pro-Phe triad in the BET bromodomains. In contrast, the central segment of the ZA-loop (residues 657–668) shows structural heterogeneity. The rigid-body displacement of this part of the ZA-loop reduces the aperture of the binding site with respect to the apo structure (PDB code 4LC2), which was solved in the same space group as our 20 holo structures (Figure 1B). The slightly narrower binding pocket in the holo structures with respect to the apo conformation is a consequence of the intrinsic flexibility of the ZA-loop and the formation of optimal van der Waals contacts between the ligand and the hydrophobic side chains of Val657, Pro658, and Val662 on one side of the pocket and Ile652 and the gatekeeper Phe714 on the other side (Figure 1C). Quantitatively, the largest backbone displacement with

DOI: 10.1021/acs.jmedchem.6b00215
J. Med. Chem. 2016, 59, 5555–5561

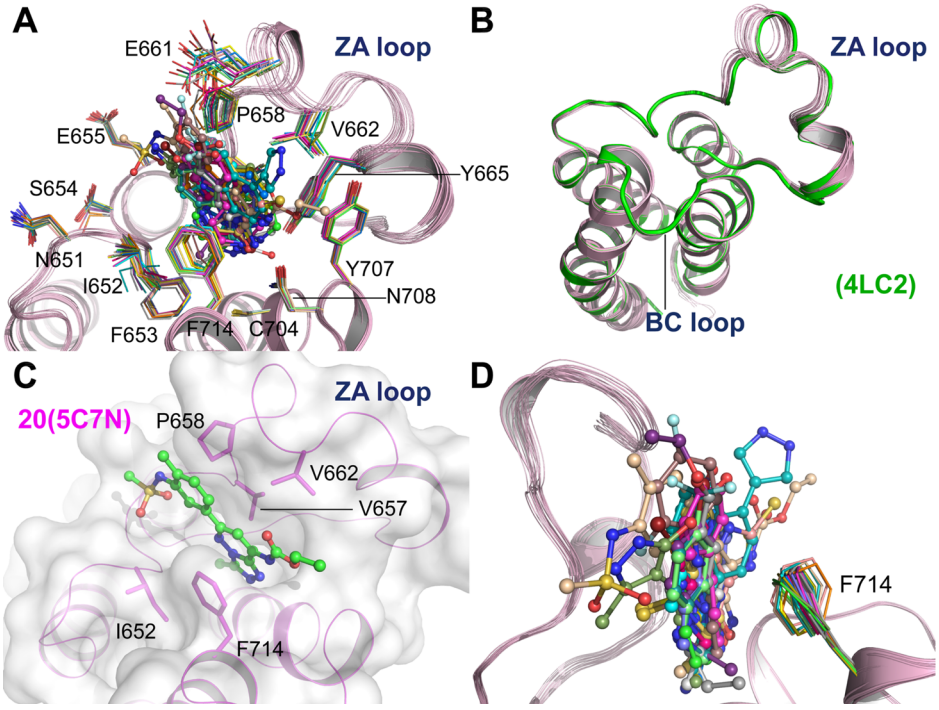

Figure 1. Structural overlap and analysis of the 20 complex structures. (A) Kac binding site of BRPF1. (B) Displacement of the ZA-loop in the 20 holo structures with respect to the apo structure (4LC2, green). (C) Hydrophobic residues lining the Kac binding site in BRPF1. (D) The phenyl ring of the gatekeeper residue Phe714 shows different orientations for different ligands.

respect to the apo structure is observed for the residues 659–661 whose Cα atoms move by up to 2.5 Å. The side chain of Glu661 shows the largest variability in the 20 structures (Figure 1A). Interestingly, the size of the ligand influences the orientation of the Glu661 side chain particularly for compounds **13**, **19**, and **20** (bromosporine), whose binding modes induce the largest displacement of the tip of the Glu661 side chain (SI, Figure S8). It is important to note that the slightly different tilting of the ligands is related not only to the rigid-body displacement of residues 657–668 of the ZA loop but also to the different orientations of the phenyl ring of the Phe714 gatekeeper (Figure 1D). The χ_2 dihedral angle of Phe714 varies in a range of about 75°, resulting in different orientations of the phenyl ring.

The two hydrogen bonds with the NH2 group of the conserved Asn708 and the buried water molecule that bridges to Tyr665 are present in all structures except for the complex with fragment **5** (Figure 2). In this complex, the oxygen atom of fragment **5** is at hydrogen bond distance to the hydroxyl oxygen of Tyr665 (2.7 Å) while its distance from the side chain nitrogen atom of Asn708 is 4.0 Å which is too long for a hydrogen bond. The scatter plot of the two hydrogen bond distances shows that the one with the structural water is shorter in 15 of 19 structures (Figure 3). This result is consistent with a previous study on BRD2 (ref 5) and provides further evidence that the hydrogen bond with the buried water molecule that bridges to the conserved Tyr665 is stronger than the one with Asn708.

The interaction with the carbonyl oxygen of the conserved Asn708 is heterogeneous. In the complexes with the ligands **9**, **10**, **12**, and **14**, there is a water molecule that acts as bridge to the side chain CO of Asn708 (Figure 4A,B). This water molecule corresponds to a structural water molecule of the apo structure (HOH1007 in 4LC2). In contrast, the bridging water

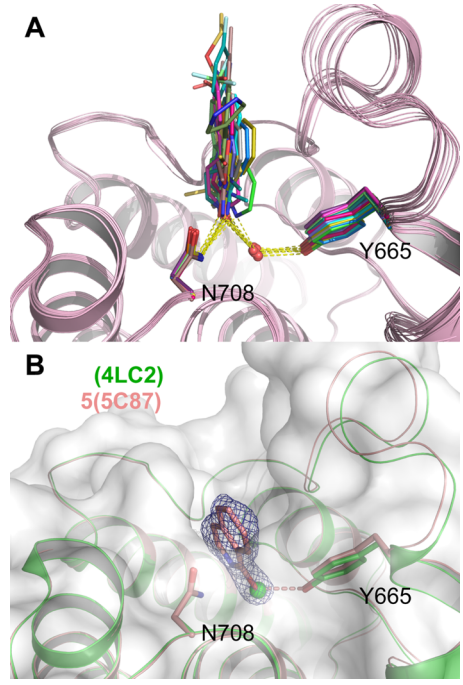

Figure 2. Only fragment **5** displaces the buried water molecule that acts as bridge to the conserved Tyr665. (A) Crystal structures overlay of all ligands but **5**. (B) Structural overlap of the complex with fragment **5** (pink) and the apo structure (green). $2F_o - F_c$ electron density map of **5** is shown in mesh contoured at 1 σ.

molecule is replaced by an NH group in ligands **3**, **4**, and **20** (Figure 4C) and the methyl group of compound **11** (Figure 4D). Similar to compound **11**, a previously reported 1, 3-dimethyl benzimidazolone inhibitor (SI, Figure S9) of the

DOI: 10.1021/acs.jmedchem.6b00215
J. Med. Chem. 2016, 59, 5555–5561

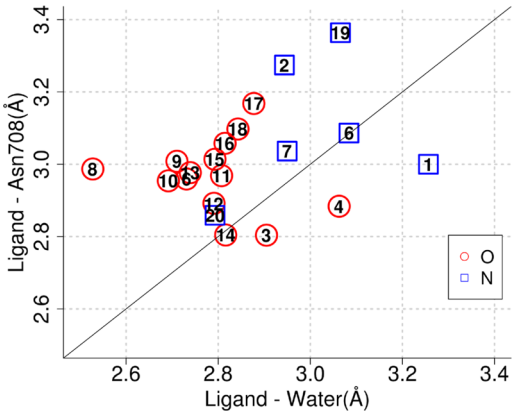

Figure 3. Scatter plot of hydrogen bond distances involving the ligand acceptor atom closest to the side chain N atom of the conserved Asn708. Numbers denote the ligand, and symbols the atomic element of the acceptor. In 15 of 19 structures, hydrogen bonds with the buried water that bridges to the Tyr665 side chain are shorter than with the Asn708.

BRPF1 bromodomain replaces the water molecule bridging to the side chain CO of Asn708 (PDB code 4UYE).

The molecules of the largest cluster (**8**–**14**) share the tetrahydroquinoxalin-2-one scaffold (Table 1). As mentioned above, these ligands do not form a direct hydrogen bond with the carbonyl oxygen of the Asn708 side chain (Figure 4, SI, Figures S7, S8). In contrast, in the structures of the complexes of the CREBBP bromodomain inhibitors[9] with the tetrahydroquinoxalin-2-one scaffold, there are two direct hydrogen bonds to the conserved asparagine (Asn1168 in CREBBP, PDB codes 4NYW and 4NYX). The structural overlap shows that the position of the scaffold in the complexes with BRPF1 is slightly shifted with respect to CREBBP (SI, Figures S9, S10).

The two mercaptopurine fragments **3** and **4** show distinct binding mode as compared with a 2-amine-9*H*-purine derived BRD9 inhibitor[17] (SI, Figure S11). In both structures of **3** and **4**, the NH group at position 7 donates a hydrogen bond to the Asn708 side chain CO while the carbonyl group at position 6 forms a bifurcated hydrogen bond with the Asn708 side chain NH and the water molecule that bridges to Tyr665. In the BRD4 and BRD9 structures, the 2-amine-9*H*-purine derivative shows a flipped orientation with the amine group at position 2, nitrogen atom at 3, and NH group at 9 involved in hydrogen bonds to the conserved asparagine and water molecule.

Finally, a polar interaction with the backbone carbonyl of Ile652 is present in the complex with several ligands. This interaction was first observed in molecular dynamics simulations of the spontaneous binding of acetyl lysine.[18] In the complex structures with the quinoxalinone derivatives **8**, **9**, **10**, and **13**, there is a direct hydrogen bond with the carbonyl of Ile562, while a bridging water molecule is present for compounds **12**, **18**, and **19** (SI, Figures S7, S8).

CONCLUSIONS

We have identified six chemotypes of ligands of the BRPF1 bromodomain by high-throughput docking of fragments, which was carried out in 1 day on a single commodity processor, followed by soaking experiments and purchase of hit analogues. Seven in silico hits have ligand efficiency in the range 0.45–0.50 kcal/mol per non-hydrogen atom (Table 1). The X-ray crystal structures of BRPF1 in complex with 19 compounds (and the complex with bromosporine, a previously disclosed promiscu-

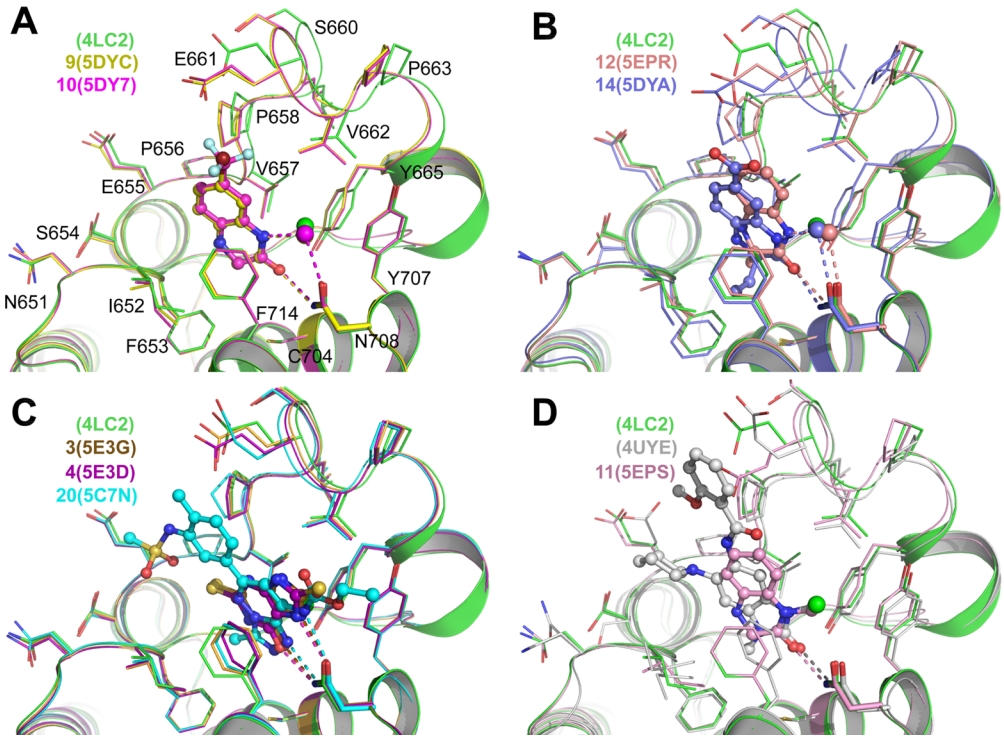

Figure 4. A water molecule acting as hydrogen bond bridge to the side chain carbonyl of Asn708 was observed in the crystal structures of the complexes with compounds (A) **9** and **10**, and (B) **12** and **14**. The bridging water molecule is replaced by the NH group of compounds **3**, **4** and **20** (C), and the methyl group of fragment **11** and a benzimidazolone derivative (4UYE) (D). The apo structure (4LC2, green) is shown in all panels as a basis of comparison.

DOI: 10.1021/acs.jmedchem.6b00215
J. Med. Chem. 2016, 59, 5555–5561

ous inhibitor) show that the overall structure of the acetyl lysine binding site is conserved. Interestingly, the water-bridged hydrogen bond with the conserved tyrosine of the ZA-loop (Tyr665) is present in all crystal structures except for the complex with fragment **5** (1-isoquinolinone), whose oxygen atom replaces the buried water molecule which does not improve affinity. The phenyl ring of the gatekeeper residue (Phe714) shows slightly different orientations, while the ZA-loop accommodates different ligands by rigid-body displacement and rearrangement of side chains, in particular Glu661.

The fragment-based high-throughput docking campaigns in our group have resulted in the identification of molecules with very favorable ligand efficiency for the bromodomains of BRD4,[19] CREBBP,[20] BAZ2B,[21] and BRPF1 (this work). These bromodomains belong to four different subfamilies of human bromodomains (viz., subfamilies II, III, IV, and V). In the case of the CREBBP bromodomain, optimization of the initial hits by chemical synthesis of derivatives has generated several selective low nanomolar inhibitors with ligand efficiency similar to the initial hits.[20] Thus, the screening of fragment libraries by docking is very efficient and shows high success rate and negligible cost. The favorable ligand efficiency of our hits and their crystal structures in the complex with the BRPF1 bromodomain are important starting points for hit optimization and the design of chemical probes to investigate the function of BRPF1. For instance, the bromine-containing fragments **8** and **9** could be grown into more potent and selective ligands by Suzuki coupling.

EXPERIMENTAL SECTION

Fragment Docking. The nearly 12 million molecules of the ZINC database (version 2014)[13] were filtered for zero rotatable bonds and molecular weight smaller than 550 g/mol by the program DAIM.[22] The resulting library of 24133 fragments was docked into the apo structure of BRPF1 (PDB code 4LC2) by the program SEED,[14] which evaluates the binding energy using a force field-based energy function with a continuum dielectric approximation of desolvation penalties.[23] The binding site for docking was defined by the conserved asparagine in the BC loop (Asn708) and four buried water molecules (numbered w1 to w4 in SI, Figures S6–S8) which are present in most crystal structures of bromodomains. The partial charges and van der Waals parameters of the protein were taken from the CHARMM36 all-atom force field,[24] while the fragments were parametrized using the CHARMM general force field (CGenFF).[25] It is important to note that CGenFF is fully consistent with the CHARMM36 force field because they use the same paradigm for the derivation of partial charges, van der Waals parameters, and parameters for bonding interactions (covalent bonds, angles, dihedrals, and improper dihedrals). The value of the dielectric constant for the continuum calculations was set to 2.0 and 78.5 in the low-dielectric region (solute) and high-dielectric region (solvent), respectively. The docking of the 24133 fragments with SEED required nearly 22 h (about 3 s per fragment) of a single core of an i7-930 processor at 2.8 GHz.

Chemistry. All screened compounds were purchased from commercial vendors and the purity of all molecules was analyzed by HPLC-MS and is determined to be at least 95%. Compound **20** (bromosporine) was purchased from Sigma-Aldrich with purity higher than 98%.

Protein Production. The gene encoding the bromo-domain of BRPF1 (aa 626–740) was amplified by PCR from the original plasmid (Addgene plasmid no. 53620) and subcloned to a modified pGEX-4T-1 vector. A tobacco etch virus (TEV) protease recognition site was introduced between the glutathione S-transferase (GST) fusion protein and BRPF1 bromodomain. The recombinant plasmid was transformed into *Escherichia coli* strain BL21(DE3). The cells were grown at 37 °C until an OD600 of 0.6 was reached. After induction (0.2 mM IPTG) and overnight expression at 16 °C, the GST-tagged protein was purified by a Glutathione Sepharose 4B column and the GST tag was removed with TEV protease afterward. The bromodomain was further purified using a Superdex 75 column in the buffer of 50 mM HEPES (pH 7.5), 0.15 M NaCl, and 0.5 mM DTT. Eluted protein was concentrated to 22 mg/mL (NanoDrop spectrophotometer) in the same buffer and frozen in liquid nitrogen.

Crystallization. Sparse-matrix crystallization screens were performed with a Phoenix crystallization robot to identify initial crystallization conditions. BRPF1 bromodomain was crystallized by vapor diffusion in hanging drops at 4 °C. Crystallization buffer is composed of 0.1 M sodium acetate pH 5.5 (or 0.1 M BIS-TRIS propane pH 6.5), 0.15–0.2 M sodium nitrate, and 18–22% PEG3350. Overnight soaking of ligands was performed by transferring the apo crystals into the crystallization buffer in which the compounds were previously dissolved at 5 mM. Soaked crystals were cryoprotected with the crystallization buffer supplemented with 20% glycerol prior to freezing in liquid nitrogen. Fragments **5** and **6** were cocrystallized with BRPF1 in the crystallization buffer and cryoprotected the same way as the soaked crystals.

Data Collection and Structure Solution. Diffraction data were collected at the Swiss Light Source, Paul Scherrer Institute (Villigen, Switzerland), beamlines PXI and PXIII. Data were processed with XDS[26] and SCALA,[27] and structures were solved by molecular replacement with Phaser[28] using PDB 4LC2 as search model. Initial models were refined iteratively with Phenix[29] and manual model building with COOT.[30] Crystal data collection and refinement statistics are summarized in SI, Tables S1–S5.

BROMOscan and AlphaScreen Assays. BROMOscan technology is a competition experiment that uses an immobilized ligand and a DNA-tagged bromodomain protein.[10] Compounds that bind to the bromodomain of interest will prevent binding of the bromodomain to the immobilized ligand. The amount of captured bromodomain is quantified by qPCR, and the dissociation constants are calculated with a standard dose–response curve. Further details about the assays can be found in the SI. AlphaScreen assays[11] consist of a donor bead that is able to transfer singlet oxygen to an acceptor bead that is in the proximity, and as a result, the acceptor bead emits a luminescent/fluorescent signal. In the presence of a bromodomain ligand, the donor/acceptor complex is disrupted, leading to a loss of singlet oxygen transfer and loss of the fluorescent signal.

ASSOCIATED CONTENT

Supporting Information

The Supporting Information is available free of charge on the ACS Publications website at DOI: 10.1021/acs.jmedchem.6b00215.

Molecular formula strings for ligands **1**–**20** (CSV)

Experimental methods, X-ray crystal structure statistic data, and structural analyses of all reported crystal structures (PDF)

Accession Codes

PDB accession codes of the structures of the BRPF1 bromodomain in the complex with molecules **1**–**20** are **1** (5EQ1), **2** (5EWD), **3** (5E3G), **4** (5E3D), **5** (5C87), **6** (5EM3), **7** (5EWH), **8** (5C85), **9** (5DYC), **10** (5DY7), **11** (5EPS), **12** (5EPR), **13** (5EWC), **14** (5DYA), **15** (5ETB), **16** (5ETD), **17** (5D7X), **18** (5EV9), **19** (5EVA), and **20** (5C7N), respectively. Authors will release the atomic coordinates and experimental data upon article publication.

AUTHOR INFORMATION

Corresponding Author

*Phone: +41 44 635 55 21. Fax: +41 44 6356862. E-mail: caflisch@bioc.uzh.ch.

DOI: 10.1021/acs.jmedchem.6b00215
J. Med. Chem. 2016, 59, 5555–5561

Notes

The authors declare no competing financial interest.

■ ACKNOWLEDGMENTS

We thank Jean-Rémy Marchand for the parametrization of the fragments, Dr. Dimitrios Spiliotopoulos for interesting discussions and Dr. Graziano Lolli for critical reading of the manuscript. We are grateful to Armin Widmer for his continuous support with the program WITNOTP which was used for the visual analysis of docked poses and the comparison with the crystal structures. We also thank the staff at PXI and PXIII beamlines, Swiss Light Source, Paul Scherrer Institute (Villigen, Switzerland) for on-site assistance. This work was supported financially by the Swiss National Science Foundation (315230_149897) and the Swiss Cancer Society (Schweizerische Krebsliga, KFS-3098).

■ ABBREVIATIONS USED

Alpha, amplified luminescent proximity homogeneous assay; proteins ATPase family, AAA domain containing 2 (ATAD2); BAZ2B, bromodomain adjacent to zinc-finger domain 2B; BET, bromodomain and extra terminal; BRD2, bromodomain-containing protein 2; BRD4, bromodomain containing protein 4; BRD9, bromodomain containing protein 9; BRPF1, bromodomain and PHD finger (BRPF) containing protein 1; CREBBP, binding protein of the cAMP response element-binding protein; GST, glutathione S-transferase; Kac, *N*-ε-acetyl-lysine; MOZ, monocytic leukemia zinc finger protein; TEV, tobacco etch virus

■ REFERENCES

(1) Laue, K.; Daujat, S.; Crump, J. G.; Plaster, N.; Roehl, H. H.; Kimmel, C. B.; Schneider, R.; Hammerschmidt, M. The multidomain protein Brpf1 binds histones and is required for Hox gene expression and segmental identity. *Development* **2008**, *135*, 1935−1946.

(2) (a) Ullah, M.; Pelletier, N.; Xiao, L.; Zhao, S. P.; Wang, K.; Degerny, C.; Tahmasebi, S.; Cayrou, C.; Doyon, Y.; Goh, S. L.; Champagne, N.; Cote, J.; Yang, X. J. Molecular architecture of quartet MOZ/MORF histone acetyltransferase complexes. *Mol. Cell. Biol.* **2008**, *28*, 6828−6843. (b) Poplawski, A.; Hu, K.; Lee, W.; Natesan, S.; Peng, D.; Carlson, S.; Shi, X.; Balaz, S.; Markley, J. L.; Glass, K. C. Molecular insights into the recognition of N-terminal histone modifications by the BRPF1 bromodomain. *J. Mol. Biol.* **2014**, *426*, 1661−1676.

(3) Lubula, M. Y.; Eckenroth, B. E.; Carlson, S.; Poplawski, A.; Chruszcz, M.; Glass, K. C. Structural insights into recognition of acetylated histone ligands by the BRPF1 bromodomain. *FEBS Lett.* **2014**, *588*, 3844−3854.

(4) Demont, E. H.; Bamborough, P.; Chung, C. W.; Craggs, P. D.; Fallon, D.; Gordon, L. J.; Grandi, P.; Hobbs, C. I.; Hussain, J.; Jones, E. J.; Le Gall, A.; Michon, A. M.; Mitchell, D. J.; Prinjha, R. K.; Roberts, A. D.; Sheppard, R. J.; Watson, R. J. 1,3-Dimethyl Benzimidazolones are potent, selective inhibitors of the BRPF1 bromodomain. *ACS Med. Chem. Lett.* **2014**, *5*, 1190−1195.

(5) Chung, C. W.; Dean, A. W.; Woolven, J. M.; Bamborough, P. Fragment-based discovery of bromodomain inhibitors part 1: inhibitor binding modes and implications for lead discovery. *J. Med. Chem.* **2012**, *55*, 576−586.

(6) (a) Hewings, D. S.; Fedorov, O.; Filippakopoulos, P.; Martin, S.; Picaud, S.; Tumber, A.; Wells, C.; Olcina, M. M.; Freeman, K.; Gill, A.; Ritchie, A. J.; Sheppard, D. W.; Russell, A. J.; Hammond, E. M.; Knapp, S.; Brennan, P. E.; Conway, S. J. Optimization of 3,5-dimethylisoxazole derivatives as potent bromodomain ligands. *J. Med. Chem.* **2013**, *56*, 3217−3227. (b) Zhao, L.; Cao, D.; Chen, T.; Wang, Y.; Miao, Z.; Xu, Y.; Chen, W.; Wang, X.; Li, Y.; Du, Z.; Xiong, B.; Li, J.; Xu, C.; Zhang, N.; He, J.; Shen, J. Fragment-based drug discovery of 2-thiazolidinones as inhibitors of the histone reader BRD4 bromodomain. *J. Med. Chem.* **2013**, *56*, 3833−3851.

(7) (a) Demont, E. H.; Chung, C. W.; Furze, R. C.; Grandi, P.; Michon, A. M.; Wellaway, C.; Barrett, N.; Bridges, A. M.; Craggs, P. D.; Diallo, H.; Dixon, D. P.; Douault, C.; Emmons, A. J.; Jones, E. J.; Karamshi, B. V.; Locke, K.; Mitchell, D. J.; Mouzon, B. H.; Prinjha, R. K.; Roberts, A. D.; Sheppard, R. J.; Watson, R. J.; Bamborough, P. Fragment-based discovery of low-micromolar ATAD2 bromodomain inhibitors. *J. Med. Chem.* **2015**, *58*, 5649−5673. (b) Harner, M. J.; Chauder, B. A.; Phan, J.; Fesik, S. W. Fragment-based screening of the bromodomain of ATAD2. *J. Med. Chem.* **2014**, *57*, 9687−9692.

(8) Ferguson, F. M.; Fedorov, O.; Chaikuad, A.; Philpott, M.; Muniz, J. R.; Felletar, I.; von Delft, F.; Heightman, T.; Knapp, S.; Abell, C.; Ciulli, A. Targeting low-druggability bromodomains: fragment based screening and inhibitor design against the BAZ2B bromodomain. *J. Med. Chem.* **2013**, *56*, 10183−10187.

(9) Rooney, T. P.; Filippakopoulos, P.; Fedorov, O.; Picaud, S.; Cortopassi, W. A.; Hay, D. A.; Martin, S.; Tumber, A.; Rogers, C. M.; Philpott, M.; Wang, M.; Thompson, A. L.; Heightman, T. D.; Pryde, D. C.; Cook, A.; Paton, R. S.; Muller, S.; Knapp, S.; Brennan, P. E.; Conway, S. J. A series of potent CREBBP bromodomain ligands reveals an induced-fit pocket stabilized by a cation-pi interaction. *Angew. Chem., Int. Ed.* **2014**, *53*, 6126−6130.

(10) Quinn, E.; Wodicka, L.; Ciceri, P.; Pallares, G.; Pickle, E.; Torrey, A.; Floyd, M.; Hunt, J.; Treiber, D. Abstract 4238: BROMOscan - a high throughput, quantitative ligand binding platform identifies best-in-class bromodomain inhibitors from a screen of mature compounds targeting other protein classes. *Cancer Res.* **2013**, *73*, 4238.

(11) Philpott, M.; Yang, J.; Tumber, T.; Fedorov, O.; Uttarkar, S.; Filippakopoulos, P.; Picaud, S.; Keates, T.; Felletar, I.; Ciulli, A.; Knapp, S.; Heightman, T. D. Bromodomain-peptide displacement assays for interactome mapping and inhibitor discovery. *Mol. BioSyst.* **2011**, *7*, 2899−2908.

(12) Hopkins, A. L.; Keseru, G. M.; Leeson, P. D.; Rees, D. C.; Reynolds, C. H. The role of ligand efficiency metrics in drug discovery. *Nat. Rev. Drug Discovery* **2014**, *13*, 105−121.

(13) Irwin, J. J.; Sterling, T.; Mysinger, M. M.; Bolstad, E. S.; Coleman, R. G. ZINC: a free tool to discover chemistry for biology. *J. Chem. Inf. Model.* **2012**, *52*, 1757−1768.

(14) (a) Majeux, N.; Scarsi, M.; Apostolakis, J.; Ehrhardt, C.; Caflisch, A. Exhaustive docking of molecular fragments with electrostatic solvation. *Proteins: Struct., Funct., Genet.* **1999**, *37*, 88−105. (b) Majeux, N.; Scarsi, M.; Caflisch, A. Efficient electrostatic solvation model for protein-fragment docking. *Proteins: Struct., Funct., Genet.* **2001**, *42*, 256−268.

(15) Unzue, A.; Zhao, H.; Lolli, G.; Dong, J.; Zhu, J.; Zechner, M.; Dolbois, A.; Caflisch, A.; Nevado, C. The ″gatekeeper″ residue influences the binding mode of acetyl indoles to bromodomains. *J. Med. Chem.* **2016**, *59*, 3087.

(16) Structural Genomics Consortium (SGC): Bromosporine. http://www.thesgc.org/chemical-probes/bromosporine (accessed January 3, 2016).

(17) Picaud, S.; Strocchia, M.; Terracciano, S.; Lauro, G.; Mendez, J.; Daniels, D. L.; Riccio, R.; Bifulco, G.; Bruno, I.; Filippakopoulos, P. 9H-purine scaffold reveals induced-fit pocket plasticity of the BRD9 bromodomain. *J. Med. Chem.* **2015**, *58*, 2718−2736.

(18) Magno, A.; Steiner, S.; Caflisch, A. Mechanism and kinetics of acetyl-lysine binding to bromodomains. *J. Chem. Theory Comput.* **2013**, *9*, 4225−4232.

(19) Zhao, H.; Gartenmann, L.; Dong, J.; Spiliotopoulos, D.; Caflisch, A. Discovery of BRD4 bromodomain inhibitors by fragment-based high-throughput docking. *Bioorg. Med. Chem. Lett.* **2014**, *24*, 2493−2496.

(20) (a) Xu, M.; Unzue, A.; Dong, J.; Spiliotopoulos, D.; Nevado, C.; Caflisch, A. Discovery of CREBBP bromodomain inhibitors by high-throughput docking and hit optimization guided by molecular dynamics. *J. Med. Chem.* **2016**, *59*, 1340−1349. (b) Unzue, A.; Xu, M.; Dong, J.; Wiedmer, L.; Spiliotopoulos, D.; Caflisch, A.; Nevado, C.

DOI: 10.1021/acs.jmedchem.6b00215
J. Med. Chem. 2016, 59, 5555−5561

Fragment-based design of selective nanomolar ligands of the CREBBP bromodomain. *J. Med. Chem.* **2016**, *59*, 1350−1356.
(21) Lolli, G.; Caflisch, A. High-Throughput Fragment Docking into the BAZ2B Bromodomain: Efficient in silico screening for X-ray crystallography. *ACS Chem. Biol.* **2016**, *11*, 800−807.
(22) Kolb, P.; Caflisch, A. Automatic and efficient decomposition of two-dimensional structures of small molecules for fragment-based high-throughput docking. *J. Med. Chem.* **2006**, *49*, 7384−92.
(23) Scarsi, M.; Apostolakis, J.; Caflisch, A. Continuum electrostatic energies of macromolecules in aqueous solutions. *J. Phys. Chem. A* **1997**, *101*, 8098−8106.
(24) (a) MacKerell, A. D.; Bashford, D.; Bellott, M.; Dunbrack, R. L.; Evanseck, J. D.; Field, M. J.; Fischer, S.; Gao, J.; Guo, H.; Ha, S.; Joseph-McCarthy, D.; Kuchnir, L.; Kuczera, K.; Lau, F. T.; Mattos, C.; Michnick, S.; Ngo, T.; Nguyen, D. T.; Prodhom, B.; Reiher, W. E.; Roux, B.; Schlenkrich, M.; Smith, J. C.; Stote, R.; Straub, J.; Watanabe, M.; Wiorkiewicz-Kuczera, J.; Yin, D.; Karplus, M. All-atom empirical potential for molecular modeling and dynamics studies of proteins. *J. Phys. Chem. B* **1998**, *102*, 3586−3616. (b) MacKerell, A. D., Jr.; Feig, M.; Brooks, C. L., 3rd Improved treatment of the protein backbone in empirical force fields. *J. Am. Chem. Soc.* **2004**, *126*, 698−699.
(25) Vanommeslaeghe, K.; Hatcher, E.; Acharya, C.; Kundu, S.; Zhong, S.; Shim, J.; Darian, E.; Guvench, O.; Lopes, P.; Vorobyov, I.; Mackerell, A. D., Jr. CHARMM general force field: A force field for drug-like molecules compatible with the CHARMM all-atom additive biological force fields. *J. Comput. Chem.* **2010**, *31*, 671−690.
(26) Kabsch, W. XDS. *Acta Crystallogr., Sect. D: Biol. Crystallogr.* **2010**, *66*, 125−132.
(27) Evans, P. Scaling and assessment of data quality. *Acta Crystallogr., Sect. D: Biol. Crystallogr.* **2006**, *62*, 72−82.
(28) McCoy, A. J.; Grosse-Kunstleve, R. W.; Adams, P. D.; Winn, M. D.; Storoni, L. C.; Read, R. J. Phaser crystallographic software. *J. Appl. Crystallogr.* **2007**, *40*, 658−674.
(29) Adams, P. D.; Afonine, P. V.; Bunkoczi, G.; Chen, V. B.; Davis, I. W.; Echols, N.; Headd, J. J.; Hung, L. W.; Kapral, G. J.; Grosse-Kunstleve, R. W.; McCoy, A. J.; Moriarty, N. W.; Oeffner, R.; Read, R. J.; Richardson, D. C.; Richardson, J. S.; Terwilliger, T. C.; Zwart, P. H. PHENIX: a comprehensive Python-based system for macromolecular structure solution. *Acta Crystallogr., Sect. D: Biol. Crystallogr.* **2010**, *66*, 213−221.
(30) Emsley, P.; Lohkamp, B.; Scott, W. G.; Cowtan, K. Features and development of Coot. *Acta Crystallogr., Sect. D: Biol. Crystallogr.* **2010**, *66*, 486−501.

DOI: 10.1021/acs.jmedchem.6b00215
J. Med. Chem. 2016, 59, 5555−5561

Supporting information

Twenty crystal structures of bromodomain and PHD finger containing protein 1 (BRPF1)/ligand complexes reveal conserved binding motifs and rare interactions

Jian Zhu and Amedeo Caflisch*

Department of Biochemistry, University of Zürich, Winterthurerstrasse 190, CH-8057 Zürich, Switzerland

*E-mail: caflisch@bioc.uzh.ch

Table of contents

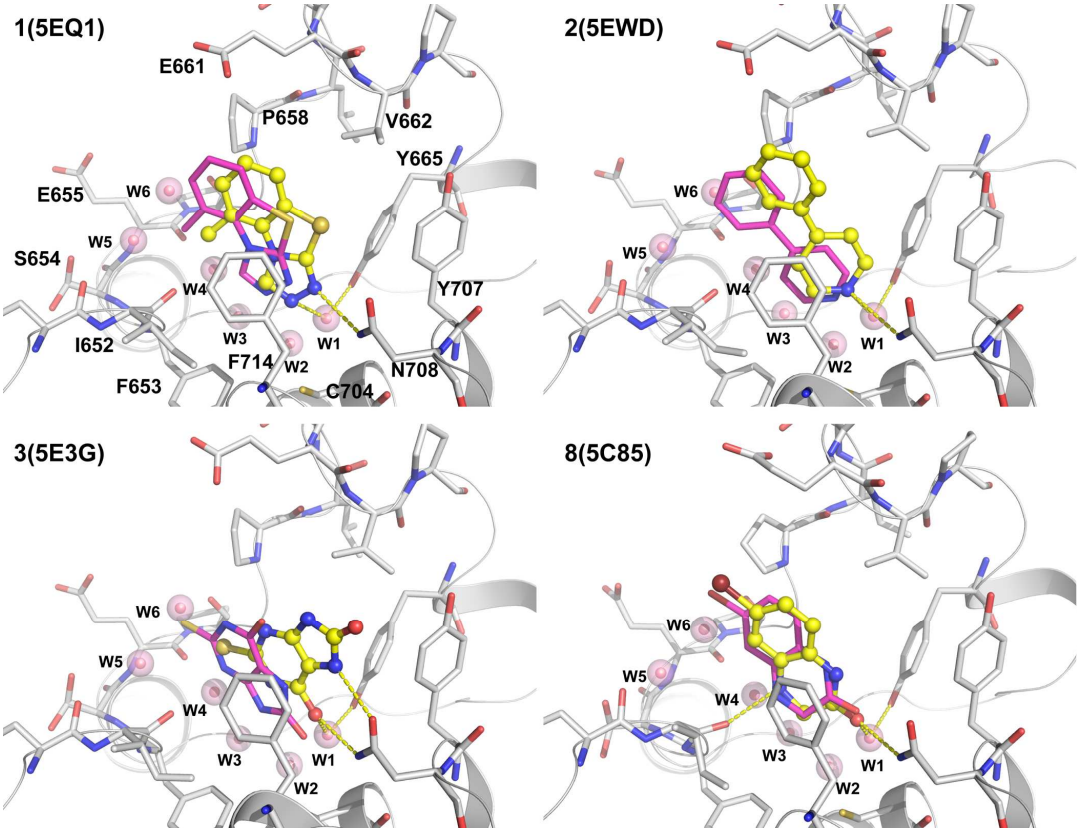

Fig S1. Comparison of docked pose obtained by the fragment-docking program SEED (carbon atoms in magenta) and binding mode in the crystal structure (carbon atoms in yellow) of fragments **1**, **2**, **3** and **8.** Heteroatoms are colored as follows: N (blue), O (red), S (yellow), and Br (maroon). The six conserved water molecules in the Kac binding pocket are labeled W1 to W6.

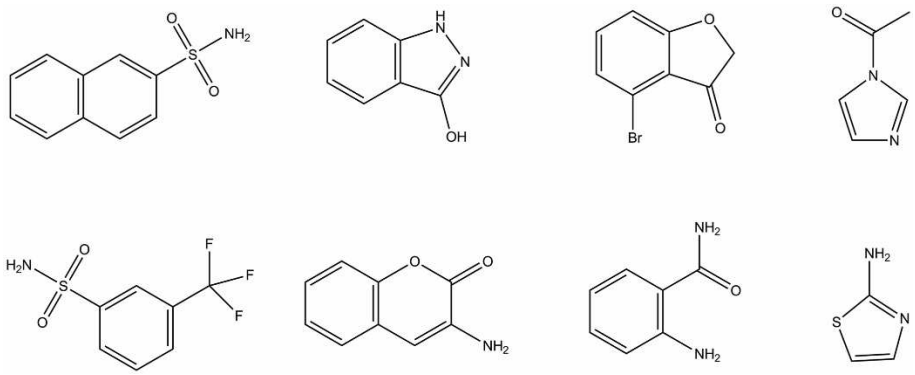

Fig S2. False positive hits from fragment docking by SEED. These fragments were among the 13 fragments purchased from 30 top ranked ones, but binding is not observed by X-ray crystallography (soaking into BRPF1 apo crystals).

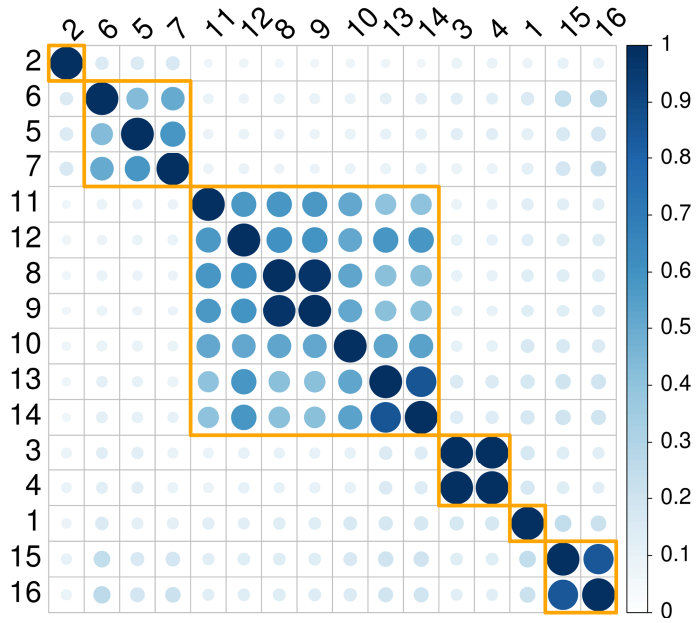

Fig S3. Similarity matrix of compounds **1** to **16**. The similarity (Tanimoto coefficient) was calculated based on the RDKit fingerprint which is implemented in the RDKit[1] toolkit. The size and darkness (vertical legend on the right) of the circles indicate similarity. The hierarchical complete-link algorithm with the R programming language generates six clusters (orange boxes).

BromoScan assay[2]

BromoScan assays on BRPF1 for the 14 compounds were performed at DiscoveRx. T7 phage strains displaying bromodomains were grown in parallel in 24-well blocks in an *E. coli* host derived from the BL21 strain. *E. coli* were grown to log-phase and infected with T7 phage from a frozen stock (multiplicity of infection= 0.4) and incubated with shaking at 32°C until lysis (90-150 minutes). The lysates were centrifuged (5,000 x g) and filtered (0.2 µm) to remove cell debris. Streptavidin-coated magnetic beads were treated with biotinylated small molecule or acetylated peptide ligands for 30 minutes at room temperature to generate affinity resins for bromodomain assays. The liganded beads were blocked with excess biotin and washed with blocking buffer (SeaBlock (Pierce), 1 % BSA, 0.05 % Tween 20, 1 mM DTT) to remove unbound ligand and to reduce non-specific phage binding. Binding reactions were assembled by combining bromodomains, liganded affinity beads, and test compounds in 1x binding buffer (17% SeaBlock, 0.33x PBS, 0.04% Tween 20, 0.02% BSA, 0.004% Sodium azide, 7.4 mM DTT). Test compounds were prepared as 1000X stocks in 100% DMSO and subsequently diluted 1:10 in monoethylene glycol (MEG) to create stocks at 100X the screening concentration (resulting stock solution is 10% DMSO/90% MEG). The compounds were then diluted directly into the assays such that the final concentration of DMSO and MEG were 0.1% and 0.9%, respectively. All reactions were performed in polystyrene 96-well plates in a final volume of 0.135 ml.

The assay plates were incubated at room temperature with shaking for 1 hour and the affinity beads were washed with wash buffer (1x PBS, 0.05% Tween 20). The beads were then re-suspended in elution buffer (1x PBS, 0.05% Tween 20, 2 µM nonbiotinylated affinity ligand) and incubated at room temperature with shaking for 30 minutes. The bromodomain concentration in the eluates was measured by qPCR. Binding constants (Kds) were calculated with a standard dose-response curve using the Hill equation:

$$\text{Response} = \text{Background} + \frac{\text{Signal} - \text{Background}}{1 + (\text{K}_\text{d}^{\text{Hill Slope}} / \text{Dose}^{\text{Hill Slope}})}$$

Curves were fitted using a non-linear least square fit with the Levenberg-Marquardt algorithm.

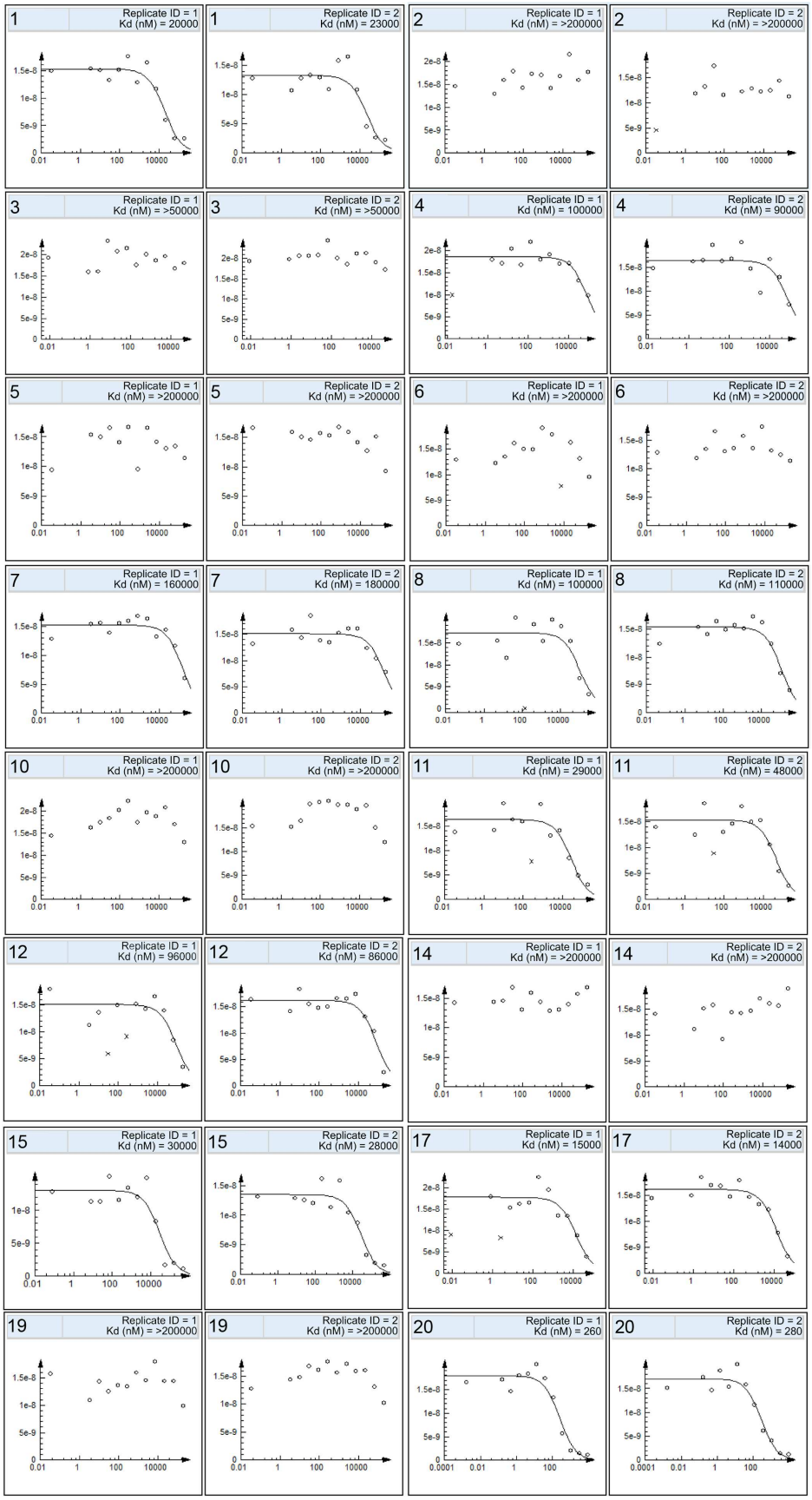

Fig S4. Dose-response curves in duplicates for the 16 compounds tested for binding to the BRPF1 bromodomain in the competition binding assay at DiscoveRx.

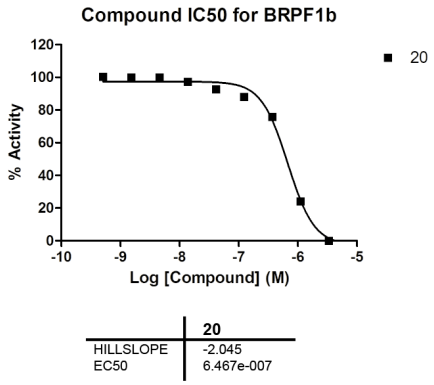

Fig S5. IC50 value of compound **20** determined by the AlphaScreen binding assay[3] at Reaction Biology.

Table S1. X-ray data collection and refinement statistics for complex structures of the BRPF1 bromodomain and compounds **1**, **2**, **3** and **4**.

Data Collection				
PDB ID	5EQ1	5EWD	5E3G	5E3D
ligand	**1**	**2**	**3**	**4**
space group	$P3_221$	$P3_221$	$P3_221$	$P3_221$
Cell dimensions				
a, b, c (Å)	60.38, 60.38, 63.20	60.67, 60.67, 63.02	60.86, 60.86, 62.99	60.73, 60.73, 62.43
α, β, γ (°)	90.00, 90.00, 120.00	90.00, 90.00, 120.00	90.00, 90.00, 120.00	90.00, 90.00, 120.00
resolution (Å)	40.29 - 1.55	40.36 - 1.58	40.40 - 1.65	40.22 - 1.71
unique observations*	19761(2835)	18839(2686)	16662(2374)	14799(2108)
completeness*	99.9 (100.0)	100.0(100.0)	100.0(100.0)	99.7(99.1)
redundancy*	9.4 (8.9)	9.6(9.6)	9.7(10.0)	9.5(9.6)
Rmerge*	0.041 (0.338)	0.029(0.359)	0.040(0.442)	0.031(0.405)
I/σI*	25.9 (6.1)	34.7(5.7)	25.6(4.9)	30.3(5.1)
Refinement				
R_{work}/R_{free}*	0.189(0.229)/0.194(0.292)	0.199(0.233)/0.225(0.252)	0.196(0.208)/0.205(0.268)	0.192(0.241)/0.222(0.319)
r.m.s deviations of bond lengths (Å)	0.008	0.006	0.007	0.007
r.m.s deviations of bond angles (°)	0.879	0.666	0.765	0.710
no. of non-hydrogen atom / average B-factor ($Å^2$)				
protein	946/37.56	946/40.90	944/45.24	936/48.64
ligand	13/40.53	12/56.25	12/57.45	12/59.34
water	80/43.30	103/46.65	64/46.49	75/48.63
residues in protein chain	628 - 739	627 - 739	628 - 739	628 -739
Ramanchandran				
Favored	98.25	100.00	99.12	99.12
allowed	1.75	0.00	0.88	0.88
disallowed	0.00	0.00	0.00	0.00
* Highest resolution shell is shown in parentheses.				

Table S2. X-ray data collection and refinement statistics for complex structures of the BRPF1 bromodomain and compounds **5**, **6**, **7** and **8**.

Data Collection				
PDB ID	5C87	5EM3	5EWH	5C85
ligand	**5**	**6**	**7**	**8**
space group	$P3_221$	$P3_221$	$P3_221$	$P3_221$
Cell dimensions				
a, b, c (Å)	60.56, 60.56, 63.60	60.14, 60.14, 63.23	60.44, 60.44, 62.68	60.72, 60.72, 61.87
α, β, γ (°)	90.00, 90.00, 120.00	90.00, 90.00, 120.00	90.00, 90.00, 120.00	90.00, 90.00, 120.00
resolution (Å)	30.00 - 1.55	40.20 - 1.40	40.18 - 1.63	40.07 - 1.70
unique observations*	20025(2861)	26409(3814)	16966(2453)	14925(2129)
completeness*	100.0(100.0)	99.7(99.7)	100.0(100.0)	100.0(100.0)
redundancy*	9.1(6.0)	9.2(8.8)	9.5(9.9)	9.7(9.5)
Rmerge*	0.048(0.341)	0.049(0.236)	0.073(0.358)	0.031(0.326)
I/σI*	26.6(4.8)	25.4(8.4)	16.3(5.3)	37.1(6.5)
Refinement				
Rwork/Rfree*	0.181(0.221)/0.198(0.26)	0.173(0.187)/0.196(0.224)	0.190(0.212)/0.223(0.288)	0.207(0.241)/0.225(0.269)
r.m.s deviations of bond lengths (Å)	0.007	0.010	0.006	0.007
r.m.s deviations of bond angles (°)	0.920	0.780	0.743	0.931
no. of non-hydrogen atom / average B-factor ($Å^2$)				
protein	947/38.01	974/19.79	955/28.65	929/50.59
ligand	11/44.55	22/22.39	11/40.01	12/55.99
water	124/44.19	170/30.45	134/40.01	79/48.55
residues in protein chain	628 - 739	625 – 739 (extra serine residue 625 at the N terminal)	627 - 739	628 -739
Ramanchandran				
Favored	99.12	99.15	99.14	99.12
allowed	0.88	0.85	0.86	0.88
disallowed	0.00	0.00	0.00	0.00
* Highest resolution shell is shown in parentheses.				

Table S3. X-ray data collection and refinement statistics for complex structures of the BRPF1 bromodomain and compounds **9**, **10**, **11** and **12**.

Data Collection				
PDB ID	5DYC	5DY7	5EPS	5EPR
ligand	**9**	**10**	**11**	**12**
space group	$P3_221$	$P3_221$	$P3_221$	$P3_221$
Cell dimensions				
a, b, c (Å)	60.81, 60.81, 63.11	60.67, 60.67, 62.38	60.63, 60.63, 62.50	60.92, 60.92, 63.02
α, β, γ (°)	90.00, 90.00, 120.00	90.00, 90.00, 120.00	90.00, 90.00, 120.00	90.00, 90.00, 120.00
resolution (Å)	40.44 - 1.65	40.19 - 1.69	40.20 - 1.47	40.45 - 1.65
unique observations*	16556(2353)	15153(2094)	23061(3316)	16718(2400)
completeness*	99.5(99.3)	99.2(95.5)	100.0(99.8)	100.0(100.0)
redundancy*	9.7(10.0)	9.5(9.3)	9.5(9.3)	9.5(9.9)
Rmerge*	0.039(0.408)	0.060(0.440)	0.042(0.285)	0.035(0.366)
I/σI*	28.2(5.4)	18.7(4.5)	25.4(6.6)	28.6(5.6)
Refinement				
Rwork/Rfree*	0.198(0.237)/0.235(0.289)	0.179(0.243)/0.204(0.306)	0.188(0.202)/0.198(0.250)	0.198(0.264)/0.220(0.285)
r.m.s deviations of bond lengths (Å)	0.006	0.007	0.007	0.008
r.m.s deviations of bond angles (°)	0.694	0.773	0.738	0.681
no. of non-hydrogen atom / average B-factor				
protein	951/43.43	956/31.17	952/32.75	948/44.14
ligand	12/53.58	15/39.11	12/47.99	12/59.44
water	82/46.97	142/37.17	111/39.47	71/45.87
residues in protein chain	627 - 739	627 - 739	627 - 739	628 -739
Ramanchandran(%)				
Favored	99.13	99.15	100.00	99.12
allowed	0.87	0.85	0.00	0.88
disallowed	0.00	0.00	0.00	0.00
* Highest resolution shell is shown in parentheses.				

Table S4. X-ray data collection and refinement statistics for complex structures of the BRPF1 bromodomain and compounds **13**, **14**, **15** and **16**.

Data Collection				
PDB ID	5EWC	5DYA	5ETB	5ETD
ligand	**13**	**14**	**15**	**16**
space group	$P3_221$	$P3_221$	$P3_221$	$P3_221$
Cell dimensions				
a, b, c (Å)	60.93, 60.93, 63.05	61.16, 61.16, 62.15	60.37, 60.37, 63.50	60.32, 60.32, 62.92
α, β, γ (°)	90.00, 90.00, 120.00	90.00, 90.00, 120.00	90.00, 90.00, 120.00	90.00, 90.00, 120.00
resolution (Å)	40.46 - 1.75	40.31 - 1.65	40.36 - 1.33	40.19 - 1.40
unique observations*	14043(1999)	16557(2370)	31032(4300)	26520(3791)
completeness*	100.0(99.9)	99.8(100.0)	99.3(95.6)	99.9(99.5)
redundancy*	9.7(9.7)	9.5(9.8)	8.7(4.9)	9.2(8.4)
Rmerge*	0.049(0.406)	0.027(0.417)	0.038(0.158)	0.044(0.334)
I/σI*	24.1(5.1)	37.1(5.2)	31.1(7.8)	22.9(5.3)
Refinement				
Rwork/Rfree*	0.194(0.252)/0.211(0.312)	0.186(0.214)/0.213(0.264)	0.174(0.204)/0.186(0.235)	0.176(0.215)/0.186(0.219)
r.m.s deviations of bond lengths (Å)	0.008	0.007	0.008	0.008
r.m.s deviations of bond angles (°)	0.731	0.790	0.791	0.756
no. of non-hydrogen atom / average B-factor				
protein	942/46.33	937/39.08	944/21.15	944/25.24
ligand	17/58.74	16/52.93	13/26.45	12/27.97
water	91/49.34	115/43.46	179/34.57	138/34.71
residues in protein chain	628 - 739	628 - 739	628 - 739	628 - 739
Ramanchandran				
Favored	99.12	99.12	98.23	99.12
allowed	0.88	0.88	1.77	0.88
disallowed	0.00	0.00	0.00	0.00
* Highest resolution shell is shown in parentheses.				

Table S5. X-ray data collection and refinement statistics for complex structures of the BRPF1 bromodomain and compounds **18**, **19**, and **20**.

Data Collection			
PDB ID	5EV9	5EVA	5C7N
ligand	**18**	**19**	**20**
space group	$P3_221$	$P3_221$	$P3_221$
Cell dimensions			
a, b, c (Å)	60.36, 60.36, 63.46	60.36, 60.36, 63.39	60.50, 60.50, 63.11
α, β, γ (°)	90.00, 90.00, 120.00	90.00, 90.00, 120.00	90.00, 90.00, 120.00
resolution (Å)	40.35 - 1.45	40.33 - 1.45	40.31 - 1.75
unique observations*	24170(3476)	24128(3476)	13890(1986)
completeness*	100.0(99.9)	99.9(100.0)	100.0(100.0)
redundancy*	9.4(9.3)	9.3(9.0)	9.7(9.8)
Rmerge*	0.032(0.285)	0.041(0.292)	0.044(0.420)
I/σI*	33.0(6.9)	27.6(7.0)	27.5(5.4)
Refinement			
Rwork/Rfree*	0.188(0.242)/0.221(0.257)	0.183(0.222)/0.197(0.235)	0.180(0.229)/0.220(0.289)
r.m.s deviations of bond angles (°)	0.009	0.008	0.010
r.m.s deviations of bond lengths (Å)	0.885	0.834	0.987
no. of non-hydrogen atom / average B-factor			
protein	939/38.50	938/32.67	955/45.50
ligand	19/50.15	17/46.97	28/62.80
water	130/46.12	152/42.00	102/48.89
residues in protein chain	628 - 739	627 - 739	628 - 739
Ramanchandran			
Favored	99.12	98.23	97.39
allowed	0.88	1.77	2.61
disallowed	0.00	0.00	0.00
* Highest resolution shell is shown in parentheses.			

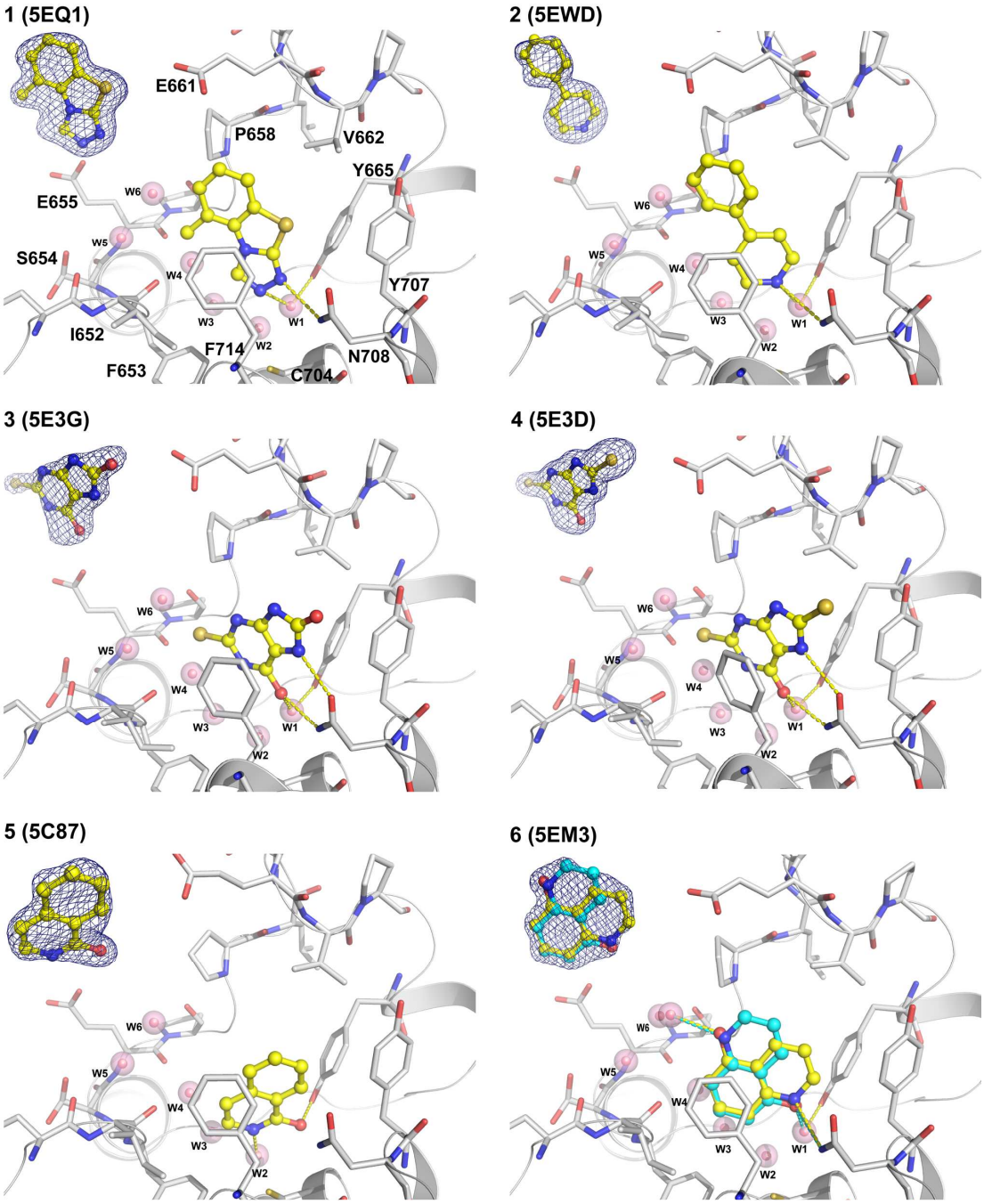

Fig S6. Close view of binding mode of compounds **1**, **2**, **3**, **4**, **5** and **6**. Conserved water molecules in the binding pocket are labeled W1 to W6 (pink spheres). 2Fo-Fc electron density maps contoured at 1 σ for ligands are shown by a mesh. Two alternative conformations of fragment **6** are shown in yellow and cyan.

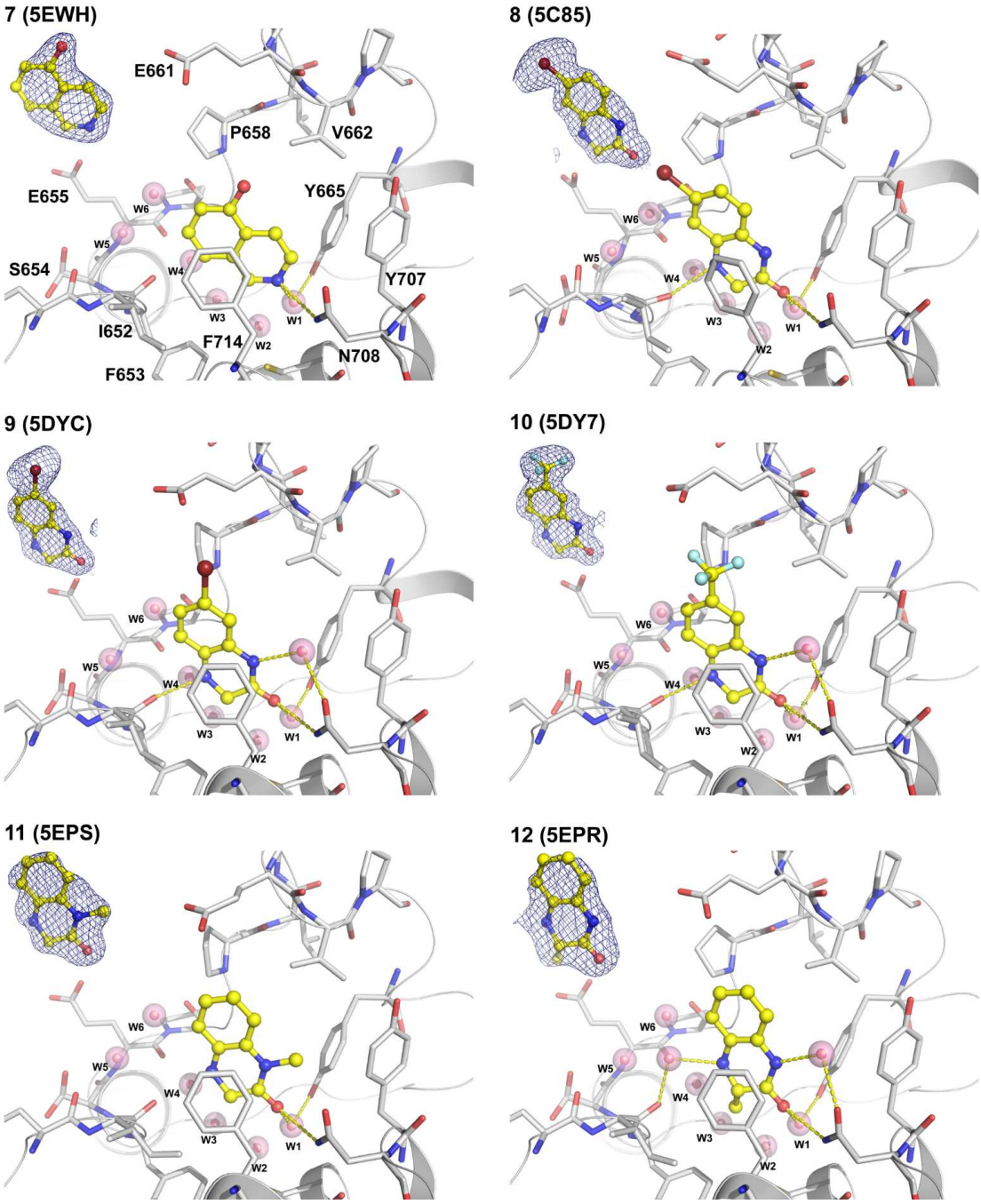

Fig S7. Same as Figure S7 for compounds **7**, **8**, **9**, **10**, **11** and **12**. For fragments **7** and **12**, 2Fo-Fc electron density maps are contoured at 0.8 σ.

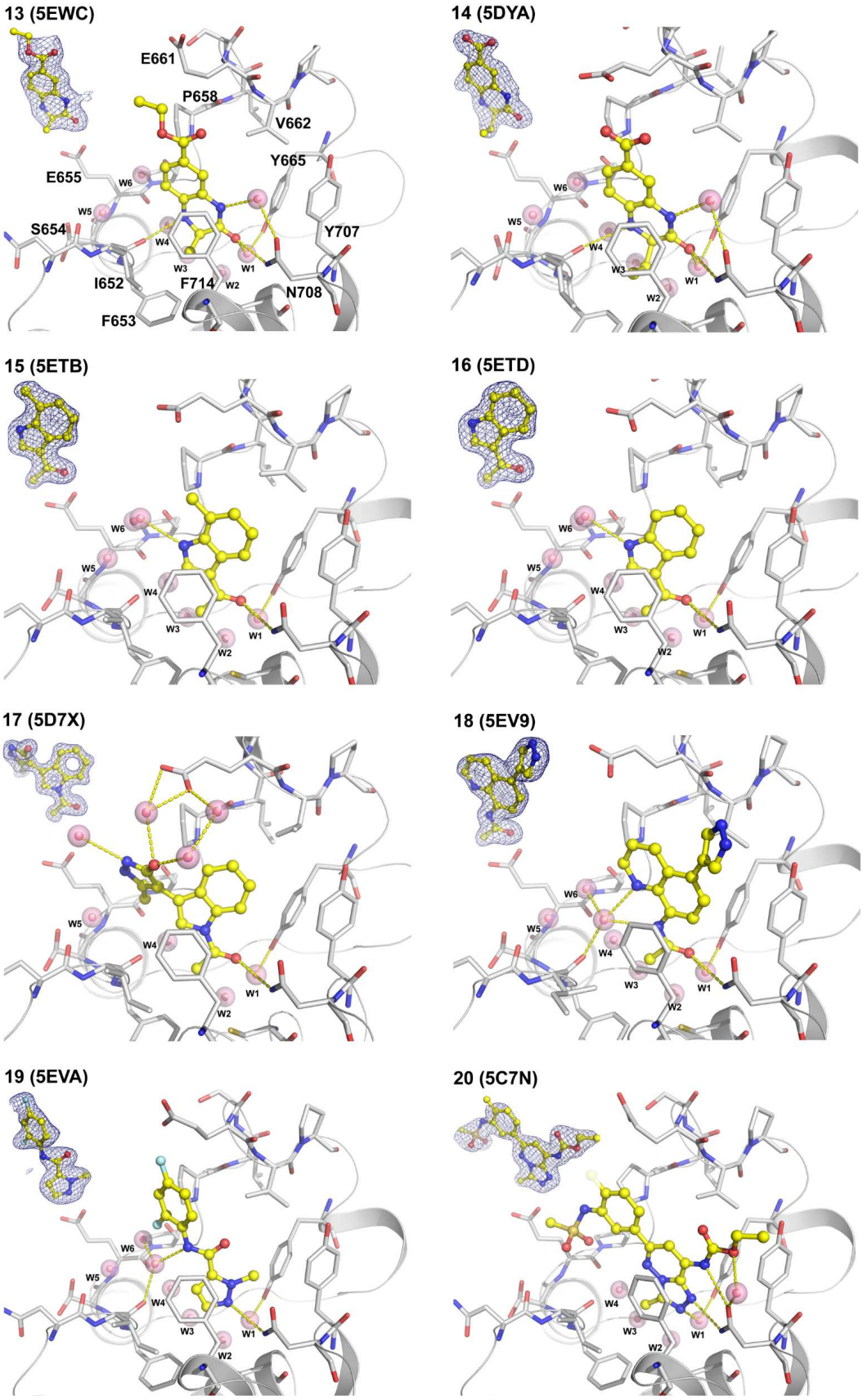

Fig S8. Same as Figure S7 for compounds **13**, **14**, **15**, **16**, **17**, **18**, **19** and **20**. For ligands **19** and **20**, 2Fo-Fc electron density maps are contoured at 0.8 σ.

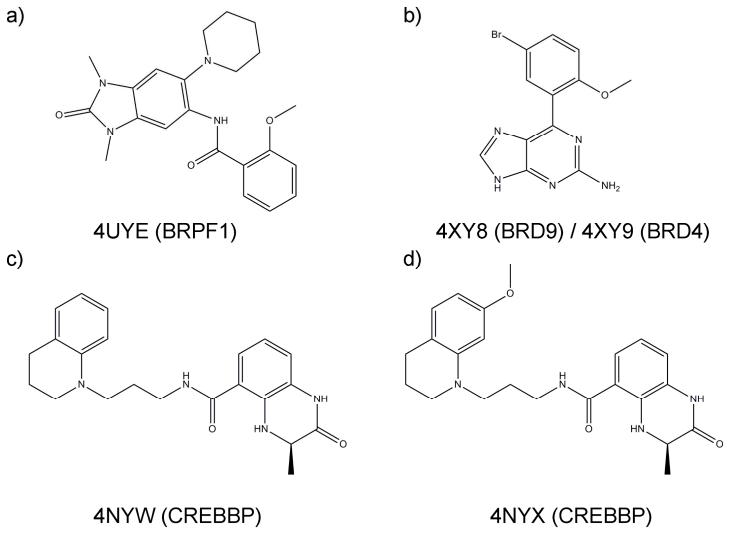

Fig S9. Chemical structures of inhibitors for structural comparison.
(a)N-[1,3-dimethyl-2-oxo-6-(piperidin-1-yl)-2,3-dihydro-1H-benzimidazol-5-yl]-2-methoxybenzamide, (b) 6-(5-bromo-2-methoxyphenyl)-9H-purin-2-amine,
(c)(3R)-N-[3-(3,4-dihydroquinolin-1(2H)-yl)propyl]-3-methyl-2-oxo-1,2,3,4-tetrahydroquinoxaline-5-carboxamide, and (d) (3R)-N-[3-(7-methoxy-3,4-dihydroquinolin-1(2H)-yl)propyl]-3-methyl-2-oxo-1,2,3,4-tetrahydroquinoxaline-5-carboxamide.

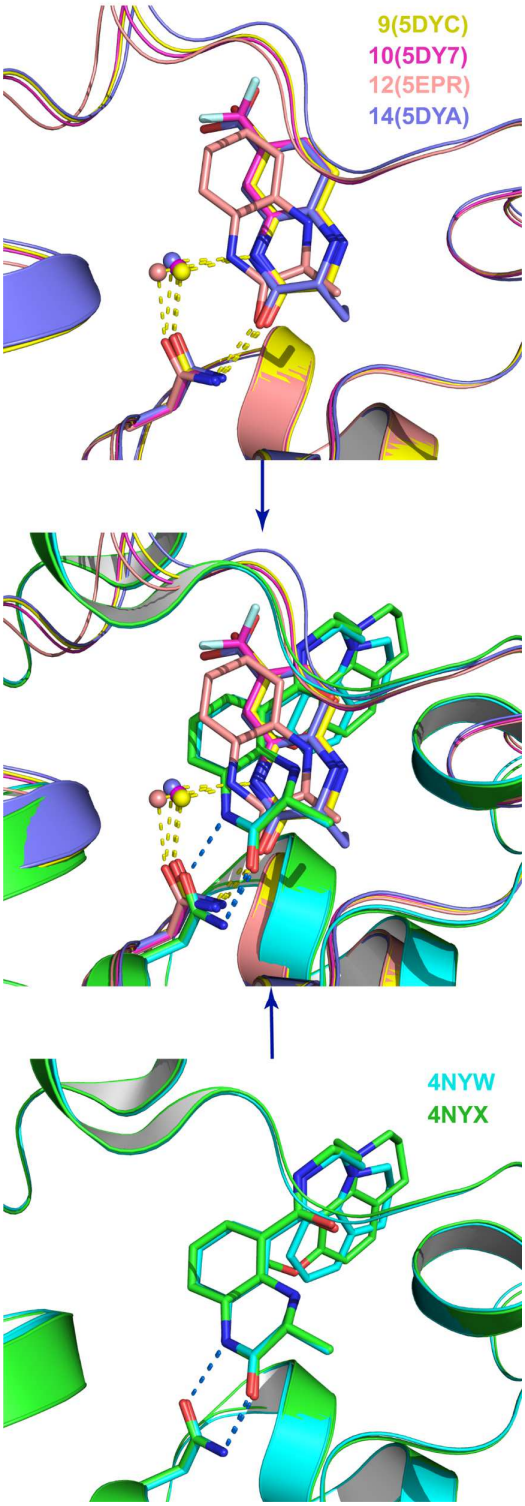

Fig S10. Comparison of the binding modes of dihydroquinoline ligands in BRPF1 (top) and CREBBP (bottom). The structural alignment (middle) shows that the binding modes are different. (Top) In BRPF1, the bromine substituent of fragment **9,** the trifluromethyl of **10**, and the carboxylate of **14** occupy the same position, while fragment **12** (5EPR) is devoid of substituent and its orientation is slightly shifted.

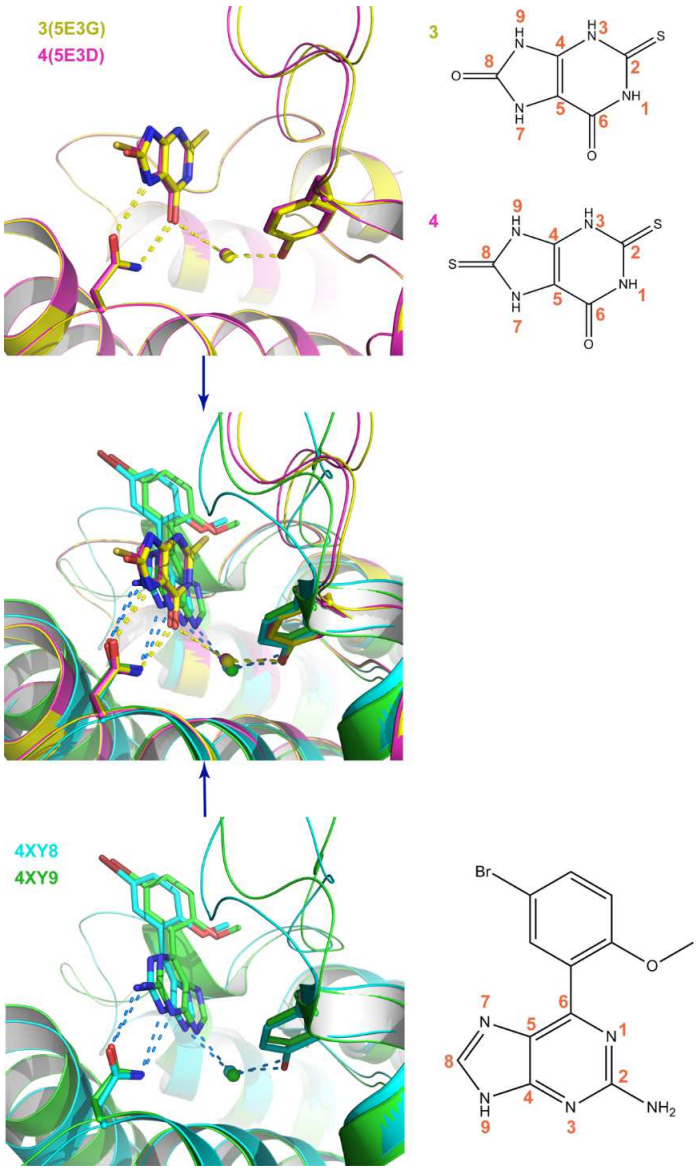

Fig S11. Comparison of the binding modes of mercaptopurine fragments **3** and **4** in BRPF1 (top) with the previously reported 2-amine-9H-purine ligands of the BRD9 (4XY8, bottom) and BRD4 (4XY9, bottom) bromodomains. The structural alignment (middle) shows that the binding modes are different which is consistent with the fact that these ligands share only the purine scaffold.

Reference

1. RDKit: cheminformatics and machine learning software. **2013**. http://www.rdkit.org (accessed January 3, 2016).

2. Quinn, E.; Wodicka, L.; Ciceri, P.; Pallares, G.; Pickle, E.; Torrey, A.; Floyd, M.; Hunt, J.; Treiber, D. Abstract 4238: BROMOscan - a high throughput, quantitative ligand binding platform identifies best-in-class bromodomain inhibitors from a screen of mature compounds targeting other protein classes *Cancer Res.* **2013**, *73*, 4238.

3. Philpott, M.; Yang, J.; Tumber, T.; Fedorov, O.; Uttarkar, S.; Filippakopoulos, P.; Picaud, S.; Keates, T.; Felletar, I.; Ciulli, A.; Knapp, S.; Heightman, T. D., Bromodomain-peptide displacement assays for interactome mapping and inhibitor discovery. *Mol. BioSyst.* **2011**, *7*, 2899-2908.

Chapter 3

Structure-based discovery of selective BRPF1 bromodomain inhibitors

Zhu J, Zhou C.X, Caflisch A. European Journal of Medicinal Chemistry 2018;155: 337-352.

European Journal of Medicinal Chemistry 155 (2018) 337–352

Contents lists available at ScienceDirect

European Journal of Medicinal Chemistry

journal homepage: http://www.elsevier.com/locate/ejmech

Research paper

Structure-based discovery of selective BRPF1 bromodomain inhibitors

Jian Zhu [a], Chunxian Zhou [b], Amedeo Caflisch [a, *]

[a] Department of Biochemistry, University of Zurich, Winterthurerstrasse 190, CH-8057, Zurich, Switzerland
[b] Department of Pathology, Shanghai University of Traditional Chinese Medicine, Cailun Road 1200, Pudong District, Shanghai, China

ARTICLE INFO

Article history:
Received 15 December 2017
Received in revised form
5 April 2018
Accepted 23 May 2018
Available online 2 June 2018

Keywords:
BRPF1 bromodomain
Pharmacophore search
Structure-based drug design
X-ray crystallography
Isothermal titration calorimetry
Molecular dynamics

ABSTRACT

Bromodomain and plant homeodomain (PHD) finger containing protein 1 (BRPF1) is a member of subfamily IV of the human bromodomains. Experimental evidence suggests that BRPF1 is involved in leukemia. In a previous high-throughput docking campaign we identified several chemotypes targeting the BRPF1 bromodomain. Here, pharmacophore searches using the binding modes of two of these chemotypes resulted in two new series of ligands of the BRPF1 bromodomain. The 2,3-dioxo-quinoxaline **21** exhibits a 2-μM affinity for the BRPF1 bromodomain in two different competition binding assays, and more than 100-fold selectivity for BRPF1 against other members of subfamily IV and representatives of other subfamilies. Cellular activity is confirmed by a viability assay in a leukemia cell line. Isothermal titration calorimetry measurements reveal enthalpy-driven binding for compounds **21**, **26** ($K_D = 3\ \mu M$), and the 2,4-dimethyl-oxazole derivative **42** ($K_D = 10\ \mu M$). Multiple molecular dynamics simulations and a dozen co-crystal structures at high resolution provide useful information for further optimization of affinity for the BRPF1 bromodomain.

1. Introduction

Bromodomains are evolutionarily conserved protein-protein interaction modules that selectively bind to acetyl-lysine (Kac) residues. They recognize acetylated histone tails, and are thus involved in the regulation of gene expression. Human proteome analysis indicates that there are eight bromodomain subfamilies, with 61 members found in 42 diverse proteins. Bromodomain-containing proteins have important role in biological process and are functionally implicated in disease processes, including cancer, inflammation and viral replication [1]. The bromodomain structure consists of approximately 110 residues folded into a bundle of four left-handed α helices (αZ, αA, αB and αC). Two variable loops termed ZA loop and BC loop, connect the helices and form the Kac binding site [2]. Despite the structural conservation of bromodomains, sequence and structural heterogeneity in the loop regions result in different druggability [3].

The most studied bromodomains are the members of the bromodomain and extra terminal domain (BET) subfamily. Highly potent and specific inhibitors for the BET subfamily have shown therapeutic potential in a number of diseases, particularly in oncology [4–6]. Outside the BET subfamily, the recent disclosure of chemical probes for bromodomains like CREBBP/EP300 [7–11], BRD7/9 [12–14], BAZ2A/B [15,16], SMARCA2/4 [17], PCAF [18], and ATAD2 [19] will facilitate the elucidation of the biological function and target validation of the non-BET bromodomains.

The bromodomain and plant homeodomain (PHD) finger containing proteins (BRPF1/2/3) are members of subfamily IV. BRPFs contain multiple epigenetic reader domains, including a unique double PHD and zinc finger assembly, a bromodomain and a C-terminal PWWP domain. As a multivalent chromatin regulator, BRPF1 recognizes histone marks via both the bromodomain and the PWWP domain [20]. The BRPF1 bromodomain preferentially binds to multiple acetyl-lysine marks in histone tails including H2AK5ac, H3K14ac, H4K5ac, H4K8ac, and H4K12ac [21]. BRPF1 is a subunit of monocytic leukemic zinc finger (MOZ) histone acetyltransferase (HAT) which acetylates free histones and affects gene transcription. In the MOZ HAT quaternary complex, BRPF1 enhances the acetylation activity of MOZ.

The MOZ HAT is involved in chromosomal translocations process found in a subtype of acute myeloid leukemia (AML) with poor prognosis [22]. The chromosomal translocation in AML leads to the production of fusion proteins in which MOZ is linked to either CREB binding proteins (CBP) [23], or CBP homolog p300 [24], or the transcriptional intermediary binding factor 2 (TIF2) [25]. MOZ fusion proteins cause aberrant expression profile of HOX genes

* Corresponding author.
E-mail address: caflisch@bioc.uzh.ch (A. Caflisch).

https://doi.org/10.1016/j.ejmech.2018.05.037
0223-5234/

mediated by the acetylation activity of MOZ during hematopoiesis, which is found to be critical for leukemogenesis [26]. Overall, the emerging body of evidence suggests the potential of BRPF1 as a therapeutic target in leukemia.

To date, only one chemical probe has been disclosed for the BRPF1 bromodomain. The 1,3-dimethylbenzimidazolone scaffold was optimized into a chemical probe for BRPF1 (GSK6853 [27]), and a dual BRPF1-TRIM24 inhibitor (compound 34 in Ref. [28]) (Fig. 1). The recently reported compounds NI-42 and NI-57 bear a structurally different scaffold N-methylquinolin-2-one [29,30]. The compounds NI-42 and NI-57 are pan-BRPF bromodomain inhibitors, showing a biased potency on BRPF1, and less than six-fold selectivity over BRPF2.

As outlined above, current development of BRPF1 chemical probes still focuses on the 1,3-dimethylbenzimidazolone and N-methylquinolin-2-one scaffolds. It would be valuable to develop compounds structurally orthogonal to the reported BRPF1 chemical probes, especially for inhibitors which are selective within the BRPF subfamily, to better elucidate the biological function of BRPF1. In our previous study, several diverse chemotypes targeting BRPF1 were discovered by high-throughput virtual screening and validated by X-ray crystallography [31]. In the present study, based on two previously identified small molecule hits, a hit-to-lead campaign was carried out using a structure-based virtual screening strategy. Two series of low micromolar inhibitors were identified which exhibit good selectivity within and outside the subfamily IV bromodomains. Isothermal titration calorimetry was used to measure thermodynamic parameters of binding and confirm selectivity. Explicit solvent molecular dynamics simulations [32,33] confirmed the stability of the head group of the ligand in the Kac binding site and revealed flexibility of the ligand tail (which is partially exposed to solvent) and part of the ZA loop.

2. Results and discussion

2.1. First pharmacophore search

Taking advantage of the rich structural information from our fragment hits [31], we set out to explore the readily available commercial chemical space by a combination of pharmacophore search followed by substructure search (Fig. 2).

At the beginning of this project, a pharmacophore search [34] using PDB coordinate 5EPS as template led to the identification of 365 molecules that include either a 1-ethyl-2,3-dioxo-4H-quinoxaline or a 1-ethyl-3-methyl-2-oxoquinoxaline core group (see section 4. Experimental). Presumably, a carbonyl group of the

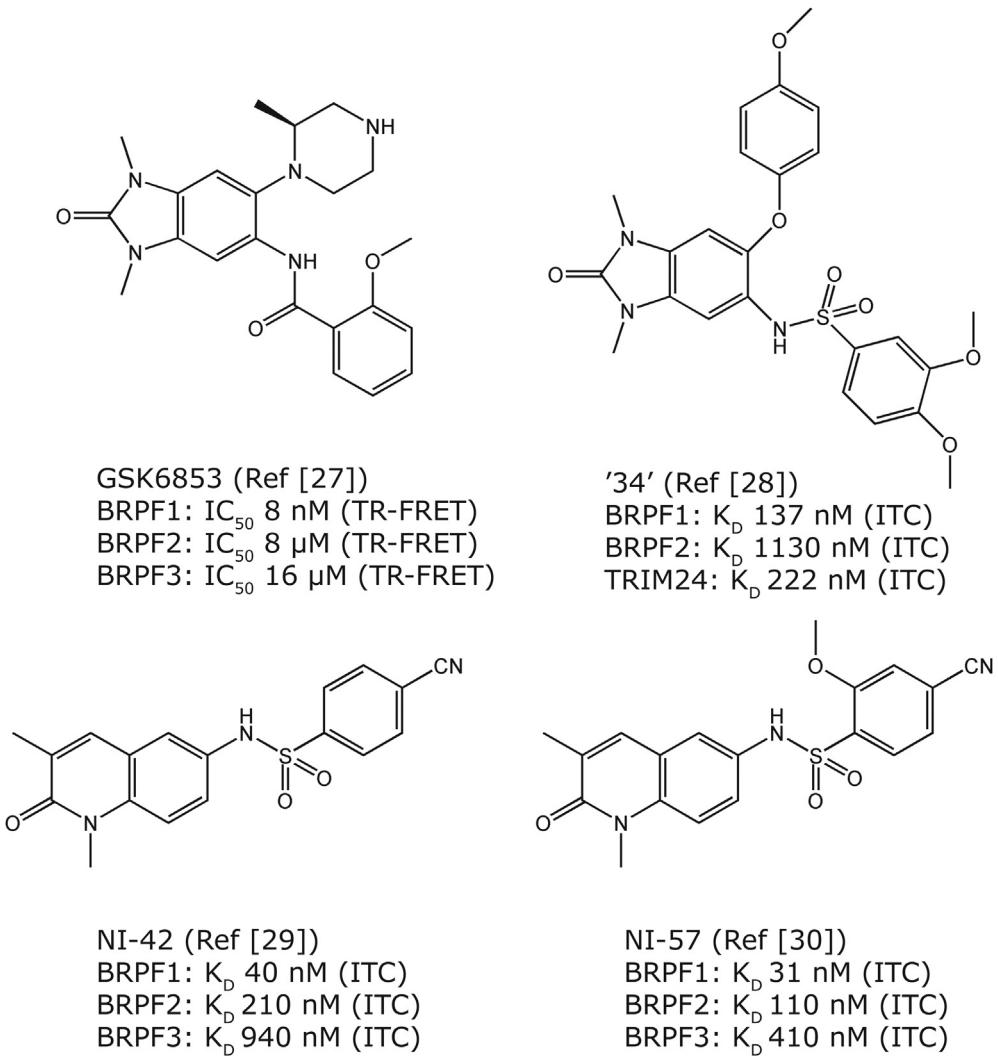

Fig. 1. Representative BRPF1 inhibitors reported previously.

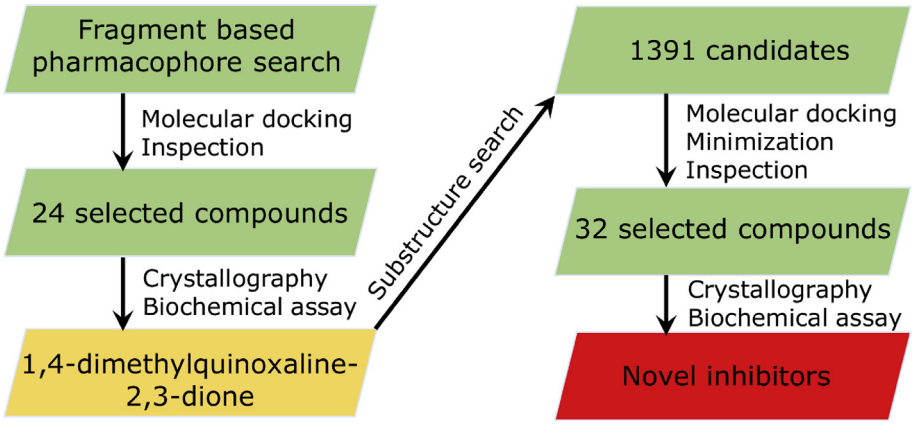

Fig. 2. Flowchart of the discovery of quinoxaline-2,3-dione derivatives.

scaffold acts as the Kac mimetic, which can form a hydrogen bond to the conserved asparagine (Asn708) in BRPF1. Therefore, this key hydrogen bond interaction was used to filter docking poses generated by Autodock Vina [35]. Seven of the 24 selected compounds exhibited K_D values below 50 μM as determined by a competition binding assay [36] (Table 1 and Table S2). Moreover, compounds **2**, **5** and **8** showed good selectivity on BRPF1 against TRIM24 ($K_D > 100$ μM) and BRD4(1) ($K_D > 100$ μM) bromodomains. Overall, this series of compounds shows reasonable *c*LogP values (<3) and have lipophilic efficiency higher than 2.0.

Crystallographic screening (soaking or co-crystallization, see Experimental) was performed to validate the pharmacophore search and pose predicted by docking. Three co-crystals of the BRPF1 bromodomain with compounds **2**, **7** and **8** were solved at resolutions higher than 1.6 Å (Table S1). As expected from the docking results (Fig. S1), the quinoxaline head group binds in the Kac pocket with the canonical hydrogen bonding to Asn708 and a buried water molecule bridging to the side chain of Tyr665 (Fig. 3). Interestingly, both of the carbonyl groups on the quinoxaline ring of **2** form hydrogen bond interactions with the bridging water molecule (Fig. 3A). In the crystal structure with compound **2**, the 3-position carbonyl group has an additional hydrogen bond interaction with the SH group of Cys704 which locates at the bottom of the Kac pocket. Furthermore, the NH group of quinoxaline of **2** is involved in a hydrogen bond to the backbone carbonyl of Ile652. Compared to **7** and **8**, the additional methyl group at the amide linker of **2** displaces a conserved water molecule in the binding site. The amide-based linkers occupy different positions in the binding site (Fig. 3D). The tail groups of these compounds pack against the nonpolar part of the side chain of Glu661.

The binding modes of **2**, **7** and **8** show two orientations of the quinoxaline scaffold: the ethyl group of **2** points towards the side chain of Tyr707 in the BC loop, whereas the ethyl group of **7** and **8** points towards the side chains of Ile652 and Phe653 in the so-called NIF shelf (i.e., the Asn651-Ile652-Phe653 triad) in the N-terminal segment of the ZA loop. The structural overlap of the crystal structures of BRPF1 in the complex with compounds **2**, **7**, and **8** shows that a modified quinoxaline with methyl or ethyl groups at both positions 1 and 4 could be accommodated in the binding pocket.

To test this hypothesis, we tried to crystallize BRPF1 with the fragment **9**, i.e., 1,4-dimethylquinoxaline-2,3-dione (Table 2). The co-crystal structure at resolution of 1.5 Å shows clear electron density for fragment **9** (Fig. 3E). Similarly to the binding mode of compound **2**, both of the carbonyl groups on the quinoxaline ring of the fragment are involved in hydrogen bonding to the structurally conserved water molecule that acts as bridge towards the hydroxyl group of the evolutionary conserved Tyr665. The hydrogen bond interactions with the side chains of Cys704 and Asn708 are also present. One of the two methyl groups on the quinoxaline ring forms van der Waals interactions with the side chain Ile652 and Phe653 of the NIF shelf.

2.2. Substructure search

Fragment **9** provided a starting point for a substructure search. Nearly 1400 compounds were retrieved via substructure search in the ZINC database [37], for which either methyl or ethyl groups are present at positions 1 and 4 on the quinoxaline core, and varied tail groups at positions 6 and 7. To in silico screen these candidate compounds, flexible docking was performed with Autodock Vina [35] and docking poses were filtered using the structure of the complex with compound **9** as reference. Next, binding poses were refined by energy minimization with CHARMM [38] using a similar protocol as in a recent work [39], and ranked with a knowledge-based scoring function DSX [40]. The top 1596 poses (of a total of 3967 poses) were inspected visually, and 32 compounds with favorable lipophilic contacts and hydrogen bonds were purchased for binding affinity measurements by BROMOscan and AlphaScreen [41]. Like before, a crystallographic screening was performed by both soaking and co-crystallization methods. Of the 32 molecules screened, compounds **13**, **16**, **21**, **26** and **36** showed binding to the Kac pocket by co-crystallization and could be unambiguously built into the electron density map.

Crystal structures of BRPF1 with **13**, **16**, **21**, **26** and **36** were solved at resolutions higher than 1.8 Å (Table S1). As expected, the quinoxaline head groups bind to the Kac pocket in a similar way as for the parent scaffold **9** (Fig. 4). The docking approach successfully predicted the crystallographic poses, as for **13**, **16**, **21** and **26**, the docked poses show root-mean-square deviation (RMSD) less than 1.6 Å with respect to the binding mode in the crystal structure (Fig. S1). In all cases, the carbonyl group at position 3 can simultaneously form hydrogen bond interactions with Asn708, Cys704 and water bridging to the conserved Tyr665. As for the other carbonyl, it acts as hydrogen bond acceptor for the NH_2 of Asn708.

The tail groups show interesting binding features in the crystal structures. The phenyl ring of **13** and **21** and aromatic ring of **16** and **26** form an edge-to-face π-π stacking interaction with the so-called gatekeeper residue which is Phe714 in BRPF1. The isobutyl group of **13** and **21** and the saturated ring of the tetralin in compounds **16** and **26** occupy a hydrophobic groove located between the side chains of Ile 713 and Phe714. The substituents at the position 6 of

Table 1
Validation of pharmacophore search results. 2D structures and binding affinity of 1-ethyl-2,3-dioxo-4H-quinoxaline and 1-ethyl-3-methyl-2-oxoquinoxaline derivatives.

Cpd	2D structure	BROMOscan K_D (μM)[a]			cLogP[b] [LiPE[c]]	PDB Code
		BRPF1	TRIM24	BRD4(1)		
1	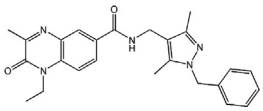	16	ND	ND	2.46 [2.34]	
2	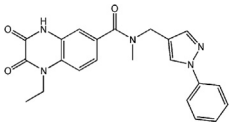	17	>100	>100	1.96 [2.81]	5O5A
3	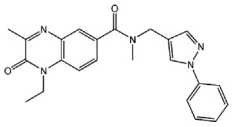	36	ND	ND	2.56 [1.88]	
4	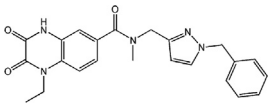	45	ND	ND	2.11 [2.24]	
5	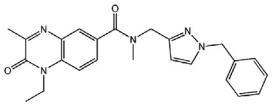	19	>100	>100	2.71 [2.01]	
6	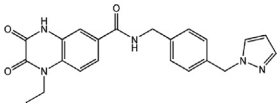	18	ND	ND	1.80 [2.94]	
7	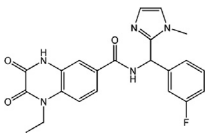	>50	ND	ND	–	5O5F
8	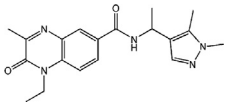	20	>100	>100	1.29 [3.41]	5O55

[a] BROMOscan is a competition binding assay. The K_D values were measured in duplicates.
[b] Calculated with ChemAxon (www.chemaxon.com).
[c] Lipophilic efficiency is calculated as LiPE = pIC_{50} - cLogP. ND indicates data not determined.

the quinoxaline point towards the NIF shelf. Furthermore, the morpholine group in **21** and **26** contacts a backbone carbonyl of Gly650 via a water mediated hydrogen bond.

The crystal structures can be employed to interpret the structure-activity relationship for this series of compounds. The substituent at position 6 seems crucial in increasing binding potency, as evidenced by some pairwise comparisons (Table 2). For example, by introduction of a morpholine group, potency of **21** is significantly increased as compared to **13** which has a pyrrolidine group, as observed in both the BROMOscan (K_D of 18 μM and 1.8 μM for compounds **13** and **21**, respectively) and AlphaScreen assay (IC_{50} of 11 μM and 1.9 μM). Similarly, improved potency was observed for **24** (IC_{50} of 3.6 μM in AlphaScreen) as compared to **10** (IC_{50} = 10.5 μM). However, compounds bearing 6-position morpholine or piperidine groups showed similar affinity. For instance, **16** (piperidine group at position 6) shows an IC_{50} of 1.7 μM in AlphaScreen and **26** (piperidine) has an IC_{50} of 3.4 μM. As seen from the crystal structure of BRPF1/**16**, the position 2 carbonyl of **16** provided an additional hydrogen bonding interaction with the bridging water molecule, which may compensate for the loss of the interaction with Gly650, as compared to **26**. Overall, for this compound series with the sulfonamide linker, it seems bulkier group at position 6 may bring higher potency. For future lead optimization, it might be beneficial to directly contact Gly650 by introduction of a modified 6-position substituent.

Due to a single crystal structure with compound **36** (IC_{50} = 16 μM) and the discrepancy between BROMOscan and AlphaScreen assay results (e.g., compound **32** has a K_D > 50 μM and IC_{50} = 4.4 μM, respectively), it is difficult to discuss the structure-activity relationship for the compounds **28**-**36** which have an amide linker. We propose that for this category of compounds, the amide and the linked group may stack against the flexible side chain of Glu661, as exemplified by the crystal structure of BRPF1/**36** (Fig. 4E). Interestingly, it seems that heterogeneous 6-position groups can be employed for this series, for instance, a diethylamino group in **28** (IC_{50} = 0.77 μM) and a methyl-piperidine substituent in **32** (IC_{50} = 4.4 μM) both result in potent compounds.

Isothermal titration calorimetry was used to characterize the

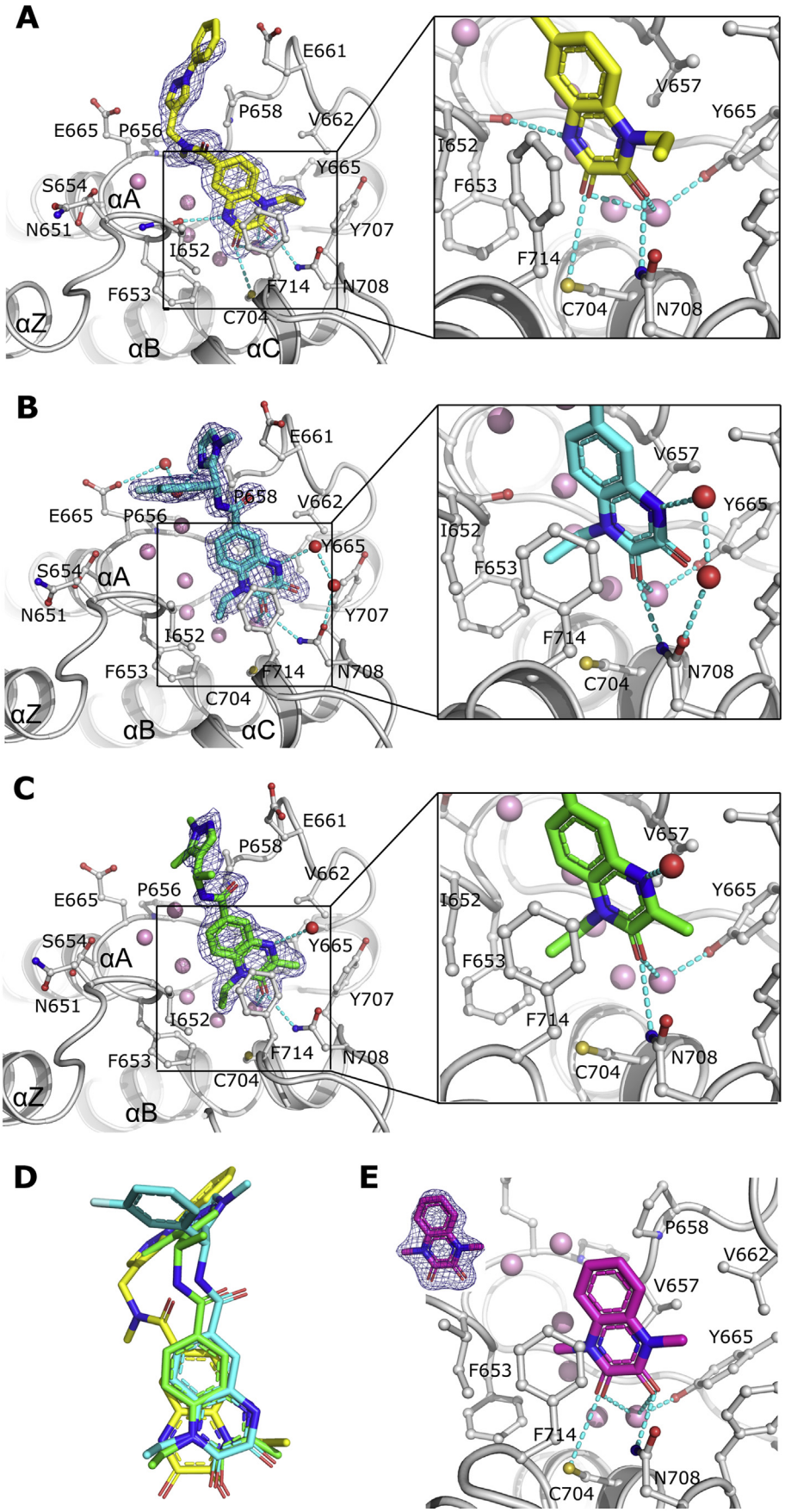

Fig. 3. Co-crystal structures of the BRPF1 bromodomain in complex with compounds **2** (A), **7** (B), **8** (C), and **9** (E). The conserved water molecules and other water molecules involved in ligand binding are shown as pink and red spheres, respectively, while hydrogen bonds are shown by dashed lines using a threshold on hydrogen bond donor and acceptor of 3.5 Å. The 2Fo − Fc electron density maps are shown in blue mesh at a contour level of 1.0 sigma. For compounds **8** and **9**, the electron density maps are shown at 0.8 sigma. (D) Superimposition of binding poses of compounds **2** (yellow), **7** (cyan) and **8** (green). (For interpretation of the references to colour in this figure legend, the reader is referred to the Web version of this article.)

binding thermodynamics of compound **21** (Fig. 5C). A K_D value of 2.7 μM was obtained, which is in good agreement with the BROMOscan (K_D of 1.8 μM) and AlphaScreen (IC_{50} of 1.9 μM) assay results. The ITC data indicated that binding of **21** to the BRPF1 bromodomain is mainly enthalpic, with an enthalpy change of −8.5 kcal mol^{-1} and a small entropy penalty of 0.9 kcal mol^{-1}. Furthermore, ITC measurements of the binding of compound **26** showed similar thermodynamic characteristics, with a K_D of 2.5 μM, ΔH of −8.6 kcal mol^{-1}, and −TΔS of 0.9 kcal mol^{-1} (Fig. S2). These measurements suggest optimal hydrogen bonding and van der Waals interactions between the BRPF1 bromodomain and this series of compounds. Overlap to the apo structure shows only minor conformational changes in BRPF1 upon binding of **21** and its analogues (Fig. 4F).

Taken together, the substructure search using fragment **9** and information on its binding mode has led to the discovery of a series of compounds with low micromolar affinity and favorable lipophilic efficiency. In total 11 compounds have IC_{50} below 10 μM, 10 compounds exhibit LiPE higher than 3.0, and even LiPE higher than 4.0 for compounds **19**, **22**, and **23**.

2.3. Selectivity

We next analyzed the selectivity profile of compound **21** by the AlphaScreen assay (Fig. 5D). The assay results showed that **21** has negligible activity on subfamily IV members BRPF2, BRPF3, and ATAD2 bromodomains, and marginal activity ($IC_{50} = 204$ μM) on BRD9 bromodomain. Moreover, **21** was inactive on promiscuous BRD4(1) (subfamily II) and CREBBP (subfamily III) bromodomains. In addition, binding of **21** to the BRPF2 bromodomain was too weak to record the thermodynamic signature in an ITC measurement (Fig. 5C, red curves). To elucidate the structural basis of the selectivity of **21**, the crystal structure of BRPF1/**21** was aligned with apo BRPF2 and BRD4(1) bromodomain structures (Fig. 5A and B, respectively). The favorable van der Waals contacts between the sulfonamide linker of **21** and Pro658 in BRPF1 are absent in BRPF2, as the side chain of the corresponding residue in BRPF2 (Ser592) points outwards the binding site. The structural overlap with BRD4(1) suggests that steric collisions may occur between the morpholine ring of **21** and Trp81 (W of the WPF shelf) in BRD4(1). Furthermore, the binding pocket of BRD4(1) is narrower than that of BRPF1, especially for the ZA loop segment surrounding Leu92, which may also cause steric clashes with **21**. Sequence alignment of BRPF1 bromodomain with other bromodomains tested in the selectivity panel provided additional information (Fig. S3). First, the gatekeeper in the BRPF subfamily members is a phenylalanine, while it is a smaller hydrophobic residue (valine or isoleucine) or a tyrosine in other bromodomains, for which the T-shaped π-π stacking with **21** cannot be formed. Secondly, Pro658 in BRPF1 corresponds to polar residues in other bromodomains (except TRIM24), and as such the lipophilic contacts with **21** are not possible.

2.4. Molecular dynamics simulations

To further investigate the binding mode and selectivity of compound **21**, three independent molecular dynamics runs were performed for its complex with the BRPF1 bromodomain and three with the BRPF2 bromodomain. The binding mode of **21** in BRPF1 is stable in the Kac pocket during the 500 ns simulation time (Fig. 6A). Conversely, **21** was not stable in BRPF2 and in one of the three MD runs it escaped from the binding pocket within the first 100 ns and there was no re-binding. The crucial hydrogen bond interaction between the NH group of Asn708 and the 3-position carbonyl group of **21** was present in 90% of the simulation time for BRPF1 while it broke in the first 100 ns in two of the three runs with the BRPF2 complex.

Besides reporting on the main intermolecular interactions, the molecular dynamics trajectories shed light on the orientation and intrinsic flexibility of the tail group. The dihedral angle distribution of the sulfonamide linker shows that **21** is mainly in a conformation with the isobutyl phenyl group projecting towards the BC loop, and sporadically this group flipped to contact the ZA loop residues (red histograms in Fig. 6B). The simulation of **21** free in solution, i.e., in the unbound state (blue histogram in Fig. 6B), showed that the most populated orientation of the sulfonamide linker is the same as in the complex with BRPF1. As for the X-ray structure, the dihedral angle of the sulfonamide is within the main state observed in the MD simulations of the free (and bound) state. Thus, compound **21** is not strained in its bound conformation observed along the MD simulations and in the X-ray structure. Concerning the relative flexibility of the BRPF1 binding site, the ZA loop region showed the largest flexibility during the simulations (Fig. S4), particularly for the segment Leu659-Ser660-Glu661 (Fig. S5). The plasticity of the ZA loop is consistent with previous simulation studies [42,43]. A bulkier substituent and/or a functional group that stacks against the flexible Glu661 side chain might reduce the flexibility of the ZA loop but it is not possible to predict if the resulting entropic penalty would be fully balanced by an enthalpic gain, i.e., additional favorable interactions.

2.5. Cellular assays

For measuring the cellular efficacy of this series of compounds, we selected compound **26**, which has higher solubility than **21** in the preliminary assay (data not shown). Cell viability was evaluated on acute myeloid leukemia cell lines THP-1 and HL-60. Compound **26** showed growth inhibition in THP-1 cells in a dose-response manner with an EC_{50} of 32 μM, while it displayed no obvious toxicity to normal fibroblast cell line BJ (Fig. 7). In contrast to the THP-1 cell with MLL translocation, **26** showed little effect on non-MLL-rearranged acute leukemia cell line HL-60 in the cell viability assay (data not shown). These observations are in line with a previous study [29] which reported that AML cell lines exhibiting MLL translocation are sensitive to inhibition of BRPF1. However, further optimization of potency is required for further investigations of the mechanism of action of this series of compounds in leukemia cells.

2.6. Second pharmacophore search; discovery of 2,4-dimethyl-oxazole derivatives

From another pharmacophore search [34] based on PDB structure 5EVA (N-methylpyrazole-based compound **19** of Ref. [37]), we identified compounds **42** and **43** (Table 3). We note that these two compounds bear a 2,4-dimethyl-oxazole head, which is different from the 3,5-dimethyl-isoxazole widely used as scaffold in BET bromodomain inhibitor [44–47]. Compound **42** exhibited a K_D of 3.5 μM in BROMOscan assay and IC_{50} of 30.6 μM in AlphaScreen assay for the BRPF1 bromodomain and no measurable binding to the TRIM24 and BRD4(1) bromodomains. Compound **43** showed substantially weaker affinity than **42**.

To validate the pharmacophore model, co-crystal structures of BRPF1 with **42** and **43** were obtained. BRPF1/**42** was solved in two different space groups (Fig. 8 and Table S1). In both cases the 2,4-dimethyl-oxazole head is positioned at the bottom of the Kac site, with the nitrogen atom on it forming hydrogen bonds with Asn708 and the bridging water molecule. The thiazole group stack against Pro658. The tail group 3,5-dimethyl-piperidine show different orientations in two crystal forms; it either points to the ZA channel

Table 2
2D structures and assay results of the 2,3-dioxo-quinoxaline derivatives.

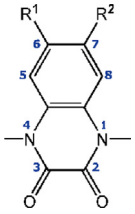

Cpd	R^1	R^2	BROMOscan			AlphaScreen		
			BRPF1 %Ctrl[a]	TRIM24 %Ctrl[a]	BRPF1 K_D (μM)	BRPF1 IC_{50} (μM)	cLogP[b] [LiPE[c]]	PDB Code
9	H	H	ND	ND	ND	>400	–	5O4T
10		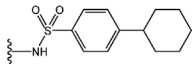	43 @100 μM	72 @100 μM	ND	10.5	3.48 [1.50]	
11		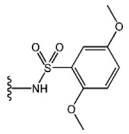	17 @100 μM	84 @100 μM	ND	ND	–	
12		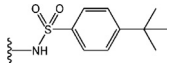	3.1 @100 μM	86 @100 μM	ND	8.7	3.35 [1.71]	
13		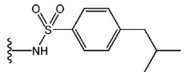	0 @100 μM	94 @100 μM	18 (n = 2)	11.0	3.05 [1.91]	5OV8
14		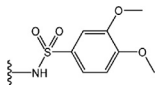	3.9 @75 μM	100 @75 μM	11 (n = 2)	ND	1.49 [3.47]	
15		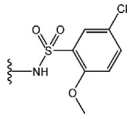	9.9 @100 μM	97 @100 μM	ND	>10	–	
16		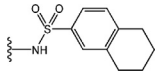	12 @100 μM	75 @100 μM	ND	1.7	3.26 [2.51]	5MWG
17		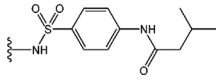	41 @100 μM	74 @100 μM	ND	3.4	2.48 [2.98]	
18		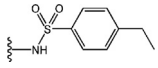	22 @100 μM	82 @100 μM	ND	ND	–	
19		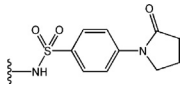	ND	ND	ND	4.4	1.13 [4.22]	
20		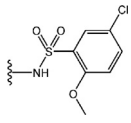	4.1 @50 μM	90 @50 μM	33 (n = 2)	ND	1.18 [3.30]	
21		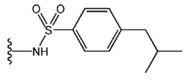	8.4 @100 μM	79 @100 μM	1.8 (n = 2)	1.9 (n = 4)	2.43 [3.29]	5MWH
22		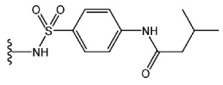	11 @100 μM	84 @100 μM	ND	2.0 (n = 2)	1.41 [4.29]	

(*continued on next page*)

Table 2 (*continued*)

Cpd	R^1	R^2	BROMOscan			AlphaScreen		
			BRPF1 %Ctrl[a]	TRIM24 %Ctrl[a]	BRPF1 K_D (μM)	BRPF1 IC_{50} (μM)	cLogP[b] [LiPE[c]]	PDB Code
23		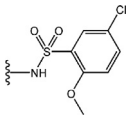	ND	ND	ND	5.4	1.18 [4.08]	
24		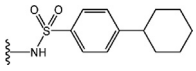	ND	ND	ND	3.6	2.85 [2.59]	
25		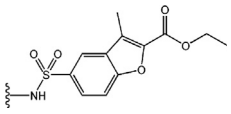	ND	ND	ND	10.1	1.69 [3.30]	
26		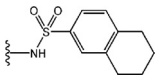	ND	ND	ND	3.4	2.19 [3.27]	5O4S
27	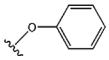	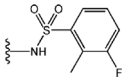	23 @100 μM	77 @100 μM	ND	23.6	3.47 [1.16]	
28		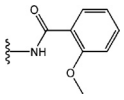	1.6 @25 μM	96 @25 μM	9.7 (n = 2)	0.77	2.12 [3.99]	
29		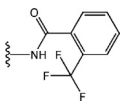	ND	ND	ND	>200	–	
30		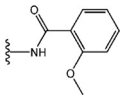	13 @100 μM	86 @100 μM	>20 (n = 2)	27.0	1.81 [2.76]	
31		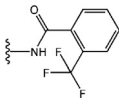	49 @50 μM	100 @50 μM	ND	ND	–	
32	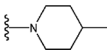	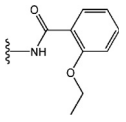	0 @50 μM	91 @50 μM	>50 (n = 2)	4.4	2.90 [2.46]	
33	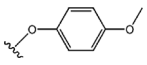	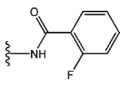	46 @25 μM	97 @25 μM	>25 (n = 2)	ND	–	
34	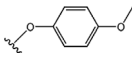	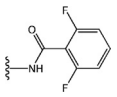	ND	ND	ND	22.3	3.08 [1.57]	
35	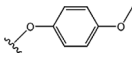	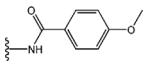	91 @25 μM	97 @25 μM	ND	ND	–	
36		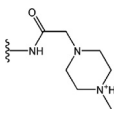	55 @20 μM	100 @20 μM	7.1 (n = 2)	16	1.23 [3.56]	5MWZ
37	H	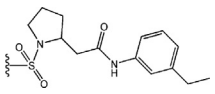	68 @100 μM	94 @100 μM	ND	ND	–	
38	H	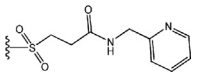	81 @50 μM	82 @50 μM	ND	ND	–	

Table 2 (*continued*)

Cpd	R^1	R^2	BROMOscan			AlphaScreen		
			BRPF1 %Ctrl[a]	TRIM24 %Ctrl[a]	BRPF1 K_D (μM)	BRPF1 IC_{50} (μM)	cLogP[b] [LiPE[c]]	PDB Code
39	H	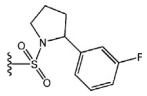	86 @75 μM	81 @75 μM	ND	ND	–	
40	H	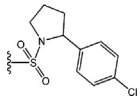	ND	ND	ND	>200	–	
41	H	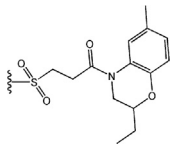	ND	ND	ND	>200	–	

[a] The single-dose value is the percentage of remaining binding of the competitor molecule with respect to DMSO solution at the compound concentration shown in μM; thus lower values indicate stronger binding of the compounds.
[b] Calculated with ChemAxon.
[c] Lipophilic efficiency is calculated as LiPE = pIC_{50}-*c*LogP. The AlphaScreen IC_{50} values are used for the pIC_{50}, except for compounds **14** and **20** for which the BROMOscan K_D value was employed as the AlphaScreen was not performed. ND indicates data not determined. Compound **36** has N-ethyl substitutions instead of N-methyl.

or the NIF shelf (Fig. 8A and B). Interestingly, the oxygen atom of the oxazole head, and three nitrogen atoms (*viz*., the NH group of the amide linker, the thiazole nitrogen, and tertiary amino in the tail group) are involved in a water-mediated hydrogen bonding network with the backbone carbonyl groups of Asn651 and Ile652. In the BRPF1/**43** crystal structure (Fig. 8C), the head group of **43** binds in a similar way as **42**, whereas the water-mediated hydrogen bond with the carbonyl group of Asn651 is lost. Compound **43** has a pyridine ring corresponding to the thiazole of **42**, and a different tail group which occupies the ZA channel. Concerning intra-ligand interactions, an intramolecular hydrogen bond between the oxazole oxygen and the NH group of the amide linker seems to contribute to the stability of the bound conformation of compounds **42** (Fig. 8A and B) and **43** (Fig. 8C).

A substructure search using 2,4-dimethyl-N-(thiazol-2-yl)oxazole-5-carboxamide yielded a single molecule in the ZINC database. Thus, we decided to perform a similarity search which yielded 15 analogues of compound **42** with a Tanimoto coefficient larger than 0.3. These 15 compounds were evaluated using the AlphaScreen assay (Table S4). They all showed weaker potency than **42**, probably due to their head groups which are different from the oxazole of **42**. In the biochemical assays (BROMOscan and AlphaScreen), compound **42** presented good selectivity over TRIM24 and BRD4(1) bromodomains (Table 3). To further analyze potency and selectivity, we measured the interaction of **42** with the bromodomains of BRPF1 and BRPF2 by means of ITC. Compound **42** showed a K_D of 10.9 μM on BRPF1 (which is consistent with the affinity of 3 μM and 30 μM measured by AlphaScreen and BROMOscan, respectively, Table 3) while binding signal was not detected for BRPF2 (Fig. 8F). Similar to **21** and **26**, compound **42** appears to be another 'enthalpic efficient' BRPF1 inhibitor, with ΔH of −7.9 kcal mol^{-1} and −TΔS of 1.2 kcal mol^{-1}. Crystal structure alignment of the BRPF1/**42** complex with apo BRPF2 clearly shows that the Pro658 is essential for the selectivity over BRPF2 (Fig. 8D), as discussed above for the 2,3-dioxo-quinoxaline derivatives. The structural overlap with the BRD4(1) structure reveals potential clashes of compound **42** with the side chains of Trp81 (in the WPF shelf) and Leu92 (Fig. 8E). These bulky side chains are oriented towards the center of the binding site in BRD4(1) while the corresponding residues in BRPF1, Asn651 and Glu661, respectively, point outside.

3. Conclusions

Our previous high-throughput fragment docking campaign [31] paved the way for the present structure-based hit-optimization study. Pharmacophore and substructure searches combined with orthogonal binding assays and X-ray crystallography have led to the identification of a series of 1,4-dimethyl-2,3-dioxo-quinoxaline derivatives, which are structurally different from previously reported BRPF1 bromodomain inhibitors. Some of these compounds showed low micromolar inhibitory activity towards the BRPF1 bromodomain, as confirmed by both biochemical and biophysical assays. Among them, **21** is a 2-μM ligand of the BRPF1 bromodomain with >100-fold selectivity over other bromodomains. Co-crystal structures of BRPF1 with this series of compounds revealed interesting binding features, e.g., a water-bridged hydrogen bond to the carbonyl of Gly650 in the ZA loop. Moreover, the X-ray structures provided structural insights into the origin of selectivity and helped to explain the structure-activity relationship. Molecular dynamics simulations were used to investigate the binding pose of **21** to BRPF1 and its flexibility. The antiproliferative activity on acute myeloid leukemia cell lines was confirmed by cell viability assay with **26**.

From another pharmacophore search, we discovered compound **42** which bears a 2,4-dimethyl-oxazole scaffold. The selective inhibition of **42** on BRPF1 over other bromodomains was demonstrated by both biochemical assay and isothermal titration calorimetry. Crystallographic study showed extensive hydrogen bond interactions formed in the Kac pocket of BRPF1 upon binding of **42**. The chemotypes discovered in the present study exhibit favorable physicochemical properties, for instance, three of the 1,4-dimethyl-2,3-dioxo-quinoxaline derivatives have lipophilic efficiency higher than 4.0. Moreover, the compounds **21**, **26**, and **42** show enthalpy-driven binding in isothermal titration calorimetry measurements, which makes them suitable candidates for optimization [48].

Taken together, a total of 74 small molecules identified in silico were evaluated by biochemical and/or biophysical assays. Of these 74 small molecules, 57 compounds originated from the pharmacophore searches that made use of the crystal structure of the BRPF1 bromodomain in the complex with 1-methyl-2-oxo-4H-

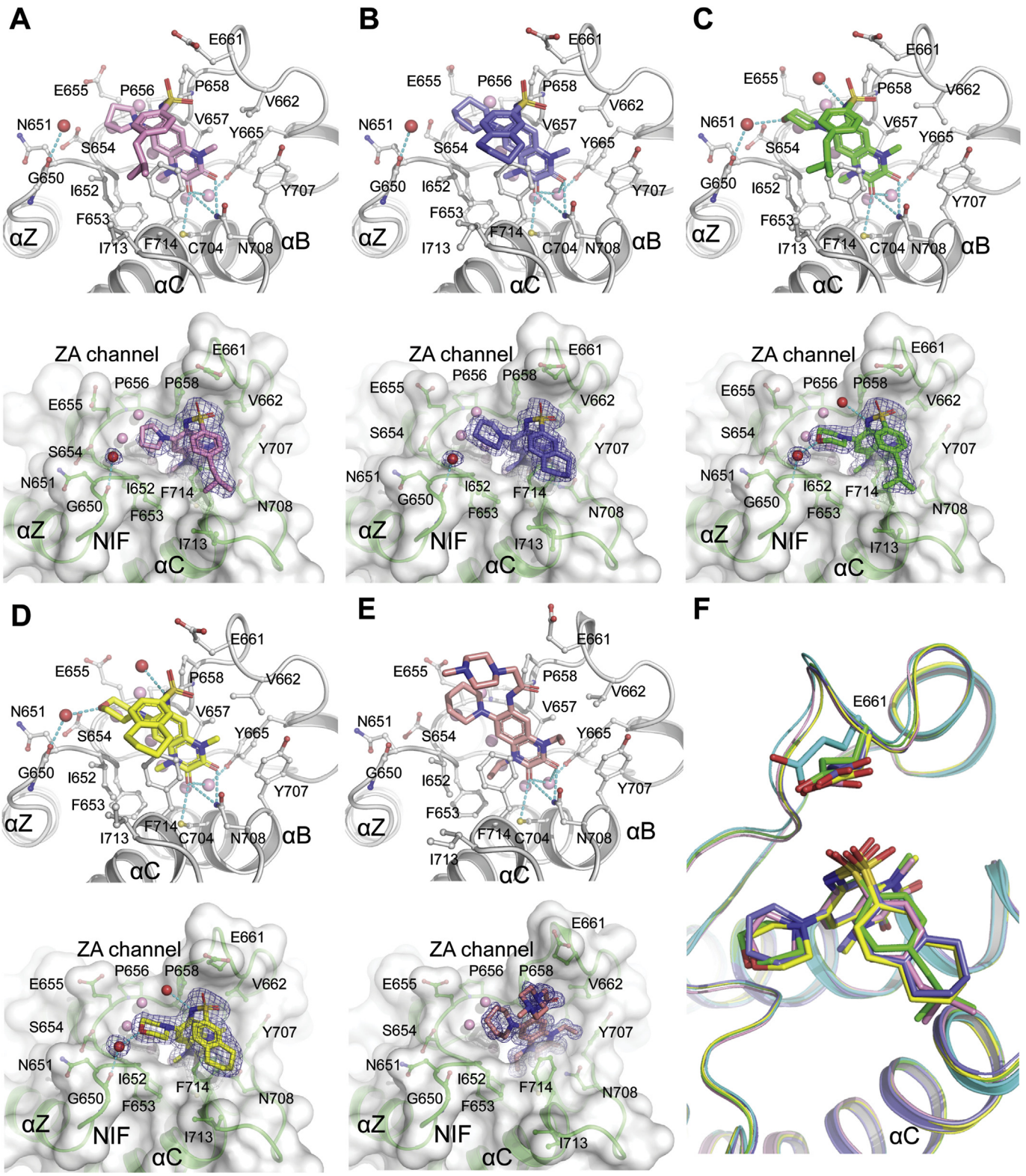

Fig. 4. Co-crystal structures of BRPF1 bound to **13** (A), **16** (B), **21** (C), **26** (D), and **36** (E). The conserved water molecules and other water molecules involved in ligand binding are shown as pink and red spheres, respectively, while hydrogen bonds are shown by dashed lines. The 2Fo − Fc electron density maps are shown in blue mesh at a contour level of 1.0 sigma. (F) Overlap of the complex structures of BRPF1/**13** (pink), BRPF1/**16** (slate), BRPF1/**21** (green), BRPF1/**26** (yellow), and apo BRPF1 4LC2 (cyan). (For interpretation of the references to colour in this figure legend, the reader is referred to the Web version of this article.)

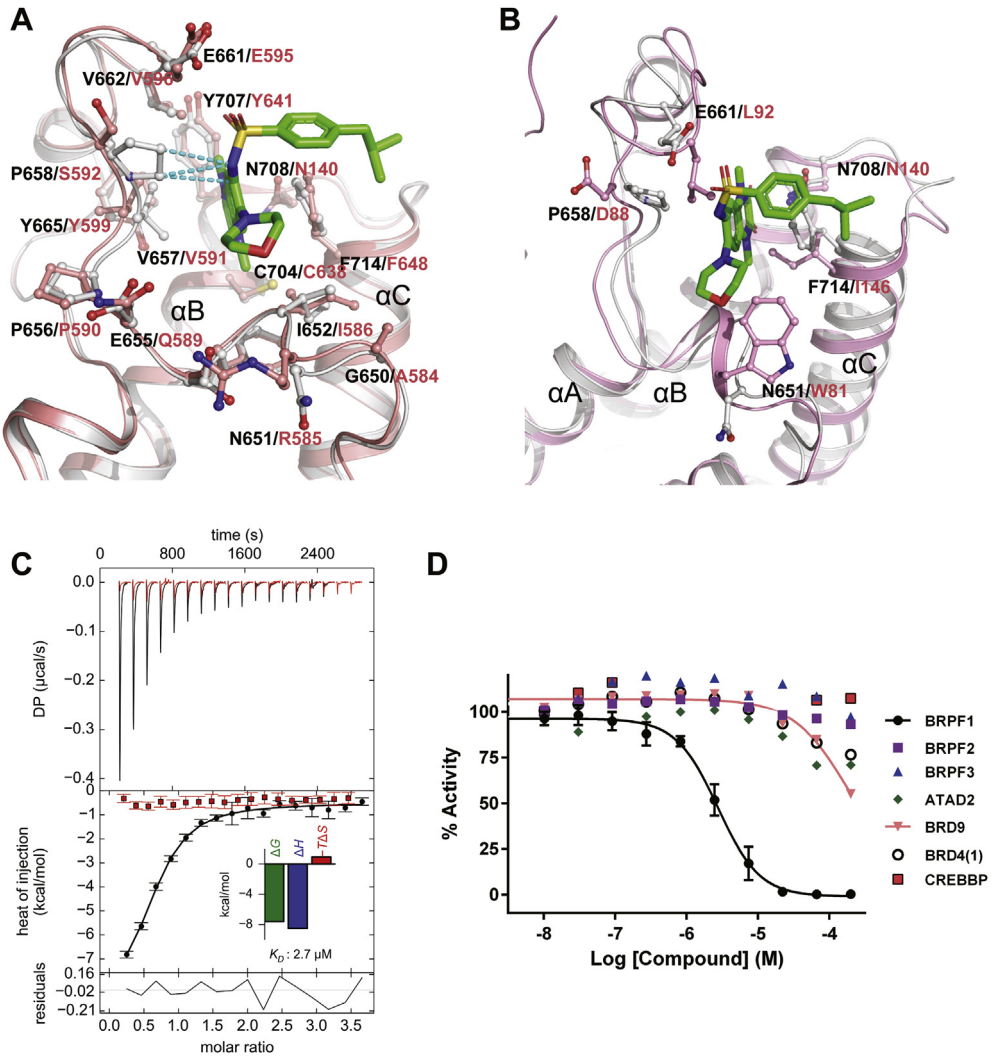

Fig. 5. Selectivity profile of compound **21**. (A) Structural comparison of BRPF1/**21** (white) with apo BRPF2 PDB code 3RCW (salmon). Dashed lines emphasize van der Waals contacts with the side chain of Pro658 in BRPF1 which corresponds to Ser592 in BRPF2 (see text). (B) Structural comparison of BRPF1/**21** (white) with apo BRD4(1) structure 2OSS (pink). (C) Thermodynamic characterization of interactions of **21** with BRPF1 (black) and BRPF2 (red) by ITC. Thermographs, fit of integrated data and fit residuals are shown in the top, middle and bottom panel, respectively. (D) Compound **21** was tested by means of AlphaScreen on bromodomains of BRPF1, BRPF2, BRPF3, ATAD2, BRD9, BRD4(1) and CREBBP. Error bars indicate SEM. Binding is not observed for the off-targets even at a 200 μM concentration of compound **21**. (For interpretation of the references to colour in this figure legend, the reader is referred to the Web version of this article.)

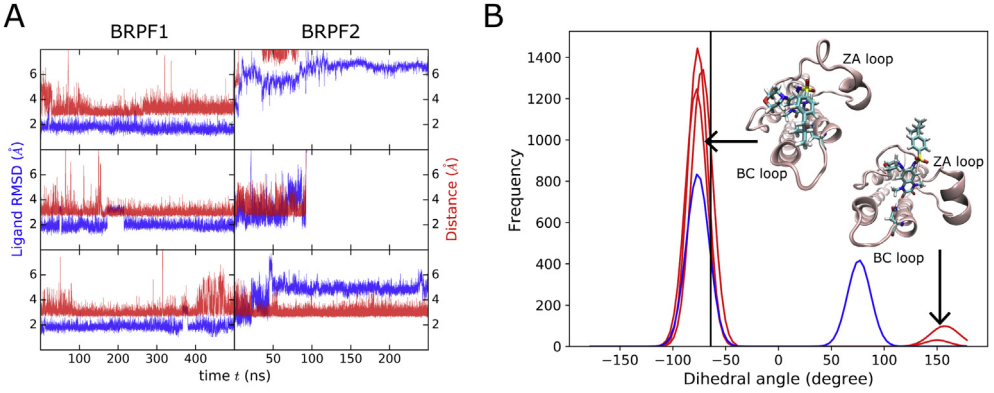

Fig. 6. MD simulations of **21** in the complex with BRPF1 or BRPF2. (A) Time series of RMSD of compound **21** from the initial structure (blue) and distance between N_δ atom of Asn708 and 3-position oxygen atom of **21** (red). Three independent MD runs were started with randomly assigned velocities for the complex with BRPF1 (left) and BRPF2 (right). (B) Histograms of the dihedral angle distribution of the sulfonamide linker of compound **21** in BRPF1 (red) or water (blue). Insets show the conformations of **21** in BRPF1. The vertical line indicate the sulfonamide dihedral angle of −64° in the crystallographic pose (PDB code 5MWH). (For interpretation of the references to colour in this figure legend, the reader is referred to the Web version of this article.)

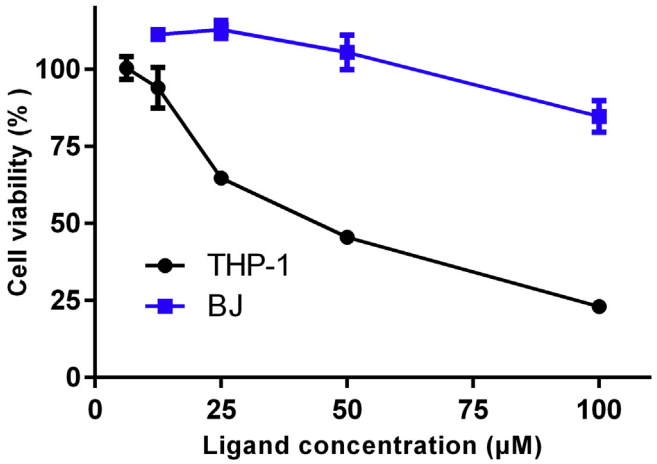

Fig. 7. Cell viability assay of **26** in leukemia cell line THP-1 and normal human fibroblast cell line BJ. The cells were treated with **26** for 72 h. Data points are triplicates and error bars represent SEM.

quinoxaline (PDB code 5EPS) and 17 compounds from the search using an N-methyl-pyrazole derivative (compound **19** of Ref. [31]; PDB code 5EVA), respectively. The pharmacophore and substructure searches were restricted to the purchasable compounds. Since the chemical diversity of the purchasable derivatives is limited it was not possible to reach low nanomolar potency which usually requires optimization by chemical synthesis of derivatives [11,49,50]. The main goal of this work was the identification of novel and selective BRPF1 ligands with structural information on their binding mode. Towards this goal, we have solved 12 holo structures of the BRPF1 bromodomain, nine complexes of BRPF1 with 1,4-dimethyl-2,3-dioxo-quinoxaline derivatives and three complexes with 2,4-dimethyl-oxazole derivatives. We propose the newly identified chemotypes and their structural information as attractive starting points for further development by medicinal chemistry.

4. Experimental

4.1. In silico screening

Two BRPF1 complex structures 5EPS and 5EVA were used for pharmacophore search with ZINCPharmer [34]. The coordinate set 5EPS contains a fragment 3,4-dihydro-1-methylquinoxalin-2(1H)-one, of which the carbonyl group on the quinoxaline ring was defined as hydrogen bond acceptor, the hydrophobic methyl group and the aromatic benzene are also included in the pharmacophores. In 5EVA, BRPF1 is complexed with a compound that bears a 1-methyl-pyrazole head. Similar to the aforementioned fragment, the methyl group on the pyrazole ring was used as hydrophobic group and the nitrogen atom served as hydrogen bond donor. The carboxamide and the aromatic difluorophenyl group were also used as pharmacophores.

Pharmacophore search based on the structure 5EPS revealed a series of compounds that possess either a 2,3-dioxo-4H-quinoxaline or a 3-methyl-2-oxoquinoxaline head. In total 365 such analogues were assembled and docked into the 5EPS structure with Autodock Vina after manual removal of the ligand. The conserved six water molecules were kept in the Kac binding site and the Glu661 was set to be flexible during docking. A filter of hydrogen bonding to the conserved Asn708 was applied and 24 compounds with a binding affinity < -6.5 kcal mol^{-1} were selected from 1753 docking poses for further experimental binding validation.

Substructure search based on fragment **9** was performed against the ZINC database using an RDKit-based python script. The retrieved 1391 compounds were docked into the 5EPS structure with Autodock Vina using same docking settings as described above. Filters of hydrogen bonding to the Asn708, binding affinity more favorable than -6.5 kcal mol^{-1}, and a RMSD calculation within 1 Å using the fragment as reference were applied, resulting in 3967 binding poses from 1174 compounds. These molecules were parameterized with CGenFF [51] which is fully consistent with the CHARMM36 force field. Next the binding poses were refined by energy minimization with CHARMM [38]. The optimized binding poses were rescored with a knowledge-based scoring function DSX [40]. In total 1596 poses from 754 compounds survived when a cutoff of DSX score at -110 was applied. The binding poses were visually inspected and 32 compounds were selected based on chemical structure diversity and availability.

Compounds **42** and **43** were identified by the pharmacophore search with structure 5EVA. The search for compounds similar to **42** was performed against ZINC database using a python script based on RDKit [52]. Totally 16 analogues with Tanimoto coefficient greater than 0.3 were selected for binding assay validation.

4.2. Chemistry

All compounds were purchased from Enamine Ltd. and Chemdiv. Their chemical structure was confirmed by HPLC-MS and proton NMR analysis (Supporting Information).

Table 3
Derivatives of 2,4-dimethyl-oxazole identified in the second pharmacophore search.

Cpd	2D structure	BROMOscan K_D (μM)			AlphaScreen IC_{50} (μM)		ITC			
							K_D (μM)	cLogP[a]	LE[c]	PDB code
		BRPF1	TRIM24	BRD4(1)	BRFP1	BRD4(1)	BRPF1	[LiPE[b]]		
42	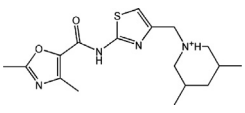	3.5 (n = 2)	>50	>50	30.6 (n = 2)	>200	10.9	2.13 [2.83]	0.29	5OWA 6EKQ
43	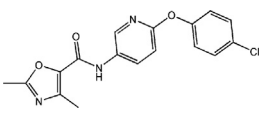	>75 (n = 2)	ND	ND	ND	ND	ND	–	–	5O5H

[a] Calculated with ChemAxon.
[b] Lipophilic efficiency is calculated as LiPE = pIC_{50}-cLogP, according to the ITC data.
[c] Ligand efficiency is calculated as LE = (1.4/HA) × pK_D, according to the ITC data. ND indicates data not aquired.

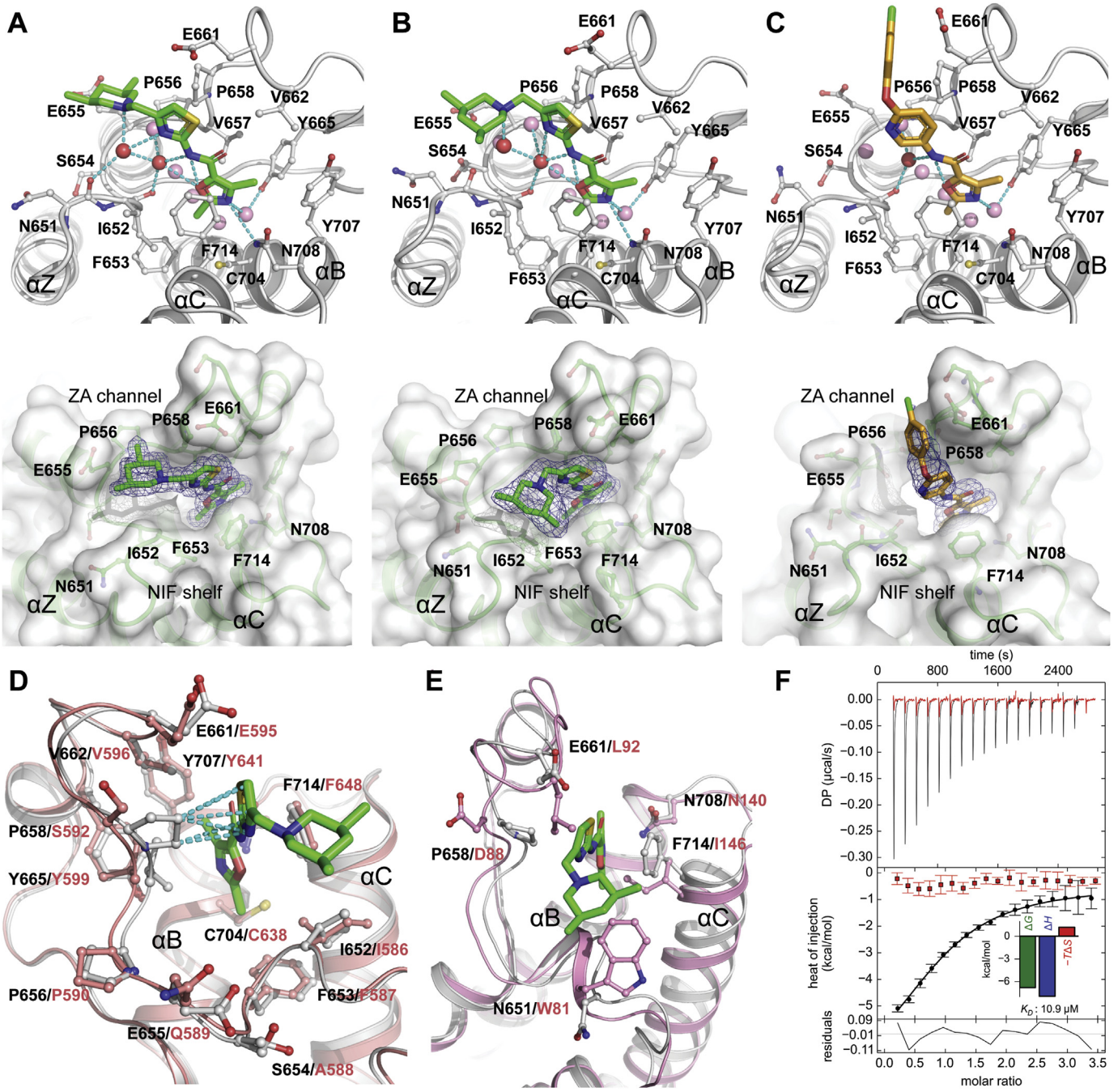

Fig. 8. Co-crystal structures of BRPF1 bound to **42** (A, B) and **43** (C). BRPF1/**42** was crystallized in $P2_1$ (A) and C2 (B) space groups.The conserved water molecules and other water molecules involved in ligand binding are shown as pink and red spheres, respectively, while hydrogen bonds are shown by dashed lines. The 2Fo − Fc electron density maps are shown in blue mesh at a contour level of 1.0 sigma. (D) Structural comparison of BRPF1/**42** (white) with apo BRPF2 structure 3RCW (salmon). (E) Structural comparison of BRPF1/**42** (white) with apo BRD4(1) structure 2OSS (pink). (F) Thermodynamic characterization of interaction of **42** with BRPF1 (black) and BRPF2 (red) by ITC. Thermographs, fit of integrated data and fit residuals are shown in the top, middle and bottom panel, respectively. (For interpretation of the references to colour in this figure legend, the reader is referred to the Web version of this article.)

4.3. BROMOscan assay

The BROMOscan assay was performed at DiscoveRx. T7 phage strains were used to display bromodomains in an *E. coli* host derived from the BL21 strain. Streptavidin-coated magnetic beads were treated with biotinylated small molecule or acetylated peptide ligands for 30 min at room temperature to generate affinity resins for bromodomain assays. Binding reactions were assembled by combining bromodomains, liganded affinity beads, and test compounds in 1x binding buffer (17% SeaBlock, 0.33 × PBS, 0.04% Tween 20, 0.02% BSA, 0.004% Sodium azide, 7.4 mM DTT). Test compounds were prepared as 1000 × stocks in DMSO and subsequently diluted 1:10 in monoethylene glycol (MEG) to create stocks at 100 × the screening concentration (resulting stock solution is 10% DMSO/90% MEG). The compounds were then diluted directly into the assays such that the final concentration of DMSO and MEG were 0.1% and 0.9%, respectively. All reactions were performed in polystyrene 96-well plates in a final volume of 0.135 ml.

The assay plates were incubated at room temperature with shaking for 1 h and the affinity beads were washed with wash buffer (1 × PBS, 0.05% Tween 20). The beads were then resuspended in elution buffer (1 × PBS, 0.05% Tween 20, 2 μM non-biotinylated affinity ligand) and incubated at room temperature with shaking for 30 min. The bromodomain concentration in the eluates was measured by qPCR. Binding constants (K_D) were calculated with a standard dose-response curve using the Hill equation. Curves were fitted using a non-linear least square fit with the Levenberg-Marquardt algorithm. Assay results are shown in Table S3 in Supporting Information.

4.4. AlphaScreen assay

The AlphaScreen assay was carried out at Reaction Biology. Recombinant His-tagged bromodomains, test compounds and biotinylated H4(1-21)K5/8/12/16Ac peptide were delivered to a 384-well OptiPlate and incubated at room temperature for 30 min with gentle shaking. Streptavidine donor beads and nickel chelate acceptor beads were added to plates followed by incubation in dark for 60 min with gentle shaking. Recombinant bromodomains, compounds, donor and acceptor beads were prepared as 4 × stock solution in the buffer of 50 mM HEPES-HCl, pH 7.5, 100 mM NaCl, 1 mg/ml BSA, 0.05% CHAPS and 0.5% DMSO. Alpha signal (Ex/Em = 680/520-620 nm) was measured with an EnSpire plate reader. Dose-response curve was fit with GraphPad Prism 6 using a nonlinear regression analysis model.

4.5. Protein production

BRPF1 bromodomain was purified as an N-terminal GST fusion protein in *E.coli* as described previously. Purified protein was changed into ITC buffer (50 mM HEPES, pH 7.5 and 150 mM NaCl) using gel filtration chromatography for the use of ITC measurements. The vector harboring N-terminal 6-His tagged BRPF2 bromodomain was purchased from Addgene (#25342). BRPF2 plasmid was transformed to BL21-CodonPlus competent cells. Protein expression was induced by adding 0.2 mM IPTG to the TB medium when OD_{600} reached 0.6–0.8, followed by overnight culturing at 18 °C. Harvested cells were disrupted using a French Press instrument in the buffer of 50 mM HEPES, pH 7.5, 300 mM NaCl, 10 mM Imidazole, and 5% Glycerol. Lysate was loaded to a nickel affinity column and contaminants were washed away using a buffer of 50 mM HEPES, pH 7.5, 300 mM NaCl, 25 mM Imidazole and 5% Glycerol. Target protein was purified using an elution buffer (50 mM HEPES, pH 7.5, 300 mM NaCl, 250 mM Imidazole and 5% Glycerol). The 6-His tag was removed by TEV protease afterwards. Finally, protein was purified using gel filtration chromatography in the ITC buffer. Protein concentration (A280) was determined using a NanoDrop spectrophotometer.

4.6. Isothermal titration calorimetry (ITC)

ITC experiments were carried out on a Microcal iTC200 instrument (GE Healthcare) at 25° with a reference power of 10 μCal/s, while stirring at a speed of 1000 rpm. Compounds were dissolved in DMSO and were diluted into the ITC buffer at appropriate concentrations and equivalent amount of DMSO was added to protein sample. Bromodomains at a concentration of 350–400 μM were injected into cell containing 20–40 μM compounds (reverse titration). An initial control injection of 0.4 μL was applied and 150 s spacing time between injections was set during titrations. Raw data were integrated and baseline corrected using NITPIC [53] and were analyzed with SEDPHAT [54] using a single-site binding model. Thermographs were plotted with GUSSI [55]. Thermodynamic parameters were calculated according to $\Delta G = \Delta H - T\Delta S$, where ΔG, ΔH, and $T\Delta S$ are changes in free energy, enthalpy, and entropy of binding, respectively.

4.7. Crystallization of BRPF1/ligand complexes

BRPF1 bromodomain was co-crystallized with inhibitors by vapor diffusion in hanging drops at 277 K. Co-crystals of BRPF1 with compound **2**, **7**, **8**, **9**, **16**, **21**, **26** and **43** were grown by mixing protein sample at 22 mg/ml concentration with an equal volume of reservoir buffer of 0.1 M Bis-tris propane, pH 6.5, 0.2 M Sodium nitrate, 20% PEG3350. For soaking trials, apo BRPF1 crystals were obtained under the same condition. Co-crystals of BRPF1 with **13** and **36** were obtained using well solution of 0.1 M Bis-Tris propane pH7.4, 5% Ethylene glycol, 0.15 M Sodium nitrate and 25% PEG3350. BRPF1/**42** complex can be crystallized either against reservoir buffer of 0.2 M $MgCl_2$ and 20% PEG3350 or a buffer of 0.1 M Bis-Tris propane, pH 9.0, 10% Ethylene glycol, 0.15 M Sodium nitrate and 25% PEG3350.

4.8. Structure determination and refinement

Crystals obtained from co-crystallization or soaking were screened for diffraction and data sets were collected at the Swiss Light Source, Paul Scherrer Institute (Villigen, Switzerland), beamlines X06DA and X06SA. Data reduction was performed with XDS [56] and scaled with Aimless [57]. Structures were solved by molecular replacement with Molrep [58] in CCP4 suite [59] using apo BRPF1 structure 4LC2 as a search model. Structures were refined with PHENIX [60] and were manually built with COOT [61] for several rounds. Topology files of compounds were obtained from the PRODRG server [62].

4.9. Molecular dynamics simulations

Molecular dynamics simulations were carried out with GROMACS [63] on Cray XC40 compute nodes at Swiss National Supercomputing Center (6900 Lugano, Switzerland). The co-crystal structure of BRPF1 in complex with **21** was used as starting coordinate set with conserved water molecules kept in the binding site. As in previous protein structure-based virtual screening campaigns [64,65] the CHARMM36 force field [66] was used for the parameters of BRPF1, the CGenFF [51] for those of compound **21**, and water was represented by the TIP3P model. All of the simulations were run in a cubic water box with minimum distance between protein and water box edge of 12 Å using periodic boundary conditions. The systems were neutralized by adding Na^+ and Cl^- counter ions and energy minimization was carried out for 10,000 steps. A 100-ps NVT run followed by a 100-ps NPT run were performed to equilibrate the system. The electrostatic interactions were calculated with the particle mesh Ewald algorithm and all bonds were constrained using the LINCS algorithm. Production simulations were carried out with a time step of 2 fs at constant temperature (300 K) and pressure (1 atm). Snapshots were saved every 10 ps and analyzed with built-in GROMACS tools.

4.10. Cell viability assay

AML cell lines THP-1 and HL-60, and normal skin fibroblast BJ were purchased from Shanghai Institute for Biological Science. Cells were maintained in RPMI-1640 medium (THP-1) and DMEM medium (HL-60 and BJ) containing 10% (v/v) fetal bovine serum (FBS), at 37 °C in a humidified atmosphere of 5% CO_2. The growth inhibitory activity of tested compounds were measured using Cell Counting Kit-8 according to manufacturer's instruction (Dojindo

Molecular Technologies). Cells were seeded in 96 well plates in 100 μL media per well. Compounds and vehicle (DMSO) were added at varying concentrations and cell cultures were incubated 37 °C for 72 h. Optical density at a wavelength of 450 nm was measured using a plate reader (Epoch, BioTek). Dose-response curves were generated and EC_{50} values were calculated using non-linear regression analysis with GraphPad Prism 6. All measurements were performed at least three times.

Accession code

The coordinate files of BRPF1 in complex with **2** (5O5A), **7** (5O5F), **8** (5O55), **9** (5O4T), **13** (5OV8), **16** (5MWG), **21** (5MWH), **26** (5O4S), **36** (5MWZ), **42** (5OWA and 6EKQ), and **43** (5O5H) have been deposited to the Protein Data Bank. Authors will release the coordinates and experimental data upon article publication.

Notes

The authors declare no conflict of interest.

Associated content

Molecular formula strings for ligands **1**-**43** (CSV).

Acknowledgments

We thank the staff at Swiss Light Source (beamlines X06SA and X06DA, Paul Scherrer Institute) for their assistance during crystal data collection. We thank Prof. W.L. Zhao, Prof. S.G. Zhu and Dr. Z.H. Su for helpful discussions. We greatly acknowledge financial support by the Swiss National Science Foundation to A.C. (31003A_169007).

Appendix A. Supplementary data

Supplementary data related to this article can be found at https://doi.org/10.1016/j.ejmech.2018.05.037.

References

[1] R. Sanchez, M.M. Zhou, The role of human bromodomains in chromatin biology and gene transcription, Curr. Opin. Drug Discov. Dev 12 (2009) 659–665.
[2] P. Filippakopoulos, S. Picaud, M. Mangos, T. Keates, J.P. Lambert, D. Barsyte-Lovejoy, I. Felletar, R. Volkmer, S. Muller, T. Pawson, A.C. Gingras, C.H. Arrowsmith, S. Knapp, Histone recognition and large-scale structural analysis of the human bromodomain family, Cell 149 (2012) 214–231.
[3] L.R. Vidler, N. Brown, S. Knapp, S. Hoelder, Druggability analysis and structural classification of bromodomain acetyl-lysine binding sites, J. Med. Chem. 55 (2012) 7346–7359.
[4] J.E. Delmore, G.C. Issa, M.E. Lemieux, P.B. Rahl, J. Shi, H.M. Jacobs, E. Kastritis, T. Gilpatrick, R.M. Paranal, J. Qi, M. Chesi, A.C. Schinzel, M.R. McKeown, T.P. Heffernan, C.R. Vakoc, P.L. Bergsagel, I.M. Ghobrial, P.G. Richardson, R.A. Young, W.C. Hahn, K.C. Anderson, A.L. Kung, J.E. Bradner, C.S. Mitsiades, BET bromodomain inhibition as a therapeutic strategy to target c-Myc, Cell 146 (2011) 904–917.
[5] S. Picaud, D. Da Costa, A. Thanasopoulou, P. Filippakopoulos, P.V. Fish, M. Philpott, O. Fedorov, P. Brennan, M.E. Bunnage, D.R. Owen, J.E. Bradner, P. Taniere, B. O'Sullivan, S. Muller, J. Schwaller, T. Stankovic, S. Knapp, PFI-1, a highly selective protein interaction inhibitor, targeting BET Bromodomains, Canc. Res. 73 (2013) 3336–3346.
[6] M.A. Dawson, R.K. Prinjha, A. Dittmann, G. Giotopoulos, M. Bantscheff, W.I. Chan, S.C. Robson, C.W. Chung, C. Hopf, M.M. Savitski, C. Huthmacher, E. Gudgin, D. Lugo, S. Beinke, T.D. Chapman, E.J. Roberts, P.E. Soden, K.R. Auger, O. Mirguet, K. Doehner, R. Delwel, A.K. Burnett, P. Jeffrey, G. Drewes, K. Lee, B.J. Huntly, T. Kouzarides, Inhibition of BET recruitment to chromatin as an effective treatment for MLL-fusion leukaemia, Nature 478 (2011) 529–533.
[7] T.D. Crawford, F.A. Romero, K.W. Lai, V. Tsui, A.M. Taylor, G. de Leon Boenig, C.L. Noland, J. Murray, J. Ly, E.F. Choo, T.L. Hunsaker, E.W. Chan, M. Merchant, S. Kharbanda, K.E. Gascoigne, S. Kaufman, M.H. Beresini, J. Liao, W. Liu, K.X. Chen, Z. Chen, A.R. Conery, A. Cote, H. Jayaram, Y. Jiang, J.R. Kiefer, T. Kleinheinz, Y. Li, J. Maher, E. Pardo, F. Poy, K.L. Spillane, F. Wang, J. Wang, X. Wei, Z. Xu, Z. Xu, I. Yen, L. Zawadzke, X. Zhu, S. Bellon, R. Cummings, A.G. Cochran, B.K. Albrecht, S. Magnuson, Discovery of a potent and selective in vivo probe (GNE-272) for the bromodomains of CBP/EP300, J. Med. Chem. 59 (2016) 10549–10563.
[8] D.A. Hay, O. Fedorov, S. Martin, D.C. Singleton, C. Tallant, C. Wells, S. Picaud, M. Philpott, O.P. Monteiro, C.M. Rogers, S.J. Conway, T.P. Rooney, A. Tumber, C. Yapp, P. Filippakopoulos, M.E. Bunnage, S. Muller, S. Knapp, C.J. Schofield, P.E. Brennan, Discovery and optimization of small-molecule ligands for the CBP/p300 bromodomains, J. Am. Chem. Soc. 136 (2014) 9308–9319.
[9] S. Picaud, O. Fedorov, A. Thanasopoulou, K. Leonards, K. Jones, J. Meier, H. Olzscha, O. Monteiro, S. Martin, M. Philpott, A. Tumber, P. Filippakopoulos, C. Yapp, C. Wells, K.H. Che, A. Bannister, S. Robson, U. Kumar, N. Parr, K. Lee, D. Lugo, P. Jeffrey, S. Taylor, M.L. Vecellio, C. Bountra, P.E. Brennan, A. O'Mahony, S. Velichko, S. Muller, D. Hay, D.L. Daniels, M. Urh, N.B. La Thangue, T. Kouzarides, R. Prinjha, J. Schwaller, S. Knapp, Generation of a selective small molecule inhibitor of the CBP/p300 bromodomain for leukemia therapy, Canc. Res. 75 (2015) 5106–5119.
[10] A.M. Taylor, A. Cote, M.C. Hewitt, R. Pastor, Y. Leblanc, C.G. Nasveschuk, F.A. Romero, T.D. Crawford, N. Cantone, H. Jayaram, J. Setser, J. Murray, M.H. Beresini, G. de Leon Boenig, Z. Chen, A.R. Conery, R.T. Cummings, L.A. Dakin, E.M. Flynn, O.W. Huang, S. Kaufman, P.J. Keller, J.R. Kiefer, T. Lai, Y. Li, J. Liao, W. Liu, H. Lu, E. Pardo, V. Tsui, J. Wang, Y. Wang, Z. Xu, F. Yan, D. Yu, L. Zawadzke, X. Zhu, X. Zhu, R.J. Sims 3rd, A.G. Cochran, S. Bellon, J.E. Audia, S. Magnuson, B.K. Albrecht, Fragment-based discovery of a selective and cell-active benzodiazepinone CBP/EP300 bromodomain inhibitor (CPI-637), ACS Med. Chem. Lett. 7 (2016) 531–536.
[11] A. Unzue, M. Xu, J. Dong, L. Wiedmer, D. Spiliotopoulos, A. Caflisch, C. Nevado, Fragment-based design of selective nanomolar ligands of the CREBBP bromodomain, J. Med. Chem. 59 (2016) 1350–1356.
[12] P.G. Clark, L.C. Vieira, C. Tallant, O. Fedorov, D.C. Singleton, C.M. Rogers, O.P. Monteiro, J.M. Bennett, R. Baronio, S. Muller, D.L. Daniels, J. Mendez, S. Knapp, P.E. Brennan, D.J. Dixon, LP99: discovery and synthesis of the first selective BRD7/9 bromodomain inhibitor, Angew Chem. Int. Ed. Engl. 54 (2015) 6217–6221.
[13] L.J. Martin, M. Koegl, G. Bader, X.L. Cockcroft, O. Fedorov, D. Fiegen, T. Gerstberger, M.H. Hofmann, A.F. Hohmann, D. Kessler, S. Knapp, P. Knesl, S. Kornigg, S. Muller, H. Nar, C. Rogers, K. Rumpel, O. Schaaf, S. Steurer, C. Tallant, C.R. Vakoc, M. Zeeb, A. Zoephel, M. Pearson, G. Boehmelt, D. McConnell, Structure-based design of an in vivo active selective BRD9 inhibitor, J. Med. Chem. 59 (2016) 4462–4475.
[14] N.H. Theodoulou, P. Bamborough, A.J. Bannister, I. Becher, R.A. Bit, K.H. Che, C.W. Chung, A. Dittmann, G. Drewes, D.H. Drewry, L. Gordon, P. Grandi, M. Leveridge, M. Lindon, A.M. Michon, J. Molnar, S.C. Robson, N.C. Tomkinson, T. Kouzarides, R.K. Prinjha, P.G. Humphreys, Discovery of I-BRD9, a selective cell active chemical probe for bromodomain containing protein 9 inhibition, J. Med. Chem. 59 (2016) 1425–1439.
[15] P. Chen, A. Chaikuad, P. Bamborough, M. Bantscheff, C. Bountra, C.W. Chung, O. Fedorov, P. Grandi, D. Jung, R. Lesniak, M. Lindon, S. Muller, M. Philpott, R. Prinjha, C. Rogers, C. Selenski, C. Tallant, T. Werner, T.M. Willson, S. Knapp, D.H. Drewry, Discovery and characterization of GSK2801, a selective chemical probe for the bromodomains BAZ2A and BAZ2B, J. Med. Chem. 59 (2016) 1410–1424.
[16] L. Drouin, S. McGrath, L.R. Vidler, A. Chaikuad, O. Monteiro, C. Tallant, M. Philpott, C. Rogers, O. Fedorov, M. Liu, W. Akhtar, A. Hayes, F. Raynaud, S. Muller, S. Knapp, S. Hoelder, Structure enabled design of BAZ2-ICR, a chemical probe targeting the bromodomains of BAZ2A and BAZ2B, J. Med. Chem. 58 (2015) 2553–2559.
[17] B.S. Gerstenberger, J.D. Trzupek, C. Tallant, O. Fedorov, P. Filippakopoulos, P.E. Brennan, V. Fedele, S. Martin, S. Picaud, C. Rogers, M. Parikh, A. Taylor, B. Samas, A. O'Mahony, E. Berg, G. Pallares, A.D. Torrey, D.K. Treiber, I.J. Samardjiev, B.T. Nasipak, T. Padilla-Benavides, Q. Wu, A.N. Imbalzano, J.A. Nickerson, M.E. Bunnage, S. Muller, S. Knapp, D.R. Owen, Identification of a chemical probe for family VIII bromodomains through optimization of a fragment hit, J. Med. Chem. 59 (2016) 4800–4811.
[18] M. Moustakim, P.G. Clark, L. Trulli, A.L. Fuentes de Arriba, M.T. Ehebauer, A. Chaikuad, E.J. Murphy, J. Mendez-Johnson, D. Daniels, C.D. Hou, Y.H. Lin, J.R. Walker, R. Hui, H. Yang, L. Dorrell, C.M. Rogers, O.P. Monteiro, O. Fedorov, K.V. Huber, S. Knapp, J. Heer, D.J. Dixon, P.E. Brennan, Discovery of a PCAF bromodomain chemical probe, Angew Chem. Int. Ed. Engl. 56 (2017) 827–831.
[19] P. Bamborough, C.W. Chung, E.H. Demont, R.C. Furze, A.J. Bannister, K.H. Che, H. Diallo, C. Douault, P. Grandi, T. Kouzarides, A.M. Michon, D.J. Mitchell, R.K. Prinjha, C. Rau, S. Robson, R.J. Sheppard, R. Upton, R.J. Watson, A chemical probe for the ATAD2 bromodomain, Angew Chem. Int. Ed. Engl. 55 (2016) 11382–11386.
[20] A. Vezzoli, N. Bonadies, M.D. Allen, S.M. Freund, C.M. Santiveri, B.T. Kvinlaug, B.J. Huntly, B. Gottgens, M. Bycroft, Molecular basis of histone H3K36me3 recognition by the PWWP domain of Brpf1, Nat. Struct. Mol. Biol. 17 (2010) 617–619.
[21] A. Poplawski, K. Hu, W. Lee, S. Natesan, D. Peng, S. Carlson, X. Shi, S. Balaz, J.L. Markley, K.C. Glass, Molecular insights into the recognition of N-terminal histone modifications by the BRPF1 bromodomain, J. Mol. Biol. 426 (2014) 1661–1676.
[22] T. Brown, J. Swansbury, M.M. Taj, Prognosis of patients with t(8;16)(p11;p13)

acute myeloid leukemia, Leuk. Lymphoma 53 (2012) 338–341.
[23] J. Borrow, V.P. Stanton Jr., J.M. Andresen, R. Becher, F.G. Behm, R.S. Chaganti, C.I. Civin, C. Disteche, I. Dube, A.M. Frischauf, D. Horsman, F. Mitelman, S. Volinia, A.E. Watmore, D.E. Housman, The translocation t(8;16)(p11;p13) of acute myeloid leukaemia fuses a putative acetyltransferase to the CREB-binding protein, Nat. Genet. 14 (1996) 33–41.
[24] I. Kitabayashi, Y. Aikawa, A. Yokoyama, F. Hosoda, M. Nagai, N. Kakazu, T. Abe, M. Ohki, Fusion of MOZ and p300 histone acetyltransferases in acute monocytic leukemia with a t(8;22)(p11;q13) chromosome translocation, Leukemia 15 (2001) 89–94.
[25] M. Carapeti, R.C. Aguiar, J.M. Goldman, N.C. Cross, A novel fusion between MOZ and the nuclear receptor coactivator TIF2 in acute myeloid leukemia, Blood 91 (1998) 3127–3133.
[26] P.J. Troke, K.B. Kindle, H.M. Collins, D.M. Heery, MOZ fusion proteins in acute myeloid leukaemia, Biochem. Soc. Symp. (2006) 23–39.
[27] P. Bamborough, H.A. Barnett, I. Becher, M.J. Bird, C.W. Chung, P.D. Craggs, E.H. Demont, H. Diallo, D.J. Fallon, L.J. Gordon, P. Grandi, C.I. Hobbs, E. Hooper-Greenhill, E.J. Jones, R.P. Law, A. Le Gall, D. Lugo, A.M. Michon, D.J. Mitchell, R.K. Prinjha, R.J. Sheppard, A.J. Watson, R.J. Watson, GSK6853, a chemical probe for inhibition of the BRPF1 bromodomain, ACS Med. Chem. Lett. 7 (2016) 552–557.
[28] J. Bennett, O. Fedorov, C. Tallant, O. Monteiro, J. Meier, V. Gamble, P. Savitsky, G.A. Nunez-Alonso, B. Haendler, C. Rogers, P.E. Brennan, S. Muller, S. Knapp, Discovery of a chemical tool inhibitor targeting the bromodomains of TRIM24 and BRPF, J. Med. Chem. 59 (2016) 1642–1647.
[29] N. Igoe, E.D. Bayle, O. Fedorov, C. Tallant, P. Savitsky, C. Rogers, D.R. Owen, G. Deb, T.C. Somervaille, D.M. Andrews, N. Jones, A. Cheasty, H. Ryder, P.E. Brennan, S. Muller, S. Knapp, P.V. Fish, Design of a biased potent small molecule inhibitor of the bromodomain and PHD finger-containing (BRPF) proteins suitable for cellular and in vivo studies, J. Med. Chem. 60 (2017) 668–680.
[30] N. Igoe, E.D. Bayle, C. Tallant, O. Fedorov, J.C. Meier, P. Savitsky, C. Rogers, Y. Morias, S. Scholze, H. Boyd, D. Cunoosamy, D.M. Andrews, A. Cheasty, P.E. Brennan, S. Muller, S. Knapp, P.V. Fish, Design of a chemical probe for the bromodomain and plant homeodomain finger-containing (BRPF) family of proteins, J. Med. Chem. 60 (2017) 6998–7011.
[31] J. Zhu, A. Caflisch, Twenty crystal structures of bromodomain and PHD finger containing protein 1 (BRPF1)/Ligand complexes reveal conserved binding motifs and rare interactions, J. Med. Chem. 59 (2016) 5555–5561.
[32] P. Sledz, A. Caflisch, Protein structure-based drug design: from docking to molecular dynamics, Curr. Opin. Struct. Biol. 48 (2017) 93–102.
[33] H. Zhao, A. Caflisch, Molecular dynamics in drug design, Eur. J. Med. Chem. 91 (2015) 4–14.
[34] D.R. Koes, C.J. Camacho, ZINCPharmer: pharmacophore search of the ZINC database, Nucleic Acids Res. 40 (2012) W409–W414.
[35] O. Trott, A.J. Olson, AutoDock Vina: improving the speed and accuracy of docking with a new scoring function, efficient optimization, and multithreading, J. Comput. Chem. 31 (2010) 455–461.
[36] L.W. Elizabeth Quinn, Pietro Ciceri, Gabriel Pallares, Elyssa Pickle, Adam Torrey, Mark Floyd, Jeremy Hunt, Daniel Treiber, BROMOscan - a high throughput, quantitative ligand binding platform identifies best-in-class bromodomain inhibitors from a screen of mature compounds targeting other protein classes, Canc. Res. 2013 (2013) 4238.
[37] J.J. Irwin, T. Sterling, M.M. Mysinger, E.S. Bolstad, R.G. Coleman, ZINC: a free tool to discover chemistry for biology, J. Chem. Inf. Model. 52 (2012) 1757–1768.
[38] B.R. Brooks, C.L. Brooks 3rd, A.D. Mackerell Jr., L. Nilsson, R.J. Petrella, B. Roux, Y. Won, G. Archontis, C. Bartels, S. Boresch, A. Caflisch, L. Caves, Q. Cui, A.R. Dinner, M. Feig, S. Fischer, J. Gao, M. Hodoscek, W. Im, K. Kuczera, T. Lazaridis, J. Ma, V. Ovchinnikov, E. Paci, R.W. Pastor, C.B. Post, J.Z. Pu, M. Schaefer, B. Tidor, R.M. Venable, H.L. Woodcock, X. Wu, W. Yang, D.M. York, M. Karplus, CHARMM: the biomolecular simulation program, J. Comput. Chem. 30 (2009) 1545–1614.
[39] J.R. Marchand, A. Dalle Vedove, G. Lolli, A. Caflisch, Discovery of inhibitors of four bromodomains by fragment-anchored ligand docking, J. Chem. Inf. Model. 57 (2017) 2584–2597.
[40] G. Neudert, G. Klebe, DSX: a knowledge-based scoring function for the assessment of protein-ligand complexes, J. Chem. Inf. Model. 51 (2011) 2731–2745.
[41] M. Philpott, J. Yang, T. Tumber, O. Fedorov, S. Uttarkar, P. Filippakopoulos, S. Picaud, T. Keates, I. Felletar, A. Ciulli, S. Knapp, T.D. Heightman, Bromodomain-peptide displacement assays for interactome mapping and inhibitor discovery, Mol. Biosyst. 7 (2011) 2899–2908.
[42] A. Magno, S. Steiner, A. Caflisch, Mechanism and kinetics of acetyl-lysine binding to bromodomains, J. Chem. Theor. Comput. 9 (2013) 4225–4232.
[43] S. Steiner, A. Magno, D. Huang, A. Caflisch, Does bromodomain flexibility influence histone recognition? FEBS Lett. 587 (2013) 2158–2163.
[44] D.S. Hewings, M. Wang, M. Philpott, O. Fedorov, S. Uttarkar, P. Filippakopoulos, S. Picaud, C. Vuppusetty, B. Marsden, S. Knapp, S.J. Conway, T.D. Heightman, 3,5-dimethylisoxazoles act as acetyl-lysine-mimetic bromodomain ligands, J. Med. Chem. 54 (2011) 6761–6770.
[45] D.S. Hewings, O. Fedorov, P. Filippakopoulos, S. Martin, S. Picaud, A. Tumber, C. Wells, M.M. Olcina, K. Freeman, A. Gill, A.J. Ritchie, D.W. Sheppard, A.J. Russell, E.M. Hammond, S. Knapp, P.E. Brennan, S.J. Conway, Optimization of 3,5-dimethylisoxazole derivatives as potent bromodomain ligands, J. Med. Chem. 56 (2013) 3217–3227.
[46] O. Mirguet, Y. Lamotte, F. Donche, J. Toum, F. Gellibert, A. Bouillot, R. Gosmini, V.L. Nguyen, D. Delannee, J. Seal, F. Blandel, A.B. Boullay, E. Boursier, S. Martin, J.M. Brusq, G. Krysa, A. Riou, R. Tellier, A. Costaz, P. Huet, Y. Dudit, L. Trottet, J. Kirilovsky, E. Nicodeme, From ApoA1 upregulation to BET family bromodomain inhibition: discovery of I-BET151, Bioorg. Med. Chem. Lett 22 (2012) 2963–2967.
[47] J. Seal, Y. Lamotte, F. Donche, A. Bouillot, O. Mirguet, F. Gellibert, E. Nicodeme, G. Krysa, J. Kirilovsky, S. Beinke, S. McCleary, I. Rioja, P. Bamborough, C.W. Chung, L. Gordon, T. Lewis, A.L. Walker, L. Cutler, D. Lugo, D.M. Wilson, J. Witherington, K. Lee, R.K. Prinjha, Identification of a novel series of BET family bromodomain inhibitors: binding mode and profile of I-BET151 (GSK1210151A), Bioorg. Med. Chem. Lett 22 (2012) 2968–2972.
[48] G. Klebe, Applying thermodynamic profiling in lead finding and optimization, Nat. Rev. Drug Discov. 14 (2015) 95–110.
[49] M. Xu, A. Unzue, J. Dong, D. Spiliotopoulos, C. Nevado, A. Caflisch, Discovery of CREBBP bromodomain inhibitors by high-throughput docking and hit optimization guided by molecular dynamics, J. Med. Chem. 59 (2016) 1340–1349.
[50] A. Unzue, H. Zhao, G. Lolli, J. Dong, J. Zhu, M. Zechner, A. Dolbois, A. Caflisch, C. Nevado, The “gatekeeper” residue influences the mode of binding of acetyl indoles to bromodomains, J. Med. Chem. 59 (2016) 3087–3097.
[51] K. Vanommeslaeghe, A.D. MacKerell Jr., Automation of the CHARMM General Force Field (CGenFF) I: bond perception and atom typing, J. Chem. Inf. Model. 52 (2012) 3144–3154.
[52] G. Landrum, RDKit: open-source cheminformatics, in.
[53] S. Keller, C. Vargas, H. Zhao, G. Piszczek, C.A. Brautigam, P. Schuck, High-precision isothermal titration calorimetry with automated peak-shape analysis, Anal. Chem. 84 (2012) 5066–5073.
[54] H. Zhao, G. Piszczek, P. Schuck, SEDPHAT–a platform for global ITC analysis and global multi-method analysis of molecular interactions, Methods 76 (2015) 137–148.
[55] C.A. Brautigam, H. Zhao, C. Vargas, S. Keller, P. Schuck, Integration and global analysis of isothermal titration calorimetry data for studying macromolecular interactions, Nat. Protoc. 11 (2016) 882–894.
[56] W. Kabsch, Integration, scaling, space-group assignment and post-refinement, Acta Crystallogr D Biol Crystallogr 66 (2010) 133–144.
[57] P.R. Evans, G.N. Murshudov, How good are my data and what is the resolution? Acta Crystallogr D Biol Crystallogr 69 (2013) 1204–1214.
[58] A. Vagin, A. Teplyakov, Molecular replacement with MOLREP, Acta Crystallogr D Biol Crystallogr 66 (2010) 22–25.
[59] M.D. Winn, C.C. Ballard, K.D. Cowtan, E.J. Dodson, P. Emsley, P.R. Evans, R.M. Keegan, E.B. Krissinel, A.G. Leslie, A. McCoy, S.J. McNicholas, G.N. Murshudov, N.S. Pannu, E.A. Potterton, H.R. Powell, R.J. Read, A. Vagin, K.S. Wilson, Overview of the CCP4 suite and current developments, Acta Crystallogr D Biol Crystallogr 67 (2011) 235–242.
[60] P.D. Adams, P.V. Afonine, G. Bunkoczi, V.B. Chen, I.W. Davis, N. Echols, J.J. Headd, L.W. Hung, G.J. Kapral, R.W. Grosse-Kunstleve, A.J. McCoy, N.W. Moriarty, R. Oeffner, R.J. Read, D.C. Richardson, J.S. Richardson, T.C. Terwilliger, P.H. Zwart, PHENIX: a comprehensive Python-based system for macromolecular structure solution, Acta Crystallogr D Biol Crystallogr 66 (2010) 213–221.
[61] P. Emsley, B. Lohkamp, W.G. Scott, K. Cowtan, Features and development of coot, Acta Crystallogr D Biol Crystallogr 66 (2010) 486–501.
[62] A.W. Schuttelkopf, D.M. van Aalten, PRODRG: a tool for high-throughput crystallography of protein-ligand complexes, Acta Crystallogr D Biol Crystallogr 60 (2004) 1355–1363.
[63] S. Pronk, S. Pall, R. Schulz, P. Larsson, P. Bjelkmar, R. Apostolov, M.R. Shirts, J.C. Smith, P.M. Kasson, D. van der Spoel, B. Hess, E. Lindahl, GROMACS 4.5: a high-throughput and highly parallel open source molecular simulation toolkit, Bioinformatics 29 (2013) 845–854.
[64] D. Spiliotopoulos, E.C. Wamhoff, G. Lolli, C. Rademacher, A. Caflisch, Discovery of BAZ2A bromodomain ligands, Eur. J. Med. Chem. 139 (2017) 564–572.
[65] D. Spiliotopoulos, J. Zhu, E.C. Wamhoff, N. Deerain, J.R. Marchand, J. Aretz, C. Rademacher, A. Caflisch, Virtual screen to NMR (VS2NMR): discovery of fragment hits for the CBP bromodomain, Bioorg. Med. Chem. Lett 27 (2017) 2472–2478.
[66] J. Huang, A.D. MacKerell Jr., CHARMM36 all-atom additive protein force field: validation based on comparison to NMR data, J. Comput. Chem. 34 (2013) 2135–2145.

Supporting Information

Structure-based discovery of selective BRPF1 bromodomain inhibitors

Jian Zhu[1], Chunxian Zhou[2] and Amedeo Caflisch*[1]

[1]Department of Biochemistry, University of Zurich, Winterthurerstrasse 190, CH-8057 Zurich, Switzerland

[2]Department of Pathology, Shanghai University of Traditional Chinese Medicine, Cailun Road 1200, Pudong District, Shanghai, China

*E-mail: caflisch@bioc.uzh.ch

Table S1. X-ray data collection and refinement statistics for the structures of the BRPF1 bromodomain in complex with small molecules identified by virtual screening.

PDB ID	**5O5A**	**5O5F**	**5O55**	**5O4T**
Compound	**2**	**7**	**8**	**9**
Data Collection				
space group	$P3_221$	$P3_221$	$P3_221$	$P3_221$
Cell dimensions a, b, c (Å)	60.69, 60.69, 63.04	60.76, 60.76, 63.52	60.86, 60.86, 62.99	60.64, 60.64, 63.47
Cell dimensions α, β, γ (°)	90.00, 90.00, 120.00	90.00, 90.00, 120.00	90.00, 90.00, 120.00	90.00, 90.00, 120.00
resolution (Å)	40.37 - 1.60	40.52 - 1.30	31.57 - 1.45	40.46 - 1.50
unique observations*	18144(900)	33637 (1591)	24259 (3462)	21891(1029)
completeness*	99.9 (100.0)	99.08 (96.04)	99.8 (99.0)	99.4(97.4)
redundancy*	10.6 (10.0)	7.3 (4.6)	9.4 (8.1)	13.2(12.9)
Rmerge*	0.043 (0.633)	0.022 (0.437)	0.031 (0.468)	0.090(0.642)
CC(1/2)	0.999 (0.879)	1.000 (0.802)	1.000 (0.999)	0.997(0.812)
I/σI*	25.5 (3.7)	37.3 (3.1)	31.2 (4.5)	16.9(3.0)
Refinement				
R_{work}/R_{free}*	0.189(0.229)/0.194(0.292)	0.199(0.233)/0.225(0.252)	0.196(0.208)/0.205(0.268)	0.182(0.247)/0.212(0.271)
r.m.s deviations bond (Å)	0.008	0.006	0.007	0.005
r.m.s deviations angles (°)	0.879	0.666	0.765	0.723
B-factors(P/L/O) ($Å^2$) **	37.5/41.9/45.5	20.7/27.0/34.1	30.6/32.0/41.7	28.9/35.3/39.5
Ramanchandran Favored	98.25	100.00	99.12	99.10
Ramanchandran Allowed	1.75	0.00	0.88	0.90
Ramanchandran Disallowed	0.00	0.00	0.00	0.00

PDB ID	**5OV8**	**5MWG**	**5MWH**	**5O4S**
Compound	**13**	**16**	**21**	**26**
Data Collection				
space group	$P2_1$	$P2_1$	$P2_1$	$P2_1$
Cell dimensions a, b, c (Å)	48.19, 56.54, 48.60	48.60, 61.14, 48.60	60.69, 60.69, 63.04	48.61, 62.69, 48.82
Cell dimensions α, β, γ (°)	90.00, 102.41, 90.00	90.00, 101.63, 90.00	90.00, 90.00, 120.00	90.00, 101.81, 90.00
resolution (Å)	47.46 - 1.80	37.56 – 1.50	38.19 - 1.65	38.00 - 1.75
unique observations*	23018(1295)	42415(1960)	34911(1685)	29072(1578)
completeness*	97.1(93.1)	95.0(89.2)	99.5 (96.7)	99.9(99.4)
redundancy*	3.9(3.9)	6.8(3.5)	13.3(9.1)	13.2(12.9)
Rmerge*	0.040(0.220)	0.209(0.253)	0.135(0.816)	0.151(0.730)
CC(1/2)	0.998(0.946)	0.990(0.914)	0.998(0.864)	0.985(0.961)
I/σI*	18.7(4.3)	12.5(5.2)	21.6 (2.1)	22.6(4.1)
Refinement				
R_{work}/R_{free}*	0.196(0.230)/0.243(0.315)	0.224(0.256)/0.243(0.320)	0.186(0.295)/0.221(0.305)	0.178(0.254)/0.220(0.297)
r.m.s deviations bond (Å)	0.006	0.006	0.006	0.006
r.m.s deviations angles (°)	0.804	0.887	0.773	0.722
B-factors(P/L/O) ($Å^2$) **	26.9/29.7/36.7	24.9/28.0/35.0	37.7/40.2/45.8	35.8/38.0/42.8
Ramanchandran Favored	99.08	99.54	98.62	100.00
Ramanchandran Allowed	0.92	0.46	1.38	0.00
Ramanchandran Disallowed	0.00	0.00	0.00	0.00

PDB ID	**5MWZ**	**5OWA**	**6EKQ**	**5O5H**
Ligand	**36**	**42**	**42**	**43**
Data Collection				
space group	$P3_221$	$P2_1$	C2	$P3_221$
Cell dimensions a, b, c (Å)	60.86, 60.86, 62.99	34.89, 92.30, 81.22	71.21, 57.78, 70.45	61.03, 61.03, 63.79
Cell dimensions α, β, γ (°)	90.00, 90.00, 120.00	90.00, 101.22, 90.00	90.00, 108.66, 90.00	90.00, 90.00, 120.00
resolution (Å)	40.46 - 1.25	39.93 - 1.95	43.89 – 1.65	40.70 – 1.85
unique observations*	37830(1871)	34898(5200)	32602(1588)	12134(740)
completeness*	99.9(99.9)	94.9(96.5)	99.7(100.0)	100.0(100.0)
redundancy*	18.4(16.8)	3.3(3.4)	4.6(4.2)	18.6(19.2)
Rmerge*	0.056(0.452)	0.083(0.469)	0.046(0.345)	0.041(0.640)
CC(1/2)	0.999(0.957)	0.991(0.762)	0.999(0.879)	1.000(0.955)
I/σI*	31.4(7.9)	12.0(2.6)	18.0(3.4)	43.9(5.4)
Refinement				
R_{work}/R_{free}*	0.163(0.165)/0.180(0.186)	0.219(0.309)/0.267(0.393)	0.156(0.188)/0.181(0.226)	0.190(0.409)/0.234(0.460)
r.m.s deviations bond (Å)	0.004	0.007	0.009	0.008
r.m.s deviations angles (°)	0.768	1.205	1.003	1.098
B-factors(P/L/O) ($Å^2$) **	15.4/22.5/29.4	40.4/44.7/42.4	20.2/18.9/35.3	35.6/51.7/43.4
Ramanchandran Favored	99.11	98.86	100.00	100
Ramanchandran Allowed	0.89	0.92	0.00	0
Ramanchandran Disallowed	0.00	0.23	0.00	0

* Statistics for the highest resolution shell is shown in parentheses.

* * P/L/O indicate protein, ligand in the active site and solvent molecules, respectively.

Table S2. 2D structures of the 1-ethyl-2,3-dioxo-4H-quinoxaline and 1-ethyl-3-methyl-2-oxoquinoxaline derivatives that did not show binding at the highest concentration tested.

2D Structure	AlphaScreen (IC50, uM) on BRPF1
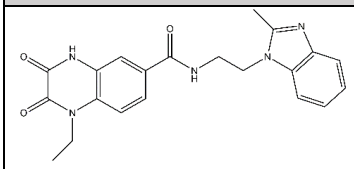	>10
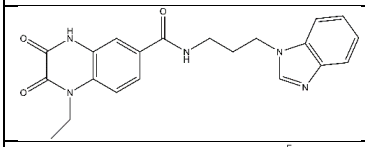	>10
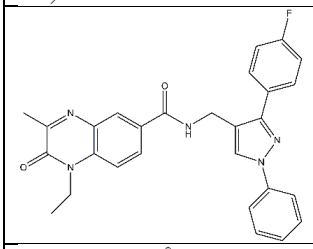	>10
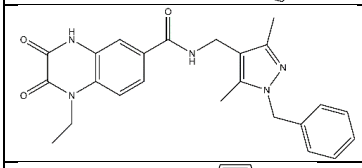	>100
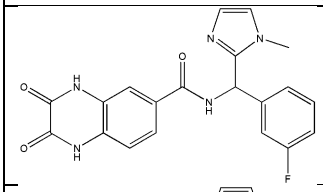	>50
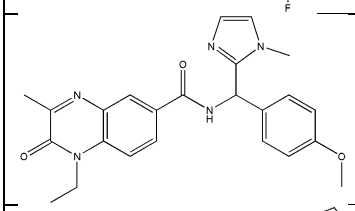	>10
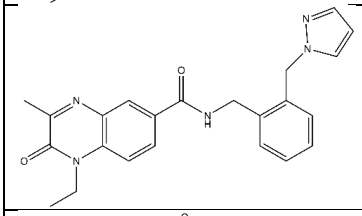	>10
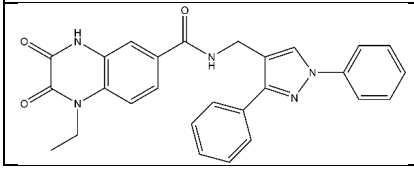	>100

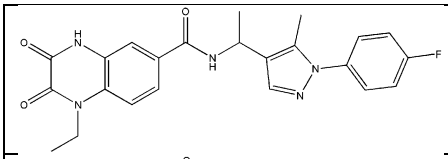	>25
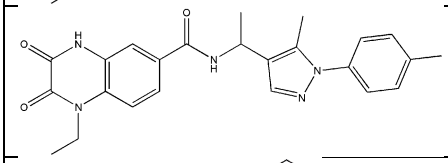	>100
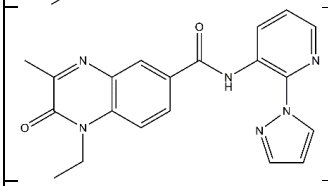	>10
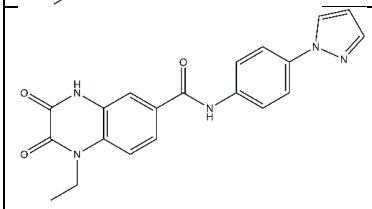	>10
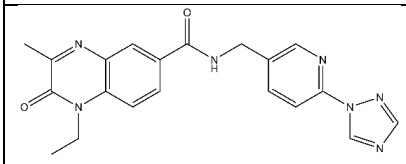	>50
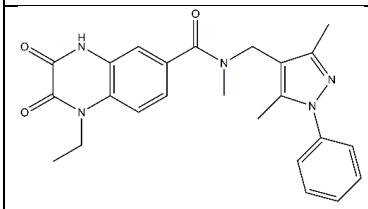	>100
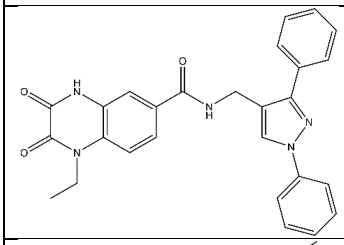	>50
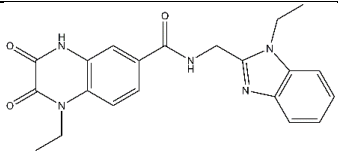	>10

Table S3. BromoScan assay results for selected compounds on BRPF1, TRIM24 and BRD4(1) bromodomains. The assays were performed in duplicate.

Cpd	BRPF1	TRIM24	BRD4(1)
1	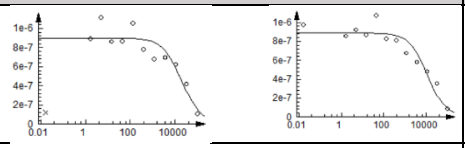		
2	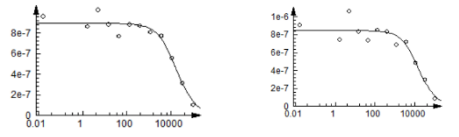	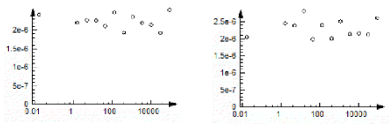	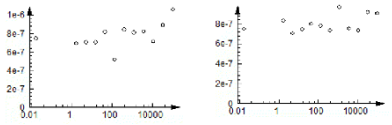
3	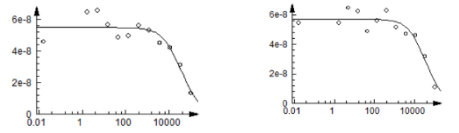		
4	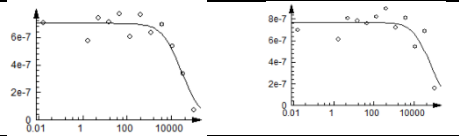		
5	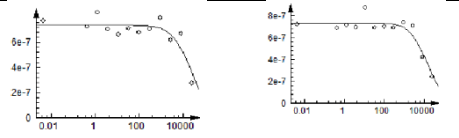	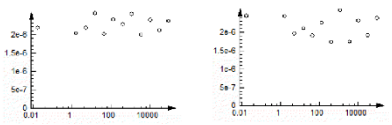	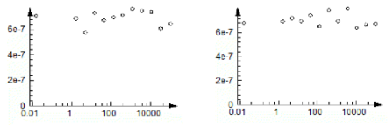
6	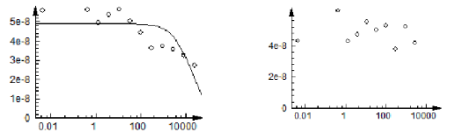		
8	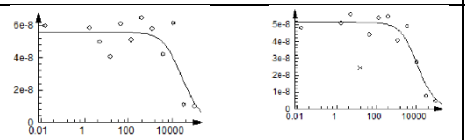	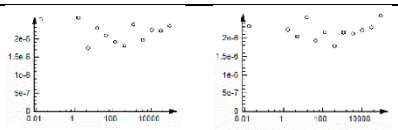	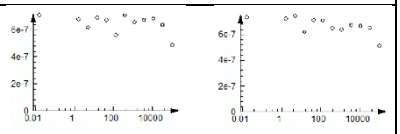
13	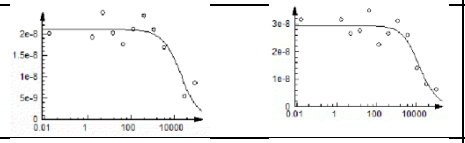		
14	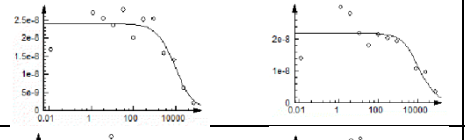		
20	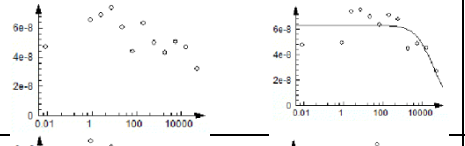		
21	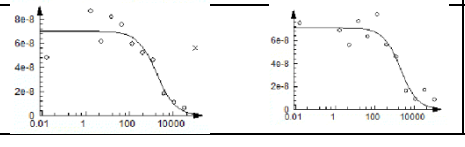		

28	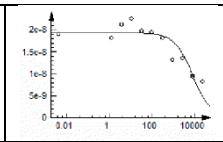	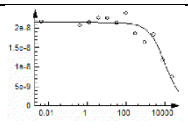		
36	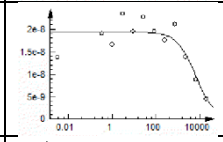	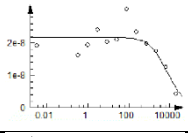		
42	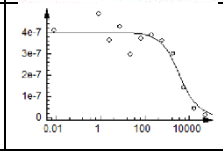	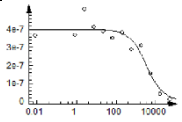	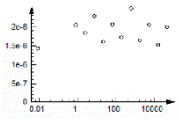 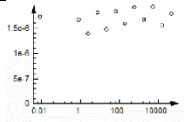	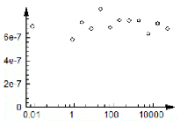 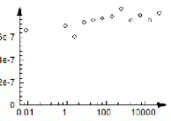

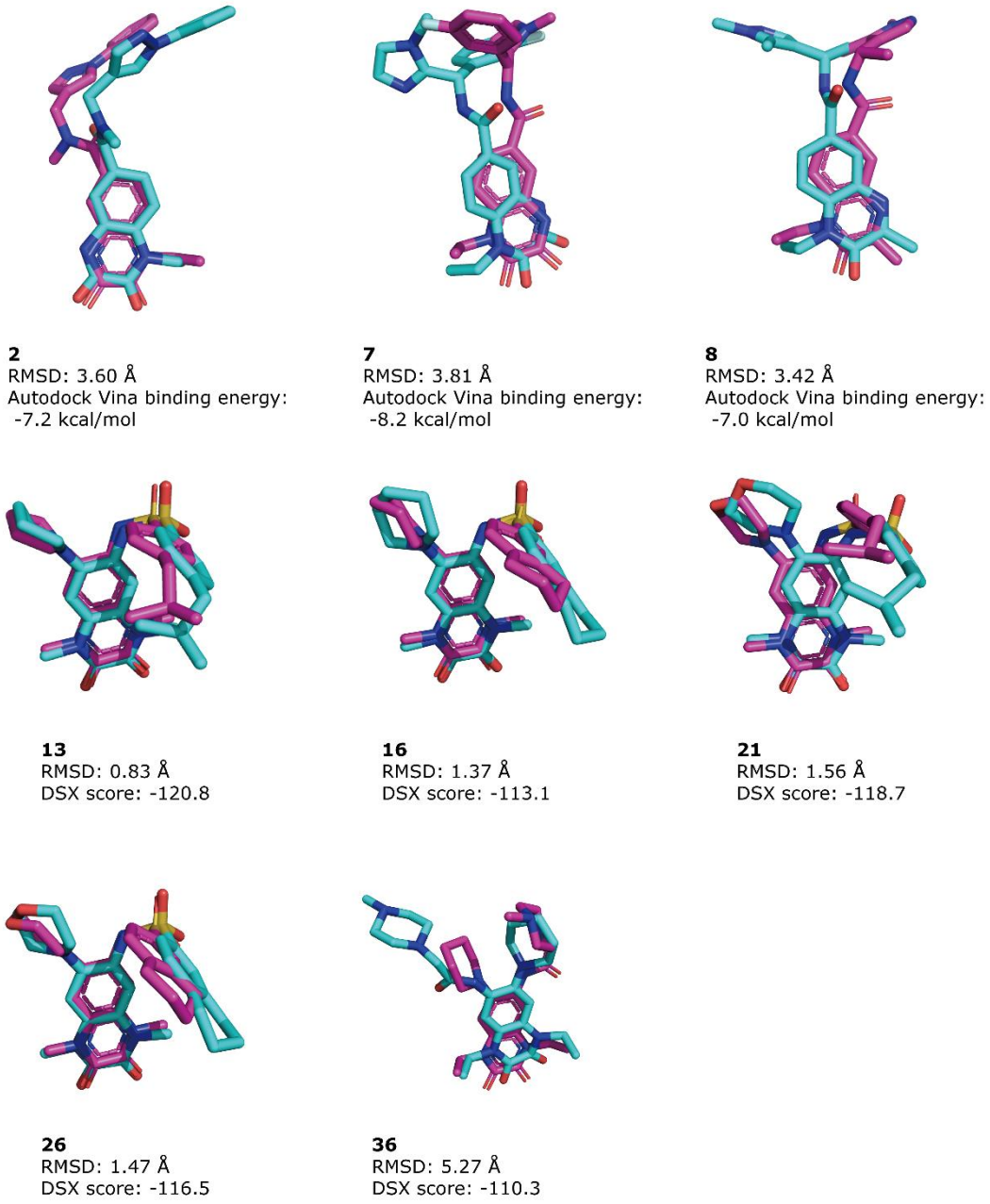

Fig. S1. Superimposition of the pose predicted by docking (cyan) and the corresponding binding mode in the crystal structures (magenta).

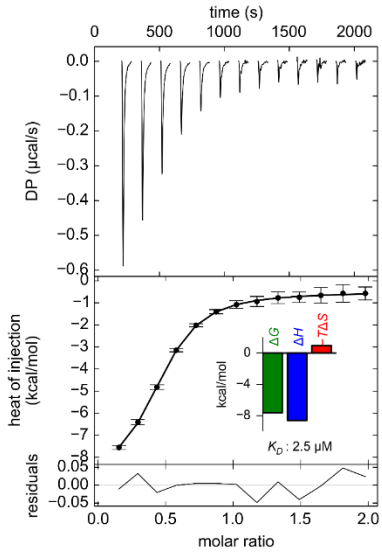

Fig. S2. Thermodynamic characterization of the BRPF1-**26** interaction by ITC. The Fig. shows thermographs (top), fit of integrated data (middle), and fit residuals (bottom).

Table S4. Analogues of compound **42** and their binding affinity measured by AlphaScreen.

2D Structure	Tanimoto coefficient with 42	AlphaScreen (IC50, uM)
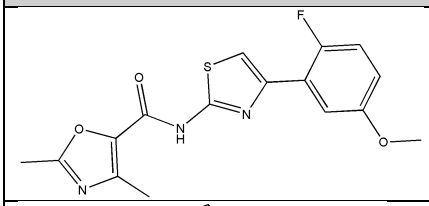	0.59	>200
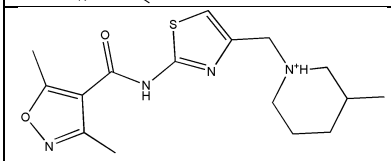	0.57	195
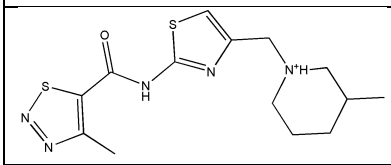	0.58	240
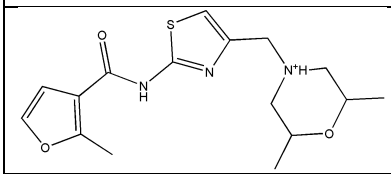	0.53	95.0 %Ctrl @100 uM
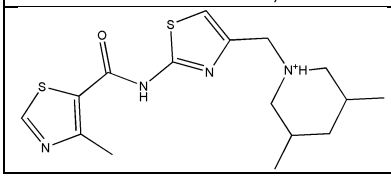	0.62	95.1 %Ctrl @100 uM

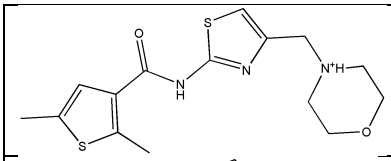	0.49	293
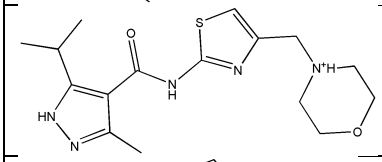	0.51	93.9 %Ctrl @100 uM
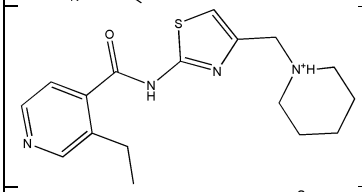	0.55	91.9 %Ctrl @100 uM
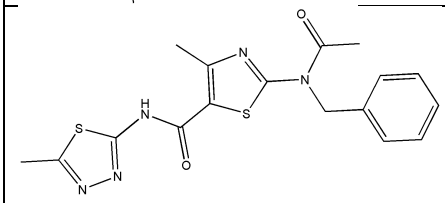	0.43	82.1 %Ctrl @100 uM
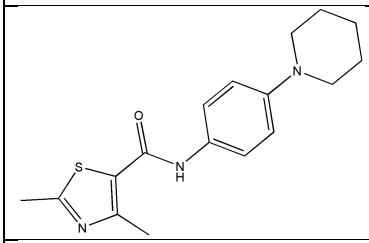	0.33	37.0 %Ctrl @100 uM
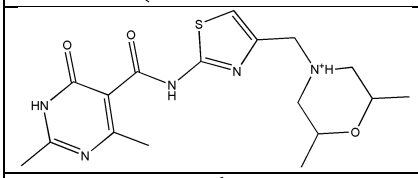	0.421	>500
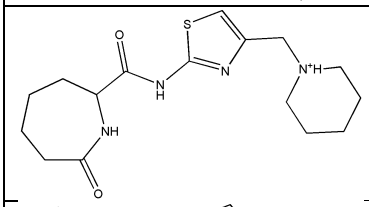	0.441	>500
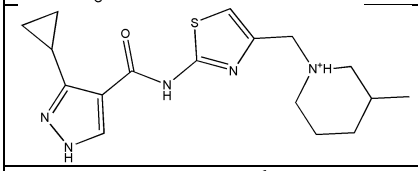	0.533	515
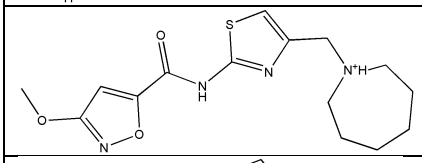	0.544	>200
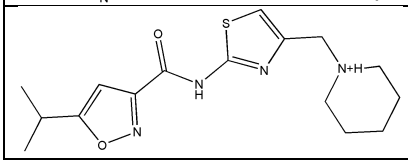	0.543	218

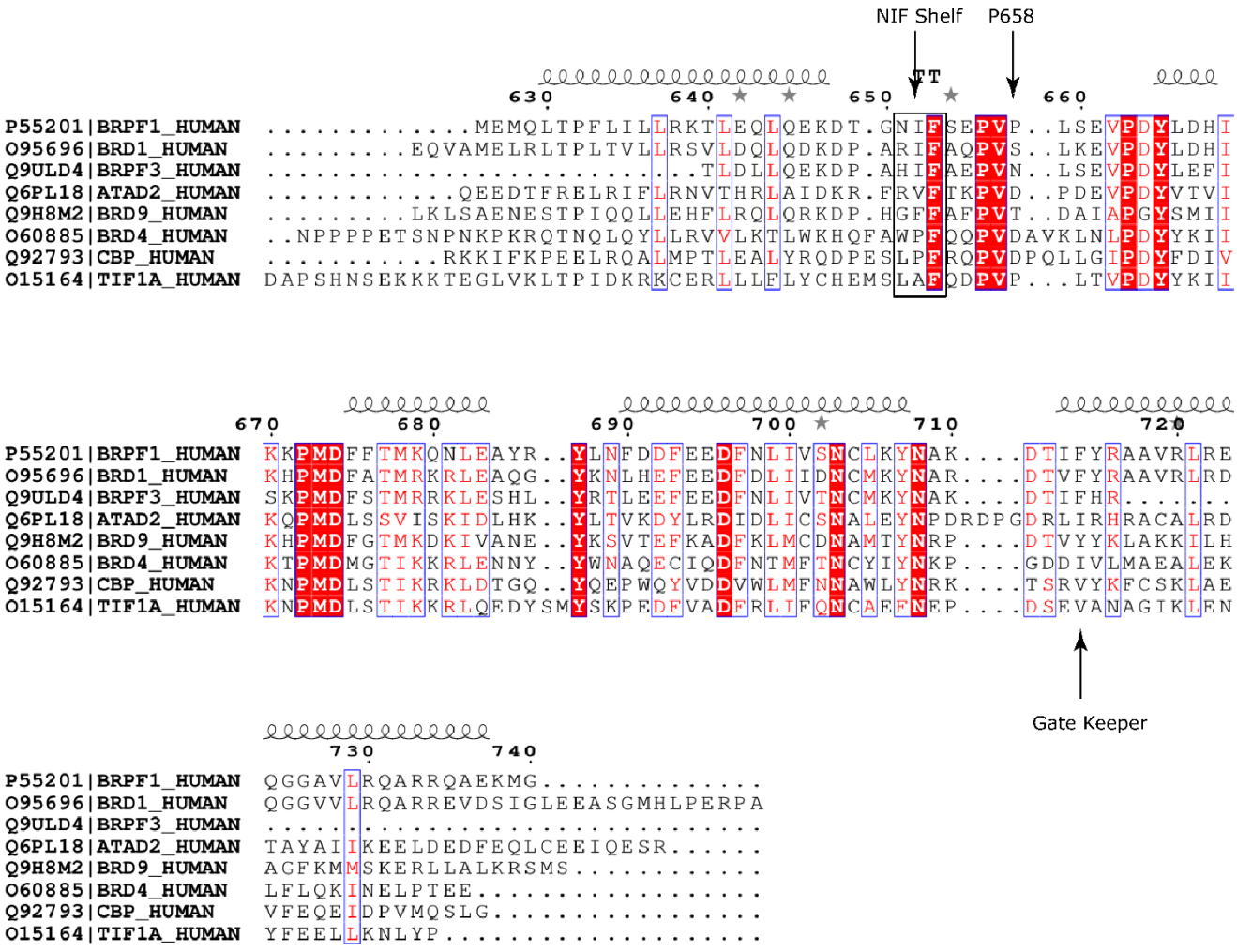

Fig. S3. Structure-based sequence alignment of the BRPF1 bromodomain with bromodomains of BRPF2 (BRD1), BRPF3, ATAD2, BRD9, BRD4(1), CREBBP (CBP) and TRIM24 (TIF1A). The sequence alignment was obtained with ESPript.[1]

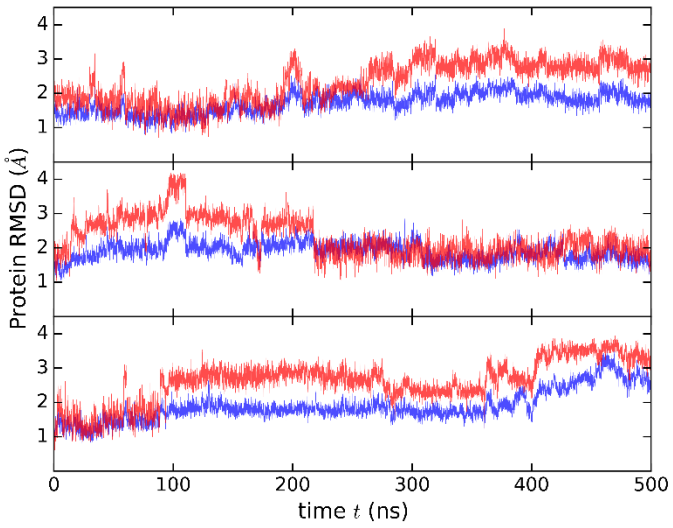

Fig. S4. Time series of RMSD from the X-ray structure along the three MD simulations of the BRPF1/**21** complex. RMSD time series for all Cα atoms (blue) and Cα atoms in the ZA loop segment 648-668(red) are shown.

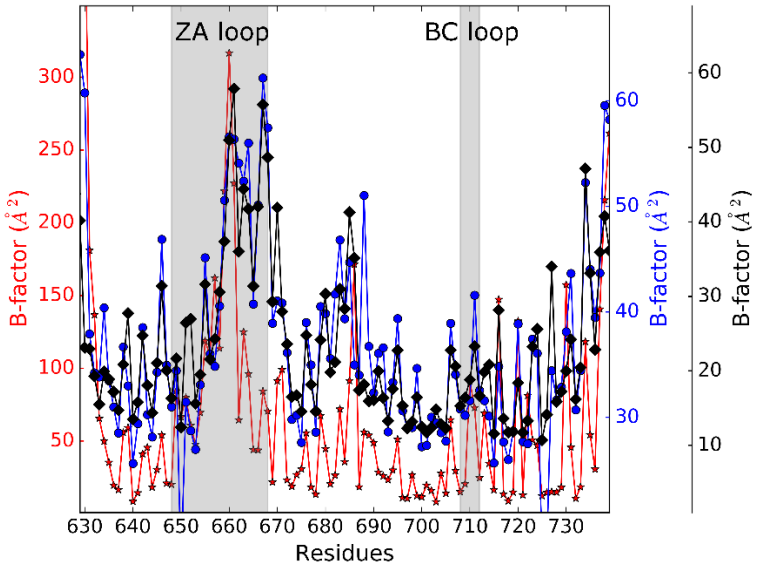

Fig. S5. Comparison of the B-factors calculated from the fluctuations of the atoms along the MD simulations of the BRPF1/**21** complex (red) and B-factors in X-ray crystals. The experimental B-factors are those of the crystal structure of the BRPF1/**21** complex (blue) and apo BRPF1 (PDB code 4LC2) (black). The ZA loop region (residues 648-668) and BC loop region (residues 708-712) are highlighted (grey vertical stripes). The function *gmx rmsf* in GROMACS was used to extract B-factors from the MD simulations.[2] B-factors were averaged over all non-hydrogen atoms for each residue.

References:

[1] X. Robert, P. Gouet, Deciphering key features in protein structures with the new ENDscript server, Nucleic Acids Res. 42 (2014) W320-324.
[2] S. Pronk, S. Pall, R. Schulz, P. Larsson, P. Bjelkmar, R. Apostolov, M.R. Shirts, J.C. Smith, P.M. Kasson, D. van der Spoel, B. Hess, E. Lindahl, GROMACS 4.5: a high-throughput and highly parallel open source molecular simulation toolkit, Bioinformatics 29 (2013) 845-854.

Chapter 4

Virtual screen to NMR (VS2NMR): Discovery of fragment hits for the CBP bromodomain

Spiliotopoulos D, **Zhu J**, Wamhoff EC, Deerain N, Marchand JR, Aretz J, Rademacher C, Caflisch A. Bioorganic & Medicinal Chemistry Letters. 2017; 27(11):2472-2478.

Bioorganic & Medicinal Chemistry Letters 27 (2017) 2472–2478

Contents lists available at ScienceDirect

Bioorganic & Medicinal Chemistry Letters

journal homepage: www.elsevier.com/locate/bmcl

Virtual screen to NMR (VS2NMR): Discovery of fragment hits for the CBP bromodomain

Dimitrios Spiliotopoulos [a,*], Jian Zhu [a], Eike-Christian Wamhoff [b,c], Nicholas Deerain [a], Jean-Rémy Marchand [a], Jonas Aretz [b,c], Christoph Rademacher [b,c], Amedeo Caflisch [a,*]

[a] Department of Biochemistry, University of Zürich, Winterthurerstrasse 190, CH-8057 Zürich, Switzerland
[b] Department of Biomolecular Systems, Max Planck Institute of Colloids and Interfaces, Am Mühlenberg 1, 14424 Potsdam, Germany
[c] Institute of Chemistry and Biochemistry, Department of Biology, Chemistry, and Pharmacy, Freie Universität Berlin, Takustraße 3, 14195 Berlin, Germany

ARTICLE INFO

Article history:
Received 7 February 2017
Revised 31 March 2017
Accepted 1 April 2017
Available online 4 April 2017

Keywords:
Docking
Virtual screening
NMR spectroscopy
Epigenetics
X-ray crystallography
Bromodomain inhibitors

ABSTRACT

Overexpression of the CREB-binding protein (CBP), a bromodomain-containing transcription coactivator involved in a variety of cellular processes, has been observed in several types of cancer with a correlation to aggressiveness. We have screened a library of nearly 1500 fragments by high-throughput docking into the CBP bromodomain followed by binding energy evaluation using a force field with electrostatic solvation. Twenty of the 39 fragments selected by virtual screening are positive in one or more ligand-observed nuclear magnetic resonance (NMR) experiments. Four crystal structures of the CBP bromodomain in complex with *in silico* screening hits validate the pose predicted by docking. Thus, the success ratio of the high-throughput docking procedure is 50% or 10% if one considers the validation by ligand-observed NMR spectroscopy or X-ray crystallography, respectively. Compounds **1** and **3** show favorable ligand efficiency in two different *in vitro* binding assays. The structure of the CBP bromodomain in the complex with the brominated pyrrole **1** suggests fragment growing by Suzuki coupling.

Bromodomains are protein-protein interaction modules that bind acetylated lysine (Kac)[1] or other acyl modifications of the lysine side chain.[2] The bromodomain fold consists of a left-handed four-helix bundle (helices Z, A, B, and C) with the interhelical loops ZA and BC flanking the rim of the acetyllysine-binding pocket.[3,4] The potential involvement of bromodomains in several types of cancer and inflammatory diseases[5] sparked interest in developing small molecules inhibiting their Kac-binding activity.[6]

The bromodomain of the lysine acetyltransferase CBP (the binding protein of the cyclic-AMP response element binding protein) has been the object of intense investigations due to the role of CBP in several cellular processes and implication in cancer.[7] Small-molecule ligands of the CBP bromodomain have been discovered by others using *in vitro* screening techniques[8–12] and in our research group by *in silico* screening (high-throughput docking).[13] The latter have been optimized by medicinal chemistry into potent and selective CBP bromodomain inhibitors.[14]

Here we report on the identification of ligand-efficient CBP bromodomain inhibitors via the computational screening of nearly 1500 small molecules. As a point of departure with respect to our previous virtual screening campaigns on CBP, here we take advantage of ligand-based NMR spectroscopy to validate the docking results. We call the sequential *in silico* to *in vitro* strategy Virtual Screen to NMR (VS2NMR).

In an effort to identify ligand-efficient small molecule inhibitors of the CBP bromodomain, we performed a rigid-ligand docking screen taking advantage of the software SEED.[16,17] A library of 1413 small molecules was docked into the acetyllysine binding site of the CBP bromodomain (Figs. 1 and S1) and the binding energy of the resulting poses was calculated using a force field-based energy function with approximation of desolvation effects in the continuum-dielectric representation.[16,17] The docked poses of the frag-

Abbreviations: Alpha, amplified luminescent proximity homogeneous assay; ATAD2, ATAD2 ATPase family, AAA domain containing 2; BAZ2A, bromodomain adjacent to zinc finger domain protein 2A; BAZ2B, bromodomain adjacent to zinc finger domain protein 2B; BRPF1, bromodomain and PHD finger (BRPF) containing protein 1; CBP, CREB-binding protein; CREB, cyclic-AMP response element binding protein; CSPs, chemical shift perturbations; DMSO, dimethyl sulfoxide; DSF, differential scanning fluorimetry; EP300, adenoviral E1A binding protein; HAC, heavy atom count; Kac, N-ε-acetyllysine; LE, ligand efficiency; NMR, nuclear magnetic resonance; qPCR, quantitative PCR polymerase chain reaction; STD, saturation transfer difference; VS2NMR, Virtual Screen to NMR.

* Corresponding authors.
E-mail addresses: d.spiliotopoulos@bioc.uzh.ch (D. Spiliotopoulos), caflisch@bioc.uzh.ch (A. Caflisch).

http://dx.doi.org/10.1016/j.bmcl.2017.04.001
0960-894X/

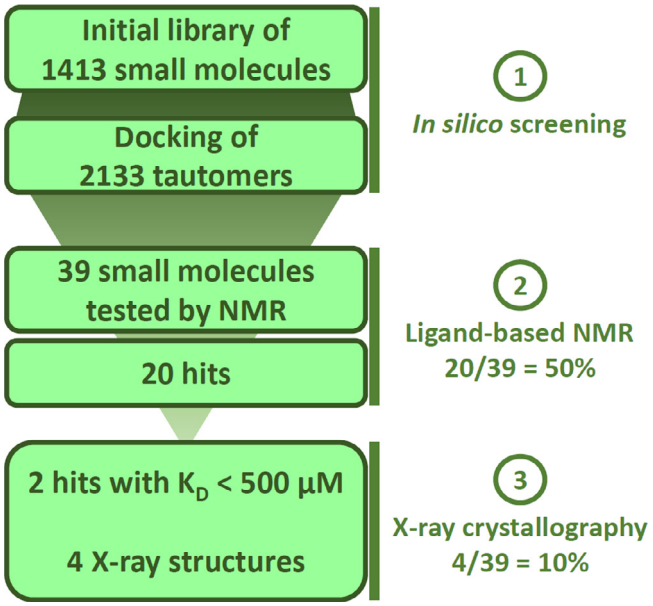

Fig. 1. Flowchart of the VS2NMR workflow and subsequent experimental validation by means of competition binding assays and X-ray crystallography. VS2NMR consisted of (1) virtual screening by high-throughput fragment docking using the program SEED[16,17] and (2) ligand-based NMR spectroscopy. This efficient screening strategy was finally validated by (3) two different *in vitro* binding assays[15,22] and X-ray crystallography. The success ratio of the *in silico* screening is 50% according to ligand-observed NMR spectroscopy and 10% according to X-ray crystallography.

ments were filtered to enforce a hydrogen bond with the conserved water molecule w_1 (Fig. S1) that bridges to the side chain hydroxyl of the conserved Tyr1125 (see Supplementary information). The remaining poses were ranked according to the median rank of a consensus scoring aimed to prioritize molecules with favorable electrostatic contribution to the binding energy (including desolvation penalties) and van der Waals interactions. Of the 60 selected fragments, 39 were ultimately chosen to be validated via NMR techniques (Table S1) based on results from experimental quality control.[18]

To experimentally validate these fragments as ligands of the CBP bromodomain, we took advantage of ligand-based NMR spectroscopy. The *in silico* hits were divided into four mixtures of 9–10 molecules each with minimal ^{1}H NMR spectral overlap. Fragments which displayed a clear evidence for binding in at least one of three ligand-observed NMR spectroscopy experiments, *viz.*, ^{1}H, STD, and R_2-filtered,[19,20] were selected for further validation. To ensure specificity for the primary binding site we included competition experiments with SGC-CBP30, a nanomolar ligand of the CBP bromodomain[8] (Fig. S2). Overall, specific interactions with the CBP bromodomain were observed for 20 of the 39 small molecules, which corresponds to a success ratio (defined as the quotient of true positives divided by the number of compounds tested by NMR) of 50% for the *in silico* screening (Fig. 1). The most pronounced effects were observed for compounds **1**–**4** (Table 1), showing STD effects as well as chemical shift perturbation (CSPs) and enhanced R_2 relaxation in presence of CBP (Table 2).

To further validate the 20 compounds that showed binding in the ligand-observed NMR experiments, competition binding assays were performed first with the AlphaScreen technology using a tetra-acetylated peptide segment from the histone H4. At 0.5 mM compound concentration, 50% or higher inhibition of the CBP bromodomain was observed for five of the 20 actives in the NMR experiments (Table 2). Two of these compounds were not investigated further because of lack of novelty of their head group. These are the 3-acetylindole **2**, which is similar to a fragment recently disclosed as a 29-µM inhibitor of the BRPF1 bromodomain,[21] and the acetylbenzene derivative **4**, which shares the same head group as our previously disclosed CBP inhibitors.[13,14] Furthermore, the pyrazole derivative **5** was discarded because of its poor affinity, also confirmed by the lack of shift in the DSF assay (Table 1). The remaining two compounds (**1** and **3**) displayed micromolar affinity in dose-response measurements using two different biochemical assays (Table 1 and Fig. S3). The IC_{50} values measured by the AlphaScreen approach[22] are about one order of magnitude less favorable than the K_D values obtained by a competition binding assay based on DNA-tagged CBP bromodomain and PCR quantification.[15] Such discrepancies have already been reported in previous studies of bromodomain ligands.[23–25] They are likely to originate from different experimental conditions, protocols, and/or the use of different competitor molecules (the AlphaScreen assay was performed using a tetra-acetylated 21-mer H4 peptide whereas a proprietary undisclosed ligand was used for the assay based on DNA-tagged bromodomain). Importantly, the ligand efficiency of compounds **1** and **3** is very favorable irrespective of the assay (Table 1).

In our previous fragment-based high-throughput docking campaigns for the bromodomains of BRD4 (N-terminal),[26] CBP,[13] BRPF1,[21] BAZ2A (PDB codes 5MGJ, 5MGK, 5MGL, 5MGM), BAZ2B,[27,28] and ATAD2 (PDB codes 5EPB, 5F3A, 5F36) the poses predicted by docking were validated by protein crystallography. Similarly, in the present VS2NMR campaign, we decided to validate the binding poses predicted by docking by means of X-ray crystallography. Towards this goal, we solved the crystal structures of the complexes of the CBP bromodomain with ligands **1** to **4** at resolution of 1.65 Å or higher (Figs. 2 and S4, Table S2).

Compound **1** forms four hydrogen bonds with the CBP bromodomain (Fig. 2A). There are two direct hydrogen bonds involving the pyrrole NH and carbonyl oxygen acting as donor and acceptor, respectively, for the side chain of the conserved Asn1168. Furthermore, two water-mediated hydrogen bonds are formed between the carbonyl oxygen of compound **1** and the side chain hydroxyl of the conserved Tyr1125 (through the structural water w_1) and between the NH of the carboxamide and the backbone carbonyl of Pro1110. The bromine substituent of **1** points towards the side chains of Leu1120 and Ile1122 in the ZA-loop, which provides stabilization by hydrophobic contacts. The pose predicted by docking is consistent with the binding mode in the crystal structure except for the relative orientation of the pyrrole and the N-methylamide, which is due to the conformer used for docking and the rigid-ligand docking protocol.

As for compound **1**, a minor discrepancy between docked pose and binding mode in the crystal structure is observed for compound **3** (Fig. 2C) which is again a consequence of the different conformer used in the rigid-docking protocol. Importantly, the position of the double-ring system and the two hydrogen bonds of the carbonyl oxygen (with the side chain of Asn1168 and the water w_1) are predicted correctly by docking. Interestingly, a second molecule **3** is present outside of the Kac binding site, with stabilization due to stacking between the indole of Trp1151 and the phenyl of Tyr1102 of a neighboring CBP bromodomain, and a hydrogen bond with the side chain of Gln1113 of the same neighboring protein (Fig. 3). Thus, the second binding mode is stabilized by crystal packing.

The pose predicted by docking for the 3-acetylindole **2** and acetylbenzene derivative **4** are essentially identical to the binding mode in the crystal structures (Fig. 2B,D). The methoxy oxygen of the acetylbenzene derivative **4** is involved in a water-bridged hydrogen bond with the backbone oxygen of Pro1110 (Fig. 2D) or the side chain oxygen of Asn1168 (Fig. S5) in the two protein chains of the asymmetric unit. As expected, the binding pose of **4** superimposes with an acetylbenzene-based sub-micromolar inhibitor reported recently (PDB code 4TQN, Fig. S6).[13] In both struc-

Table 1
In silico identified ligands of the CBP bromodomain.

	2D structure	HAC[a]	PDB code	DSF (°C)[b]		AlphaScreen			BROMOscan	
				CBP	EP300	%[c]	IC50 (μM)[d]	LE[e]	K_D (μM)[f]	LE[e]
1	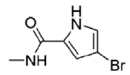	10	5MQE	7.3	7.0	0.1	40	0.60	4	0.74
2	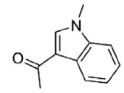	13	5MQK	2.9	2.6	31	n.d.[g]	n.d.	n.d.	n.d.
3	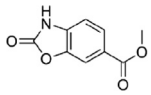	14	5MPZ	2.3	1.4	34	455	0.33	85	0.40
4	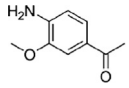	12	5MQG	2.4	2.6	37	n.d.	n.d.	n.d.	n.d.
5	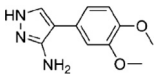	16	–	−0.1	−1.3	48	n.d.	n.d.	n.d.	n.d.

[a] HAC: heavy atom count.
[b] Differential scanning fluorimetry (DSF) measurements were carried out at a bromodomain concentration of 2 μM and a ligand concentration of 1 mM. For each ligand/bromodomain pair, the shift in the melting temperature is the median value of at least nine measurements. Standard error of the mean values were smaller than 0.3 °C in all cases.
[c] Binding of the CBP bromodomain to a labelled acetylated peptide in the presence of 0.5 mM of the ligand with respect to DMSO solution, with lower percentage values indicating stronger inhibition.
[d] IC50 values were determined by curve fitting of 10-point dose responses.
[e] Ligand efficiency (LE) values are reported in kcal/mol per heavy atom.
[f] K_D values, as determined by curve fitting of 12-point dose responses in duplicates in a competition-binding experiment based on DNA-tagged CBP bromodomain and quantitative PCR.[15]
[g] n.d.: not determined.

tures, the acetyl oxygen of the ligand acts as acceptor in a direct hydrogen bond with the side chain NH_2 of the conserved Asn1168 and a water-bridged hydrogen bond to the side chain of Tyr1125. As reported previously,[21,29,30] the distance between the acetyl oxygen and the bridging water (2.7 Å for both compounds **2** and **4**) is shorter than the distance to the nitrogen atom of the Asn1168 side chain (3.0 Å). A shorter distance to the bridging w_1 oxygen than the Asn1168 side chain nitrogen is also observed for the carbonyl oxygen of compounds **1** and **3** (Fig. S7).

An essential element of our fragment-docking procedure is the efficient evaluation of the binding energy which is the sum of the van der Waals interaction and electrostatic energy in the continuum dielectric approximation (see original papers on the SEED software).[16,17] The electrostatic contribution to the binding energy is the sum of the screened interaction between the (partial) charges in the protein and the ligand, and the desolvation penalty of the receptor and fragment upon binding. It is useful to analyze the individual contributions to the binding energy. Here, we focus the analysis on the top two poses (according to total binding energy as calculated by SEED) as the third ranking pose was significantly less favorable for the four fragment hits **1**–**4**. The total SEED energy favors the pose that is close to the binding mode observed in the crystal structure (Fig. 4). On the other hand, the van der Waals contribution does not consistently favor the binding mode observed in the crystal structure. The van der Waals energy is always favorable because it consists of only the fragment/protein contribution, while the loss of solute/solvent van der Waals energy upon binding is neglected. In contrast, the electrostatic contribution to the binding energy (ΔG_{elec}), which includes desolvation effects, always favors the pose close to the binding mode observed in the crystal structure over the second best pose. More precisely, for compound **3** the desolvation penalty is less unfavorable for the top pose than the second best pose while for compounds **1**, **2**, and **4** it is rather the intermolecular electrostatic contribution that favors the top pose. This analysis provides evidence that a simple scoring function, e.g., based on only van der Waals energy, would not have sufficient predictive ability. It also highlights the importance of the evaluation of the electrostatic energy with solvation for identifying the correct binding mode among the multiple poses generated by docking.

In conclusion, we efficiently identified inhibitors of the CBP bromodomain by means of a VS2NMR campaign using high-throughput fragment docking (by the program SEED)[16,17] followed by ligand-observed NMR spectroscopy. First, the initial 1413 fragments were reduced to 39 candidate ligands by *in silico* screening, which required only two hours of a commodity computer. Twenty of these molecules showed specific, competitive binding in ligand-observed NMR experiments. In contrast to the present study in which NMR measurements were performed on a small set of molecules preselected by high-throughput docking, in previous reports by others NMR spectroscopy has been employed as primary screening with the following protocols: 2D HSQC or HMQC NMR,[31–36] ligand-observed NMR,[37,38] protein observed fluorine NMR,[39,40] and target immobilized NMR screening.[41] Importantly, with the present VS2NMR campaign, 50% of the small molecules predicted by docking as candidate ligands of the CBP bromodomain were confirmed by ligand-observed NMR spectroscopy, a higher success ratio than that of primary NMR screens on bromodomains, which range from 0.3%[33] to 13.5%.[40] Although it is not possible to directly compare different screening protocols and targets, the present study provides evidence that the VS2NMR strategy is time and resource efficient. As a matter of fact, the primary screening of nearly 1500 compounds by NMR, including data analysis, would have required about three weeks, while the present VS2NMR campaign took about two days.

We have recently carried out a VS2NMR campaign for the BAZ2A bromodomain starting from the same 1413-fragment library as in the present study and with the same validation by ligand-based NMR as secondary screening (D. Spiliotopoulos et al., manuscript in preparation). The success ratio for CBP (20

Table 2
Ligand-based NMR spectroscopy validation of the molecules predicted *in silico* as CBP bromodomain ligands.

	2D structure	HAC[a]	NMR screening[b]			AlphaScreen %[c]
			^{1}H	STD	CPMG	
1	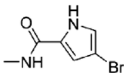	10	+	+	+	0.1
2	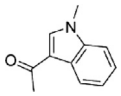	13	–	+	+	31
3	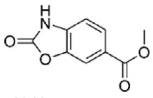	14	+	+	+	34
4	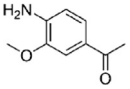	11	+	+	+	37
5	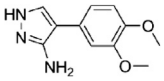	16	–	–	+	48
6	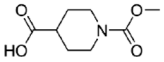	12	–	–	+	56
7	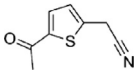	11	+	–	+	56
8	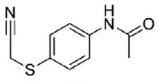	14	+	+	+	74
9	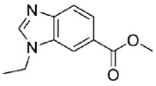	15	+	+	+	79
10	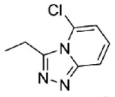	12	+	+	+	85
11	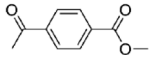	12	–	+	+	92
12	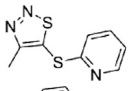	13	+	–	+	92
13	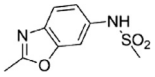	15	–	+	+	92
14	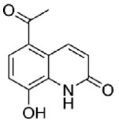	15	+	+	+	93
15	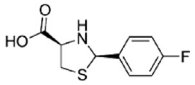	15	+	–	+	94
16	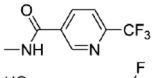	14	–	–	+	96
17	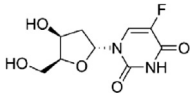	17	+	–	+	98
18	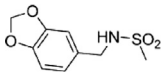	15	–	–	+	100
19	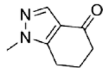	11	+	+	+	100
20	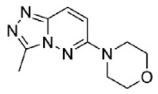	17	–	–	+	102

[a] HAC: heavy atom count.
[b] NMR spectroscopy techniques included ^{1}H, saturation transfer difference (STD) NMR and Carr-Purcell-Meiboom-Gill (CPMG).
[c] Binding of the CBP bromodomain to an acetylated peptide in the presence of 0.5 mM of the ligand with respect to DMSO solution, with lower values indicating stronger inhibition. The compounds are sorted according to percentage binding.

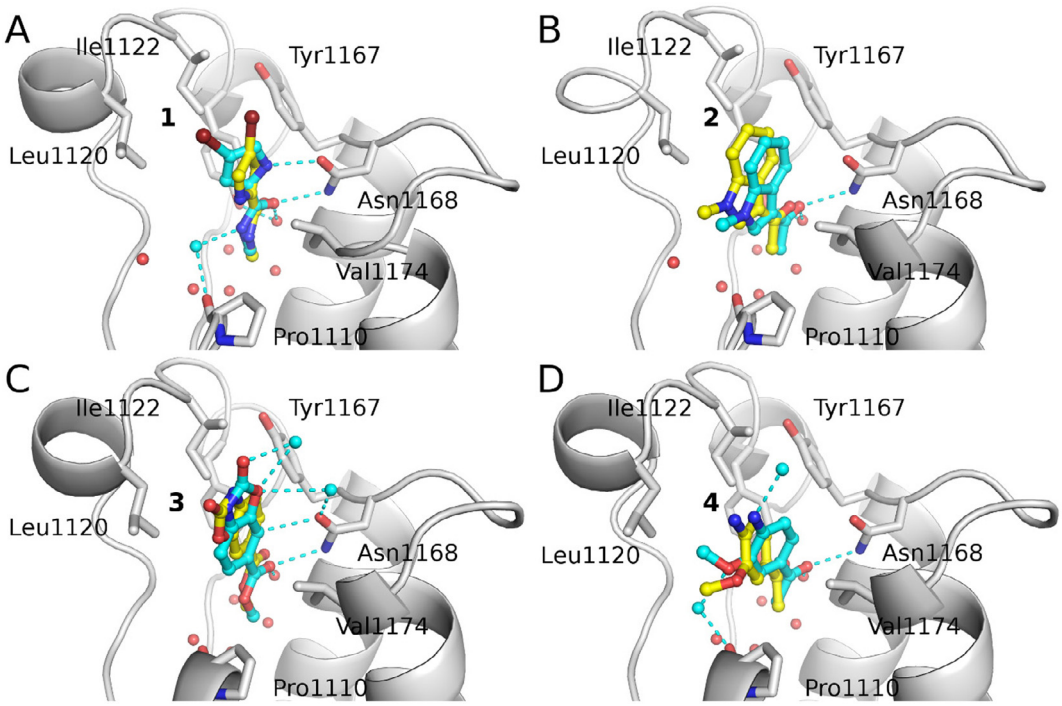

Fig. 2. Structural validation of the fragment-based *in silico* screening campaign for CBP. (A–D) The binding mode in the crystal structures (carbon atoms of ligands in cyan) are compared to the binding pose predicted by docking with SEED[16,17] (carbon atoms in yellow) for compounds (A) **1**, (B) **2**, (C) **3**, and (D) **4** (PDB codes: 5MQE, 5MQK, 5MPZ, and 5MQG, respectively). Conserved water molecules and water molecules present in the crystal structure but not used for docking are shown as red and cyan spheres, respectively. Compounds **1** and **3** have a different relative orientation of the substituents, which could not be predicted by SEED since the compounds were docked as rigid molecules.

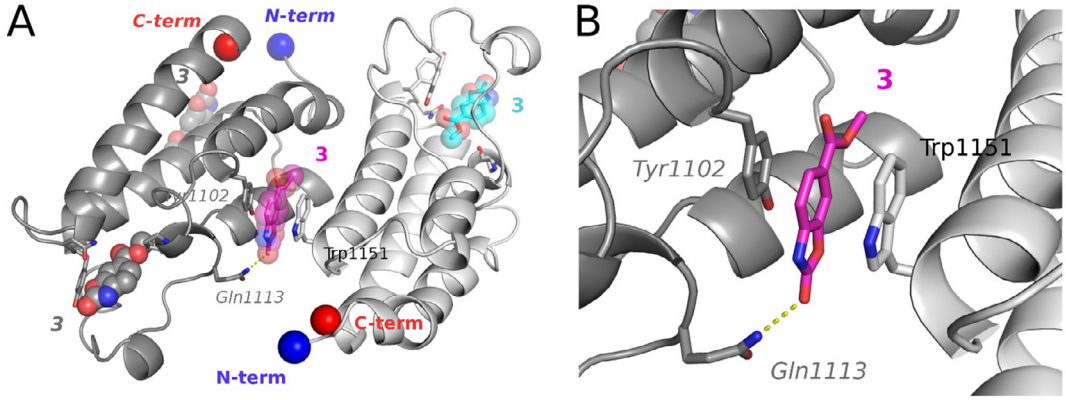

Fig. 3. Two molecules of compound **3** bind to the CBP bromodomain in the crystal structure. (A) The two compound **3** molecules present in the crystallographic unit of the CBP/**3** complex (gray cartoons) are shown as sticks and transparent spheres. A description of the pose of the molecule bound to the Kac-binding site (carbon atoms in cyan or gray) can be found in the text. The second molecule (magenta) stacks between the side chains of Trp1151 and Tyr1102 of a neighboring CBP bromodomain. The N- and C-termini of the bromodomains are shown with a blue and red sphere, respectively. (B) Zoom on the additional compound **3** molecule and the protein residues surrounding it. The polar interaction between the carbonyl oxygen of the ligand and the side chain of the Gln1113 of the neighboring CBP bromodomain is shown with dashed lines. The two bromodomains are shown with dark and light gray, respectively.

actives according to NMR out of 39 candidate ligands) is higher than for the BAZ2A bromodomain (7 actives out of 20 candidate ligands) which is a more difficult target as it has a shallower Kac biding site.

The high ligand efficiency of the *in silico* identified fragments calls for hit expansion. In a cellular *milieu*, the methylester of compound **3** is likely to be converted into a carboxyl group. The resulting negative charge on the carboxyl group would hinder binding to the Kac pocket because of the electrostatic desolvation penalty. On the other hand, the binding mode of the brominated pyrrole **1** is compatible with fragment growing by Suzuki coupling.

Author contribution

J. A. and C. R. compiled the library of compounds and J.-R. M. parametrized it. D.S. and A.C. performed and analyzed the virtual screening. N. D. purified the protein samples for the NMR screening and performed and analyzed the DSF measurements. E.-C. W. and D. S. performed and analyzed the NMR screen. J. Z. purified the protein for X-ray crystallography, grew the crystals and solved the structures. D.S. and A.C. wrote the manuscript with contributions from all authors.

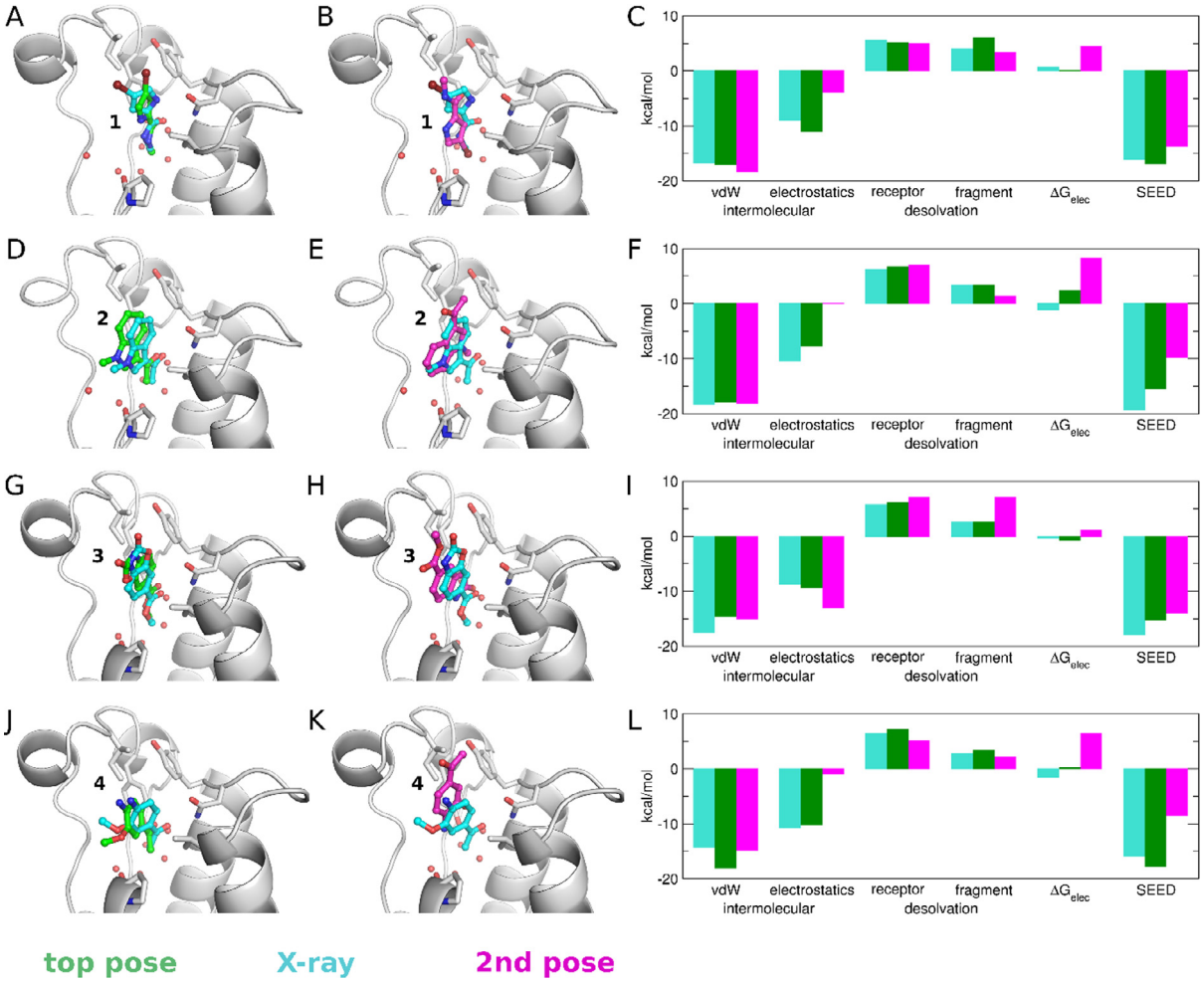

Fig. 4. Insights into the energetic terms calculated using SEED for the two top poses of compounds **1** (A–C), **2** (D–F), **3** (G–I), and **4** (J–L). The CBP bromodomain is shown as a cartoon and sticks with white carbon atoms, whereas the ligands are shown as sticks. The color coding is consistent in all panels (cyan, green, and magenta for binding mode in the crystal structure, top pose and 2nd best pose according to total SEED energy, respectively). (C, F, I, L) The contributions to the binding energy are the intermolecular van der Waals energy, the intermolecular electrostatics energy calculated in the solvent using a continuum dielectric representation, the electrostatic desolvation energy of the receptor and ligand upon binding. These terms sum up to the total energy. The electrostatic contribution to the binding free energy in the solvent (ΔG_{elec}) is the sum of intermolecular electrostatic energy and desolvation penalties.

Accession codes

Structure were deposited to the PDB with accession numbers 5MQE (CBP/**1**), 5MQK (CBP/**2**), 5MPZ (CBP/**3**), and 5MQG (CBP/**4**).

Conflict of interest

The authors declare no competing interest.

Acknowledgements

We thank the Structural Genomics Consortium at University of Oxford for providing the plasmid of the CBP bromodomain. EP300 was a gift from Nicola Burgess-Brown (Addgene plasmid # 39018). The AlphaScreen and BROMOscan measurements were performed at Reaction Biology Corporation and DiscoverX, respectively. This work was supported in part by the Swiss National Science Foundation (grant to A.C.) and Max Planck Society and the German Research Foundation (DFG, RA1944/2-1) (C.R., J. A. and E.W.). D.S. is a recipient of the SystemsX.ch translational postdoc fellowship and gratefully acknowledges support from the Holcim Foundation.

A. Supplementary data

Supplementary data associated with this article can be found, in the online version, at http://dx.doi.org/10.1016/j.bmcl.2017.04.001.

References

1. Dhalluin C, Carlson JE, Zeng L, He C, Aggarwal AK, Zhou MM. Structure and ligand of a histone acetyltransferase bromodomain. *Nature*. 1999;399(6735):491–496.
2. Flynn EM, Huang OW, Poy F, et al. A subset of human bromodomains recognizes butyryllysine and crotonyllysine histone peptide modifications. *Structure*. 2015;23(10):1801–1814.
3. Zhang G, Smith SG, Zhou MM. Discovery of chemical inhibitors of human bromodomains. *Chem Rev*. 2015;115(21):11625–11668.
4. Filippakopoulos P, Knapp S. Targeting bromodomains: Epigenetic readers of lysine acetylation. *Nat Rev Drug Discov*. 2014;13(5):337–356.
5. Muller S, Filippakopoulos P, Knapp S. Bromodomains as therapeutic targets. *Expert Rev Mol Med*. 2011;13:e29.
6. Ferri E, Petosa C, McKenna CE. Bromodomains: structure, function and pharmacology of inhibition. *Biochem Pharmacol*. 2016;106:1–18.
7. Iyer NG, Ozdag H, Caldas C. P300/CBP and cancer. *Oncogene*. 2004;23(24):4225–4231.
8. Hay DA, Fedorov O, Martin S, et al. Discovery and optimization of small-molecule ligands for the CBP/p300 bromodomains. *J Am Chem Soc*. 2014;136(26):9308–9319.

9. Rooney TP, Filippakopoulos P, Fedorov O, et al. A series of potent CREBBP bromodomain ligands reveals an induced-fit pocket stabilized by a cation-pi interaction. *Angew Chem Int Ed*. 2014;53(24):6126–6130.
10. Picaud S, Fedorov O, Thanasopoulou A, et al. Generation of a selective small molecule inhibitor of the CBP/p300 bromodomain for leukemia therapy. *Cancer Res*. 2015;75(23):5106–5119.
11. Taylor AM, Cote A, Hewitt MC, et al. Fragment-based discovery of a selective and cell-active benzodiazepinone CBP/EP300 bromodomain inhibitor (CPI-637). *ACS Med Chem Lett*. 2016;7(5):531–536.
12. Crawford TD, Romero FA, Lai KW, et al. Discovery of a potent and selective in vivo probe (GNE-272) for the bromodomains of CBP/EP300. *J Med Chem*. 2016;59(23):10549–10563.
13. Xu M, Unzue A, Dong J, Spiliotopoulos D, Nevado C, Caflisch A. Discovery of CREBBP bromodomain inhibitors by high-throughput docking and hit optimization guided by molecular dynamics. *J Med Chem*. 2016;59(4):1340–1349.
14. Unzue A, Xu M, Dong J, et al. Fragment-based design of selective nanomolar ligands of the CREBBP bromodomain. *J Med Chem*. 2016;59(4):1350–1356.
15. Quinn E, Wodicka L, Ciceri P, et al. BROMOscan – a high throughput, quantitative ligand binding platform identifies best-in-class bromodomain inhibitors from a screen of mature compounds targeting other protein classes. *Cancer Res*. 2013;73:4238.
16. Majeux N, Scarsi M, Apostolakis J, Ehrhardt C, Caflisch A. Exhaustive docking of molecular fragments with electrostatic solvation. *Proteins*. 1999;37:88–105.
17. Majeux N, Scarsi M, Caflisch A. Efficient electrostatic solvation model for protein-fragment docking. *Proteins*. 2001;42(2):256–268.
18. Aretz J, Wamhoff EC, Hanske J, Heymann D, Rademacher C. Computational and experimental prediction of human C-type lectin receptor druggability. *Front Immunol*. 2014;5:323.
19. Mayer M, Meyer B. Characterization of ligand binding by saturation transfer difference NMR spectroscopy. *Angew Chem Int Ed*. 1999;38(12):1784–1788.
20. Hajduk PJ, Olejniczak ET, Fesik SW. One-dimensional relaxation- and diffusion-edited NMR methods for screening compounds that bind to macromolecules. *J Am Chem Soc*. 1997;119(50):12257–12261.
21. Zhu J, Caflisch A. Twenty crystal structures of bromodomain and PHD finger containing protein 1 (BRPF1)/ligand complexes reveal conserved binding motifs and rare interactions. *J Med Chem*. 2016;59(11):5555–5561.
22. Philpott M, Yang J, Tumber T, et al. Bromodomain-peptide displacement assays for interactome mapping and inhibitor discovery. *Mol BioSyst*. 2011;7(10):2899–2908.
23. Theodoulou NH, Bamborough P, Bannister AJ, et al. Discovery of I-BRD9, a selective cell active chemical probe for bromodomain containing protein 9 inhibition. *J Med Chem*. 2016;59(4):1425–1439.
24. Crawford TD, Tsui V, Flynn EM, et al. Diving into the water: inducible binding conformations for BRD4, TAF1(2), BRD9, and CECR2 bromodomains. *J Med Chem*. 2016;59(11):5391–5402.
25. Tanaka M, Roberts JM, Seo HS, et al. Design and characterization of bivalent BET inhibitors. *Nat Chem Biol*. 2016;12(12):1089–1096.
26. Zhao H, Gartenmann L, Dong J, Spiliotopoulos D, Caflisch A. Discovery of BRD4 bromodomain inhibitors by fragment-based high-throughput docking. *Bioorg Med Chem Lett*. 2014;24(11):2493–2496.
27. Lolli G, Caflisch A. High-throughput fragment docking into the BAZ2B bromodomain: efficient in silico screening for X-ray crystallography. *ACS Chem Biol*. 2016;11(3):800–807.
28. Marchand JR, Lolli G, Caflisch A. Derivatives of 3-amino-2-methylpyridine as BAZ2B bromodomain ligands: in silico discovery and in crystallo validation. *J Med Chem*. 2016;59(21):9919–9927.
29. Chung C-W, Dean AW, Woolven JM, Bamborough P. Fragment-based discovery of bromodomain inhibitors part 1: inhibitor binding modes and implications for lead discovery. *J Med Chem*. 2011;55(2):576–586.
30. Marchand JR, Caflisch A. Binding mode of acetylated histones to bromodomains: variations on a common motif. *ChemMedChem*. 2015;10(8):1327–1333.
31. Zeng L, Li J, Muller M, et al. Selective small molecules blocking HIV-1 Tat and coactivator PCAF association. *J Am Chem Soc*. 2005;127(8):2376–2377.
32. Sachchidanand, Resnick-Silverman L, Yan S, et al. Target structure-based discovery of small molecules that block human p53 and CREB binding protein association. *Chem Biol*. 2006;13(1):81–90.
33. Borah JC, Mujtaba S, Karakikes I, et al. A small molecule binding to the coactivator CREB-binding protein blocks apoptosis in cardiomyocytes. *Chem Biol*. 2011;18(4):531–541.
34. Harner MJ, Frank AO, Fesik SW. Fragment-based drug discovery using NMR spectroscopy. *J Biomol NMR*. 2013;56(2):65–75.
35. Chaikuad A, Petros AM, Fedorov O, Xu J, Knapp S. Structure-based approaches towards identification of fragments for the low-druggability ATAD2 bromodomain. *Med Chem Commun*. 2014;5(12):1843–1848.
36. Ghosh S, Taylor A, Chin M, et al. Regulatory T cell modulation by CBP/EP300 bromodomain inhibition. *J Biol Chem*. 2016;13014–13027.
37. Demont EH, Bamborough P, Chung CW, et al. 1,3-Dimethyl benzimidazolones are potent, selective inhibitors of the BRPF1 bromodomain. *ACS Med Chem Lett*. 2014;5(11):1190–1195.
38. Wang N, Li F, Bao H, Li J, Wu J, Ruan K. NMR Fragment screening hit induces plasticity of BRD7/9 bromodomains. *ChemBioChem*. 2016;17(15):1456–1463.
39. Mishra NK, Urick AK, Ember SW, Schonbrunn E, Pomerantz WC. Fluorinated aromatic amino acids are sensitive 19F NMR probes for bromodomain-ligand interactions. *ACS Chem Biol*. 2014;9(12):2755–2760.
40. Urick AK, Hawk LM, Cassel MK, et al. Dual screening of BPTF and Brd4 using protein-observed fluorine NMR uncovers new bromodomain probe molecules. *ACS Chem Biol*. 2015;10(10):2246–2256.
41. Chaikuad A, Lang S, Brennan PE, et al. Structure-based identification of inhibitory fragments targeting the p300/CBP-associated factor bromodomain. *J Med Chem*. 2016;59(4):1648–1653.

Supporting Information

Virtual Screen to NMR (VS2NMR): Discovery of fragment hits for the CBP bromodomain

Dimitrios Spiliotopoulos,[*,a] Jian Zhu,[a] Eike-Christian Wamhoff,[b,c] Nicholas Deerain,[a] Jean-Rémy Marchand,[a] Jonas Aretz,[b,c] Christoph Rademacher,[b,c] and Amedeo Caflisch[*,a]

Author Affiliations:
[a]Department of Biochemistry University of Zürich, Winterthurerstrasse 190, CH-8057 Zürich, Switzerland
[b]Department of Biomolecular Systems, Max Planck Institute of Colloids and Interfaces, Am Mühlenberg 1, 14424 Potsdam, Germany
[c]Institute of Chemistry and Biochemistry, Department of Biology, Chemistry, and Pharmacy, Freie Universität Berlin, Takustraße 3, 14195 Berlin, Germany

Corresponding Authors:
*E-mail: A.C., caflisch@bioc.uzh.ch. Phone: +41 44 635 55 21. D.S., d.spiliotopoulos@bioc.uzh.ch. Phone: +41 44 635 55 92.

EXPERIMENTAL SECTION

Fragment Docking and Scoring. The initial library consisted of 1413 fragments available in the laboratory of one of the authors (C.R.). These molecules were selected from a large panel of commercial suppliers and academic collaborations according mainly to diversity. From this library, a total of 2133 tautomers were generated using the calculator plugins of Marvin 15.8.17, 2015, Chemaxon.

The in-house developed program SEED[1, 2] was used for docking. The target structure was the CBP bromodomain complexed to acetylated lysine (PDB code: 3P1C), and the binding site was defined as the side chain of the conserved Asn1168 and the six water molecules that are found in most crystal structures of this bromodomain (Figure S1).

The partial charges and van der Waals parameters for the protein and the fragments were taken from the CHARMM36 all-atom force field[3, 4] and the CHARMM general force field (CGenFF),[5] respectively. Importantly, the same paradigm was used to derive the partial charges and van der Waals parameters for the CHARMM36 force field and CGenFF, making the force fields completely consistent. SEED uses a force field-based energy function with a continuum dielectric approximation of desolvation penalties based on the generalized Born paradigm to evaluate the binding energy.[6] The continuum calculations were performed setting the dielectric constant to 2.0 and 78.5 for the solute (low-dielectric region) and solvent (high-dielectric region), respectively. The docking of the 2133 tautomers with SEED required approximately 2 h (about 3 s per fragment) of a single core of an Intel Xeon E5410 processor at 2.33 GHz.

The docked poses were first evaluated for the presence of an acceptor atom involved in a hydrogen bond with the conserved water molecule w_1 (Figure S1). Moreover, poses with buried polar groups of fragment and/or protein not involved in hydrogen bonds were filtered out using an in-house developed software (Hydrogen bond penalty lower than 1).[7, 8] The final ranking was based on the median value of a consensus scoring function that included the ranks of (1) the difference between (1a) the electrostatic contribution to the protein/ligand interaction energy in the solvent and (1b) the solvation energy of the ligand, (2) the predicted binding energy (SEED total energy), and (3) the van der Waals efficiency, i.e., the intermolecular van der Waals contribution divided by the number of non-hydrogen atoms. These three terms are meant to prioritize compounds that (1) establish favorable polar interactions with the targeted protein considering the opposing free energy of hydration, (2) have favorable total energy calculated by SEED, including van der Waals and polar interactions, and (3) are fully buried in the binding site. Compounds were sorted using the median of the three rankings. The median (and not the mean value) was used as it is less sensitive to outliers.[9, 10] Note that SEED treats the docked compounds as rigid molecules, meaning that all the terms (including 1a and 1b) are computed for the small molecule in the conformation under investigation. A total of 60 small molecules were selected using the *in silico* approach. Of these 60 compounds, 21 were subsequently filtered out due to experimental issues (e.g., poor solubility, binding promiscuity and/or chemical reactivity).

Protein Expression and Purification. Proteins were expressed and purified as described in [11].

NMR Spectroscopy. All NMR experiments were performed on a PremiumCompact 600 MHz spectrometer at 25°C equipped with a OneNMR probe (Agilent). Data were processed using MestReNova software suite (Mestrelab Research S. L.). A DPFGSE pulse sequence was utilized for solvent suppression.[12]

During STD NMR experiments a saturation time t_{sat} of 4.0 s utilizing a train of 50 ms Gauss pulses for used with an on- and off-resonance frequency of 0.0 ppm (ν_{sat}) and 80.0 ppm (ν_{ref}).[13] For each spectrum, 256 scans were recorded in 5 mm sample tubes at sample volumes of 500 to 550 µL. No prescan relaxation delay d_1 was included and the acquisition time t_{acq} was set to 2.0 s. A $T_{1,rho}$ filter of 35 ms duration was utilized for receptor resonances suppression. A Carr−Purcell−Meiboom−Gill (CPMG) pulse sequence was used to perform R_2-filtered NMR experiments with a prescan relaxation delay d_1 of 2.0 s and an acquisition time t_{acq} of 2.0 s.[14] The frequency of 180° pulses (ν_{CPMG}) was set to 100 Hz and the total relaxation time T was set to 0.4 s. The induction of chemical shift perturbations in presence of CBP was analyzed using regular ^{1}H NMR experiments. The relaxation delay d_1 was set to 2.0 s and the acquisition time t_{acq} was set to 2.0 s. Spectra were recorded at 128 scans.

From the 39 selected compounds, four fragment mixtures with minimal 1H NMR spectral overlap were predicted using a genetic algorithm. Briefly, this approach was implementing by first generating a list of chemical shifts for each fragment. Assignment of the NMR resonances was based on previously acquired ^{1}H NMR spectra of the individual fragments. The lists were then randomly combined to yield a population of 50 individual virtual fragment mixtures. Assuming a tolerance of 0.3 ppm for the spectra overlap, a fitness score was calculated. Based on this score, a set of fit fragment mixtures is selected and its composition is randomly varied by mutation (mutation rate = 0.01) or crossover (crossover rate = 0.8) to generate the next generation of fragment mixtures. This procedure was repeated for 1000 generations until convergence to yield fragment mixtures with optimized spectral overlap. The termination criterion was the existence of at least one resonance not displaying spectral overlap for each fragment.

Optimized sample mixtures were prepared at 200 µM of each fragment in 50 mM H_3PO_4 with 100% D_2O, 2% DMSO-d_6, 150 mM NaCl at pH 7.4. 100 µM TSP-d_4 served as an internal reference. The stability of the fragment mixtures over 16 h at room temperature was monitored via ^{1}H NMR. CPMG and STD-based fragment screening was conducted first in absence of CBP, followed by the addition of 20 µM CBP. Finally, competitive binding experiments were conducted in presence of 20 µM SGC-CBP30.[15] Hits from virtual screening were considered as validated in case either an STD effect, an increased R_2 relaxation rate or a ^{1}H chemical shift perturbation occurred in presence of CBP, and the nanomolar inhibitor SGC-CBP30 showed competitive binding. The analysis was based on a visual and qualitative assessment of the recorded spectra. Fragments displaying an STD effect in absence of protein were considered artifacts and were excluded from further analysis.

AlphaScreen and BROMOscan assays. AlphaScreen is a bead-based proximity assay technology that has been applied to identify small molecules able to displace histone peptides from bromodomains.[16] Briefly, donor and acceptor beads are coupled to the interaction partners and, as the bromodomain ligand inhibits this interaction, the detected signal is reduced. A histone H4 tetra-acetylated peptide ($H4_{1-21}$Kac5Kac8Kac12Kac16) was used for the measurements with the CBP bromodomain ligands in the presence of 0.1% DMSO.

BROMOscan is a competition-based technology using a ligand immobilized to a solid support and DNA-tagged bromodomains. The ligand is incubated with the bromodomains in the presence and absence of the putative inhibitors and the bromodomains are eluted and quantified by qPCR. The amount of bromodomain captured will be reduced if small molecules inhibiting the bromodomain binding to the immobilized ligand are present, which results in a reduction of the detected qPCR signal.[17] Dissociation constants (K_D) were calculated in the presence of 0.09% DMSO fitting a 12-point dilution with starting concentration of 0.5 mM and dilution factor of 3.0.

AlphaScreen and BROMOscan assays were carried out at Reaction Biology Corporation and DiscoverX Corporation, respectively.

Thermal Shift Measurements. Thermal shift measurements were performed using a 2 μM and 1 mM concentration for the bromodomains and ligands, respectively, with 0.3% (v/v) DMSO.

Crystallization, Data Collection and Structure Solution. CBP bromodomain was crystallized by vapor diffusion in sitting drops at 4°C. Apo crystals for compound soaking were grown from 0.1 M Bis-Tris pH 5.5, 0.2 M potassium thiocynate, 5% ethylene glycol and 23% PEG3350. Overnight soaking of compounds **1** and **4** were performed by transferring the apo crystals into the crystallization buffer in which compounds were previously dissolved at 5-10 mM. Compound **2** was co-crystallized with CBP bromodomain using the crystallization buffer of 0.15 M KSCN, 10% ethylene glycol and 20% PEG3350. Co-crystal structure of compound **3** bound to CBP bromodomain was determined from crystals grown from 0.1 M Bis-Tris pH 6.5, 0.2 M $MgCl_2$, 5% ethylene glycol and 23% PEG3350. Crystals were cryoprotected by crystallization buffer supplemented with 20% ethylene glycol prior to freezing in liquid nitrogen. Diffraction data from a single crystal was acquired at the X06SA beamline at the Swiss Light Source, Paul Scherrer Institut, Villigen, Switzerland. Data was processed with XDS[18] and scaled with SCALA[19] or AIMLESS,[20] structures were solved by molecular replacement with Phaser[21] or MOLREP[22] using PDB 3DWY as search model. Clear difference electron densities for compounds in the Kac binding pocket can be unambiguously modelled. Rounds of manual model building were carried out with COOT[23] and refinement was performed with Phenix.[24] Crystal data collection and refinement statistics are summarized in Table S2.

Table S1. 2D structures and contributions to the binding energy (in kcal/mol) for the 39 molecules predicted as candidate ligands of the CBP bromodomain by the docking program SEED[a].

	2D structure	intermolecular		electrostatic desolvation		total	Total
		vdW	elect.	protein	fragment	elect.	energy
1	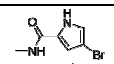	–16.9	–11.0	5.1	6.0	0.1	–16.8
2		–17.9	–7.7	6.7	3.4	2.4	–15.5
3	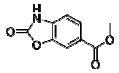	–14.5	–9.4	6.1	2.6	–0.7	–15.2
4	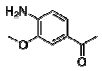	–18.0	–10.3	7.2	3.3	0.2	–17.8
5	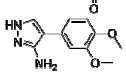	–18.2	–15.2	8.2	8.7	1.7	–16.5
6	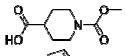	–20.1	–9.7	6.9	6.0	3.2	–16.9
7	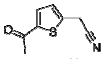	–16.1	–7.7	6.9	3.0	2.2	–13.9
8	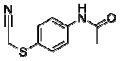	–14.8	–10.9	6.4	4.4	–0.1	–14.9
9	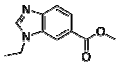	–19.1	–10.2	8.0	2.9	0.7	–18.4
10		–22.6	–7.5	5.6	4.8	2.9	–19.7
11	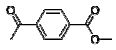	–16.8	–9.4	6.5	2.8	–0.1	–16.9
12		–22.2	–5.9	7.8	2.2	4.1	–18.1
13	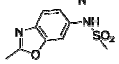	–18.6	–5.0	7.5	2.7	5.2	–13.4
14		–20.7	–12.2	8.3	6.6	2.7	–18.0
15	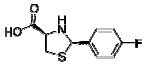	–17.8	–21.9	11.2	15.1	4.4	–13.4
16	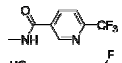	–17.1	–11.5	5.6	5.2	–0.7	–17.8
17	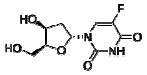	–19.2	–12.4	8.9	9.1	5.6	–13.6
18	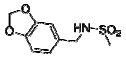	–15.3	–3.0	6.5	4.0	7.5	–7.8
19		–17.5	–8.1	5.3	2.6	–0.2	–17.7
20	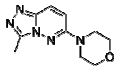	–19.5	–10.1	9.0	4.4	3.3	–16.2
21	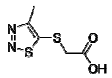	–20.7	–9.4	6.2	5.3	2.1	–18.6
22		–20.8	–8.3	6.1	1.6	–0.5	–21.4
23	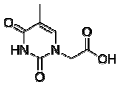	–17.8	–11.1	6.7	8.2	3.8	–14.0
24	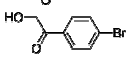	–16.3	–12.1	5.6	5.0	–1.5	–17.8
25		–18.1	–12.5	6.5	6.2	0.2	–17.9
26		–18.4	–12.4	6.4	6.3	0.3	–18.0
27	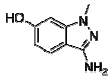	–17.9	–8.7	5.8	7.5	4.6	–13.3
28	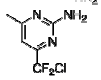	–18.4	–6.2	6.0	5.9	5.7	–12.7

29	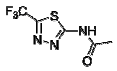	–16.2	–12.8	5.2	8.9	1.3	–14.9
30	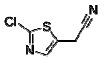	–17.7	–6.3	5.2	2.9	1.8	–15.9
31	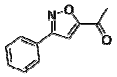	–16.3	–8.0	6.0	2.8	0.8	–15.5
32		–15.5	–7.4	5.4	2.8	0.8	–14.7
33		–18.3	–7.0	5.7	2.8	1.5	–16.8
34	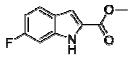	–16.5	–9.7	6.0	3.4	–0.3	–16.8
35	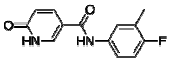	–17.3	–16.2	8.9	7.4	0.1	–17.2
36	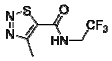	–17.7	–7.3	7.4	2.4	2.5	–15.2
37	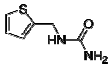	–11.9	–14.4	5.6	5.6	–3.2	–15.1
38		–11.0	–9.0	4.9	3.5	–0.6	–11.6
39	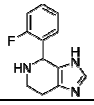	–15.9	–14.3	9.1	6.3	1.1	–14.8

[a]The SEED total energy (total energy) is the sum of the intermolecular van der Waals energy (vdW) and the total electrostatic energy. The total electrostatic is the sum of intermolecular electrostatic energy and desolvation penalties for protein and fragment.

Table S2. X-ray data collection and refinement statistics for complex structures of the CBP bromodomain and compounds 1, 2, 3 and 4.

Data Collection				
PDB ID	5MQE	5MQK	5MPZ	5MQG
ligand	**1**	**2**	**3**	**4**
space group	H3	H3	$P2_12_12_1$	H3
Cell dimensions				
a, b, c (Å)	122.37, 122.37, 39.35	122.36,122.36, 40.37	44.06, 44.06, 60.21	121.44, 121.44, 40.27
α, β, γ (°)	90.00, 90.00, 120.00	90.00, 90.00, 120.00	90.00, 90.00, 90.00	90.00, 90.00, 120.00
resolution (Å)	37.38 - 1.65	37.72 - 1.53	44.06 - 1.40	37.61 - 1.35
unique observations[a]	26769(1347)	33860(4964)	23766(1057)	48059(6756)
completeness[a]	99.7(99.5)	99.6(99.9)	98.9(90.1)	98.8(95.4)
redundancy[a]	5.1(4.5)	5.1(4.9)	5.8(3.3)	4.9(4.2)
Rmerge[a]	0.038(0.425)	0.041(0.485)	0.044(0.336)	0.030(0.335)
I/σI[a]	20.2(3.0)	16.5(3.3)	21.2(4.0)	20.7(3.6)
Refinement				
Rwork/Rfree[a]	0.184(0.260) /0.223(0.322)	0.183(0.278)/ 0.210(0.275)	0.157(0.206)/ 0.176(0.273)	0.171(0.244) /0.191(0.252)
r.m.s. deviations of bond lengths (Å)	0.007	0.007	0.005	0.006
r.m.s. deviations of bond angles (°)	0.909	0.915	0.957	0.891
Average B-factor (Å^2)				
protein	36.13	37.04	17.66	28.87
ligand	24.69	30.31	24.05	27.71
water	40.83	41.61	31.76	37.04
Ramachandran				
favored (%)	98.57	99.06	100	99.50
allowed (%)	1.43	0.94	0	0.50
disallowed (%)	0	0	0	0

[a]Highest resolution shell is shown in parentheses.

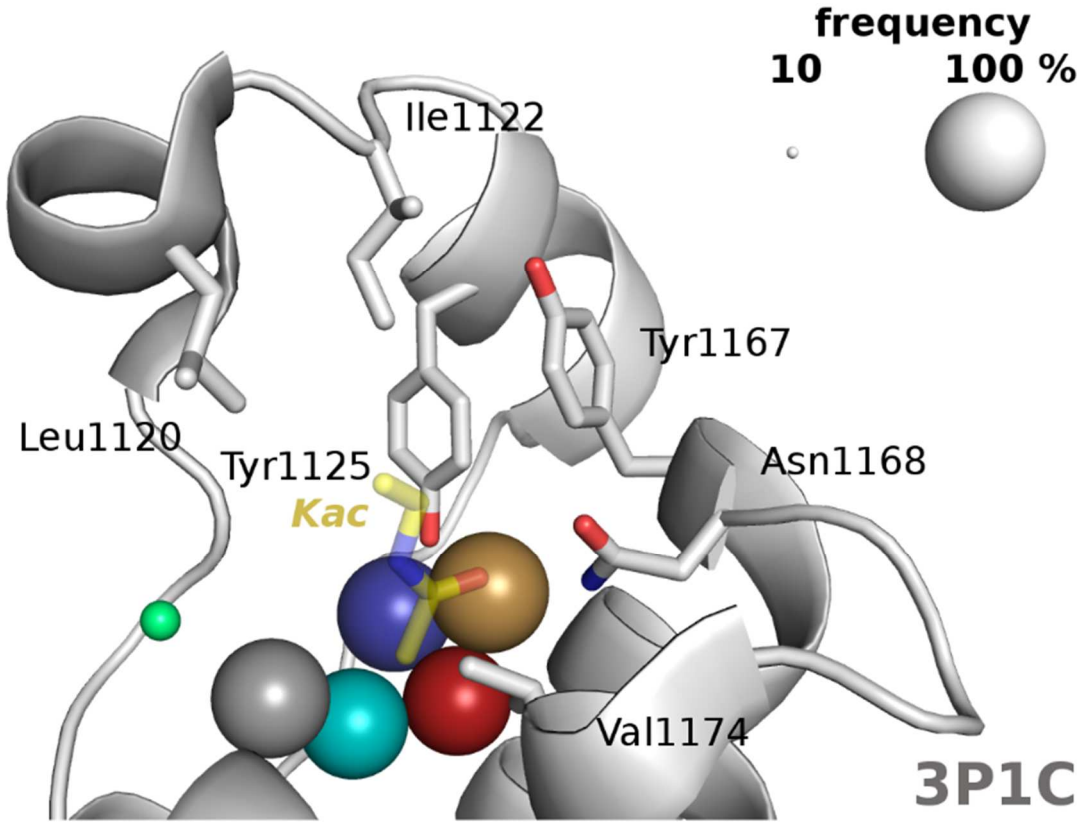

Figure S1. CBP bromodomain structure used for docking (PDB code: 3P1C). The six water molecules kept for the docking procedures are shown as spheres, with w_1 colored in gold (color code for the water molecules as in Figure 1B of [25]). The size of each sphere is proportional to the frequency of the corresponding water molecule (legend on top, right) in 44 inspected crystal structures of bromodomains bound to an acetyllysine (one structure each for PCAF, BRD2(2), BRD3(2), BRD4(2), BRDT(1), BRDT(2), and BAZ2A; two structures for TAF1(2); three structures each for CBP, BAZ2B, and TRIM24; four structures each for BRD2(1), ATAD2, and BRPF1; seven structures each for BRD4(1) and BRD9). The side chain of the residues discussed in the main text and the acetyllysine are shown as sticks (carbon atoms in gray and yellow, respectively).

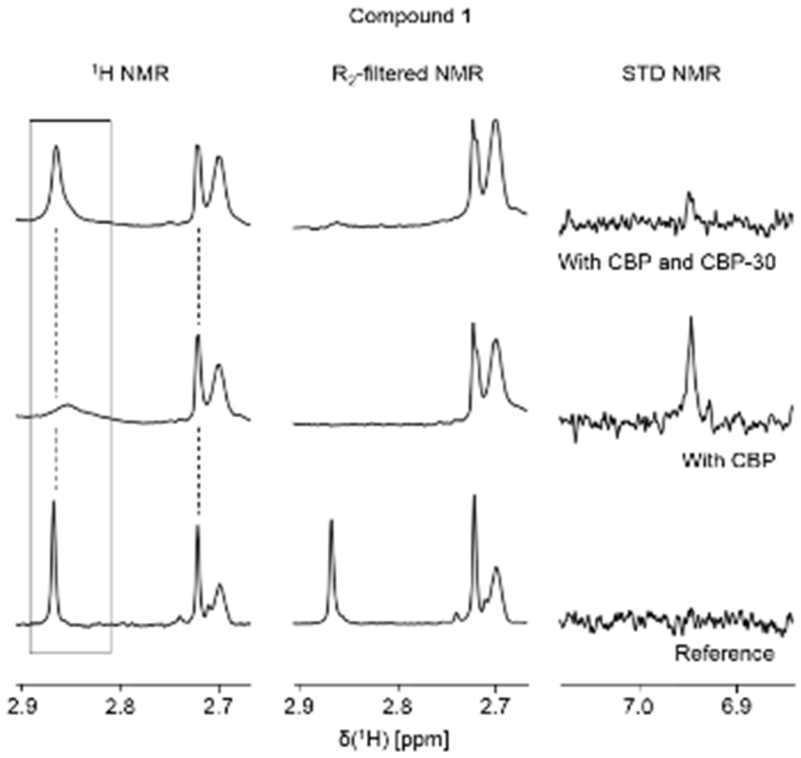

Figure S2. Ligand-observed NMR screening experiments for compound **1**. Peaks of the compound undergo ^{1}H chemical shift perturbation (left), an increase in the R_2 relaxation (middle) and STD effects (right) in the presence of the CBP bromodomain. Binding occurs in the acetyllysine binding site as titration of the nanomolar inhibitor SGC-CBP30 reverses all three observables.

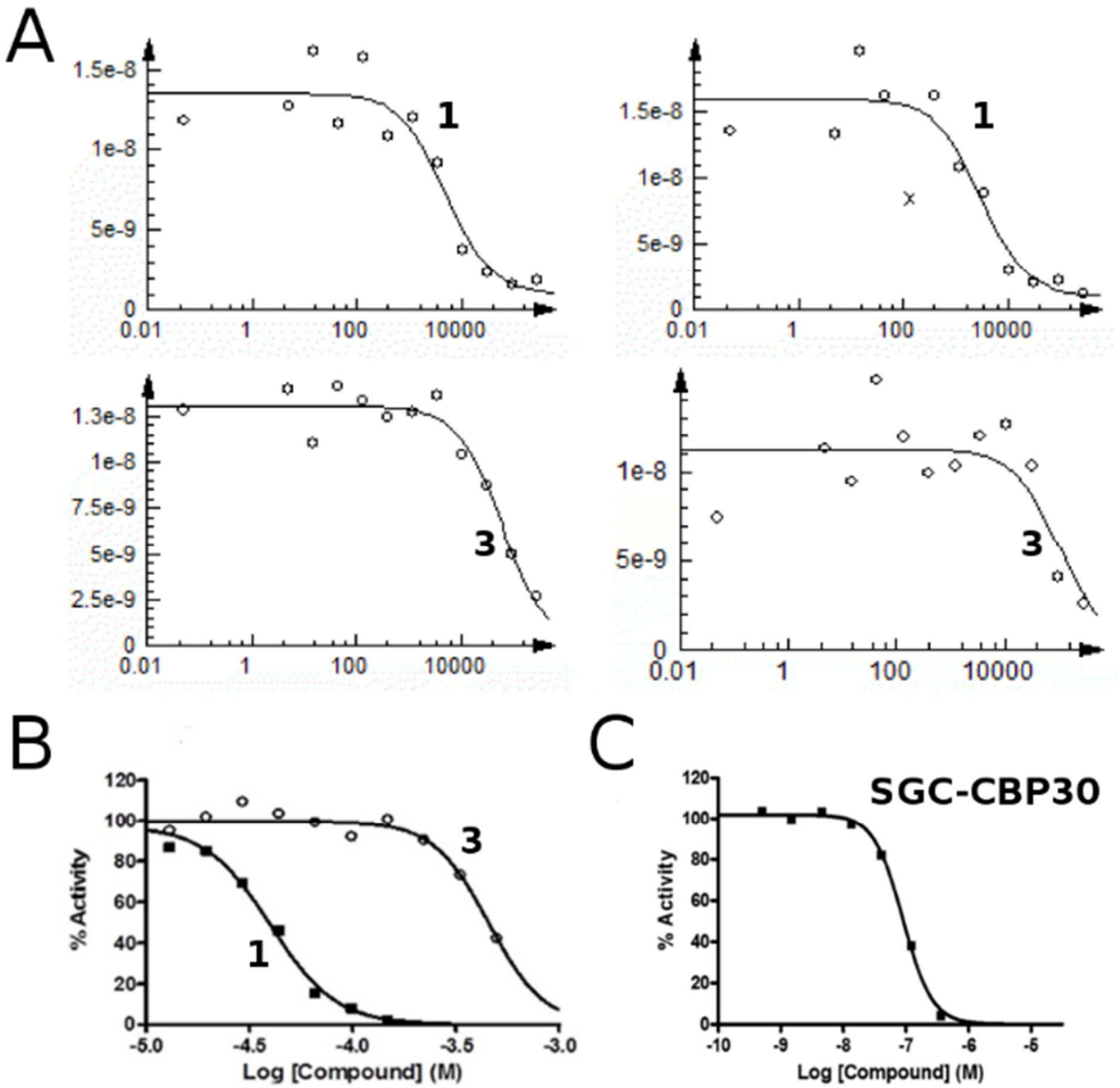

Figure S3. Competition binding assays for compounds **1** and **3**. (A) Dose-response curves in duplicates for the compounds **1** (top) and **3** (bottom) tested for binding to the CBP bromodomain in the BROMOscan competition binding assay. (B) Dose response curves for binding of hit fragments **1** (black squares) and **3** (open circles) to the CBP bromodomain as measured by the AlphaScreen assay using a biotinylated H4 peptide as competitive ligand at Reaction Biology Corporation. (C) SGC-CBP30 is used as a positive control; it consists of 36 heavy atoms and has a ligand efficiency of 0.31 kcal mol^{-1} HAC^{-1}.

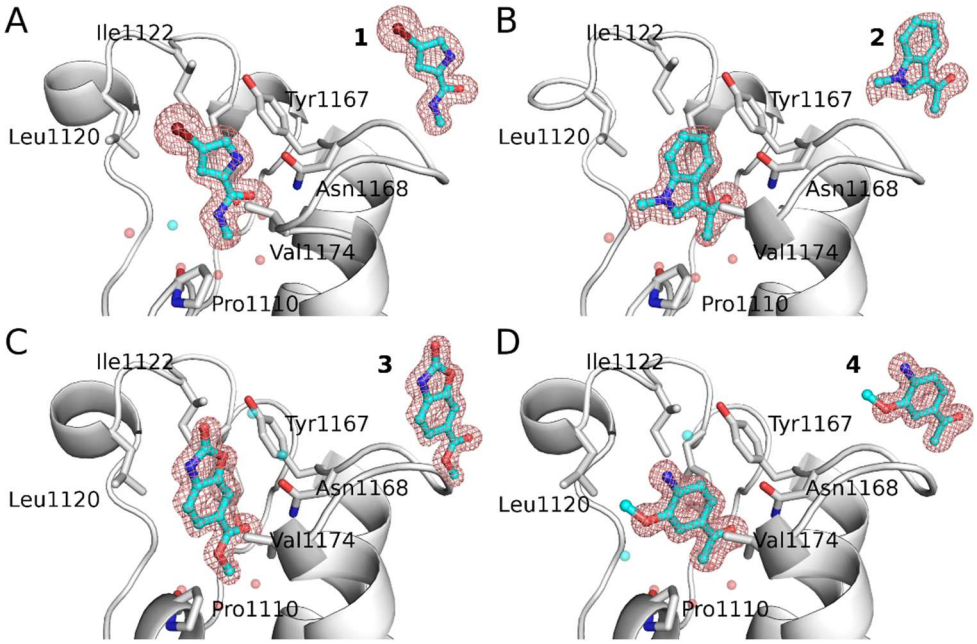

Figure S4. Close view of binding mode of compounds **1**–**4**. Conserved water molecules in the binding pocket are shown as transparent spheres color coded as in Figure 3. Fo – Fc omit map for each compounds is shown in mesh contoured at 3 σ.

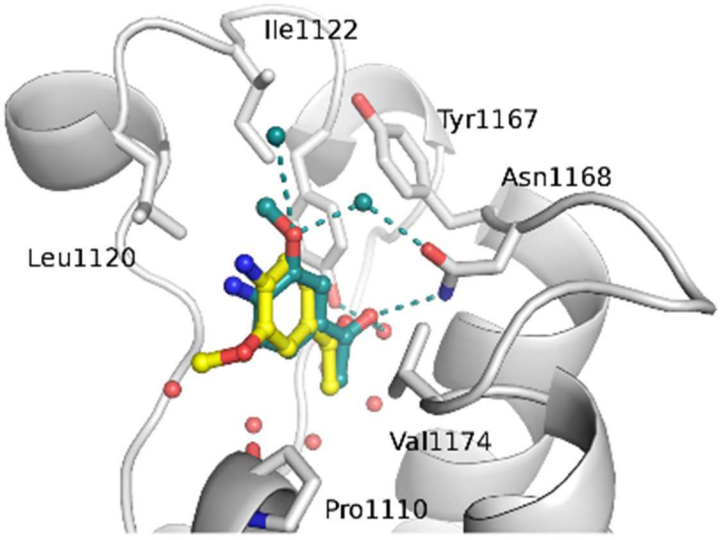

Figure S5. Comparison of the binding mode in the chain A of the crystal structure of the CBP/**4** complex (carbon atoms in deep teal, PDB code: 5MQG) with the binding pose predicted by docking with SEED [1, 2] (carbon atoms in yellow). The oxygen atom of the methoxy group forms a water-mediated hydrogen bond with the side chain of the conserved asparagine. Conserved water molecules (red spheres) and crystallographic water molecules not used for docking (deep teal spheres) are shown. Hydrogen bonds are shown as deep teal dashed lines.

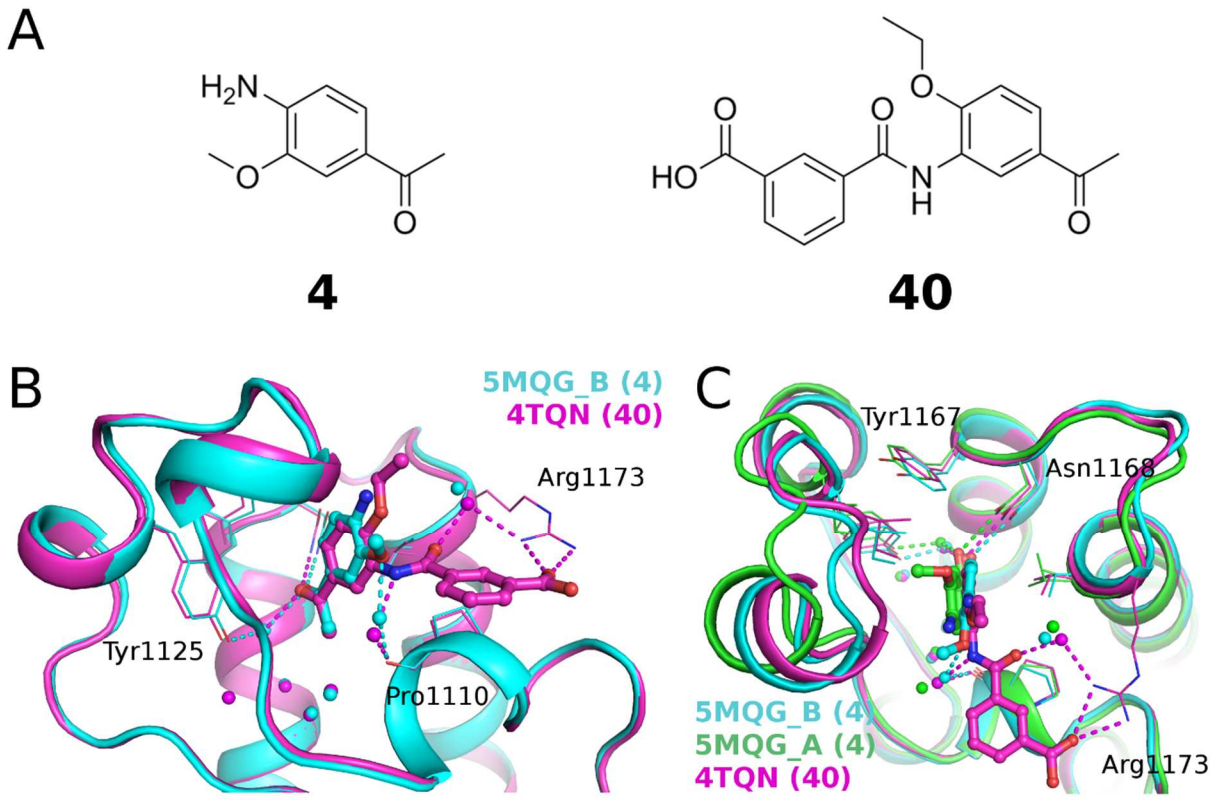

Figure S6. Comparison of the binding poses of compound **4** and the previously reported compound **40**. (A) Chemical structure of compounds **4** and **40**. (B) Comparison of the CBP/**4** complex (cyan) to the CBP/**40** complex (magenta, PDB code: 4TQN). Compound **4** recapitulates many polar interactions of the larger compound **40** (color-coded dashed lines), including a water-bridged hydrogen bond with the backbone oxygen of Pro1110. The smaller compound **4**, though, does not establishes any interaction with the side chain of Arg1173. (C) Comparison of the binding pose of compound **4** in the two chains of the asymmetric unit (cyan and green) and compound **40** (magenta).

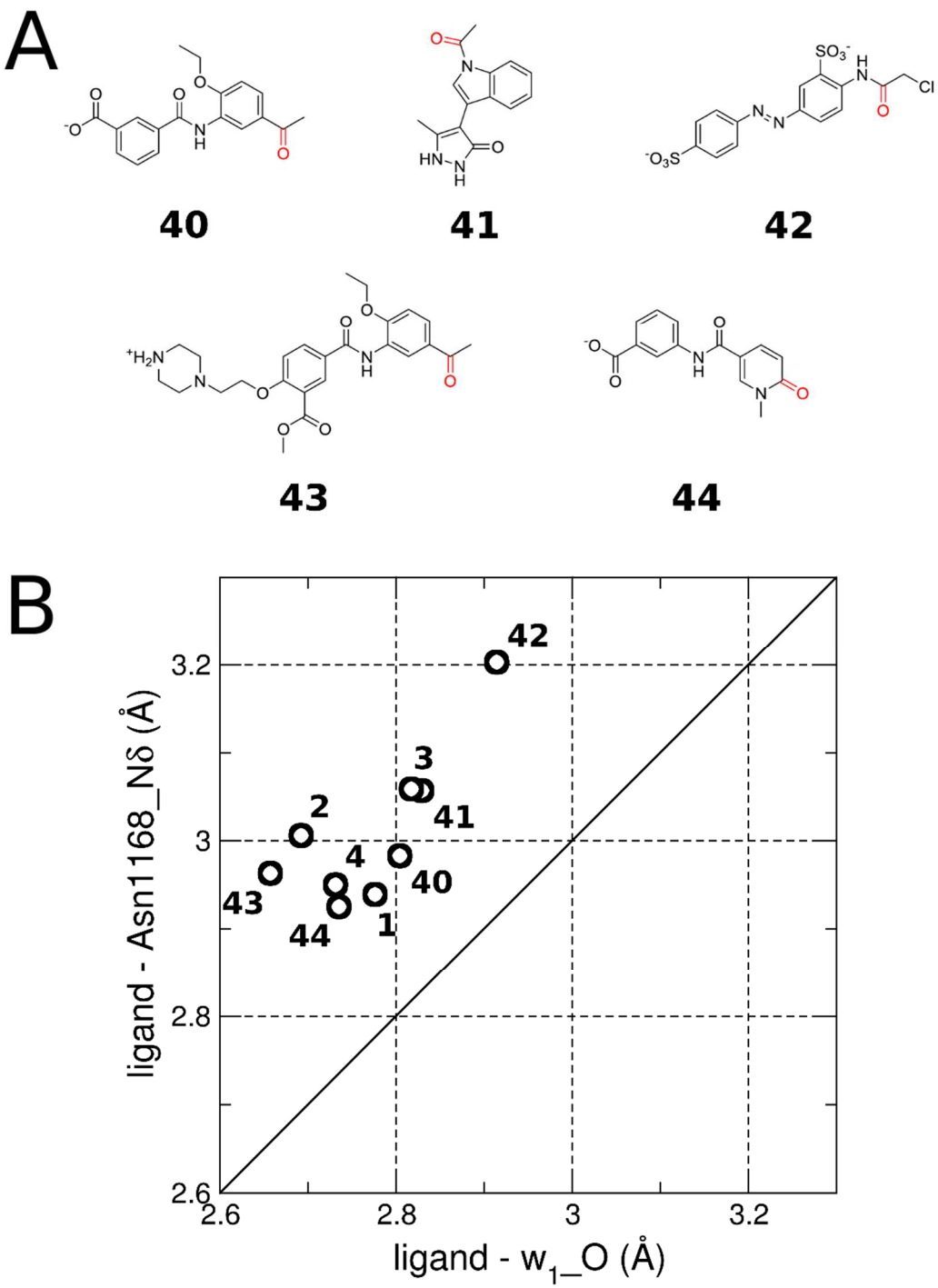

Figure S7. Analysis of the H-bonds of the group that mimics the acetyl of Kac. (A) 2D structures of compounds **40** (**10** in [26], PDB code: 4TQN), **41** (**1b** in [27], PDB code: 4TS8), **42** (PDB code: 5EIC), **43** (PDB code: 5ENG), and **44** (PDB code: 5EP7). The carbonyl group involved in the H-bond is in red. (B) Scatter plot of the distances involving the side chain nitrogen of Asn1168, with numbers indicating the ligand. In all cases the hydrogen bond distance with the conserved water w_1 that bridges to the Tyr1125 side chain is shorter than the distance to the Asn1168.

REFERENCES

1. Majeux N, Scarsi M, Apostolakis J, Ehrhardt C, Caflisch A. Exhaustive docking of molecular fragments with electrostatic solvation. *Proteins.* 1999;37: 88-105.
2. Majeux N, Scarsi M, Caflisch A. Efficient electrostatic solvation model for protein-fragment docking. *Proteins.* 2001;42(2): 256-268.
3. MacKerell AD, Bashford D, Bellott M, et al. All-atom empirical potential for molecular modeling and dynamics studies of proteins. *J Phys Chem B.* 1998;102(18): 3586-3616.
4. MacKerell AD, Feig M, Brooks CL, 3rd. Improved treatment of the protein backbone in empirical force fields. *J Am Chem Soc.* 2004;126(3): 698–699.
5. Vanommeslaeghe K, Hatcher E, Acharya C, et al. CHARMM general force field: A force field for drug-like molecules compatible with the CHARMM all-atom additive biological force fields. *J Comput Chem.* 2010;31(4): 671-690.
6. Scarsi M, Apostolakis J, Caflisch A. Continuum electrostatic energies of macromolecules in aqueous solutions. *J Phys Chem A.* 1997;101(43): 8098-8106.
7. Zhao H, Huang D. Hydrogen bonding penalty upon ligand binding. *PLoS ONE.* 2011;6(6): e19923.
8. Zhao H, Gartenmann L, Dong J, Spiliotopoulos D, Caflisch A. Discovery of BRD4 bromodomain inhibitors by fragment-based high-throughput docking. *Bioorg Med Chem Lett.* 2014;24(11): 2493-2496.
9. Huang D, Caflisch A. Library screening by fragment-based docking. *J Mol Recognit.* 2010;23(2): 183-193.
10. Zhao H, Caflisch A. Molecular dynamics in drug design. *Eur J Med Chem.* 2015;91: 4-14.
11. Filippakopoulos P, Picaud S, Mangos M, et al. Histone recognition and large-scale structural analysis of the human bromodomain family. *Cell.* 2012;149(1): 214-231.
12. Hwang T-L, Shaka AJ. Water suppression that works. Excitation sculpting using arbitrary waveforms and pulse field gradients. *J Magn Reson A.* 1995;112: 275-279.
13. Mayer M, Meyer B. Characterization of ligand binding by saturation transfer difference NMR spectroscopy. *Angew Chem, Int Ed.* 1999;38: 1784-1788.
14. Carr HY, Purcell EM. Effects of diffusion on free precession in nuclear magnetic resonance experiments. *Phys Rev.* 1954;94(3): 630-638.
15. Hay DA, Fedorov O, Martin S, et al. Discovery and optimization of small-molecule ligands for the CBP/p300 bromodomains. *J Am Chem Soc.* 2014;136(26): 9308-9319.
16. Philpott M, Yang J, Tumber T, et al. Bromodomain-peptide displacement assays for interactome mapping and inhibitor discovery. *Mol bioSyst.* 2011;7(10): 2899-2908.
17. Quinn E, Wodicka L, Ciceri P, et al. BROMOscan - a high throughput, quantitative ligand binding platform identifies best-in-class bromodomain inhibitors from a screen of mature compounds targeting other protein classes. *Cancer Res.* 73. 2013:4238.
18. Kabsch W. Xds. *Acta Crystallogr D Biol Crystall.* 2010;66(Pt 2): 125-132.
19. Winn MD, Ballard CC, Cowtan KD, et al. Overview of the CCP4 suite and current developments. *Acta Crystallogr D Biol Crystall.* 2011;67(Pt 4): 235-242.
20. Evans PR, Murshudov GN. How good are my data and what is the resolution? *Acta Crystallogr D Biol Crystall.* 2013;69(Pt 7): 1204-1214.
21. McCoy AJ, Grosse-Kunstleve RW, Adams PD, Winn MD, Storoni LC, Read RJ. Phaser crystallographic software. *J Appl Crystallogr.* 2007;40(Pt 4): 658-674.
22. Vagin A, Teplyakov A. Molecular replacement with MOLREP. *Acta Crystallogr D Biol Crystall.* 2010;66(Pt 1): 22-25.
23. Emsley P, Lohkamp B, Scott WG, Cowtan K. Features and development of Coot. *Acta Crystallogr D Biol Crystall.* 2010;66(Pt 4): 486-501.
24. Adams PD, Afonine PV, Bunkoczi G, et al. PHENIX: a comprehensive Python-based system for macromolecular structure solution. *Acta Crystallogr D Biol Crystall.* 2010;66(Pt 2): 213-221.
25. Huang D, Rossini E, Steiner S, Caflisch A. Structured water molecules in the binding site of bromodomains can be displaced by cosolvent. *ChemMedChem.* 2014;9(3): 573-579.
26. Xu M, Unzue A, Dong J, Spiliotopoulos D, Nevado C, Caflisch A. Discovery of CREBBP bromodomain inhibitors by high-throughput docking and hit optimization guided by molecular dynamics. *J Med Chem.* 2016;59(4): 1340-1349.

27. Unzue A, Zhao H, Lolli G, et al. The "gatekeeper" residue influences the mode of binding of acetyl indoles to bromodomains. *J Med Chem.* 2016;59(7): 3087-3097.

Chapter 5

Chemical space expansion of bromofomain ligands guided by in silico virtual couplings (Autocouple)

Batiste L, Unzue A, Dolbois A, Hassler F, Wang X, Deerain N, **Zhu J**, Spiliotopoulos D, Nevado C, Caflisch A. ACS Central Science 2018, 4 (2): 180–188.

ACS central science

Research Article

Cite This: ACS Cent. Sci. 2018, 4, 180−188

Chemical Space Expansion of Bromodomain Ligands Guided by in Silico Virtual Couplings (AutoCouple)

Laurent Batiste,[†,‡] Andrea Unzue,[‡,§] Aymeric Dolbois,[§] Fabrice Hassler,[§] Xuan Wang,[†,§] Nicholas Deerain,[†] Jian Zhu,[†] Dimitrios Spiliotopoulos,[†] Cristina Nevado,*[,§] and Amedeo Caflisch*[,†]

[†]Department of Biochemistry, University of Zurich, Winterthurerstrasse 190, CH-8057, Zürich, Switzerland

[§]Department of Chemistry, University of Zurich, Winterthurerstrasse 190, CH-8057, Zürich, Switzerland

Supporting Information

ABSTRACT: Expanding the chemical space and simultaneously ensuring synthetic accessibility is of upmost importance, not only for the discovery of effective binders for novel protein classes but, more importantly, for the development of compounds against hard-to-drug proteins. Here, we present AutoCouple, a de novo approach to computational ligand design focused on the diversity-oriented generation of chemical entities via virtual couplings. In a benchmark application, chemically diverse compounds with low-nanomolar potency for the CBP bromodomain and high selectivity against the BRD4(1) bromodomain were achieved by the synthesis of about 50 derivatives of the original fragment. The binding mode was confirmed by X-ray crystallography, target engagement in cells was demonstrated, and antiproliferative activity was showcased in three cancer cell lines. These results reveal AutoCouple as a useful in silico coupling method to expand the chemical space in hit optimization campaigns resulting in potent, selective, and cell permeable bromodomain ligands.

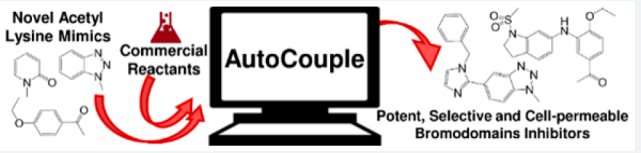

INTRODUCTION

The druglike chemical space is estimated at 10^{60} organic molecules, but only 100 million have been synthesized to date, and an even smaller fraction thereof is commercially available.[1,2] Libraries of purchasable molecules are biased toward certain classes of targets, in particular G-protein-coupled receptors and kinases.[3,4] Repositories of pharmaceutical companies consist of 10^6 to 10^7 compounds which barely scratch the surface of chemical space. Success in high-throughput screening ultimately relies on the screening library:[5−7] the exploration of chemical space that is not biased toward already investigated targets is decisive not only for the discovery of effective binders for novel protein classes but, more importantly, for the development of compounds against protein targets that are hard-to-drug.[8−11] Classical de novo strategies can potentially populate new areas of chemical space,[12−16] and thus, programs have been developed to disconnect molecules following retrosynthesis rules[17,18] producing fragments that can be used later on to construct new libraries.[19] Nevertheless, significant challenges when reaching the synthesis stage might prevent those new molecular entities from being prepared and, ultimately, becoming useful chemical probes.[13] In addition, time pressure in drug-discovery campaigns demands new tools to improve the identification of hits and streamline their optimization into lead compounds.[20] Computational tools for de novo generation of molecular entities via virtual couplings have been reported.[21−24] The method proposed here, called AutoCouple, distinguishes itself by starting from a set of available building blocks that are assembled via virtual organic reactions in such a way that, at the coupling step, the reaction partners are parsed automatically and are coupled only if no undesired group is contained (e.g., groups that would require additional protection steps or lead to cross reactivity products are discarded). As such, AutoCouple generates libraries of compounds that are, ideally, synthesizable in one step.

Bromodomains are protein modules that bind acetylated lysine (KAc) residues in histone tails and other proteins. Among the 61 known human bromodomains,[25] the BET family, in particular BRD4(1) (the first bromodomain of the protein called BRD4), has been widely targeted because of its involvement in cancer, type 2 diabetes, and cardiovascular diseases.[26−30] Several small molecule ligands of BET bromodomains are currently in clinical trials, which highlights the potential of regulating post-transcriptional modifications of histone tails in the current landscape of drug discovery.[31−34] In contrast, selective and potent bromodomain ligands, aiming to unravel the biological implications of bromodomains outside the BET family, have only recently started to be developed.[35−54] In particular, the bromodomain of CBP (the epigenetic reader of the cyclic AMP response element binding protein) is an interesting target due to its key role in several diseases including cancer and neurological disorders.[55] Despite recent efforts toward developing novel and selective CBP bromodomain inhibitors, the chemotypes that are able to act as KAc mimic are still rather limited and, except for GNE-781, demand exquisite absolute stereocontrol, thus complicating their synthetic accessibility (Figure 1A).[56−67]

Our groups have recently reported the fragment-based design[68,69] of acetyl benzene derivatives as selective nanomolar

Received: August 29, 2017
Published: February 7, 2018

DOI: 10.1021/acscentsci.7b00401
ACS Cent. Sci. 2018, 4, 180−188

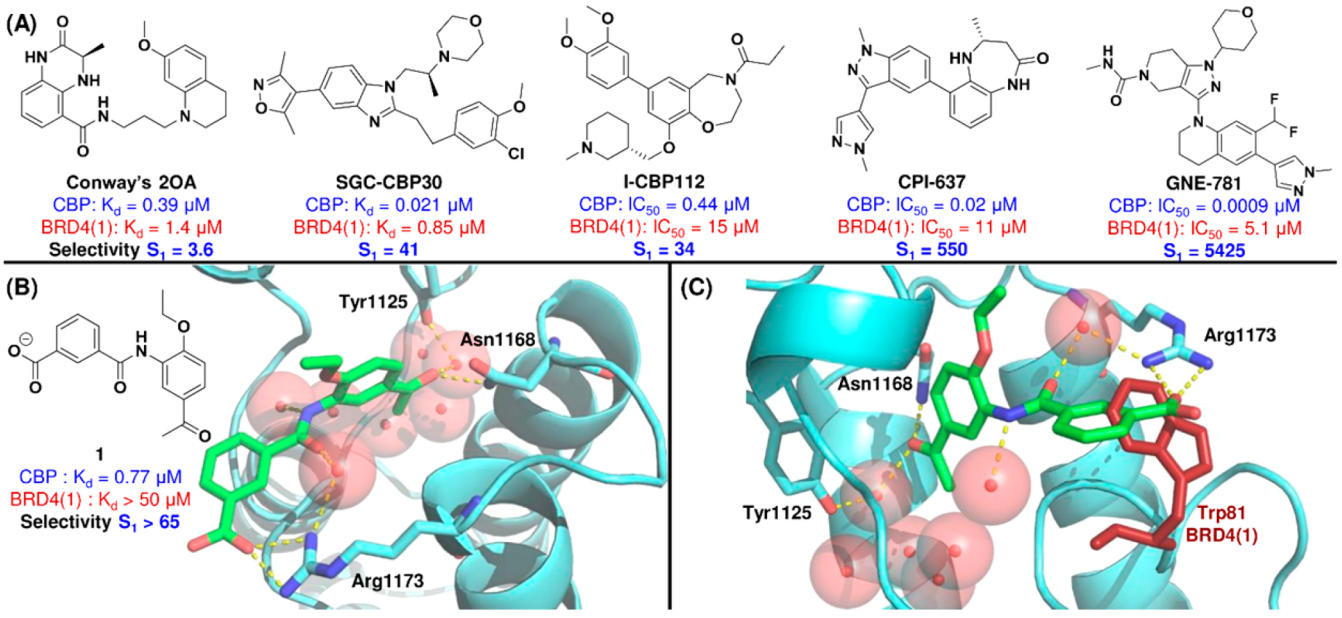

Figure 1. (A) List of current nM inhibitors of the CBP bromodomain.[44,56−58,60] Dissociation constant (K_d) determined by isothermal titration calorimetry (ITC). Half-maximal inhibitory concentration (IC_{50}) determined by time-resolved fluorescence resonance energy transfer (TR-FRET). Selectivity for CBP over BRD4(1) bromodomains (S_1) determined by the ratio of K_d or IC_{50} values. (B) Crystal structure of the CBP bromodomain (cyan) in complex with compound **1** (green) (PDB code: 4TQN).[70,71] The acetyl benzene moiety acts as a KAc mimic interacting directly and through a water molecule with the side chains of the conserved residues Asn1168 and Tyr1125, respectively. The carboxylate function of the tail group forms a salt bridge with the guanidinium of Arg1173. The amide linker is involved in two water-bridged hydrogen bonds with the CBP bromodomain. (C) Overlay of the complex of compound **1** (green) with the CBP bromodomain (cyan) and the structure of BRD4(1) (4PCI) shows that the selectivity is due to bumping of the benzoate into the Trp81 side chain (red) of the so-called WPF triad of BRD4(1).

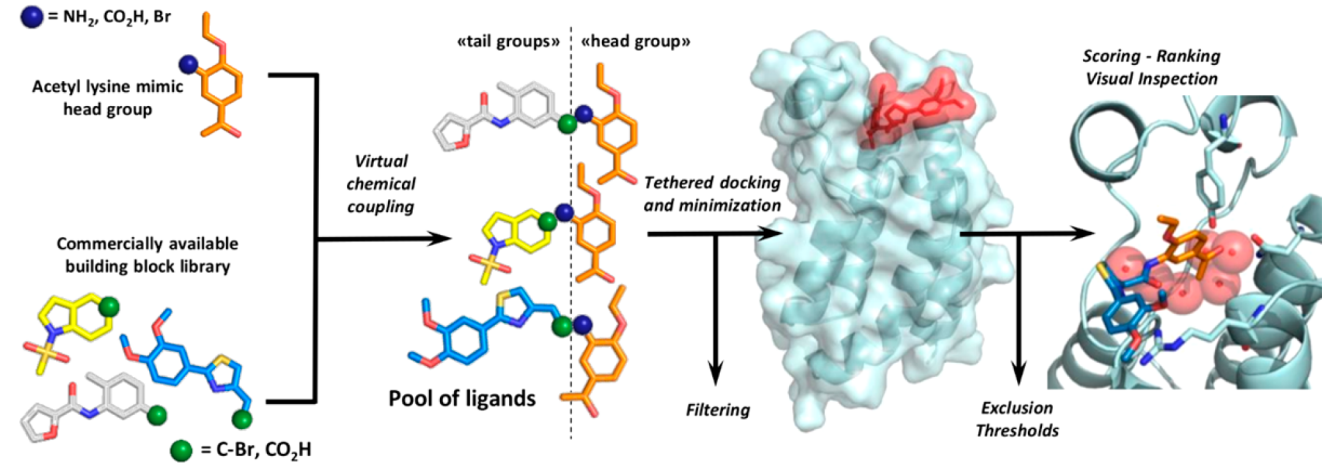

Figure 2. Schematic representation of AutoCouple. A headgroup (here the KAc mimic is shown in orange) is virtually coupled to commercially available building blocks. The resulting library is filtered out to remove any protein-reactive functionalities and subsequently docked while maintaining key interactions of the headgroup inside the target's binding site. The compounds are ranked according to binding energy calculated by a force field with continuum electrostatic solvation.

CBP bromodomain ligands.[70,71] Compound **1** (Figure 1B), bearing a benzoic acid moiety, proved to be a synthetically accessible molecule with an equilibrium dissociation constant (K_d) of 770 nM for the CBP bromodomain and good selectivity over BRD4(1) (selectivity >65-fold according to the ratio of K_d values). The overlap of the crystal structures of the complex of compound **1** with the CBP bromodomain and the structure of BRD4(1) (Figure 1C) shows that the selectivity is due to the steric clash between the benzoate group and the Trp81 side chain of the so-called WPF triad of BRD4(1). Further development of this compound was not pursued given its lack of target engagement in cells, likely due to the negative effect of the carboxylate on the compound's permeability, a commonly encountered problem in medicinal chemistry optimization campaigns.[72−74] We thus set out to identify new chemotypes enabling interactions at the outer part of the binding site of the CBP bromodomain (Arg1173 and/or the so-called ZA loop) that could potentially translate into ligands with improved potency, selectivity, and cell permeability compared to hit **1**.

To this end, we sought to establish an efficient method for growing fragments into potent and selective ligands taking chemical accessibility into account at the outset of the computation.[75,76] This early on synthesis oriented approach

DOI: 10.1021/acscentsci.7b00401
ACS Cent. Sci. 2018, 4, 180−188

Scheme 1. AutoCouple Results for the CBP Bromodomain Using (A) Amide Condensation, (B) Buchwald−Hartwig Amination, and (C) Suzuki Cross-Coupling Reactions from Aniline (2), Bromobenzene (3), and Aryl Boronic Ester (4) as "Headgroups", Respectively[a]

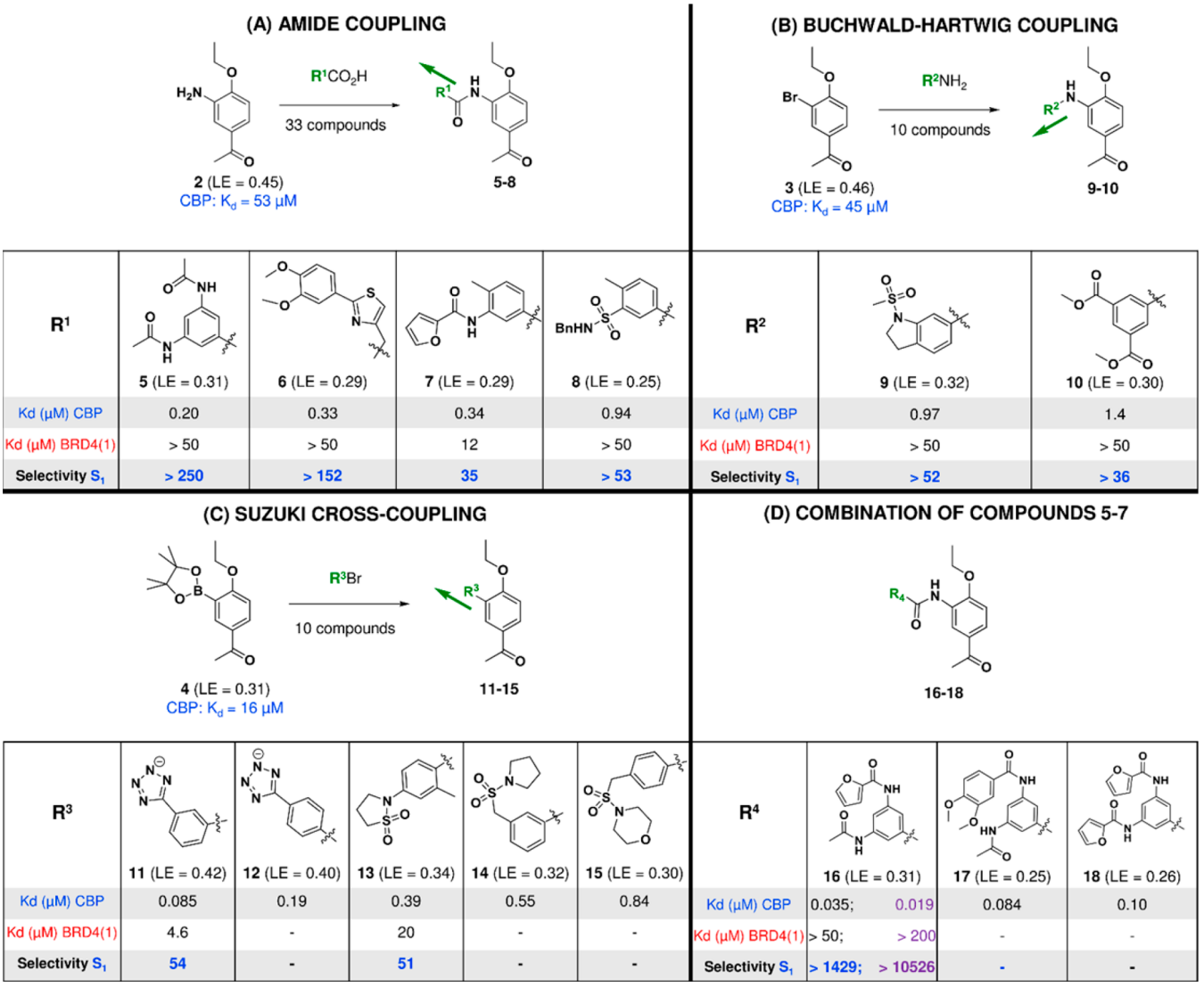

R1	5 (LE = 0.31)	6 (LE = 0.29)	7 (LE = 0.29)	8 (LE = 0.25)
Kd (µM) CBP	0.20	0.33	0.34	0.94
Kd (µM) BRD4(1)	> 50	> 50	12	> 50
Selectivity S_1	> 250	> 152	35	> 53

R2	9 (LE = 0.32)	10 (LE = 0.30)
Kd (µM) CBP	0.97	1.4
Kd (µM) BRD4(1)	> 50	> 50
Selectivity S_1	> 52	> 36

R3	11 (LE = 0.42)	12 (LE = 0.40)	13 (LE = 0.34)	14 (LE = 0.32)	15 (LE = 0.30)
Kd (µM) CBP	0.085	0.19	0.39	0.55	0.84
Kd (µM) BRD4(1)	4.6	-	20	-	-
Selectivity S_1	54	-	51	-	-

R4	16 (LE = 0.31)		17 (LE = 0.25)	18 (LE = 0.26)
Kd (µM) CBP	0.035;	0.019	0.084	0.10
Kd (µM) BRD4(1)	> 50;	> 200	-	-
Selectivity S_1	> 1429;	> 10526	-	-

[a] K_d values (µM) were determined by a competition binding assay in duplicates (BROMOscan).[88] IC_{50} values for compound **16** are indicated in purple and were determined by amplified luminescent proximity homogeneous assay (Alpha) screen technology (Reaction Biology). Ligand efficiency (LE) values refer to the CBP bromodomain. Selectivity for CBP over BRD4(1) bromodomains (S_1) determined by the ratio of K_d or IC_{50} values. (D) Chimerization of compounds **5**−**7**. The growing vectors (green arrows) of the different coupling strategies show the similarity between the amide and the C−C coupled products compared to the amine linker in orienting the tail group.

would confer on our method the possibility to overcome the limitations of previously released software tools which typically suggest hard-to-synthesize molecules, hampering follow-up medicinal chemistry efforts. Here, we present the realization of this concept with AutoCouple, a novel approach to de novo computational ligand design that focuses on the diversity-oriented generation of chemical entities via virtual chemical couplings. AutoCouple is the first fragment-growing software tool that generates synthetically accessible molecules with a force field based prediction of their binding energy without any fitting parameter. Its operative and pragmatic value has been demonstrated by the discovery of novel chemical blueprints which translated into nM potent and cell-permeable inhibitors of the CBP bromodomain with high selectivity over BRD4(1). Further, the preliminary biological evaluation of cell permeable ligands points toward the potential use of these compounds to unravel the role of CBP in several types of solid tumors and hematological malignancies.[77]

RESULTS AND DISCUSSION

Implementation of AutoCouple and Application to CBP Bromodomain. First, a suite of Python scripts[78,79] was assembled (see section 1 in the Supporting Information) to generate a virtual library from commercially available reagents by a set of coupling reactions suited for medicinal chemistry (Figure 2). Three reactions were established based on the following criteria:[5,80] (a) the robustness of the intended chemical coupling, (b) the applicability to a wide variety of reactants, (c) the proven relevance/use in drug-discovery campaigns. The acetyl benzene moiety within **1** was retained as

DOI: 10.1021/acscentsci.7b00401
ACS Cent. Sci. 2018, 4, 180−188

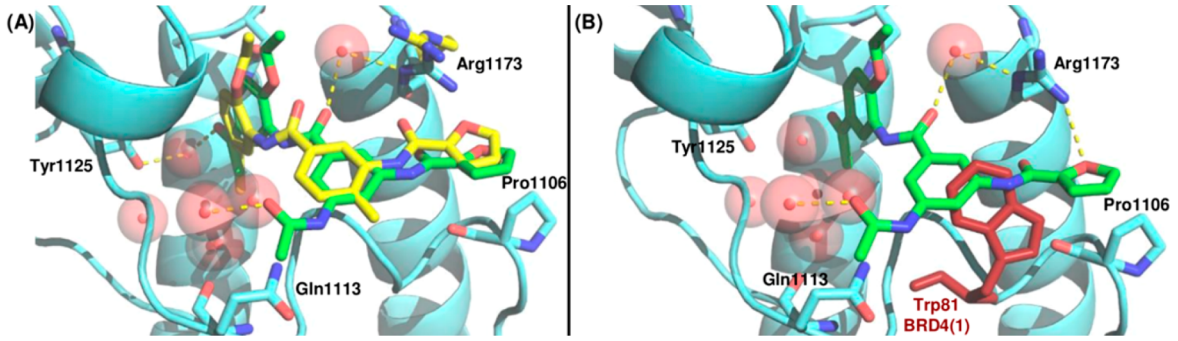

Figure 3. (A) Structural alignment of the crystal structure of the CBP bromodomain (cyan) in complex with ligand **16** (green) (PDB code 5NLK) and the pose of ligand **7** (yellow) as predicted by docking into the CBP structure 4NYX (Arg1173 side chain in yellow). (B) Overlay of the complex of compound **16** (green) with the CBP bromodomain (cyan) and the structure of BRD4(1) (4PCI) shows that the selectivity is due to bumping of the phenyl into the Trp81 side chain (red) of the so-called WPF triad of BRD4(1).

the KAc mimic (from now on referred to as "headgroup"), and we thus decided to explore the chemical space of the "tail group" adjacent to the KAc mimic.

First, commercially available building block libraries were generated, followed by coupling in silico to the KAc mimic in compound **1**. Aniline **2**, bromobenzene **3**, and aryl boronic ester **4** were selected as "headgroups" for amide condensation, Buchwald−Hartwig amination, and Suzuki cross-coupling, respectively (Schemes 1A, 1B, and 1C respectively). For the tail, a library of ∼270,000 commercially available compounds was sorted according to chemical functionalities. A series of filters were applied to limit the final molecular complexity and to discard molecular patterns known to react non-specifically with most proteins[81,82] as well as heavy metals containing molecules. Moreover, to avoid redundancies, any building blocks with the same CAS number were merged. Considering that chemical couplings imply an increase in the molecular complexity (except for cleavage reactions),[22] and that the coupling products should preferably satisfy the Lipinski rule of 5 for druglikeness, building blocks meeting any of the following criteria were discarded: (a) >5 rotatable bonds; (b) number of heavy atoms (= non-hydrogen) smaller than 3 or larger than 35; (c) >2 chiral centers. Each virtual reaction was also encoded to discard any building block that contained undesired chemical functionalities that would require a protecting group or lead to cross-reactivity problems. For instance, for the Buchwald−Hartwig coupling, the amine building blocks containing a halide (which would ultimately lead to self-condensation) were not kept for the virtual reactions.

A total of ∼70,000 virtual compounds were generated: 32,000 carboxylic amides (A), 19,000 anilines (B), and 19,000 C−C coupled ligands (C). Five independent docking campaigns were carried out with libraries A, B, and C using the CBP bromodomain structures 3P1C, 4TQN, and 4NYX (see section 1.3 in the Supporting Information). Multiple crystal structures were used because of the flexibility of the Arg1173 side chain and the rigid-protein protocol employed for docking by the open-source software rDock.[83] The acetyl benzene was initially oriented in the binding site to mimic the KAc residue as observed in the crystal structure and then underwent flexible docking. The poses obtained by docking were subsequently minimized using the CHARMM program[84] and the CHARMM36/CGenFF force field[85,86] with evaluation of desolvation effects in the continuum dielectric approximation.[87] Receiver operating characteristic (ROC) curves using known positive controls[70,71] were plotted as to ensure the ability of the force field and implicit solvent approximation (finite-difference Poisson) to prioritize active ligands.

Synthesis of de Novo Ligand Binders: Potency, Selectivity, and Binding Mode Validation. Overall, 53 top-ranking compounds were synthesized (Scheme 1A−C) and a competition binding assay (BROMOscan)[88] was used to measure dissociation constants (for exhaustive data on all synthesized ligands, see section 2 in the Supporting Information). Using amide coupling for fragment assembly enabled us to identify arylsulfonamides, -acetamides, and -thiazoles with diverse substitution patterns (**5**−**8**) as suitable motifs to replace the original benzoate "tail group". These de novo synthesized ligands displayed comparable or even improved levels of potency and selectivity compared to those previously observed for **1**. Compound **5** showed not only a 4-fold improvement in potency (K_d = 200 nM) but also a remarkably high selectivity (>250-fold) against BRD4(1). Furthermore, the "amide-coupling" campaign resulted in 33 synthesized molecules, four of which display submicromolar affinity (compounds **5**−**8**, Scheme 1A), 17 are low micromolar binders (1.2−6.5 μM), and 10 have K_d values between 10 μM and 45 μM (see Figure S1). Compounds stemming from both Buchwald−Hartwig amination (**9**, **10**) and Suzuki cross-coupling (**11**−**15**) consistently showed improved affinities and good selectivity while offering additional motifs (cyclic and linear alkylsulfonamides, diester, tetrazoles) to the portfolio of "tail groups" for CBP ligands (Scheme 1B,C).

Interestingly, five out of 10 molecules synthesized by Suzuki cross-couplings are nanomolar binders with K_d values ranging from 85 to 840 nM (Scheme 1C, compounds **11**−**15**), thus confirming the ability of AutoCouple to identify good binders.

The comparison between the three series of compounds (A, B, C) confirms that the amide linker does not contribute significantly to binding affinity, which is consistent with previous molecular dynamics simulations that showed rotations of the amide group on the 100 ns time scale.[70,89] In addition, the analysis of the growing vectors of the three coupling strategies reveals interesting trends. As shown by the green arrows (growing vectors) in Scheme 1, a geometric similarity between the amide and the C−C coupled products (A, C) can be found, in line with the consistently higher potency observed for the compounds obtained via these two reactions compared to those introducing the amine linker (B).

The preparation of an analogue of compound **1** bearing a triazole as KAc mimic (Table S2) turned out to be more selective for BRD4(1) over CBP, suggesting that the selectivity

DOI: 10.1021/acscentsci.7b00401
ACS Cent. Sci. 2018, 4, 180−188

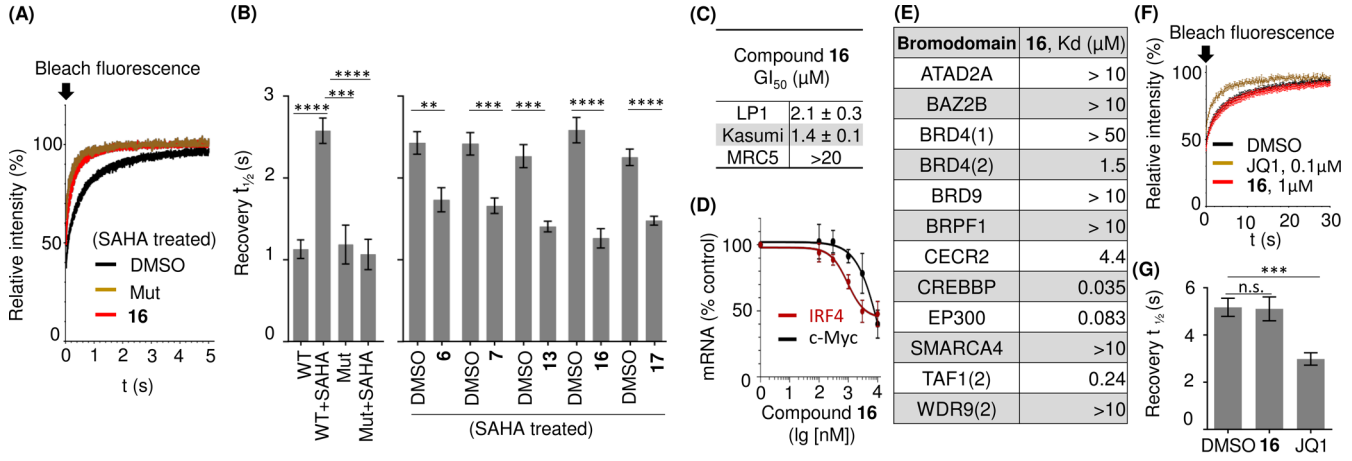

Figure 4. (A,B) FRAP assay for compounds **6**, **7**, **13**, **16**, and **17**; U2OS cells were transfected with plasmids encoding GFP-fused to wild-type (WT) or mutant (N1168F) multimerized CBP bromodomain, with or without 2.5 μM suberoylanilide hydroxamic acid (SAHA, a deacetylase inhibitor) and indicated compounds at a concentration of 1 μM. (A) Fluorescent recovery curves after photobleaching (normalized to the intensity before bleaching). (B) Half-times of the fluorescence recovery ($t_{1/2}$) ($n \geq 7$ cells per group, error bars: standard error of the mean). The recovery $t_{1/2}$ of the compound-treated cells was compared to that of DMSO-treated cells (bar on the left) within the same experiment setup using Mann−Whitney test. **, $P < 0.01$; ***, $P < 0.001$; ****, $P < 0.0001$. (C) Concentration of compound **16** that results in 50% growth inhibition (GI50). LP1 and Kasumi are human tumor cell lines while the nontransformed fibroblast MRC5 is a negative control. GI50 values were determined by a resazurin assay after 72 h compound incubation. (D) Dose-dependent inhibition of IRF4 and c-Myc mRNA transcription (RT-qPCR) by compound **16** in LP1 cells after 6 h of treatment. (C, D) Values represent the mean of at least three biological replicates ± SD. The curves are fits by a four-parameter logistic function. (E) Selectivity profile of compound **16** in a panel of bromodomains representing all subfamilies of human bromodomains. The K_d values were determined by a competition binding assay.[88] (F, G) FRAP assay for compound **16** in U2OS cells transfected with a plasmid encoding GFP-BRD4. Cells were treated with compound **16** (1 μM) or a BRD4 ligand JQ1 (0.1 μM). (F) Fluorescent recovery curves after photobleaching (normalized to the intensity before bleaching). (G) $t_{1/2}$ in the FRAP assay of F ($n \geq 7$ cells per group, error bars: standard error of the mean, Mann−Whitney test; ***, $P < 0.001$; n.s., not significant).

can possibly arise from the KAc mimic moiety.[90] AutoCouple was therefore further validated through a virtual-coupling campaign to design BRD4(1) inhibitors (detailed information is available in section 3 in the Supporting Information).

Hybridization Strategies. Aiming to further improve the affinity of these compounds, we decided to combine the best performing motifs in the amide-coupling campaign (acetamide **5**, dimethoxybenzene **6**, and furan **7**) into compounds **16**−**18**. This hybridization approach resulted in additional low nanomolar CBP ligands (Scheme 1D). Remarkably, compound **16** shows an affinity for the CBP bromodomain higher by a factor of more than 10,000 with respect to the affinity for the BRD4(1) bromodomain while still exhibiting an excellent ligand efficiency for the target of 0.31 and 0.32 kcal mol^{-1} per non-hydrogen atom (according to BROMOscan and AlphaScreen, respectively) in line with recommendations for maintaining druglike properties throughout the optimization process.[91,92]

The crystal structure of CBP in complex with ligand **16** (PDB code 5NLK) could be obtained, confirming that the binding mode predicted by AutoCouple is correct (Figure 3A): the furan ring of compound **16** is at favorable van der Waals distance to the Pro1106 side chain as predicted by the docked pose of the parent compound **7**. The overlap of the crystal structure of the CBP/ligand **16** complex with the BRD4(1) structure shows steric conflicts with the Trp81 side chain (Figure 3B), which explains its high selectivity.[59,60] Compound **16** was further profiled via a BROMOscan against a panel of bromodomains covering all subfamilies (Figure 4E). While the strong binding to CREBBP and EP300 could again be confirmed, only moderate affinity for the bromodomains of CECR2 (the bromodomain of the cat eye syndrome critical region protein 2) and TAF1(2) (the second bromodomain of human transcription initiation factor TFIID subunit 2) was observed.[93]

Target Engagement in Cells and Preliminary Biological Evaluation. The target engagement of some of these ligands and thus their cell permeability were evaluated by means of a fluorescence recovery after photobleaching (FRAP) assay.[94] In human osteosarcoma U2OS cells, compounds **6**, **7**, **13**, **16**, and **17** at a concentration of 1 μM showed significant displacement of the GFP-fused CBP bromodomain from chromatin. In particular, compound **16**, which displayed the highest affinity for the CBP bromodomain in the biochemical assay (K_d = 35 nM), showed also the strongest effect in the FRAP assay (Figure 4A,B). The compounds' purity was evaluated by peak integration of the UV/visible HPLC chromatograms for compounds **6** (99%), **7** (94%), **13** (99%), **16** (97%), and **17** (92%) (see section 11 in the SI).

Compound **16** was further tested in cellular proliferation assays. Three cell lines known to be sensitive to CBP bromodomain inhibition, i.e., LP1 (multiple myeloma), Kasumi, and HL-60 (acute myeloblastic leukemia),[59,95] were selected as well as nontransformed primary fibroblast MRC5.[96] The MRC5 cells are used as control as they are noncancer cells and with limited lifespan caused by replicative senescence.[97] The resazurin assay was employed with compound incubation for 72 h (LP1, Kasumi, and MRC5; Figure 4C) or 144 h (LP1, Kasumi, and HL-60; Figure S9).[98] Remarkably, compound **16** selectively inhibited the proliferation of the three cancer cell lines, but was not toxic in MRC5 cells (GI50 > 20 μM) (Figure 4C, Figures S8 and S9). Since CBP and EP300 regulate the transcription of the lymphocyte-specific transcription factor IRF4 and the IRF4 target gene c-MYC in myeloma cells,[59,60] we investigated the transcription of IRF4 and c-MYC in the LP1 cell line using RT-qPCR (reverse transcription quantitative

DOI: 10.1021/acscentsci.7b00401
ACS Cent. Sci. 2018, 4, 180−188

polymerase chain reaction). The dose−response curves showed that the mRNA levels of IRF4 and c-MYC were reduced after incubation for 6 h with compound **16** (Figure 4D). Since the inhibition of BRD4 bromodomains also has a strong effect on c-MYC expression,[99] one could argue that the c-MYC inhibition by compound **16** arises from a weak binding to the BRD4 protein. To address this issue, we evaluated the BRD4 engagement in cells by FRAP. Compound **16** at 1 μM showed no effect on the fluorescence recovery time (Figure 4F,G), thus confirming the potential of compound **16** as a useful tool to unravel the specific role of CBP bromodomain in disease.

CONCLUSIONS

A de novo design approach based on virtual chemical reactions starting from commercially available building blocks (AutoCouple) has been developed and successfully applied to the identification of potent and selective bromodomain ligands. This novel approach makes full use of the three-dimensional structure of the protein target and calculates the binding energy by molecular mechanics (transferable force field including electrostatic solvation by the Poisson equation) without any fitting parameter. Thus, AutoCouple is a fragment-growing program that generates synthetically accessible molecules with an accurate and efficient prediction of their binding energy. Our in silico guided medicinal chemistry optimization represents a very efficient strategy to expand the chemical diversity while swiftly acquiring knowledge on previously unexplored areas of chemical space for the target of choice.

AutoCouple has been benchmarked on the CBP bromodomain taking an existing hit as starting point for a ligand optimization campaign. While only potency and synthetic accessibility were encoded in the design working principles of AutoCouple, highly potent and selective ligands with improved solubility and cell permeability have been identified, thus underpinning the importance of chemical diversity in tackling properties that are hard to predict with existing softwares. Hit expansion by AutoCouple resulted in compound **16**, a cell-permeable ligand of the CBP bromodomain with low-nanomolar potency and high selectivity against BRD4(1). This probe represents a useful chemical tool to unravel the individual role of CBP in several types of diseases including cancer, inflammation, and hematological malignancies among others. Further biological evaluation of these compounds and application of AutoCouple to other protein targets are currently ongoing in our laboratories.

ASSOCIATED CONTENT

Supporting Information

The Supporting Information is available free of charge on the ACS Publications website at DOI: 10.1021/acscentsci.7b00401.

Computational methods, organic syntheses, NMR traces, UV traces, biophysical analyses, and crystallographic data (PDF)

AUTHOR INFORMATION

Corresponding Authors

*E-mail: caflisch@bioc.uzh.ch.

*E-mail: cristina.nevado@chem.uzh.ch.

ORCID

Cristina Nevado: 0000-0002-3297-581X

Amedeo Caflisch: 0000-0002-2317-6792

Author Contributions

‡L.B. and A.U. contributed equally to this work.

Notes

The authors declare no competing financial interest.

ACKNOWLEDGMENTS

The Swiss National Science Foundation (200020_157083), the *Synapsis Foundation - Alzheimer Research Switzerland*, the *Heidi Seiler-Stiftung*, and the *Hartmann Müller Stiftung für medizinische Forschung* are acknowledged for their financial support. We would like to thank Dr. Claudia Jessen-Trefzer for her invaluable help in cloning the plasmid for FRAP experiments. Isabel Córdoba and Charel Prost are also acknowledged for preliminary work on the preparation of some of the ligands. We are grateful to the Paul Scherrer Institut (PSI) for the use of beamlines at the Swiss Light Source.

ABBREVIATIONS

BET, bromo- and extraterminal domain; BRD4(1), first bromodomain of the protein called BRD4; CBP, binding protein of the cyclic AMP response element binding protein; KAc, acetylated lysine; ROC, receiver operating characteristic; FRAP, fluorescence recovery after photobleaching; K_d, dissociation constant; SEED, solvation energy for exhaustive docking; GFP, green fluorescent protein

REFERENCES

(1) Fink, T.; Reymond, J.-L. Virtual Exploration of the Chemical Universe up to 11 Atoms of C, N, O, F: Assembly of 26.4 Million Structures (110.9 Million Stereoisomers) and Analysis for New Ring Systems, Stereochemistry, Physicochemical Properties, Compound Classes, and Drug Discovery. *J. Chem. Inf. Model.* **2007**, *47*, 342−353.

(2) Dragone, V.; Sans, V.; Henson, A. B.; Granda, J. M.; Cronin, L. An autonomous organic reaction search engine for chemical reactivity. *Nat. Commun.* **2017**, 8:15733.

(3) Warne, T.; Serrano-Vega, M. J.; Baker, J. G.; Moukhametzianov, R.; Edwards, P. C.; Henderson, R.; Leslie, A. G. W.; Tate, C. G.; Schertler, G. F. X. Structure of a β1-adrenergic G-protein-coupled receptor. *Nature* **2008**, *454*, 486−491.

(4) Lucas, X.; Grüning, B. A.; Bleher, S.; Günther, S. The Purchasable Chemical Space: A Detailed Picture. *J. Chem. Inf. Model.* **2015**, *55*, 915−924.

(5) Hartenfeller, M.; Eberle, M.; Meier, P.; Nieto-Oberhuber, C.; Altmann, K.-H.; Schneider, G.; Jacoby, E.; Renner, S. Probing the Bioactivity-Relevant Chemical Space of Robust Reactions and Common Molecular Building Blocks. *J. Chem. Inf. Model.* **2012**, *52*, 1167−1178.

(6) Wetzel, S.; Bon, R. S.; Kumar, K.; Waldmann, H. Biology-Oriented Synthesis. *Angew. Chem., Int. Ed.* **2011**, *50*, 10800−10826.

(7) Burke, M. D.; Schreiber, S. L. A Planning Strategy for Diversity-Oriented Synthesis. *Angew. Chem., Int. Ed.* **2004**, *43*, 46−58.

(8) Dandapani, S.; Marcaurelle, L. A. Grand challenge commentary: Accessing new chemical space for 'undruggable' targets. *Nat. Chem. Biol.* **2010**, *6*, 861−863.

(9) Vidler, L. R.; Brown, N.; Knapp, S.; Hoelder, S. Druggability Analysis and Structural Classification of Bromodomain Acetyl-lysine Binding Sites. *J. Med. Chem.* **2012**, *55*, 7346−7359.

(10) Zhang, G.; Sanchez, R.; Zhou, M.-M. Scaling the Druggability Landscape of Human Bromodomains, a New Class of Drug Targets. *J. Med. Chem.* **2012**, *55*, 7342−7345.

(11) Valeur, E.; Guéret, S. M.; Adihou, H.; Gopalakrishnan, R.; Lemurell, M.; Waldmann, H.; Grossmann, T. N.; Plowright, A. T. New Modalities for Challenging Targets in Drug Discovery. *Angew. Chem., Int. Ed.* **2017**, *56*, 10294−10323.

(12) Hartenfeller, M.; Schneider, G. In *Chemoinformatics and Computational Chemical Biology*; Bajorath, J., Ed.; Humana Press: Totowa, NJ, 2011; pp 299−323.
(13) Schneider, G.; Fechner, U. Computer-based de novo design of drug-like molecules. *Nat. Rev. Drug Discovery* **2005**, *4*, 649−663.
(14) Chéron, N.; Jasty, N.; Shakhnovich, E. I. OpenGrowth: An Automated and Rational Algorithm for Finding New Protein Ligands. *J. Med. Chem.* **2016**, *59*, 4171−4188.
(15) Yuan, Y.; Pei, J.; Lai, L. LigBuilder 2: A Practical de Novo Drug Design Approach. *J. Chem. Inf. Model.* **2011**, *51*, 1083−1091.
(16) Wang, R.; Gao, Y.; Lai, L. LigBuilder: A Multi-Purpose Program for Structure-Based Drug Design. *J. Mol. Model.* **2000**, *6*, 498−516.
(17) Liu, T.; Naderi, M.; Alvin, C.; Mukhopadhyay, S.; Brylinski, M. Break Down in Order To Build Up: Decomposing Small Molecules for Fragment-Based Drug Design with eMolFrag. *J. Chem. Inf. Model.* **2017**, *57*, 627−631.
(18) Ghersi, D.; Singh, M. molBLOCKS: decomposing small molecule sets and uncovering enriched fragments. *Bioinformatics* **2014**, *30*, 2081−2083.
(19) Naderi, M.; Alvin, C.; Ding, Y.; Mukhopadhyay, S.; Brylinski, M. A graph-based approach to construct target-focused libraries for virtual screening. *J. Cheminf.* **2016**, *8*, 14.
(20) Cooper, T. W. J.; Campbell, I. B.; Macdonald, S. J. F. Factors Determining the Selection of Organic Reactions by Medicinal Chemists and the Use of These Reactions in Arrays (Small Focused Libraries). *Angew. Chem., Int. Ed.* **2010**, *49*, 8082−8091.
(21) Hartenfeller, M.; Zettl, H.; Walter, M.; Rupp, M.; Reisen, F.; Proschak, E.; Weggen, S.; Stark, H.; Schneider, G. DOGS: Reaction-Driven de novo Design of Bioactive Compounds. *PLoS Comput. Biol.* **2012**, *8*, e1002380.
(22) Chevillard, F.; Kolb, P. SCUBIDOO: A Large yet Screenable and Easily Searchable Database of Computationally Created Chemical Compounds Optimized toward High Likelihood of Synthetic Tractability. *J. Chem. Inf. Model.* **2015**, *55*, 1824−1835.
(23) Vinkers, H. M.; de Jonge, M. R.; Daeyaert, F. F. D.; Heeres, J.; Koymans, L. M. H.; van Lenthe, J. H.; Lewi, P. J.; Timmerman, H.; Van Aken, K.; Janssen, P. A. J. SYNOPSIS: SYNthesize and OPtimize System in Silico. *J. Med. Chem.* **2003**, *46*, 2765−2773.
(24) Schneider, G.; Lee, M.-L.; Stahl, M.; Schneider, P. De novo design of molecular architectures by evolutionary assembly of drug-derived building blocks. *J. Comput.-Aided Mol. Des.* **2000**, *14*, 487−494.
(25) Filippakopoulos, P.; Knapp, S. Targeting bromodomains: epigenetic readers of lysine acetylation. *Nat. Rev. Drug Discovery* **2014**, *13*, 337−356.
(26) Muller, S.; Filippakopoulos, P.; Knapp, S. Bromodomains as therapeutic targets. *Expert Rev. Mol. Med.* **2011**, *13*, e29.
(27) Lucas, X.; Wohlwend, D.; Hügle, M.; Schmidtkunz, K.; Gerhardt, S.; Schüle, R.; Jung, M.; Einsle, O.; Günther, S. 4-Acyl Pyrroles: Mimicking Acetylated Lysines in Histone Code Reading. *Angew. Chem., Int. Ed.* **2013**, *52*, 14055−14059.
(28) Hügle, M.; Lucas, X.; Ostrovskyi, D.; Regenass, P.; Gerhardt, S.; Einsle, O.; Hau, M.; Jung, M.; Breit, B.; Günther, S.; Wohlwend, D. Beyond the BET Family: Targeting CBP/p300 with 4-Acyl Pyrroles. *Angew. Chem., Int. Ed.* **2017**, *56*, 12476−12480.
(29) Filippakopoulos, P.; Qi, J.; Picaud, S.; Shen, Y.; Smith, W. B.; Fedorov, O.; Morse, E. M.; Keates, T.; Hickman, T. T.; Felletar, I.; Philpott, M.; Munro, S.; McKeown, M. R.; Wang, Y.; Christie, A. L.; West, N.; Cameron, M. J.; Schwartz, B.; Heightman, T. D.; La Thangue, N.; French, C. A.; Wiest, O.; Kung, A. L.; Knapp, S.; Bradner, J. E. Selective inhibition of BET bromodomains. *Nature* **2010**, *468*, 1067−1073.
(30) Zhao, H.; Gartenmann, L.; Dong, J.; Spiliotopoulos, D.; Caflisch, A. Discovery of BRD4 bromodomain inhibitors by fragment-based high-throughput docking. *Bioorg. Med. Chem. Lett.* **2014**, *24*, 2493−2496.
(31) Conway, S. J.; Woster, P. M.; Greenlee, W. J.; Georg, G.; Wang, S. Epigenetics: Novel Therapeutics Targeting Epigenetics. *J. Med. Chem.* **2016**, *59*, 1247−1248.
(32) Andrieu, G.; Belkina, A. C.; Denis, G. V. Clinical trials for BET inhibitors run ahead of the science. *Drug Discovery Today: Technol.* **2016**, *19*, 45−50.
(33) Wadhwa, E.; Nicolaides, T. Bromodomain Inhibitor Review: Bromodomain and Extra-terminal Family Protein Inhibitors as a Potential New Therapy in Central Nervous System Tumors. *Cureus* **2016**, *8*, e620.
(34) Zhang, G.; Smith, S. G.; Zhou, M.-M. Discovery of Chemical Inhibitors of Human Bromodomains. *Chem. Rev.* **2015**, *115*, 11625−11668.
(35) Romero, F. A.; Taylor, A. M.; Crawford, T. D.; Tsui, V.; Côté, A.; Magnuson, S. Disrupting Acetyl-Lysine Recognition: Progress in the Development of Bromodomain Inhibitors. *J. Med. Chem.* **2016**, *59*, 1271−1298.
(36) Hewings, D. S.; Rooney, T. P. C.; Jennings, L. E.; Hay, D. A.; Schofield, C. J.; Brennan, P. E.; Knapp, S.; Conway, S. J. Progress in the Development and Application of Small Molecule Inhibitors of Bromodomain−Acetyl-lysine Interactions. *J. Med. Chem.* **2012**, *55*, 9393−9413.
(37) Gallenkamp, D.; Gelato, K. A.; Haendler, B.; Weinmann, H. Bromodomains and Their Pharmacological Inhibitors. *ChemMedChem* **2014**, *9*, 438−464.
(38) Berthon, C.; Raffoux, E.; Thomas, X.; Vey, N.; Gomez-Roca, C.; Yee, K.; Taussig, D. C.; Rezai, K.; Roumier, C.; Herait, P.; Kahatt, C.; Quesnel, B.; Michallet, M.; Recher, C.; Lokiec, F.; Preudhomme, C.; Dombret, H. Bromodomain inhibitor OTX015 in patients with acute leukaemia: a dose-escalation, phase 1 study. *Lancet Haematology* **2016**, *3*, e186−e195.
(39) Clark, P. G. K.; Vieira, L. C. C.; Tallant, C.; Fedorov, O.; Singleton, D. C.; Rogers, C. M.; Monteiro, O. P.; Bennett, J. M.; Baronio, R.; Müller, S.; Daniels, D. L.; Méndez, J.; Knapp, S.; Brennan, P. E.; Dixon, D. J. LP99: Discovery and Synthesis of the First Selective BRD7/9 Bromodomain Inhibitor. *Angew. Chem., Int. Ed.* **2015**, *54*, 6217−6221.
(40) Bamborough, P.; Chung, C.-w.; Furze, R. C.; Grandi, P.; Michon, A.-M.; Sheppard, R. J.; Barnett, H.; Diallo, H.; Dixon, D. P.; Douault, C.; Jones, E. J.; Karamshi, B.; Mitchell, D. J.; Prinjha, R. K.; Rau, C.; Watson, R. J.; Werner, T.; Demont, E. H. Structure-Based Optimization of Naphthyridones into Potent ATAD2 Bromodomain Inhibitors. *J. Med. Chem.* **2015**, *58*, 6151−6178.
(41) Hay, D. A.; Rogers, C. M.; Fedorov, O.; Tallant, C.; Martin, S.; Monteiro, O. P.; Müller, S.; Knapp, S.; Schofield, C. J.; Brennan, P. E. Design and synthesis of potent and selective inhibitors of BRD7 and BRD9 bromodomains. *MedChemComm* **2015**, *6*, 1381−1386.
(42) Lolli, G.; Caflisch, A. High-Throughput Fragment Docking into the BAZ2B Bromodomain: Efficient in Silico Screening for X-Ray Crystallography. *ACS Chem. Biol.* **2016**, *11*, 800−807.
(43) Theodoulou, N. H.; Bamborough, P.; Bannister, A. J.; Becher, I.; Bit, R. A.; Che, K. H.; Chung, C.-w.; Dittmann, A.; Drewes, G.; Drewry, D. H.; Gordon, L.; Grandi, P.; Leveridge, M.; Lindon, M.; Michon, A.-M.; Molnar, J.; Robson, S. C.; Tomkinson, N. C. O.; Kouzarides, T.; Prinjha, R. K.; Humphreys, P. G. Discovery of I-BRD9, a Selective Cell Active Chemical Probe for Bromodomain Containing Protein 9 Inhibition. *J. Med. Chem.* **2016**, *59*, 1425−1439.
(44) Zucconi, B. E.; Luef, B.; Xu, W.; Henry, R. A.; Nodelman, I. M.; Bowman, G. D.; Andrews, A. J.; Cole, P. A. Modulation of p300/CBP Acetylation of Nucleosomes by Bromodomain Ligand I-CBP112. *Biochemistry* **2016**, *55*, 3727−3734.
(45) Navratilova, I.; Aristotelous, T.; Picaud, S.; Chaikuad, A.; Knapp, S.; Filappakopoulos, P.; Hopkins, A. L. Discovery of New Bromodomain Scaffolds by Biosensor Fragment Screening. *ACS Med. Chem. Lett.* **2016**, *7*, 1213−1218.
(46) Palmer, W. S. Development of small molecule inhibitors of BRPF1 and TRIM24 bromodomains. *Drug Discovery Today: Technol.* **2016**, *19*, 65−71.
(47) Palmer, W. S.; Poncet-Montange, G.; Liu, G.; Petrocchi, A.; Reyna, N.; Subramanian, G.; Theroff, J.; Yau, A.; Kost-Alimova, M.; Bardenhagen, J. P.; Leo, E.; Shepard, H. E.; Tieu, T. N.; Shi, X.; Zhan, Y.; Zhao, S.; Barton, M. C.; Draetta, G.; Toniatti, C.; Jones, P.; Geck

DOI: 10.1021/acscentsci.7b00401
ACS Cent. Sci. 2018, 4, 180−188

Do, M.; Andersen, J. N. Structure-Guided Design of IACS-9571, a Selective High-Affinity Dual TRIM24-BRPF1 Bromodomain Inhibitor. *J. Med. Chem.* **2016**, *59*, 1440−1454.
(48) Bamborough, P.; Barnett, H. A.; Becher, I.; Bird, M. J.; Chung, C.-w.; Craggs, P. D.; Demont, E. H.; Diallo, H.; Fallon, D. J.; Gordon, L. J.; Grandi, P.; Hobbs, C. I.; Hooper-Greenhill, E.; Jones, E. J.; Law, R. P.; Le Gall, A.; Lugo, D.; Michon, A.-M.; Mitchell, D. J.; Prinjha, R. K.; Sheppard, R. J.; Watson, A. J. B.; Watson, R. J. GSK6853, a Chemical Probe for Inhibition of the BRPF1 Bromodomain. *ACS Med. Chem. Lett.* **2016**, *7*, 552−557.
(49) Zhu, J.; Caflisch, A. Twenty Crystal Structures of Bromodomain and PHD Finger Containing Protein 1 (BRPF1)/Ligand Complexes Reveal Conserved Binding Motifs and Rare Interactions. *J. Med. Chem.* **2016**, *59*, 5555−5561.
(50) Demont, E. H.; Bamborough, P.; Chung, C.-w.; Craggs, P. D.; Fallon, D.; Gordon, L. J.; Grandi, P.; Hobbs, C. I.; Hussain, J.; Jones, E. J.; Le Gall, A.; Michon, A.-M.; Mitchell, D. J.; Prinjha, R. K.; Roberts, A. D.; Sheppard, R. J.; Watson, R. J. 1,3-Dimethyl Benzimidazolones Are Potent, Selective Inhibitors of the BRPF1 Bromodomain. *ACS Med. Chem. Lett.* **2014**, *5*, 1190−1195.
(51) Bennett, J.; Fedorov, O.; Tallant, C.; Monteiro, O.; Meier, J.; Gamble, V.; Savitsky, P.; Nunez-Alonso, G. A.; Haendler, B.; Rogers, C.; Brennan, P. E.; Müller, S.; Knapp, S. Discovery of a Chemical Tool Inhibitor Targeting the Bromodomains of TRIM24 and BRPF. *J. Med. Chem.* **2016**, *59*, 1642−1647.
(52) Demont, E. H.; Chung, C.-w.; Furze, R. C.; Grandi, P.; Michon, A.-M.; Wellaway, C.; Barrett, N.; Bridges, A. M.; Craggs, P. D.; Diallo, H.; Dixon, D. P.; Douault, C.; Emmons, A. J.; Jones, E. J.; Karamshi, B. V.; Locke, K.; Mitchell, D. J.; Mouzon, B. H.; Prinjha, R. K.; Roberts, A. D.; Sheppard, R. J.; Watson, R. J.; Bamborough, P. Fragment-Based Discovery of Low-Micromolar ATAD2 Bromodomain Inhibitors. *J. Med. Chem.* **2015**, *58*, 5649−5673.
(53) Bamborough, P.; Chung, C.-w.; Demont, E. H.; Furze, R. C.; Bannister, A. J.; Che, K. H.; Diallo, H.; Douault, C.; Grandi, P.; Kouzarides, T.; Michon, A.-M.; Mitchell, D. J.; Prinjha, R. K.; Rau, C.; Robson, S.; Sheppard, R. J.; Upton, R.; Watson, R. J. A Chemical Probe for the ATAD2 Bromodomain. *Angew. Chem., Int. Ed.* **2016**, *55*, 11382−11386.
(54) Moustakim, M.; Clark, P. G. K.; Trulli, L.; Fuentes de Arriba, A. L.; Ehebauer, M. T.; Chaikuad, A.; Murphy, E. J.; Mendez-Johnson, J.; Daniels, D.; Hou, C.-F. D.; Lin, Y.-H.; Walker, J. R.; Hui, R.; Yang, H.; Dorrell, L.; Rogers, C. M.; Monteiro, O. P.; Fedorov, O.; Huber, K. V. M; Knapp, S.; Heer, J.; Dixon, D. J.; Brennan, P. E. Discovery of a PCAF Bromodomain Chemical Probe. *Angew. Chem., Int. Ed.* **2017**, *56*, 827−831.
(55) Theodoulou, N. H.; Tomkinson, N. C. O.; Prinjha, R. K.; Humphreys, P. G. Progress in the Development of non-BET Bromodomain Chemical Probes. *ChemMedChem* **2016**, *11*, 477−487.
(56) Rooney, T. P. C.; Filippakopoulos, P.; Fedorov, O.; Picaud, S.; Cortopassi, W. A.; Hay, D. A.; Martin, S.; Tumber, A.; Rogers, C. M.; Philpott, M.; Wang, M.; Thompson, A. L.; Heightman, T. D.; Pryde, D. C.; Cook, A.; Paton, R. S.; Müller, S.; Knapp, S.; Brennan, P. E.; Conway, S. J. A Series of Potent CREBBP Bromodomain Ligands Reveals an Induced-Fit Pocket Stabilized by a Cation−π Interaction. *Angew. Chem., Int. Ed.* **2014**, *53*, 6126−6130.
(57) Hammitzsch, A.; Tallant, C.; Fedorov, O.; O'Mahony, A.; Brennan, P. E.; Hay, D. A.; Martinez, F. O.; Al-Mossawi, M. H.; de Wit, J.; Vecellio, M.; Wells, C.; Wordsworth, P.; Müller, S.; Knapp, S.; Bowness, P. CBP30, a selective CBP/p300 bromodomain inhibitor, suppresses human Th17 responses. *Proc. Natl. Acad. Sci. U. S. A.* **2015**, *112*, 10768−10773.
(58) Taylor, A. M.; Côté, A.; Hewitt, M. C.; Pastor, R.; Leblanc, Y.; Nasveschuk, C. G.; Romero, F. A.; Crawford, T. D.; Cantone, N.; Jayaram, H.; Setser, J.; Murray, J.; Beresini, M. H.; de Leon Boenig, G.; Chen, Z.; Conery, A. R.; Cummings, R. T.; Dakin, L. A.; Flynn, E. M.; Huang, O. W.; Kaufman, S.; Keller, P. J.; Kiefer, J. R.; Lai, T.; Li, Y.; Liao, J.; Liu, W.; Lu, H.; Pardo, E.; Tsui, V.; Wang, J.; Wang, Y.; Xu, Z.; Yan, F.; Yu, D.; Zawadzke, L.; Zhu, X.; Zhu, X.; Sims, R. J.; Cochran, A. G.; Bellon, S.; Audia, J. E.; Magnuson, S.; Albrecht, B. K. Fragment-Based Discovery of a Selective and Cell-Active Benzodiazepinone CBP/EP300 Bromodomain Inhibitor (CPI-637). *ACS Med. Chem. Lett.* **2016**, *7*, 531−536.
(59) Crawford, T. D.; Romero, F. A.; Lai, K. W.; Tsui, V.; Taylor, A. M.; de Leon Boenig, G.; Noland, C. L.; Murray, J.; Ly, J.; Choo, E. F.; Hunsaker, T. L.; Chan, E. W.; Merchant, M.; Kharbanda, S.; Gascoigne, K. E.; Kaufman, S.; Beresini, M. H.; Liao, J.; Liu, W.; Chen, K. X.; Chen, Z.; Conery, A. R.; Côté, A.; Jayaram, H.; Jiang, Y.; Kiefer, J. R.; Kleinheinz, T.; Li, Y.; Maher, J.; Pardo, E.; Poy, F.; Spillane, K. L.; Wang, F.; Wang, J.; Wei, X.; Xu, Z.; Xu, Z.; Yen, I.; Zawadzke, L.; Zhu, X.; Bellon, S.; Cummings, R.; Cochran, A. G.; Albrecht, B. K.; Magnuson, S. Discovery of a Potent and Selective in Vivo Probe (GNE-272) for the Bromodomains of CBP/EP300. *J. Med. Chem.* **2016**, *59*, 10549−10563.
(60) Romero, F. A.; Murray, J.; Lai, K. W.; Tsui, V.; Albrecht, B. K.; An, L.; Beresini, M. H.; de Leon Boenig, G.; Bronner, S. M.; Chan, E. W.; Chen, K. X.; Chen, Z.; Choo, E. F.; Clagg, K.; Clark, K.; Crawford, T. D.; Cyr, P.; de Almeida Nagata, D.; Gascoigne, K. E.; Grogan, J. L.; Hatzivassiliou, G.; Huang, W.; Hunsaker, T. L.; Kaufman, S.; Koenig, S. G.; Li, R.; Li, Y.; Liang, X.; Liao, J.; Liu, W.; Ly, J.; Maher, J.; Masui, C.; Merchant, M.; Ran, Y.; Taylor, A. M.; Wai, J.; Wang, F.; Wei, X.; Yu, D.; Zhu, B.-Y.; Zhu, X.; Magnuson, S. GNE-781, A Highly Advanced Potent and Selective Bromodomain Inhibitor of Cyclic Adenosine Monophosphate Response Element Binding Protein, Binding Protein (CBP). *J. Med. Chem.* **2017**, *60*, 9162.
(61) Hay, D. A.; Fedorov, O.; Martin, S.; Singleton, D. C.; Tallant, C.; Wells, C.; Picaud, S.; Philpott, M.; Monteiro, O. P.; Rogers, C. M.; Conway, S. J.; Rooney, T. P. C.; Tumber, A.; Yapp, C.; Filippakopoulos, P.; Bunnage, M. E.; Müller, S.; Knapp, S.; Schofield, C. J.; Brennan, P. E. Discovery and Optimization of Small-Molecule Ligands for the CBP/p300 Bromodomains. *J. Am. Chem. Soc.* **2014**, *136*, 9308−9319.
(62) Picaud, S.; Fedorov, O.; Thanasopoulou, A.; Leonards, K.; Jones, K.; Meier, J.; Olzscha, H.; Monteiro, O.; Martin, S.; Philpott, M.; Tumber, A.; Filippakopoulos, P.; Yapp, C.; Wells, C.; Che, K. H.; Bannister, A.; Robson, S.; Kumar, U.; Parr, N.; Lee, K.; Lugo, D.; Jeffrey, P.; Taylor, S.; Vecellio, M. L.; Bountra, C.; Brennan, P. E.; O'Mahony, A.; Velichko, S.; Müller, S.; Hay, D.; Daniels, D. L.; Urh, M.; La Thangue, N. B.; Kouzarides, T.; Prinjha, R.; Schwaller, J.; Knapp, S. Generation of a Selective Small Molecule Inhibitor of the CBP/p300 Bromodomain for Leukemia Therapy. *Cancer Res.* **2015**, *75*, 5106−5119.
(63) Denny, R. A.; Flick, A. C.; Coe, J.; Langille, J.; Basak, A.; Liu, S.; Stock, I.; Sahasrabudhe, P.; Bonin, P.; Hay, D. A.; Brennan, P. E.; Pletcher, M.; Jones, L. H.; Chekler, E. L. P. Structure-Based Design of Highly Selective Inhibitors of the CREB Binding Protein Bromodomain. *J. Med. Chem.* **2017**, *60*, 5349−5363.
(64) Popp, T. A.; Tallant, C.; Rogers, C.; Fedorov, O.; Brennan, P. E.; Müller, S.; Knapp, S.; Bracher, F. Development of Selective CBP/P300 Benzoxazepine Bromodomain Inhibitors. *J. Med. Chem.* **2016**, *59*, 8889−8912.
(65) Moustakim, M.; Clark, P. G.; Hay, D. A.; Dixon, D. J.; Brennan, P. E. Chemical probes and inhibitors of bromodomains outside the BET family. *MedChemComm* **2016**, *7*, 2246−2264.
(66) Ghosh, S.; Taylor, A.; Chin, M.; Huang, H.-R.; Conery, A. R.; Mertz, J. A.; Salmeron, A.; Dakle, P. J.; Mele, D.; Cote, A.; et al. Regulatory T cell modulation by CBP/EP300 bromodomain inhibition. *J. Biol. Chem.* **2016**, *291*, 13014−13027.
(67) Gerona-Navarro, G.; Yoel-Rodríguez; Mujtaba, S.; Frasca, A.; Patel, J.; Zeng, L.; Plotnikov, A. N.; Osman, R.; Zhou, M.-M. Rational Design of Cyclic Peptide Modulators of the Transcriptional Coactivator CBP: A New Class of p53 Inhibitors. *J. Am. Chem. Soc.* **2011**, *133*, 2040−2043.
(68) Majeux, N.; Scarsi, M.; Apostolakis, J.; Ehrhardt, C.; Caflisch, A. Exhaustive docking of molecular fragments with electrostatic solvation. *Proteins: Struct., Funct., Genet.* **1999**, *37*, 88−105.
(69) Majeux, N.; Scarsi, M.; Caflisch, A. Efficient electrostatic solvation model for protein-fragment docking. *Proteins: Struct., Funct., Genet.* **2001**, *42*, 256−268.

DOI: 10.1021/acscentsci.7b00401
ACS Cent. Sci. 2018, 4, 180−188

(70) Xu, M.; Unzue, A.; Dong, J.; Spiliotopoulos, D.; Nevado, C.; Caflisch, A. Discovery of CREBBP Bromodomain Inhibitors by High-Throughput Docking and Hit Optimization Guided by Molecular Dynamics. *J. Med. Chem.* **2016**, *59*, 1340−1349.
(71) Unzue, A.; Xu, M.; Dong, J.; Wiedmer, L.; Spiliotopoulos, D.; Caflisch, A.; Nevado, C. Fragment-Based Design of Selective Nanomolar Ligands of the CREBBP Bromodomain. *J. Med. Chem.* **2016**, *59*, 1350−1356.
(72) Paul, S. M.; Mytelka, D. S.; Dunwiddie, C. T.; Persinger, C. C.; Munos, B. H.; Lindborg, S. R.; Schacht, A. L. How to improve R&D productivity: the pharmaceutical industry's grand challenge. *Nat. Rev. Drug Discovery* **2010**, *9*, 203−214.
(73) Kubinyi, H. Drug research: myths, hype and reality. *Nat. Rev. Drug Discovery* **2003**, *2*, 665−668.
(74) Kola, I.; Landis, J. Can the pharmaceutical industry reduce attrition rates? *Nat. Rev. Drug Discovery* **2004**, *3*, 711−716.
(75) Coley, C. W.; Barzilay, R.; Jaakkola, T. S.; Green, W. H.; Jensen, K. F. Prediction of Organic Reaction Outcomes Using Machine Learning. *ACS Cent. Sci.* **2017**, *3*, 434−443.
(76) Kayala, M. A.; Baldi, P. ReactionPredictor: Prediction of Complex Chemical Reactions at the Mechanistic Level Using Machine Learning. *J. Chem. Inf. Model.* **2012**, *52*, 2526−2540.
(77) Dutta, R.; Tiu, B.; Sakamoto, K. M. CBP/p300 acetyltransferase activity in hematologic malignancies. *Mol. Genet. Metab.* **2016**, *119*, 37−43.
(78) VanRossum, G.; Drake, F. L.; *The Python Language Reference*; Python software foundation: Amsterdam, Netherlands, 2010.
(79) Landrum, G.; RDKit, Open-Source Cheminformatics; *Online:* http://www.rdkit.org.
(80) Hartenfeller, M.; Eberle, M.; Meier, P.; Nieto-Oberhuber, C.; Altmann, K.-H.; Schneider, G.; Jacoby, E.; Renner, S. A Collection of Robust Organic Synthesis Reactions for In Silico Molecule Design. *J. Chem. Inf. Model.* **2011**, *51*, 3093−3098.
(81) Rishton, G. M. Reactive compounds and in vitro false positives in HTS. *Drug Discovery Today* **1997**, *2*, 382−384.
(82) Baell, J. B.; Holloway, G. A. New Substructure Filters for Removal of Pan Assay Interference Compounds (PAINS) from Screening Libraries and for Their Exclusion in Bioassays. *J. Med. Chem.* **2010**, *53*, 2719−2740.
(83) Ruiz-Carmona, S.; Alvarez-Garcia, D.; Foloppe, N.; Garmendia-Doval, A. B.; Juhos, S.; Schmidtke, P.; Barril, X.; Hubbard, R. E.; Morley, S. D. rDock: A Fast, Versatile and Open Source Program for Docking Ligands to Proteins and Nucleic Acids. *PLoS Comput. Biol.* **2014**, *10*, e1003571.
(84) Brooks, B. R.; Brooks, C. L.; Mackerell, A. D.; Nilsson, L.; Petrella, R. J.; Roux, B.; Won, Y.; Archontis, G.; Bartels, C.; Boresch, S.; Caflisch, A.; Caves, L.; Cui, Q.; Dinner, A. R.; Feig, M.; Fischer, S.; Gao, J.; Hodoscek, M.; Im, W.; Kuczera, K.; Lazaridis, T.; Ma, J.; Ovchinnikov, V.; Paci, E.; Pastor, R. W.; Post, C. B.; Pu, J. Z.; Schaefer, M.; Tidor, B.; Venable, R. M.; Woodcock, H. L.; Wu, X.; Yang, W.; York, D. M.; Karplus, M. CHARMM: The biomolecular simulation program. *J. Comput. Chem.* **2009**, *30*, 1545−1614.
(85) Vanommeslaeghe, K.; Hatcher, E.; Acharya, C.; Kundu, S.; Zhong, S.; Shim, J.; Darian, E.; Guvench, O.; Lopes, P.; Vorobyov, I.; Mackerell, A. D. CHARMM general force field: A force field for drug-like molecules compatible with the CHARMM all-atom additive biological force fields. *J. Comput. Chem.* **2010**, *31*, 671−690.
(86) MacKerell, A. D.; Feig, M.; Brooks, C. L. Improved Treatment of the Protein Backbone in Empirical Force Fields. *J. Am. Chem. Soc.* **2004**, *126*, 698−699.
(87) Im, W.; Beglov, D.; Roux, B. Continuum solvation model: Computation of electrostatic forces from numerical solutions to the Poisson-Boltzmann equation. *Comput. Phys. Commun.* **1998**, *111*, 59−75.
(88) Quinn, E.; Wodicka, L.; Ciceri, P.; Pallares, G.; Pickle, E.; Torrey, A.; Floyd, M.; Hunt, J.; Treiber, D. Abstract 4238: BROMOscan - a high throughput, quantitative ligand binding platform identifies best-in-class bromodomain inhibitors from a screen of mature compounds targeting other protein classes. *Cancer Res.* **2013**, *73*, 4238−4238.
(89) Spiliotopoulos, D.; Caflisch, A. Molecular Dynamics Simulations of Bromodomains Reveal Binding-Site Flexibility and Multiple Binding Modes of the Natural Ligand Acetyl-Lysine. *Isr. J. Chem.* **2014**, *54*, 1084−1092.
(90) Unzue, A.; Zhao, H.; Lolli, G.; Dong, J.; Zhu, J.; Zechner, M.; Dolbois, A.; Caflisch, A.; Nevado, C. The "Gatekeeper" Residue Influences the Mode of Binding of Acetyl Indoles to Bromodomains. *J. Med. Chem.* **2016**, *59*, 3087−3097.
(91) Hopkins, A. L.; Keserü, G. M.; Leeson, P. D.; Rees, D. C.; Reynolds, C. H. The role of ligand efficiency metrics in drug discovery. *Nat. Rev. Drug Discovery* **2014**, *13*, 105−121.
(92) Hopkins, A. L.; Groom, C. R.; Alex, A. Ligand efficiency: a useful metric for lead selection. *Drug Discovery Today* **2004**, *9*, 430−431.
(93) For a recent report on a high affinity binder of the bromodomains BRD9, TAF1(2) and of CBP see: Sdelci, S.; Lardeau, C.-H.; Tallant, C.; Klepsch, F.; Klaiber, B.; Bennett, J.; Rathert, P.; Schuster, M.; Penz, T.; Fedorov, O.; Superti-Furga, G.; Bock, C.; Zuber, J.; Huber, K. V. M.; Knapp, S.; Müller, S.; Kubicek, S. Mapping the chemical chromatin reactivation landscape identifies BRD4-TAF1 cross-talk. *Nat. Chem. Biol.* **2016**, *12*, 504−510.
(94) Philpott, M.; Rogers, C. M.; Yapp, C.; Wells, C.; Lambert, J.-P.; Strain-Damerell, C.; Burgess-Brown, N. A.; Gingras, A.-C.; Knapp, S.; Müller, S. Assessing cellular efficacy of bromodomain inhibitors using fluorescence recovery after photobleaching. *Epigenet. Chromatin* **2014**, *7*, 14.
(95) Conery, A. R.; Centore, R. C.; Neiss, A.; Keller, P. J.; Joshi, S.; Spillane, K. L.; Sandy, P.; Hatton, C.; Pardo, E.; Zawadzke, L.; et al. Bromodomain inhibition of the transcriptional coactivators CBP/EP300 as a therapeutic strategy to target the IRF4 network in multiple myeloma. *eLife* **2016**, *5*, e10483.
(96) Jacobs, J.; Jones, C.; Baille, J. Characteristics of a human diploid cell designated MRC-5. *Nature* **1970**, *227*, 168−170.
(97) Hutter, E.; Renner, K.; Pfister, G.; Stöckl, P.; Jansen-Dürr, P.; Gnaiger, E. Senescence-associated changes in respiration and oxidative phosphorylation in primary human fibroblasts. *Biochem. J.* **2004**, *380*, 919−928.
(98) Anoopkumar-Dukie, S.; Carey, J. B.; Conere, T.; O'Sullivan, E.; Pelt, F. N. v.; Allshire, A. Resazurin assay of radiation response in cultured cells. *Br. J. Radiol.* **2005**, *78*, 945−947.
(99) Mertz, J. A.; Conery, A. R.; Bryant, B. M.; Sandy, P.; Balasubramanian, S.; Mele, D. A.; Bergeron, L.; Sims, R. J. Targeting MYC dependence in cancer by inhibiting BET bromodomains. *Proc. Natl. Acad. Sci. U. S. A.* **2011**, *108*, 16669−16674.

DOI: 10.1021/acscentsci.7b00401
ACS Cent. Sci. 2018, 4, 180−188

Supporting Information

Chemical Space Expansion of Bromodomain Ligands Guided by In Silico Virtual Couplings (AutoCouple)

Laurent Batiste,[a,c] Andrea Unzue,[b,c] Aymeric Dolbois,[b] Fabrice Hassler,[b] Xuan Wang,[a,b] Nicholas Deerain,[a] Jian Zhu,[a] Dimitrios Spiliotopoulos,[a] Cristina Nevado[b],* and Amedeo Caflisch[a],*

[a] Department of Biochemistry, University of Zurich. [b] Department of Chemistry, University of Zurich. Winterthurerstrasse 190, CH-8057. Zürich, Switzerland. [c] These authors contributed equally to this work.

Table of contents

1. Computational methods

1.1 Python scripts for AutoCouple

The scripts presented herein were written using the *Python* programming language[1] calling the following Object Oriented Libraries: *Numpy*,[2] *RDkit*.[3]
All molecular files were stored under the *structure data file* (*sdf*) format.[4]

Building-blocks library preparation
Building-blocks' libraries from various chemical providers, namely Acros Organics, AK Scientific, Alfa Aesar, ApolloChem, FluoroChem, Sigma-Aldrich, SpiroChem were retrieved under the computer-readable *sdf*-format with appended information about the molecule's Chemical Abstract Service (*CAS*) registration number (widely used by chemists), catalog number, prices and amounts.
Script Procedure:
To avoid redundancies, any building-block with the same *CAS* (hence same chemical formula) were merged. By mean of substructure-search, all the building-blocks containing the structures reported as toxic functional groups,[5] and heavy-metal containing molecules were detected and filtered-out. Considering that chemical couplings imply an increase of the molecular complexity (exception taken for cleavage reactions), and that the coupling products should preferably satisfy the Lipinski rule of 5 for druglikeliness,[6] building-blocks meeting the following criteria were discarded: (a) number of rotatable bonds larger than 5, since most non-cyclisation reactions create one to two additional rotatable bonds;[7] (b) number of heavy atoms (= non-hydrogen) smaller than 3 or larger than 35; (c) chiral centers larger than 2 (depending on the nature of the reagents and the reaction itself, additional chiral centers can be created upon coupling).
In this way, a collection of building-blocks containing ~270'000 unique molecules stored under the *sdf*-format was generated.

Reactants filters
Literature reviews estimated around ~20 reagent classes.[7-8] Those classes were redefined and merged giving 12 categories of building-blocks : (a) alcohols; (b) I- and II-amines (including anilines); (c) alkyl halides; (d) aryl/vinyl halides; (e) boronic acids/esters; (f) carboxylic acids/esters, nitriles, acylchlorides; (g) epoxides; (h) isocyanates; (i) aldehydes, ketones; (j) phophorus ylids, (k) sulfonyl chlorides, (l) terminal alkenes.
Script Procedure:
An RDkit-based Python script using substructure search parsed the building-blocks library and sorted out the molecules onto separate reactant libraries. Molecules containing several functions of the same type were saved in a different library than for the mono-functionalized ones (to avoid protection/deprotection steps). Ultimately, the reactant libraries contained the following information about the compounds: (a) reactivity (amine, carboxylic acid, halide, etc.) (b) position of the reactive centers (c) functional groups inducing side-reactions (see Reactions Pool, such data helps to foresee the reagent's adequacy for a single-step synthesis) (d) CAS number. Once the library was established, it was used multiple times and enriched on demand.

Reactions pool
The present collection comprises three reactions:[8-9] (a) Amide condensation : I- or II-amines/anilines addition onto carboxylic acids; (b) Suzuki coupling of boronic acids with aryl halides; (c) Buchwald-Hartwig coupling of I- or II-amines/anilines with aryl halides. Libraries or software making use of similar reaction collections were recently developed for *in-silico* drug design.[7-8,10]
Script Procedure:
The python script for virtual coupling parsed the *sdf* files of the two reaction partners retrieving information on the possible presence of undesired functionalities (if a competing functional group was present, the script would discard the building block). Subsequently it generated a new *sdf* file of the coupling product. Relying on the robustness of the used reaction and on the fact that compounds were generated in one step from the building-blocks, no assessment of the synthetic accessibility score[11-12] was needed for the product.

The python scripts used in AutoCouple were released on GitHub in the following repository: https://github.com/Caflisch-Group/AutoCouple_Python-based.

1.2 Conformers and protonation states

The software suite *ChemAxon* (*Marvins Beans*)[13] and the chemical toolbox *OpenBabel*[14] were used for preparation of the ligand libraries before docking. The command line program *cxcalc* within *Marvins Beans* performed various calculations such as lowest conformer generation (*leconformer*), generation of multiple conformers (*conformers*), major microspecies at given pH (*majormicrospecies*), microspecies list with distributions at given pH (*microspeciesdistribution*). *OpenBabel* was used for conversion between different chemical data formats.

1.3 Flexible ligand docking and binding energy evaluation

Target Preparation

The 3D coordinates of CBP, that were used for docking, originated from the crystallographic structures of the CBP bromodomain in complex with three different ligands, viz., 3P1C, CBP bromodomain in complex with the endogenous acetylated lysine ligand; 4TQN, CBP bromodomain in complex with our previously reported acetylbenzene ligand **1**;[15-16] 4NYX, CBP bromodomain in complex with a dihydroquinoxalinone ligand.[17] Only one structure of BRD4(1) was used for docking, from the complex with benzodiazepin-2-one (4PCI).[18] To do so, the target coordinates were extracted from the crystal structure. Protons and missing side-chains were added to the coordinates using the module AutoPSF of VMD based on the topology from CHARMM param36 force field for protein. The hereby prepared crystal structure in complex with the ligand and either 5, 6 or 7 structural water molecules was used for optimization of the positions of the hydrogen atoms by steepest descent and conjugate gradient methods implemented in the CHARMM program (version 38b1).[19]

Flexible ligand docking with tethered head group

The subsequently extracted bromodomain's coordinates as well as the optimized structural water molecules were used for flexible docking with the open-source software *rDock*.[20] During flexible ligand docking, the head groups were tethered in the binding site (command *sdtether*) to mimic the KAc residue.

Pose minimization

Atom typing, assignment of parameters and charges for the ligand were performed with the CHARMM General Force Field (CGenFF) program using the CHARMM param36 force field topology.[21,22] The minimization of the ligand's poses within the binding site was performed successively by steepest descent and conjugate gradient methods implemented in the CHARMM program (version 38b1).[19] All target's atoms were fixed during optimization.

Binding energy evaluation

The binding energy is the sum of protein/ligand van der Waals and electrostatic contribution. The electrostatic energy is the sum of bromodomain desolvation, ligand desolvation, and intermolecular interaction screened by the solvent which is treated implicitly by the finite-difference Poisson-Boltzmann method using the PBEQ module in CHARMM.[23] The dielectric constant of the solute was set to 4.0 and for the solvent to 78.5.

2. Molecules suggested by AutoCouple for CBP

- **Amide linker (Amide coupling):**

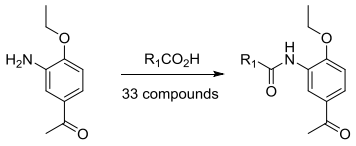

2 (LE = 0.45)
CBP: K_d = 53 μM

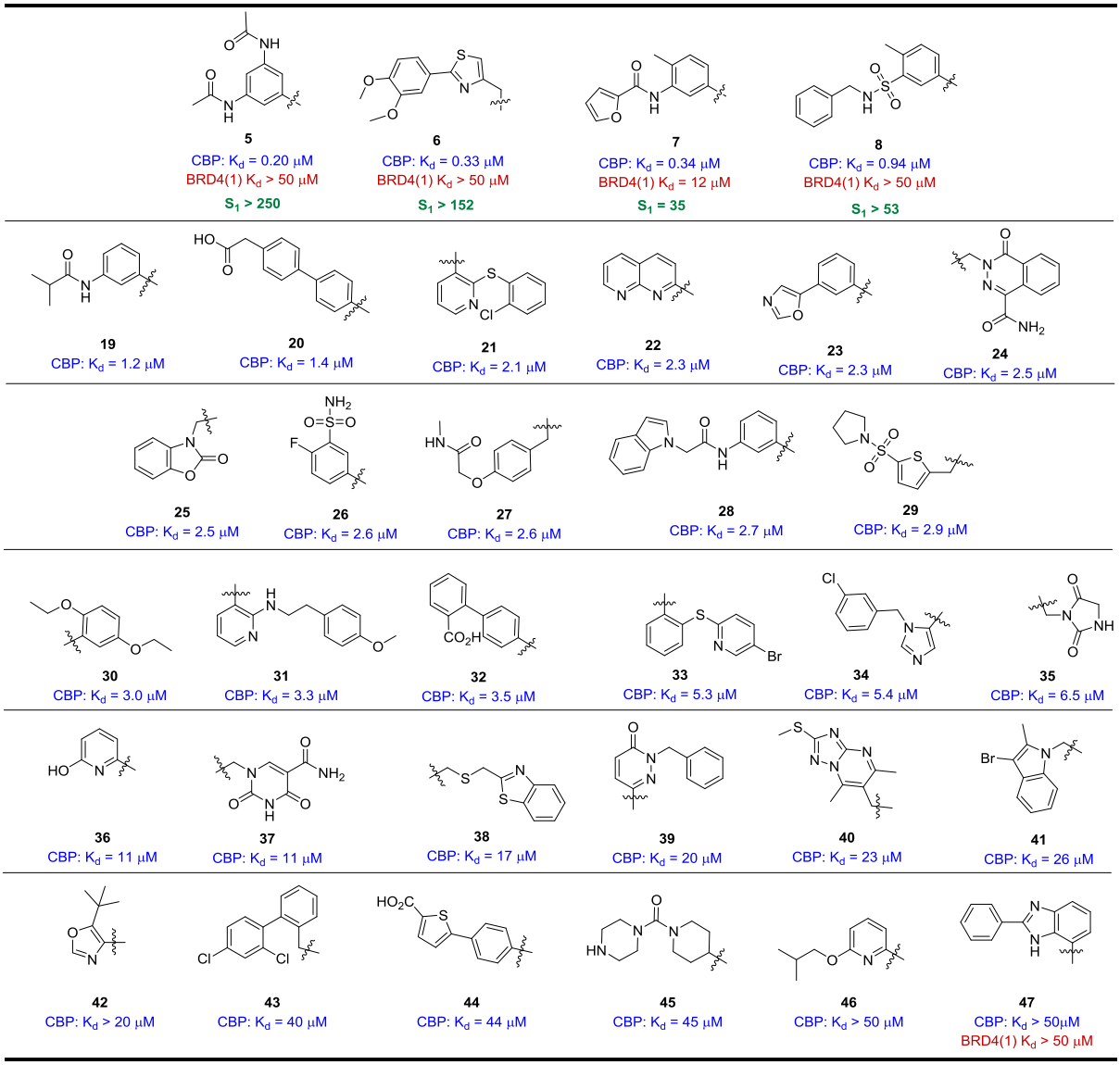

Figure S1. CBP inhibitors with an amide linker that originate from the virtual chemical reaction campaign by AutoCouple. The molecules are ordered from lowest to highest K_d for binding on CBP bromodomain. The K_d was determined in a competition binding assay (see section 6 for further details) onto CBP bromodomain (blue) or BRD4(1) bromodomain (red). Selectivity (S_1) for CBP bromodomain over BRD4(1) bromodomain determined by the ratio of K_d values.

- **Amine linker (Buchwald-Hartwig coupling)**

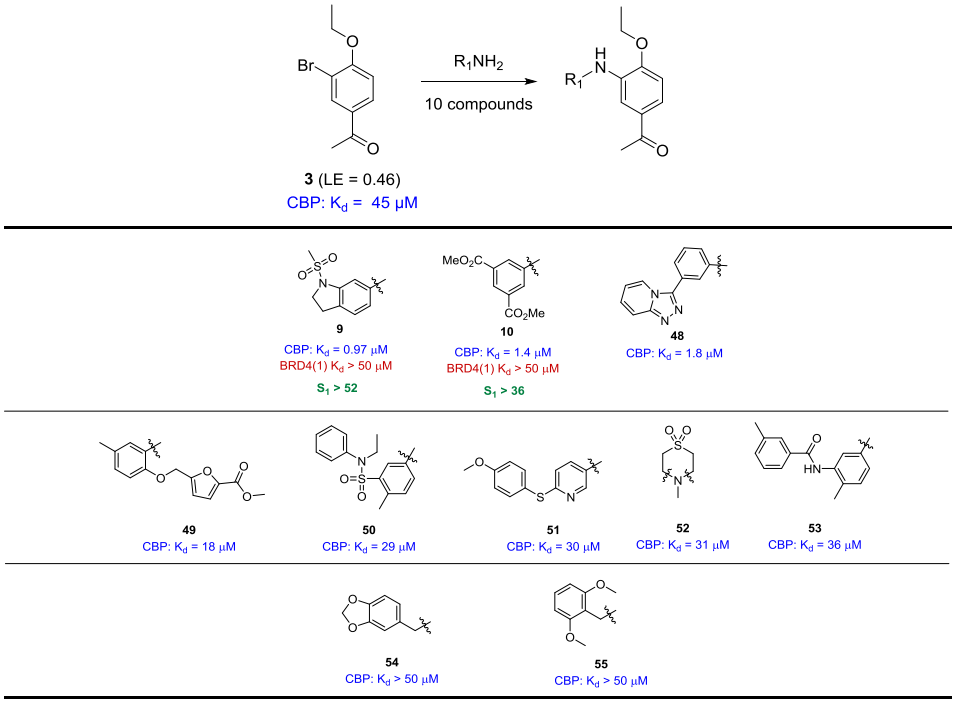

Figure S2. same as Figure S1 - synthesized CBP inhibitors containing an amine linker.

- **No linker (Suzuki cross-coupling)**

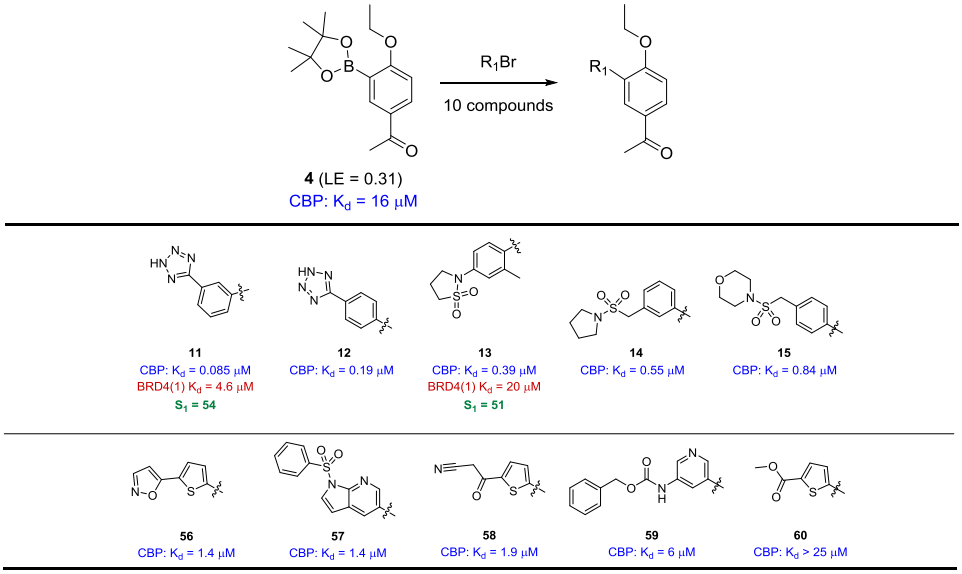

Figure S3. same as Figure S1 - synthesized CBP inhibitors without a linker (Suzuki coupling).

3. Molecules suggested by SEED and AutoCouple for BRD4(1)

3.1 Selective ligands of BRD4(1) identified by SEED

3.1.1 Fragment docking (SEED)

To further validate AutoCouple, we decided to focus on alternative KAc mimic fragments that, in contrast with the acetyl benzene moiety **61**, would exhibit higher affinity for BRD4(1) than for CBP. Preceding the present work, alternative "head-group" fragments (Table S1) had been identified by the fragment-docking program SEED (version 3.3.6):[24-25] A library of 419 heteroaromatics[22] was docked to the crystal structure of the CBP bromodomain (PDB code 3P1C) and the BRD4(1) bromodomain (PDB code 3MXF). The SEED docking of 419 fragments required about 15 minutes of a single core of a Xeon® Processor E3-1245 at 3.5 GHz. The CHARMM36[21] and CGenFF force fields[22] were used for the protein and fragments, respectively. The electrostatic energy is the sum of bromodomain desolvation, fragment desolvation, and intermolecular interaction screened by the solvent which is treated implicitly by the generalized Born approximation.

Table S1. Fragments with favorable binding energy as predicted by SEED.

	Fragment	CBP			BRD4(1)		
		van der Waals	electrostatic	total	van der Waals	electrostatic	total
61	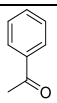	-14.0	-2.3	-16.3	-14.6	0.5	-14.0
62		-18.5	-1.4	-19.9	-17.5	-0.8	-18.3
63		-17.5	-1.9	-19.4	-16.6	2.1	-14.5
64	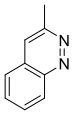	-15.3	-4.6	-19.9	-17.7	1.1	-16.5

3.1.2 Molecules suggested by SEED for BRD4(1)

Compounds **65-67** (Table S2) are analogs of compound **1** bearing a benzoic acid moiety as tail group and are connected via an amide linker to those SEED-identified hit fragments as KAc mimic (head group, see Table S1). Although these three compounds had high affinity for CBP (blue column in Table S2), compound **65** turned out to be slightly more potent towards BRD4(1) (Kd of 6.9 μM) than CBP (Kd of 17 μM), suggesting that the selectivity can possibly arise from the KAc mimic moiety. The benzotriazole moiety of compound **65** thus appeared as an alternative KAc mimic head group for targeting preferentially BRD4(1). We therefore set out to generate novel ligands via AutoCouple that would bear the benzotriazole moiety **65** as a KAc mimic.

Table S2. Affinity of compounds **1**, **65-67** for the CBP and BRD4(1) bromodomains.

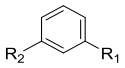

Cmpd	R_1	R_2	LE CBP	K_d (μM)[a] CBP	K_d (μM)[a] BRD4(1)	S_1[b]	S_2[b]	ΔT_m(°C)[c] CBP	ΔT_m(°C)[c] BRD4(1)
1	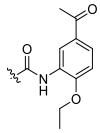	CO_2H	0.35	0.77	> 50	> 65	< 0.02	3.8	0.4
65	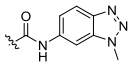	CO_2H	0.30	17	6.9	0.4	2.5	2.0	2.8
66	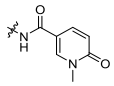	CO_2H	0.37	4.1	33	8.0	0.1	1.9	0.9
67	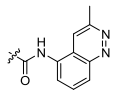	CO_2H	0.35	1.1	41	37	0.03	4.0	1.4

[a] K_d values were determined by a competition binding assay[26] in duplicates for CBP (blue) and BRD4(1) (red). [b] Selectivity (S_1) for CBP bromodomain over BRD4(1) bromodomain and selectivity (S_2) for BRD4(1) bromodomain over CBP bromodomain as determined by the ratio of K_d values obtained via the competition binding assay.[26] [c] Median value of the shift in the melting temperature (number of measurements > 12). The thermal shift assay was carried out with a 2 μM concentration of the bromodomain and 100 μM compound concentration (see section 5: Thermal shift measurements).

3.2 Molecules suggested by AutoCouple for BRD4(1)

Following the same strategy as described for CBP in the main text, virtual libraries were generated in silico by coupling of the benzotriazole moiety with commercially-available reactants. Two campaigns involving amide condensation and Suzuki cross-coupling reactions on the benzotriazole head groups **68** (see Figure S5) and **69** (see Figure S6) provided 32'000 amides and 19'000 C−C coupled compounds, respectively. A crystal structure of BRD4(1) in complex with a low micromolar benzodiazepine-2-one ligand previously resolved in our groups was used as the target[18] for flexible ligand docking. During the latter, the benzotriazole was tethered in the binding site (command *sdtether*) to mimic the KAc residue as observed in SEED pose (for BRD4(1), see Figure S4).

A total of 20 compounds were prioritized and synthesized (10 for the amide condensation and 10 for the Suzuki coupling). Nine of these compounds (**70-74** with amide linkers and **80-83** via direct C-C coupling) presented a K_d lower than 10 μM with promising LE values (up to 0.37 kcal mol^{-1} per non-hydrogen atom for compound **81**; see Figure S6). Furthermore, the selectivity towards BRD4(1) was improved from 2.5 fold for compound **65** up to 11 and 12 fold for pyridine **71** and sulfonamide **70**, respectively. Interestingly, compound **70** is 26 times more potent than the original fragment **68**. As in the previous campaign, AutoCouple offered significant structural diversity with a broad range of functional groups, including sulfonamides (**70**, **74**, **83**), pyridines (**71**, **80**), and diverse five membered ring heterocycles (**72**, **73**, **82**) among others, thus demonstrating the ability of this in silico tool to identify alternative motifs streamlining hit-optimization efforts.

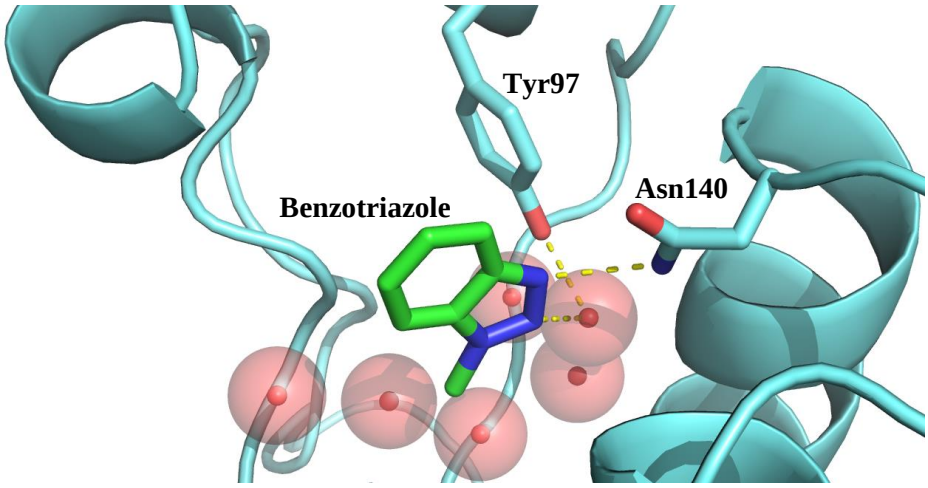

Figure S4: SEED pose of the Benzotriazole fragment (green) in BRD4(1) – During the docking of ligands generated by virtual couplings, the benzotriazole head groups were tethered to reproduce the pose within the binding site (*sdtether* command).

- **Amide linker (Amide coupling)**

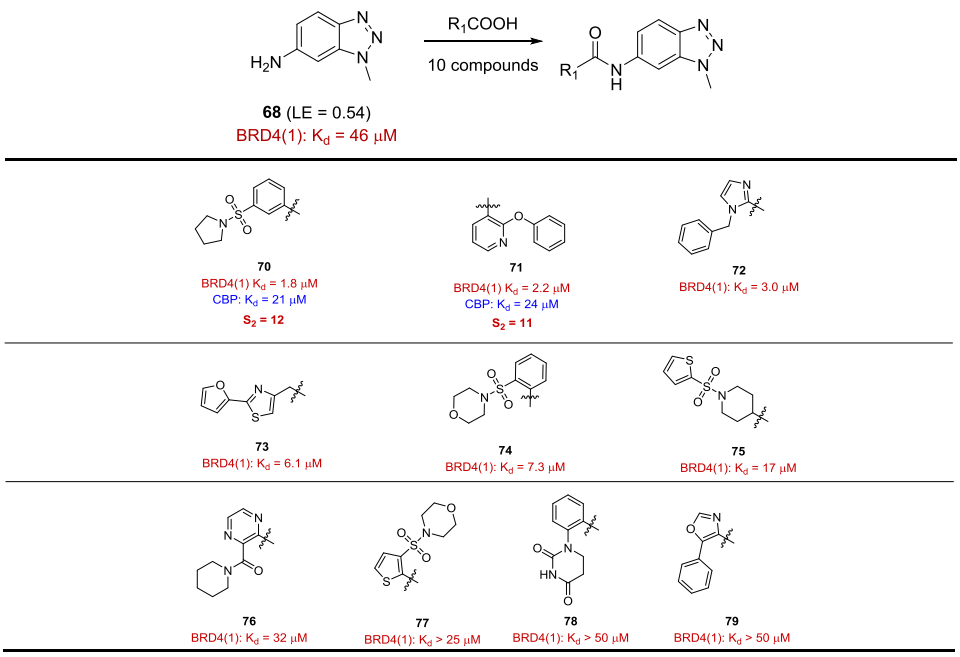

Figure S5. BRD4(1) inhibitors with an amide linker that originate from the virtual chemical reaction campaign by AutoCouple. The molecules are ordered from lowest to highest K_d for binding on BRD4(1) bromodomain. The K_d was determined in a competition binding assay (see section 6 for further details) onto CBP bromodomain (blue) or BRD4(1) bromodomain (red). Selectivity (S_2) for BRD4(1) bromodomain over CBP bromodomain determined by the ratio of K_d values.

- **No linker (Suzuki cross-coupling)**

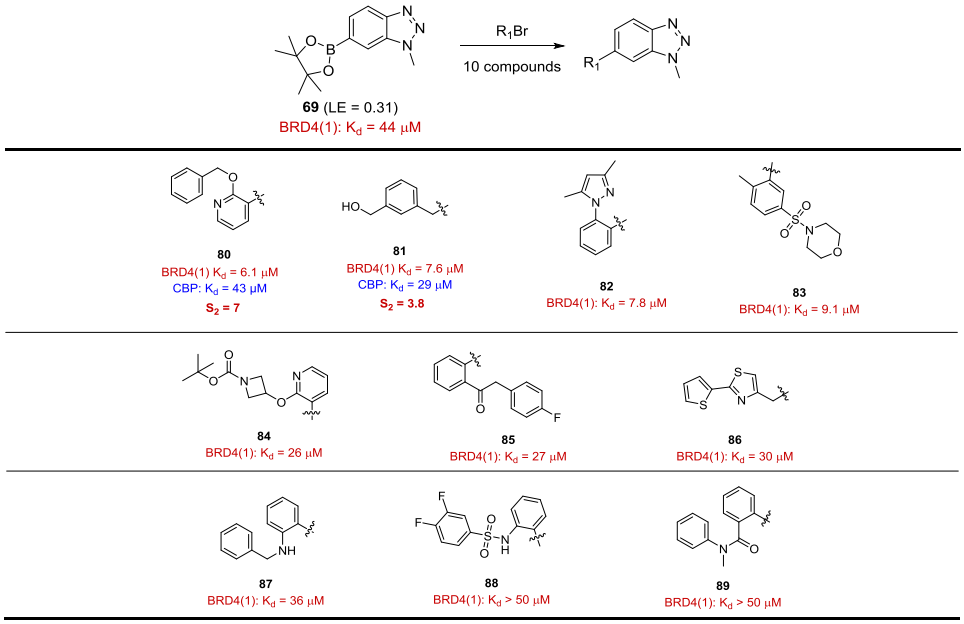

Figure S6. same as Figure S5 - synthesized BRD4(1) inhibitors without a linker (Suzuki cross-couplings).

4. Bromodomain expression and purification

Proteins were purified as described previously.[27] Briefly, Poly-Histidine-tagged (His-tag) bromodomains were expressed in *Escherichia coli* BL21(DE3) cells upon induction with isopropyl thio-beta-D-galactoside (IPTG, final concentration 0.1 mM) for 16 h at 18 °C. Bacteria were lysed and (when required) the resulting extract was treated to remove DNA, and 0.15% polyethylenimine (PEI) was added. The His-tagged proteins were purified on HisTrap columns (GE Healthcare) and eluted using a step gradient of imidazole. The His-tags were removed by overnight incubation with His-tagged tobacco etch virus (TEV) protease purified in-house (if required by the purification protocol, in the meantime the sample was exchanged via dialysis). A size-exclusion chromatography step (HiLoad 16/600 Superdex75 column) and a Ni-affinity chromatography step were subsequently performed to finally purify the cleaved bromodomains. Samples were then concentrated, flash frozen and stored at –80 °C.

5. Thermal shift measurements

Thermal shift measurements were performed using a 2 μM and 100 μM concentration for the bromodomains and ligands, respectively, as precedently described.[28] The reported values (ΔTm) were calculated as the difference between the transition midpoints of an individual sample and the average of the reference wells (containing the protein and the DMSO only) in the same plate. DMSO concentration was kept at 0.2% (v/v).

6. BROMOscan assays[26]

The binding constant (K_d) determinations by means of BROMOscan technology were carried out at DiscoverX. An E. *coli* strain derived from BL21 was used as the host to grow T7 phage strains displaying the bromodomains. E. *coli*, grown to log-phase, were infected with T7 phage (from a frozen stock, being the multiplicity of infection 0.4) and incubated while shaking at 32 °C for 90-150 minutes until lysis. In order to remove cell debris, lysates were centrifuged at 5,000 x g and filtered (0.2 μm). Affinity resins were obtained by treating streptavidin-coated magnetic beads with biotinylated acetylated peptide ligands for 30 minutes at 25°C. Those beads were then blocked with excess of biotin and washed with blocking buffer (SeaBlock (Pierce), 1 % bovine serum albumin (BSA), 0.05 % Tween 20, 1 mM dithiothreitol (DTT)) to remove the unbound ligand and reduce non-specific phage binding.

During the experiment, the bromodomain, ligand-bound affinity beads and test compounds were combined in a buffer composed of 17% SeaBlock, 33% phosphate-buffered solution (PBS), 0.04% Tween 20, 0.02% BSA, 0.004% sodium azide and 7.4 mM DTT. Test compounds were prepared as 50 mM in pure DMSO and diluted to 5 mM with monoethylene gycol, MEG (100× concentrated in respect to the top screening concentration 50 μM). During the assay the DMSO and MEG final concentrations were 0.1% and 0.9%, respectively. The assays were carried out in polystyrene 96-well plates in a final volume of 0.135 mL. The assay plates were incubated at 25 °C with shaking for 1 hour and the affinity beads were washed with a buffer composed of 0.05% Tween 20 in PBS. The beads were then re-suspended in the elution buffer (1x PBS, 0.05% Tween 20, 2 μM non-biotinylated affinity ligand) and incubated at 25°C with shaking for 30 minutes. The bromodomain concentration in the elutes was measured by qPCR. K_d values were calculated with a standard dose-response curve using the Hill equation and curves were fitted using a non-linear least square fit with the Levenberg-Marquardt algorithm.

7. Alpha Screen assays[29]

IC_{50} determinations by means of Amplified Luminescent Proximity Homogeneous Assay (Alpha) Screen technology were carried out at Reaction Biology. Compounds were tested in 10-dose IC_{50} mode with 2 or 3-fold serial dilution starting at varying concentrations. The competitive ligand was H4/4Ac: Histone H4 peptide (1-21) K5/8/12/16Ac-Biotin. The detection was performed by the AlphaScreen

Binding assay in Envision (Ex/Em=680/520-620 nm). Data include raw data (signal-Background, Background was measured without BRD but all other components.), % binding (relative to DMSO controls), and curve fits. An IC_{50} value higher than the starting compound concentration was estimated based on the best curve fitting available.

Compound **16**

Bromodomain	**IC_{50} (µM)**
CBP	0.019
BRD4(1)	>200
Selectivity	>10526

Table S3. Half maximal inhibitory concentration (IC_{50}) as determined by Alpha Screen assays for compound **16** with BRD4(1) and the bromodomain of CBP. The selectivity is calculated as the ratio of the IC_{50} values.

8. Target engagement in cells and preliminary biological evaluation

8.1 FRAP assays[30]

In order to determine if our inhibitors engage CBP bromodomain within a cellular setting, we conducted a fluorescence recovery after photo-bleaching (FRAP) assay for the most potent and chemically diverse inhibitors. Compounds **6**, **7**, **13**, **16** and **17** were able to displace the CBP bromodomain from chromatin at concentration of 1 µM (Figure S8 and Scheme 1D in the main text). The half times ($t_{1/2}$) required to recover the fluorescence in a photobleach area of U2OS cells expressing GFP-tagged multimerized (3X) CBP bromodomains were measured (Figure 4A, 4B in the main text and Figure S7). The presence of our inhibitors reduced the recovery $t_{1/2}$ compared to cells without compound treatment, in the presence of 2.5 µM of the histone deacetylase inhibitor suberoylanilide hydroxamic acid (SAHA). Moreover, in the case of compound **16**, the $t_{1/2}$ value resembles that of the N1168F mutant, indicating that our compound interacts with the KAc binding site of the CBP bromdomain efficiently, displacing it from chromatin (Figure 4A, 4B in the main text and Figure S7).

Plasmids:

The GFP-BRD4 plasmid was a gift from Kyle Miller (Addgene plasmid # 65378).[55]

CBP Plasmid cloning

The CBP multimerised bromodomain construct was made as previously reported.[30] Plasmids containing the fragments shown below were purchased from GenScript and their PCR products were cloned with Gateway BP Clonase II enzyme mix (MultiSite Gateway System, ThermoFisher) into either pDONR221 P4r-P3r, pDONR221 P3-P2 or pDONR221 P1-P4 to create entry clones.

pENTR221 P4r-P3r **CBP aa868-1341**	GGGGACAACTTTTCTATACAAAGTTGCTCTCCAGCACACGACACCACCTGGGATGACTCCTCCC CAGCCAGCAGCTCCCACTCAGCCATCAACTCCTGTGTCGTCTTCCGGGCAGACTCCCACCCCGA CTCCTGGCTCAGTGCCCAGTGCTACCCAAACCCAGAGCACCCCTACAGTCCAGGCAGCAGCCC AGGCCCAGGTGACCCCGCAGCCTCAAACCCCAGTTCAGCCCCCGTCTGTGGCTACCCCTCAGTC ATCGCAGCAACAGCCGACGCCTGTGCACGCCCAGCCTCCTGGCACACCGCTTTCCCAGGCAGC AGCCAGCATTGATAACAGAGTCCCTACCCCCTCCTCGGTGGCCAGCGCAGAAACCAATTCCCA GCAGCCAGGACCTGACGTACCTGTGCTGGAAATGAAGACGGAGACCCAAGCAGAGGACACTG AGCCCGATCCTGGTGAATCCAAAGGGGAGCCCAGGTCTGAGATGATGGAGGAGGATTTGCAAG GAGCTTCCCAAGTTAAAGAAGAAACAGACATAGCAGAGCAGAAATCAGAACCAATGGAAGTG GATGAAAAGAAACCTGAAGTGAAAGTAGAAGTTAAAGAGGAAGAAGAGAGTAGCAGTAACG GCACAGCCTCTCAGTCAACATCTCCTTCGCAGCCGCGCAAAAAAATCTTTAAACCAGAGGAGT TACGCCAGGCCCTCATGCCAACCCTAGAAGCACTGTATCGACAGGACCCAGAGTCATTACCTTT CCGGCAGCCTGTAGATCCCCAGCTCCTCGGAATTCCAGACTATTTTGACATCGTAAAGAATCCC ATGGACCTCTCCACCATCAAGCGGAAGCTGGACACAGGGCAATACCAAGAGCCCTGGCAGTAC GTGGACGACGTCTGGCTCATGTTCAACAATGCCTGGCTCTATAATCGCAAGACATCCCGAGTCT ATAAGTTTTGCAGTAAGCTTGCAGAGGTCTTTGAGCAGGAAATTGACCCTGTCATGCAGTCCCT TGGATATTGCTGTGGACGCAAGTATGAGTTTTCCCCACAGACTTTGTGCTGCTATGGGAAGCAG

	CTGTGTACCATTCCTCGCGATGCTGCCTACTACAGCTATCAGAATAGGTATCATTTCTGTGAGA AGTGTTTCACAGAGATCCAGGGCGAGAATGTGACCCTGGGTGACGACCCTTCACAGCCCCAGA CGACAATTTCAAAGGATCAGTTTGAAAAGAAGAAAAATGATACCTTAGACCCCGAACCTTTCG TTGATTGCAAGGAGTGTGGCCGGAAGATGCATCAGATTTGCGTTCTGCACTATGACATCATTTG GCCTTCAGGTTTTGTGTGCGACAACTGCTTGAAGAAAACTGGCAGACCTCGAAAAGAAAACAA ATTCAGTGCTAAGAGGCTGCAGACCACAAGACTGGGAAACCACTTGGAAGACCGAACAACTTT GTATAATAAAGTTGTCCCC
pENTR221 P3-P2 **CBP aa868-1341**	GGGGACAACTTTGTATAATAAAGTTGCTCTCCAGCACACGACACCACCTGGGATGACTCCTCCC CAGCCAGCAGCTCCCACTCAGCCATCAACTCCTGTGTCGTCTTCCGGGCAGACTCCCACCCCGA CTCCTGGCTCAGTGCCCAGTGCTACCCAAACCCAGAGCACCCCTACAGTCCAGGCAGCAGCCC AGGCCCAGGTGACCCCGCAGCCTCAAACCCCAGTTCAGCCCCCGTCTGTGGCTACCCCTCAGTC ATCGCAGCAACAGCCGACGCCTGTGCACGCCCAGCCTCCTGGCACACCGCTTTCCCAGGCAGC AGCCAGCATTGATAACAGAGTCCCTACCCCCTCCTCGGTGGCCAGCGCAGAAACCAATTCCCA GCAGCCAGGACCTGACGTACCTGTGCTGGAAATGAAGACGGAGACCCAAGCAGAGGACACTG AGCCCGATCCTGGTGAATCCAAAGGGGAGCCCAGGTCTGAGATGATGGAGGAGGATTTGCAAG GAGCTTCCCAAGTTAAAGAAGAAACAGACATAGCAGAGCAGAAATCAGAACCAATGGAAGTG GATGAAAAGAAACCTGAAGTGAAAGTAGAAGTTAAAGAGGAAGAAGAGAGTAGCAGTAACG GCACAGCCTCTCAGTCAACATCTCCTTCGCAGCCGCGCAAAAAAATCTTTAAACCAGAGGAGT TACGCCAGGCCCTCATGCCAACCCTAGAAGCACTGTATCGACAGGACCCAGAGTCATTACCTTT CCGGCAGCCTGTAGATCCCCAGCTCCTCGGAATTCCAGACTATTTTGACATCGTAAAGAATCCC ATGGACCTCTCCACCATCAAGCGGAAGCTGGACACAGGGCAATACCAAGAGCCCTGGCAGTAC GTGGACGACGTCTGGCTCATGTTCAACAATGCCTGGCTCTATAATCGCAAGACATCCCGAGTCT ATAAGTTTTGCAGTAAGCTTGCAGAGGTCTTTGAGCAGGAAATTGACCCTGTCATGCAGTCCCT TGGATATTGCTGTGGACGCAAGTATGAGTTTTCCCCACAGACTTTGTGCTGCTATGGGAAGCAG CTGTGTACCATTCCTCGCGATGCTGCCTACTACAGCTATCAGAATAGGTATCATTTCTGTGAGA AGTGTTTCACAGAGATCCAGGGCGAGAATGTGACCCTGGGTGACGACCCTTCACAGCCCCAGA CGACAATTTCAAAGGATCAGTTTGAAAAGAAGAAAAATGATACCTTAGACCCCGAACCTTTCG TTGATTGCAAGGAGTGTGGCCGGAAGATGCATCAGATTTGCGTTCTGCACTATGACATCATTTG GCCTTCAGGTTTTGTGTGCGACAACTGCTTGAAGAAAACTGGCAGACCTCGAAAAGAAAACAA ATTCAGTGCTAAGAGGCTGCAGACCACAAGACTGGGAAACCACTTGGAAGACCGATAGTACCC AGCTTTCTTGTACAAAGTGGTCCCC
pENTR221 P1-P4 **NLS/CBP aa868-1341**	GGGGACAAGTTTGTACAAAAAAGCAGGCTTAATGCCCAAGAAGAAGAGGAAAGTCTCTCTCCA GCACACGACACCACCTGGGATGACTCCTCCCCAGCCAGCAGCTCCCACTCAGCCATCAACTCCT GTGTCGTCTTCCGGGCAGACTCCCACCCCGACTCCTGGCTCAGTGCCCAGTGCTACCCAAACCC AGAGCACCCCTACAGTCCAGGCAGCAGCCCAGGCCCAGGTGACCCCGCAGCCTCAAACCCCAG TTCAGCCCCCGTCTGTGGCTACCCCTCAGTCATCGCAGCAACAGCCGACGCCTGTGCACGCCCA GCCTCCTGGCACACCGCTTTCCCAGGCAGCAGCCAGCATTGATAACAGAGTCCCTACCCCCTCC TCGGTGGCCAGCGCAGAAACCAATTCCCAGCAGCCAGGACCTGACGTACCTGTGCTGGAAATG AAGACGGAGACCCAAGCAGAGGACACTGAGCCCGATCCTGGTGAATCCAAAGGGGAGCCCAG GTCTGAGATGATGGAGGAGGATTTGCAAGGAGCTTCCCAAGTTAAAGAAGAAACAGACATAG CAGAGCAGAAATCAGAACCAATGGAAGTGGATGAAAAGAAACCTGAAGTGAAAGTAGAAGTT AAAGAGGAAGAAGAGAGTAGCAGTAACGGCACAGCCTCTCAGTCAACATCTCCTTCGCAGCCG CGCAAAAAAATCTTTAAACCAGAGGAGTTACGCCAGGCCCTCATGCCAACCCTAGAAGCACTG TATCGACAGGACCCAGAGTCATTACCTTTCCGGCAGCCTGTAGATCCCCAGCTCCTCGGAATTC CAGACTATTTTGACATCGTAAAGAATCCCATGGACCTCTCCACCATCAAGCGGAAGCTGGACA CAGGGCAATACCAAGAGCCCTGGCAGTACGTGGACGACGTCTGGCTCATGTTCAACAATGCCT GGCTCTATAATCGCAAGACATCCCGAGTCTATAAGTTTTGCAGTAAGCTTGCAGAGGTCTTTGA GCAGGAAATTGACCCTGTCATGCAGTCCCTTGGATATTGCTGTGGACGCAAGTATGAGTTTTCC CCACAGACTTTGTGCTGCTATGGGAAGCAGCTGTGTACCATTCCTCGCGATGCTGCCTACTACA GCTATCAGAATAGGTATCATTTCTGTGAGAAGTGTTTCACAGAGATCCAGGGCGAGAATGTGA CCCTGGGTGACGACCCTTCACAGCCCCAGACGACAATTTCAAAGGATCAGTTTGAAAAGAAGA AAAATGATACCTTAGACCCCGAACCTTTCGTTGATTGCAAGGAGTGTGGCCGGAAGATGCATC AGATTTGCGTTCTGCACTATGACATCATTTGGCCTTCAGGTTTTGTGTGCGACAACTGCTTGAA GAAAACTGGCAGACCTCGAAAAGAAAACAAATTCAGTGCTAAGAGGCTGCAGACCACAAGAC TGGGAAACCACTTGGAAGACCGACACCCAACTTTTCTATACAAAGTTGTCCCC

The three entry clones were then combined by LR cloning (MultiSite Gateway System, ThermoFisher) into the pcDNA6.2/N-EmGFP-DEST vector creating an expression clone for three tandem repeats of the CBP bromodomain fused to an N-terminal GFP.

The N1168F CBP bromodomain mutant plasmid was generated using the QuikChange Lightning Multi Site-Directed Mutagenesis Kit (Agilent Technologies) starting from the non-mutagenic plasmid. The mutagenic primer was designed in the Agilent Technologies' website:
5'- GGATGTCTTGCGAAAATAGAGCCAGGCATTGTTGAACATG-3'

Cell culture

U2OS cells are kind gift from Dr. Sander Botter (Balgrist University Hospital, Zurich, Switzerland). Cells were grown at 37°C with 5% CO2 in a humidified incubator in Dulbecco's modified medium (DMEM) (GibcoTM, ThermoFischer Scientific). The medium contained 10% FCS, 100U/ml penicillin and 100mg/ml streptomycin.

FRAP assay

FRAP studies were performed according to a published protocol,[30] with slight modifications. In brief, U2OS cells in a 8-well chamber (ibidi) were transfected (Lipofectamine 2000, ThermoFisher) with the GFP-CBP-bromodomain plasmid (WT), GFP-CBP mutant plasmid (N1168F) or GFP-BRD4 plasmid. Six hours after transfection, culture medium was replaced with or without 2.5 μM SAHA (only for CBP plasmids), and the inhibitors (1 μM for CBP compounds and 0.1 μM for JQ1) were added 23 hours after transfection. Cells were then imaged 24 hours after transfection.

The FRAP experiments were conducted with a Leica SP5 confocal microscope (Leica microsystems GmbH, Wetzla, Germany) equipped with a HCX PL APO 40× Objective (NA 1.25) (Leica) and a controlled chamber set at 37°C and 5% CO_2. Bleaching and GFP fluorescence imaging were carried out with an argon laser (488 nm) and a detector set to detect fluorescence between 500 and 550 nm. Cells with nuclei just below saturation within the gain range of 650 to 850 were bleached. A square region (16 μm^2) of a GFP-positive nucleus was selected, and, after five prescans, the region was bleached. A time-lapse series was then taken to record GFP recovery. During the time-lapse series, images were acquired with a frame size of 256 pixels × 256 pixels with line-stepping of 2, bidirectional scanning and a zoom factor of 6, which allowed for a time interval time of 0.1-0.2 seconds. The laser power was set to 100% for photobleaching and attenuated to 2% for acquisition.

Data analysis

The fluorescence signal was measured with FIJI and normalized according to a published method.[30] All experiments were transferred to Prism (GraphPad) and fit on an exponential FRAP curve (one-way association). Different groups were compared by determining the half time ($t_{½}$) of the fluorescence recovery to reach a plateau level.

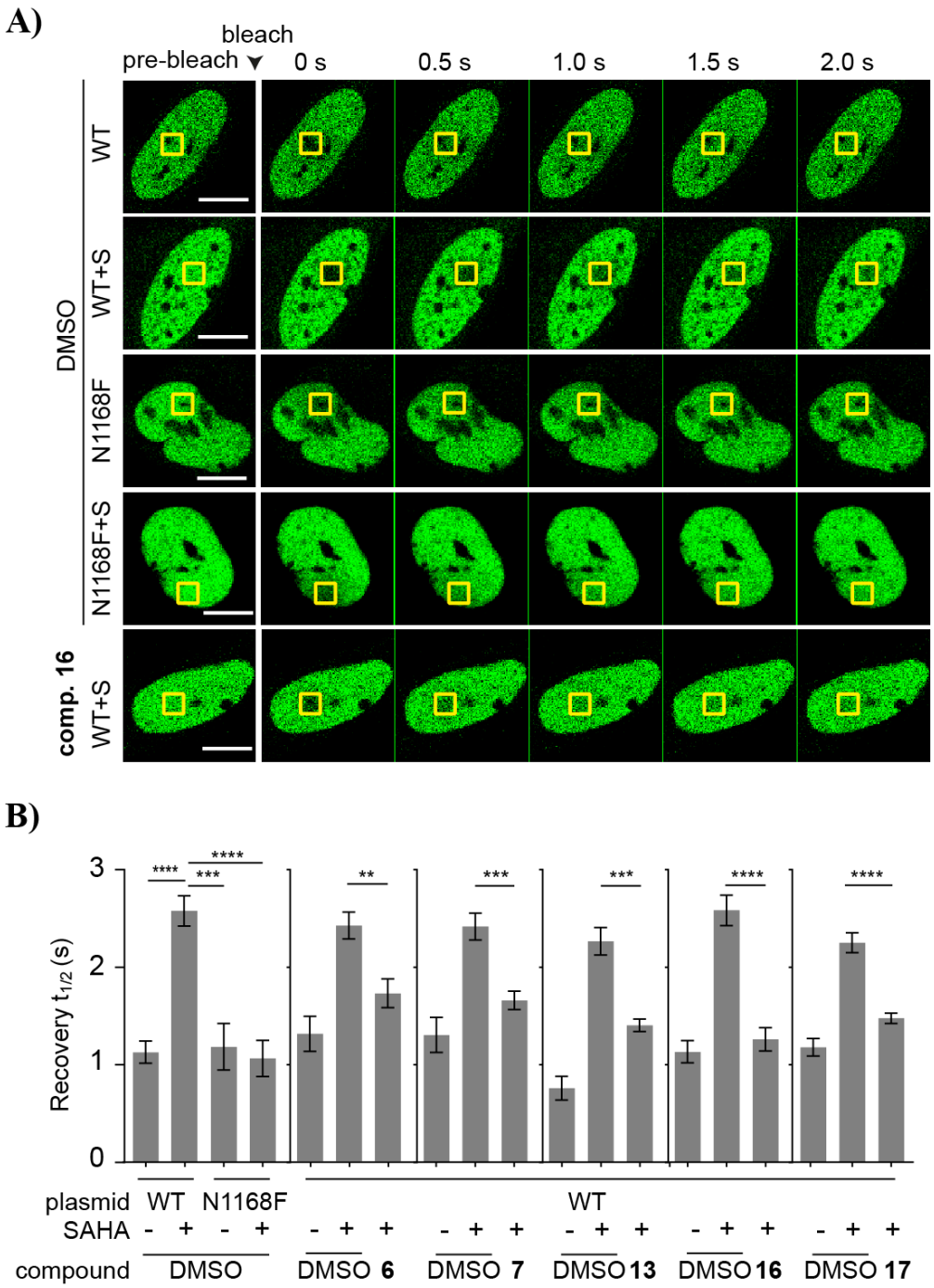

Figure S7. Fluorescence recovery after photo-bleaching (FRAP) demonstrating the displacement of CBP bromodomain from chromatin. U2OS cells were transfected with plasmids encoding GFP fused to wild-type (WT) or mutant (N1168F) multimerised CBP bromodomain, with or without 2.5 μM suberoylanilide hydroxamic acid (SAHA) and indicated compounds (1 μM). A) Representative images of the nuclei of cells treated with DMSO or compound **16**, with the presence of SAHA. The bleached area (16 μm^2) is indicated by a square. B) Half-times of fluorescence recovery ($t_{½}$) in the FRAP assays. Bars represent the mean $t_{½}$ calculated from individual recovery curves of at least 7 cells per group, and error bars represent the standard error of the mean. (statistics: Man-Whitney, always compared to SAHA-treated cells within the same experiment setup (significance: **P< 0.01, ***P<0.001 and ****P < 0.0001.)

8.2 Proliferation assays and Reverse Transcription Quantitative Polymerase Chain Reaction (RT-qPCR)

Cell proliferation assays

Cellular proliferation was assessed by Resazurin assay. Cells were plated at 10^4 cells/well of a 96-well plate for 24 h prior to incubation for three or six days with two-fold compound dilutions from 50µM or DMSO 1% control. Resazurin at 86µM (#R12204, ThermoFisher) was added and the metabolic activity was measured after six hours incubation at excitation of 560nM and detecting emission at 590nM. Procedures referred to Conery et al.[31]

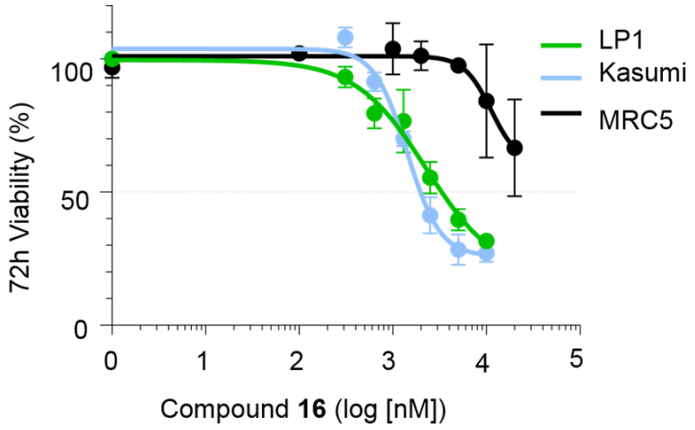

Figure S8. Proliferation assay of compound **16** in cells: LP1, Kasumi and non-transformed fibroblast MRC5, resazurin assay, 72 h incubation. Curves represent non-linear fit by a four-parameter logistic function; data points are mean values of at least three independent experiments; error bars: S.D. Hill coefficients for LP1 = -1.2, Kasumi = -2.5, MRC5 = -3.0.

6-DAYS ASSAY:

	GI_{50} (µM)
LP1	1.1 ± 0.4
Kasumi	1.8 ± 0.2
HL-60	3.2 ± 0.3

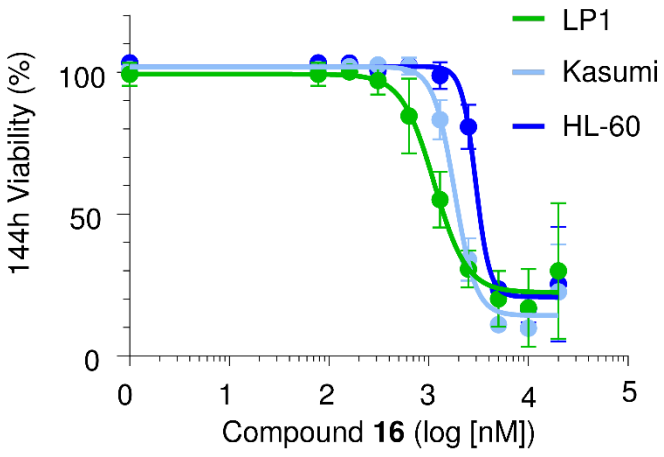

Figure S9. Same as Figure S8 with 144 h incubation and an additional cell line, the leukemia cell line HL-60. Hill coefficients for LP1 = -2.7, Kasumi = -4.1, HL-60 = -6.2.

Reverse Transcription Quantitative Polymerase Chain Reaction (RT-qPCR)

LP1 cells were incubated with compounds or DMSO control at 0.1% for six hours. RNA was isolated with an RNeasy kit (#74104, Qiagen) or by consistent quality with TRIzol reagent (#15596026, ThermoFisher) following manufacturer's instructions. RNA was converted to cDNA by Applied Biosystems' reverse transcriptase (#4368814, ThermoFisher). qPCR was operated in a Roche LightCycler®480 and performed by fluorescence detection of SYBRgreen® (#4368577, ThermoFisher) cycled from 1µg converted cDNA. Transcript specific primers are: IRF4: 5'-GCCAAGATTCCAGGTGACTC 3'-CTGGCTAGCAGAGGTTCTACG; cMYC: 5'-TACAACACCCGAGCAAGGAC 3'-GAGGCTGCTGGTTTTCCACT; and control transcript GAPDH: 5'-AGCCACATCGCTCAGACAC 3'-GCCCAATACGACCAAATCC.

12. Protein purification, crystallization and structural determination

CBP bromodomain was expressed and purified by following the protocol described previously.[27] Protein was concentrated to 20 mg/ml in the buffer of 20 mM HEPES, pH 7.4, 500 mM NaCl, 5% glycerol and 0.5 mM TCEP for crystallization. The co-crystal of **16** bound to CBP bromodomain was grown by sitting-drop vapor diffusion at 277 K in 0.1 M Morpheus® Buffer System 3, pH 8.5, 37.50% v/v MPD_P1K_P3350 and 0.09 M NPS at a1:1 (v/v) ratio of protein/ligand to reservoir buffer. Crystals were cryoprotected by crystallization buffer supplemented with 20% ethylene glycol prior to freezing in liquid nitrogen. Diffraction data were collected at the X06SA beamline at the Swiss Light Source, Paul Scherrer Institut, Villigen, Switzerland. Data was integrated with XDS[49] and scaled with AIMLESS.[50] Structure was solved by molecular replacement with Phaser[51] using PDB 3DWY as a search model. Model building and refinement was performed with Coot[52] and Phenix,[53] respectively. Programs used for crystallographic data processing and analysis were supported by the SBGrid Consortium[54]. The statistics of data process and refinement are summarized in Table S3.

Table S4. X-ray data collection and refinement statistics for co-crystal structure of the CBP bromodomain with compound **16**.

Data Collection	
PDB ID	5NLK
Space group	$P2_12_12_1$
Cell dimensions	
a, b, c (Å)	37.38, 40.81, 87.38
α, β, γ (°)	90.00, 90.00, 90.00
Resolution (Å)	40.81 - 1.80
Unique observations[a]	12880(745)
Completeness[a]	99.3(99.8)
Redundancy[a]	12.6(13.5)
Rmerge[a]	0.164(0.689)
I/σI[a]	9.9(2.6)
$CC_{1/2}$[a]	0.99(0.94)
Refinement	
Rwork/Rfree[a]	0.176(0.227) /0.216(0.333)
R.m.s. deviations of bond lengths (Å)	0.005
R.m.s. deviations of bond angles (°)	0.989
Average B-factor ($Å^2$)	
Protein	35.23
Ligand	32.10
Wwater	42.50
Ramachandran	
Favored (%)	99.12
Allowed (%)	0.88
Disallowed (%)	0
[a] Highest resolution shell is shown in parentheses.	

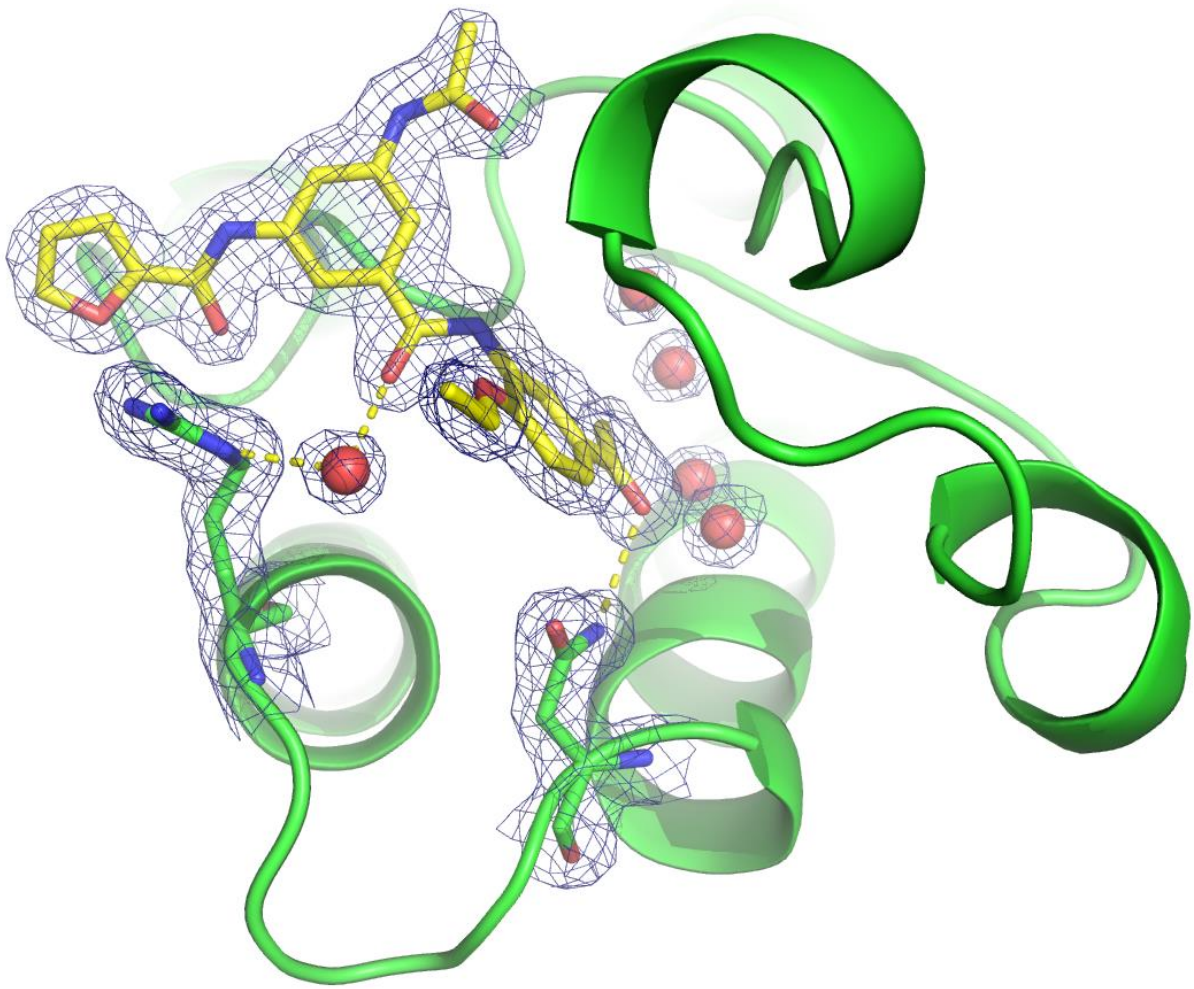

Figure S10. 2mFo – DFc electron density maps of ligand **16**, structural water molecules and key residues of the CBP bromodomain; PDB code : 5NLK

13. References

1. G. VanRossum, F. L. Drake, *The Python Language Reference*, Python software foundation Amsterdam, Netherlands, **2010**.
2. S. v. d. Walt, S. C. Colbert, G. Varoquaux, *Computing in Science & Engineering* **2011**, *13*, 22–30.
3. Landrum, G.; RDKit, Open-Source Cheminformatics; *Online: http://www.rdkit.org*.
4. A. Dalby, J. G. Nourse, W. D. Hounshell, A. K. Gushurst, D. L. Grier, B. A. Leland, J. Laufer, *Journal of chemical information and computer sciences* **1992**, *32*, 244–255.
5. G. M. Rishton, *Drug discovery today* **1997**, *2*, 382–384.
6. C. A. Lipinski, *Drug Discovery Today: Technologies* **2004**, *1*, 337–341.
7. F. Chevillard, P. Kolb, *Journal of chemical information and modeling* **2015**, *55*, 1824–1835.
8. M. Hartenfeller, H. Zettl, M. Walter, M. Rupp, F. Reisen, E. Proschak, S. Weggen, H. Stark, G. Schneider, *PLoS Comput Biol* **2012**, *8*: e1002380.
9. M. Hartenfeller, M. Eberle, P. Meier, C. Nieto-Oberhuber, K.-H. Altmann, G. Schneider, E. Jacoby, S. Renner, *Journal of chemical information and modeling* **2012**, *52*, 1167–1178.
10. H. M. Vinkers, et al. *Journal of medicinal chemistry* **2003,** *46*, 2765–2773.
11. P. Ertl, A. Schuffenhauer, *Journal of cheminformatics* **2009**, *1*, 1:8.
12. K. Boda, T. Seidel, J. Gasteiger, *Journal of computer-aided molecular design* **2007**, *21*, 311–325.
13. Marvin Suite (version 16.2.15.0) , calculation module developed by ChemAxon, https://www.chemaxon.com/download/marvin-suite/#marvin, 2015.
14. N. M. O'Boyle, M. Banck, C. A. James, C. Morley, T. Vandermeersch, G. R. Hutchison, *Journal of cheminformatics* **2011**, *3*:33.
15. A. Unzue, M. Xu, J. Dong, L. Wiedmer, D. Spiliotopoulos, A. Caflisch, C. Nevado, *Journal of medicinal chemistry* **2015**, *59*, 1350–1356.
16. M. Xu, A. Unzue, J. Dong, D. Spiliotopoulos, C. Nevado, A. Caflisch, *Journal of medicinal chemistry* **2015**, *59*, 1340–1349.
17. T. P. Rooney, P. Filippakopoulos, O. Fedorov, S. Picaud, W. A. Cortopassi, D. A. Hay, S. Martin, A. Tumber, C. M. Rogers, M. Philpott, *Angewandte Chemie International Edition* **2014**, *53*, 6126–6130.
18. H. Zhao, L. Gartenmann, J. Dong, D. Spiliotopoulos, A. Caflisch, *Bioorganic & medicinal chemistry letters* **2014**, *24*, 2493–2496.
19. B. R. Brooks, C. L. Brooks, A. D. MacKerell, L. Nilsson, R. J. Petrella, B. Roux, Y. Won, G. Archontis, C. Bartels, S. Boresch, *Journal of computational chemistry* **2009**, *30*, 1545–1614.
20. S. Ruiz-Carmona, D. Alvarez-Garcia, N. Foloppe, A. B. Garmendia-Doval, S. Juhos, P. Schmidtke, X. Barril, R. E. Hubbard, S. D. Morley, *PLOS Comput Biol* **2014**, *10*, e1003571.
21. A. D. MacKerell, M. Feig, C. L. Brooks, *Journal of the American Chemical Society* **2004**, *126*, 698–699.
22. K. Vanommeslaeghe, et al. *J. Comput. Chem.* **2010,** *31*, 671–690.
23. W. Im, D. Beglov, B. Roux, *Computer physics communications* **1998**, *111*, 59–75.
24. N. Majeux, M. Scarsi, J. Apostolakis, C. Ehrhardt, A. Caflisch, *Proteins: Structure, Function, and Bioinformatics* **1999**, *37*, 88–105.
25. N. Majeux, M. Scarsi, A. Caflisch, *Proteins: Structure, Function, and Bioinformatics* **2001**, *42*, 256–268.
26. E. Quinn, L. Wodicka, P. Ciceri, G. Pallares, E. Pickle, A. Torrey, M. Floyd, J. Hunt, D. Treiber, *Cancer Research* **2013**, *73*, 4238–4238.
27. P. Filippakopoulos, S. Picaud, M. Mangos, T. Keates, J. P. Lambert, D. Barsyte-Lovejoy, I. Felletar, R. Volkmer, S. Müller, T. Pawson, A. C. Gingras, C. H. Arrowsmith, S. Knapp, *Cell* **2012**, *149*, 214–231.
28. P. Filippakopoulos, J. Qi, S. Picaud, Y. Shen, W. B. Smith, O. Fedorov, E. M. Morse, T. Keates, T. T. Hickman, I. Felletar, M. Philpott, S. Munro, M. R. McKeown, Y. Wang, A. L. Christie, N. West, M. J. Cameron, B. Schwartz, T. D. Heightman, N. La Thangue, C. A. French, O. Wiest, A. L. Kung, S. Knapp, J. E. Bradner, *Nature* **2010**, *468*, 1067–1073.
29. A. M. Quinn, et al. *Nucleic Acids Res.*, **2010**, *38*, 2:e11, D750-D753.
30. M. Philpott, C. M. Rogers, C. Yapp, C. Wells, J. P. Lambert, C. Strain-Damerell, N. A. Burgess-Brown, A. C. Gingras, S. Knapp, S. Muller, *Epigenetics & Chromatin* **2014**, *7*:14, 1–12
31. Conery, A. R. et al. *eLife* **2016**, *5*, e10483
32. C. Deutsch, D. Kuhn, T. Ross, L. Burgdorf, *Merck* **2013**, *WO2013/124026 A1*.
33. N. Kaila, B. Follows, L. Leung, J. Thomason, A. Huang, A. Moretto, K. Janz, M. Lowe, T. Mansour, C. Hubeau, K. Page, P. Morgan, S. Fish, X. Xu, C. Williams, E. Saiah, *Journal of Medicinal Chemistry* **2014**, *57*, 1299–1322.
34. M. A. Palladino, G. K. Lloyd, Y. Hayashi, **2008,** *US2008/221122 A1*.
35. H. Iwata, Y. Kohara, S. X. Cao, P. Guntupalli, S. L. Gwaltney, D. J. Hosfield, Y. Liu, J. A. Stafford, B. Throop, **2010**, *US2010/69431 A1*; *WO2007/028135*
36. B. F. Mcguinness, K. K. Ho, S. Babu, G. Dong, J. Duo, T. X. H. Le, K. W. Saionz, **2010**, *WO2010/102154 A2*.
37. N. Carruthers, W. Chai, S. Dax, J. Jablonowski, X. Li, T. Lovenberg, W. Murray, D. Rudolph, M. Seierstad, M. Youngman, **2005**, *US2005/0070534 A1*.
38. V. S. Padalkar, V. S. Patil, K. R. Phatangare, P. G. Umape, N. Sekar, *Synthetic Communications* **2011**, *41*, 925–938.
39. E. Altmann, C. Betschart, K. Gohda, M. Horiuchi, R. Lattmann, M. Missbach, J. Sakaki, M. Takai, N. Teno, S. D. Cowen, **2002**, *US6353017 B1*.
40. E. A. Hamed, A. A. ElBardan, E. F. Saad, G. A. Gohar, G. M. Hassan, *Journal of the Chemical Society-Perkin Transactions 2* **1997**, 2415–2421.
41. W. J. Hoekstra, C. M. Yates, S. W. Rafferty, **2014**, *WO2014/117090 A1*.

42. G. Wu, K. Chan, T. Ewing, P. N. Ibrahim, J. Lin, M. Nespi, W. Spevak, Y. Zhang, **2014**, *WO2014/100620 A2*.
43. R. Lavoie, J. A. Bender, C. Bachand, E. H. Ruediger, J. F. Kadow, **2010**, *WO2010/120621 A1*.
44. R. A. Bit, A. Hall, D. N. Hurst, T. Scoccitti, **2006**, *WO2006/114274 A1*.
45. X. Q. Wang, K. Sarris, K. Kage, D. Zhang, S. P. Brown, T. Kolasa, C. Surowy, O. F. El Kouhen, S. W. Muchmore, J. D. Brioni, A. O. Stewart, *Journal of Medicinal Chemistry* **2009**, *52*, 170–180.
46. M. E. Christy, C. D. Colton, M. Mackay, W. H. Staas, J. B. Wong, E. L. Engelhardt, M. Torchiana, C. A. Stone, *Journal of Medicinal Chemistry* **1977**, *20*, 421–430.
47. S. Wurtz, C. Lohre, R. Frohlich, K. Bergander, F. Glorius, *Journal of the American Chemical Society* **2009**, *131*, 8344–8345.
48. S. Matsumoto, D. Takada, H. Kageyama, M. Akazome, *Tetrahedron Letters* **2014**, *55*, 1082–1085.
49. W. Kabsch, *Acta crystallographica. Section D, Biological crystallography* **2010**, *66*, 125–132.
50. P. R. Evans, G. N. Murshudov, *Acta crystallographica. Section D, Biological crystallography* **2013**, *69*, 1204–1214.
51. A. J. McCoy, R. W. Grosse-Kunstleve, P. D. Adams, M. D. Winn, L. C. Storoni, R. J. Read, *Journal of applied crystallography* **2007**, *40*, 658–674.
52. P. Emsley, B. Lohkamp, W. G. Scott, K. Cowtan, *Acta Crystallographica Section D* **2010**, *66*, 486–501.
53. P. D. Adams, P. V. Afonine, G. Bunkoczi, V. B. Chen, I. W. Davis, N. Echols, J. J. Headd, L.-W. Hung, G. J. Kapral, R. W. Grosse-Kunstleve, A. J. McCoy, N. W. Moriarty, R. Oeffner, R. J. Read, D. C. Richardson, J. S. Richardson, T. C. Terwilliger, P. H. Zwart, *Acta Crystallographica Section D* **2010**, *66*, 213–221.
54. A. Morin, B. Eisenbraun, J. Key, P. C. Sanschagrin, M. A. Timony, M. Ottaviano, P. Sliz, *eLife* **2013**, *2*, e01456.
55. F. Gong, L.Y. Chiu, B. Cox, F. Aymard, T. Clouaire, J.W. Leung, M. Cammarata, M. Perez, P. Agarwal, J.S. Brodbelt, G. Legube, K.M. Miller. *Genes Dev.* **2015**, *29*,197–211.

Chapter 6

The "gatekeeper" residue influences the mode of binding of acetyl indoles to bromodomains

Unzue A, Zhao H, Lolli G, Dong J, **Zhu J**, Zechner M, Dolbois A, Caflisch A, Nevado C. Journal of Medicinal Chemistry 2016; 59(7):3087-3097.

Journal of Medicinal Chemistry

Article

pubs.acs.org/jmc

The "Gatekeeper" Residue Influences the Mode of Binding of Acetyl Indoles to Bromodomains

Andrea Unzue,[†] Hongtao Zhao,[‡] Graziano Lolli,[‡] Jing Dong,[‡] Jian Zhu,[‡] Melanie Zechner,[†] Aymeric Dolbois,[†] Amedeo Caflisch,*[,‡] and Cristina Nevado*[,†]

[†]Department of Chemistry and [‡]Department of Biochemistry, University of Zürich, Winterthurerstrasse 190, CH-8057 Zürich, Switzerland

Supporting Information

ABSTRACT: Small-molecule hits for the bromodomains of CREBBP and BAZ2B have been identified by scaffold hopping followed by docking of a set of ∼200 compounds containing the acetyl indole scaffold. Chemical synthesis of nearly 30 derivatives has resulted in ligands of representatives of three subfamilies of human bromodomains with favorable ligand efficiency. The X-ray crystal structures of three different bromodomains (CREBBP, BAZ2B, and BRPF1b) in complex with acetyl indole derivatives reveal the influence of the gatekeeper residue on the orientation of small-molecule ligands in the acetyl lysine binding site.

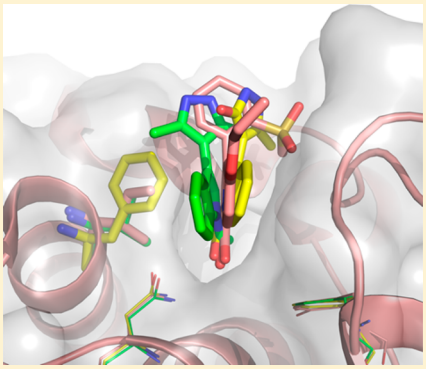

INTRODUCTION

Acetylation of lysine residues is an important post-translational modification of histone proteins that contributes to the regulation of chromatin structure and transcription.[1,2] Bromodomains are protein modules with four-helix bundle topology that specifically recognize ("read") acetylated lysine residues, as well as butyryllysine and crotonyllysine,[3] and are considered protein targets of interest for the development of chemical probes and clinical tools for the treatment of cancer, inflammation, and other diseases.[4−8]

The BET (bromodomain and extra terminal) subfamily (BRD2/3/4/T) has been widely addressed, and as a consequence, several potent and selective inhibitors have been developed, some of which are currently undergoing clinical trials for the treatment of NUT midline carcinoma (NMC), solid tumors, leukemia, lymphoma, hematological malignancies, atherosclerosis, and type II diabetes.[7,9,10] In contrast, the specific function and potential pharmacological relevance of other bromodomains, including CREB binding protein (CREBBP), E1A binding protein p300 (EP300), BRD7/9, and bromodomain adjacent to zinc finger domain (BAZ2B), are much less understood, and thus, small-molecule inhibitors will be valuable tools for unraveling their biological roles.

The bromodomains of EP300 and CREBBP, which belong to the same subfamily and share 96% sequence identity,[11] play important roles in DNA replication and repair, cell growth and cell cycle regulation, and genomic stability.[12,13] As an example, EP300 and CREBBP are able to acetylate p53 on its K382 residue through the histone acetyl transferase (HAT) domain upon extracellular stress or DNA damage, and they are also known to specifically bind to acetylated p53 via their bromodomain module.[14] As a consequence, changes in the p53-dependent activation of target genes result in cell cycle arrest, senescence, or apoptosis.[15−17] On one hand, chromosome translocations resulting in gene fusions containing CREBBP or EP300 have been linked to leukemias and lymphomas.[18,19] On the other hand, CREBBP and EP300 are mutated in solid tumors and B-cell lymphoma, suggesting they possess a tumor-suppressing role.[13,20] Thus, because both oncogene or tumor suppressor roles have been reported for CREBBP and EP300,[18,21] the development of chemical probes will be instrumental for the analysis of their biological function(s).

The bromodomains of BRD7 and BRD9 belong to the same subfamily and share 72% sequence identity.[22] Both BRD7 and BRD9 are part of the SWI/SNF (SWItch/Sucrose Non-Fermentable) chromatin remodelling complex, which plays a key role in the regulation of gene expression.[23−25] Recent reports have linked BRD9 to oncology, including non-small cell lung[26] and cervical cancer.[27] Its paralogue, BRD7, is frequently downregulated in cancer[28−30] and is able to regulate the tumor suppressor protein p53.[31−33] The bromodomain of BRPF1b (bromodomain-PHD finger protein 1b) belongs to the same subfamily as BRD7 and BRD9. Despite the function of the BRPF1b bromodomain not being yet fully understood, the availability of BRPF1b ligands might help in the elucidation of its role.[34−36]

Received: November 10, 2015
Published: March 16, 2016

DOI: 10.1021/acs.jmedchem.5b01757
J. Med. Chem. 2016, 59, 3087−3097

BAZ2B is another bromodomain-containing protein whose role in physiology and disease is not clear. Biophysical screening of a library of 1300 fragments resulted in the identification of 10 small molecules that bind in the micromolar range to BAZ2B.[37] Recently, the first submicromolar selective CREBBP,[11,38,39] BAZ2B,[40,41] and BRD7/9[22,42,43] inhibitors have been reported.

Here we present the result of a combined scaffold hopping and docking approach that has permitted the discovery of acetyl indoles as ligands of the bromodomains of CREBBP, BAZ2B, BRPF1b, and/or BRD9, which belong to three different subfamilies that lie outside of the BET bromodomain subfamily. A comparative analysis of four crystal structures of bromodomain/acetyl indole complexes shows the importance of the so-called gatekeeper residue with respect to the binding mode of the ligand.

RESULTS AND DISCUSSION

***In Silico* Screening by Scaffold Hopping and Docking.** In the past few years, our groups have successfully identified several low micromolar to nanomolar kinase[44−47] and bromodomain[39,48,49] inhibitors by high-throughput virtual screening campaigns. In this work, we decided to dock a small subset of compounds containing a moiety identified by scaffold hopping (see Experimental Section). First, the ZINC all-now library was decomposed into approximately 600000 fragments retaining key functional groups. These fragments were queried by the indolizine fragment **A**, which is present in the potent BAZ2B ligand GSK2801 (**1a**)[41] and more recently has been identified in BRD7 and BRD9 ligands.[22] (Capital letters are used to label generic chemical blueprints. **1a−i** correspond to commercially available compounds. **1−50** represent the synthetic intermediates and self-made products.) The acetyl indole **B** was identified as the top-ranking fragment with an activity-oriented fingerprint similarity of 0.975 with respect to **A**. The high degree of similarity is due to almost identical geometry and connecting vectors in fragments **A** and **B** (Figure 1).

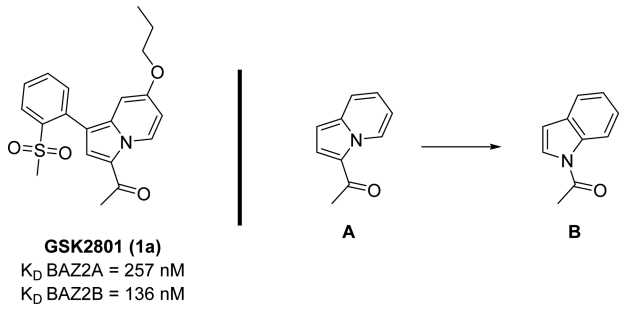

Figure 1. GSK2801 (**1a**), a nanomolar chemical probe for BAZ2A and BAZ2B bromodomains.[22,41] Core fragment hopping by activity-oriented fingerprint using fragment **A** as the query molecule. **A** and **B** respresent generic chemical blueprints.

In a second step, we retrieved ∼200 commercially available compounds containing fragment **B**. As in our previous fragment-based virtual screening approach,[46,48,49] the retrieved compounds were docked into crystal structures of the targets, namely, the bromodomains of CREBBP [Protein Data Bank (PDB) entry 4A9K] and BAZ2B (PDB entry 3Q2F). An in-house-developed program for automatic docking was used.[48,50−52] The docking poses were subsequently rescored by a transferable scoring function (see Experimental Section).[45,50−54] Finally, 14 molecules were selected for experimental validation by means of a competition binding assay.[55,56] At a concentration of 50 μM, seven compounds showed significant competition [i.e., a percentage of residual binding of CREBBP to the acetylated histone peptide of <70% with respect to the DMSO control (Figure 2)], which corresponds to a hit rate of 50% for the *in silico* screening approach based on scaffold hopping and docking. The most active compound, **1b**, exhibits an equilibrium dissociation constant (K_d) of 20 μM for CREBBP. Using the same threshold of 70% as for CREBBP, the hit rate for BAZ2B was 29% (Figure 2). Interestingly, at a concentration of 50 μM, only compound **1g** shows a significantly higher affinity for BAZ2B than for CREBBP.

Binding Mode of Compound 1b: Validation by X-ray Protein Crystallography. The opposite selectivity toward CREBBP and BAZ2B observed for compounds **1b** and **1g** (Figure 2) prompted us to study their binding mode. While we could not determine the structure with compound **1g**, the crystal structure of CREBBP in complex with compound **1b** was determined at 2.0 Å resolution (Figure 3, green, PDB entry 4TS8), which revealed an overall binding mode essentially identical to the docked pose of compound **1b** (Figure 3, blue). The binding of compound **1b** in CREBBP is characterized by a lipophilic sandwich of its bicyclic core between residues Phe1111, Val1174, and Ala1164 on one side and Val1115, Leu1120, and Ile1122 on the other side of the binding pocket. The carbonyl oxygen of the acetyl indole acts as the acetylated lysine mimic and is engaged in hydrogen bonding interactions with the side chains of the conserved Asn1168 (BC loop) and Tyr1125 (ZA loop), where the latter is bridged by a water molecule. Another four water molecules present at the bottom of the pocket are conserved. In addition, there is a water molecule bridging the dihydro-pyrazole ring and the guanidinium group of Arg1173 (Figure 3).

Assessing the Affinity Difference between Indolizine and Indole Ligands. Compound **1a** is reported to be a potent ligand for the BAZ2B bromodomain with a K_d of 136 nM.[41] To study the influence on the binding affinity of the position of the nitrogen atom in our hit compound **1b**, we decided to synthesize the indole analogue of indolizine **1a**. Commercially available 1*H*-indol-5-ol (**1**) was transformed into compound **3** via alkylation of the phenol moiety with 1-iodopropane, followed by introduction of an *N*-benzenesulfonyl group and bromination at C3 in the presence of molecular bromine (Scheme 1). Bromo indole **3** was then coupled to [2-(methylsulfonyl)phenyl]boronic acid, affording compound **4** in moderate yield. Removal of the sulfonyl group under basic conditions preceded the incorporation of the acetyl group to give the indole analogue of compound **1a** (**5**).

Interestingly, a 24-fold reduction in binding affinity toward BAZ2B was observed for acetyl indole **5** with respect to **1a** [IC_{50} values of 8.55 and 0.36 μM, respectively, determined by AlphaScreen (see the Supporting Information)], which indicates that the position of the nitrogen atom in the double-ring system is crucial.

Synthesis. We decided to focus our derivatization campaign on compounds **1b** and **1g** as ligands. Compound **1b** was selected because of its ligand efficiency for CREBBP (0.34 kcal/mol per heavy atom) and the availability of the crystal structure (Figure 3), while compound **1g** was chosen because of its selectivity toward BAZ2B (Figure 2).

DOI: 10.1021/acs.jmedchem.5b01757
J. Med. Chem. 2016, 59, 3087−3097

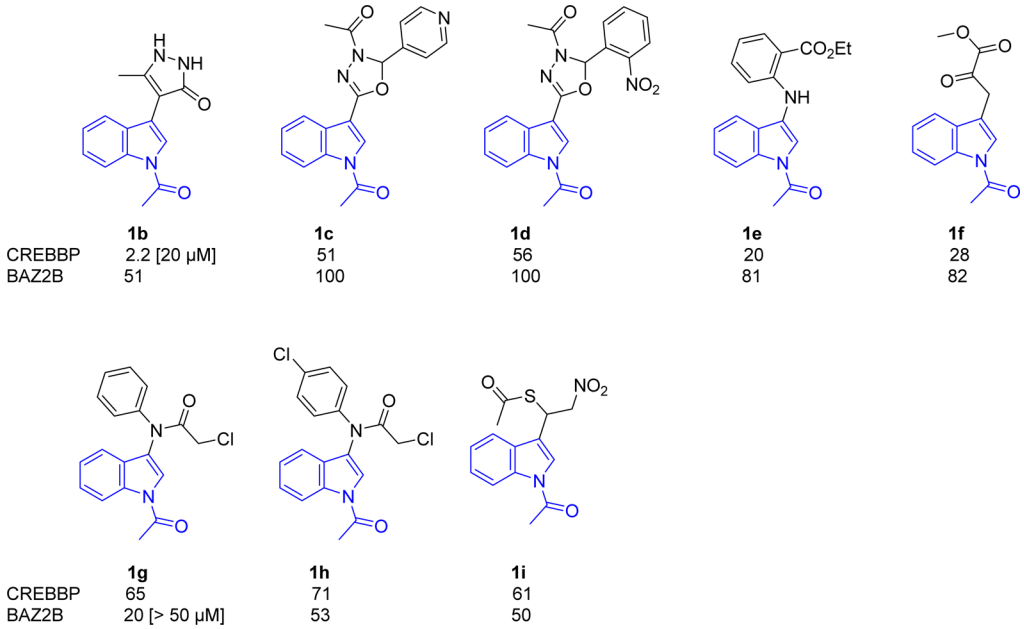

Figure 2. Binding affinity and two-dimensional structures of acetyl indole derivatives **1b–i** identified by core fragment hopping and docking. The values are a percentage of residual binding of the CREBBP or BAZ2B bromodomain to an acetylated histone peptide at a compound concentration of 50 μM with respect to the DMSO control. Thus, lower percentages indicate higher affinities of the compound. Values in brackets are equilibrium dissociation constants (K_d) determined by two independent dose–response measurements of 11 doses each. Compounds **1c**, **1d**, and **1i** were measured as a racemic mixture. All values were determined by the BROMOscan competition binding assay.[55,56]

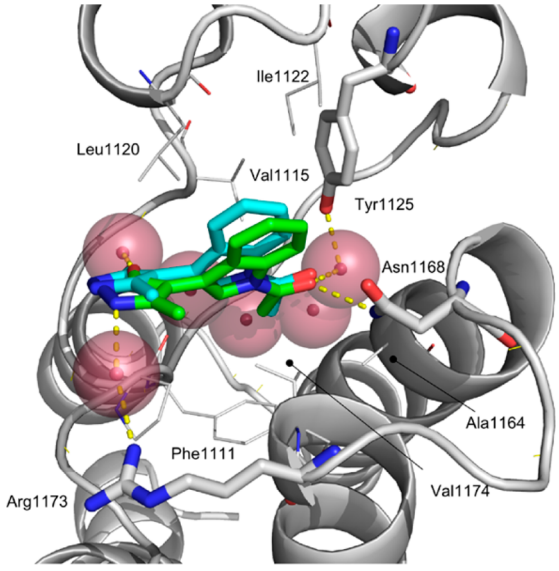

Figure 3. Crystal structure (green) and docked pose (blue) of the CREBBP bromodomain (gray) in complex with compound **1b** (PDB entry 4TS8). The conserved Tyr1125 and Asn1168 residues, together with Arg1173 (a characteristic residue for the CREBBP bromodomain),[11,38,39,49] are shown as sticks. Hydrogen bonds are shown as yellow dashed lines, and the crystallographic water molecules are represented by red spheres.

Synthesis of Compound ***1b*** *and Its Derivatives.* The synthesis of CREBBP hit **1b** is shown in Scheme 2. The carboxylic acid of commercially available 2-(1*H*-indol-3-yl)-acetic acid (**6**) was transformed into the corresponding methyl ester. Acetylation of the N atom afforded indole **7**. Deprotonation of **7** in the presence of *in situ*-generated lithium diisopropylamide (LDA) followed by reaction with acetic anhydride or 4-methoxyphenylacetic anhydride delivered

Scheme 1[a]

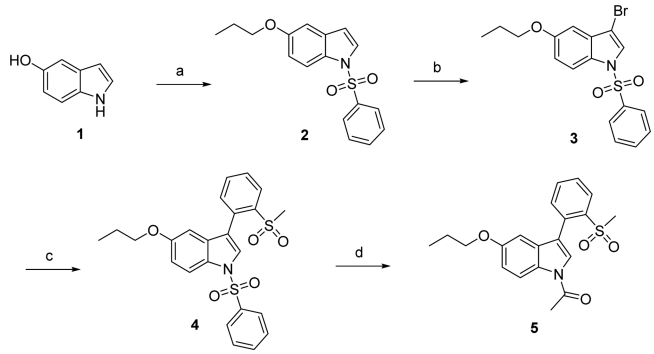

[a]Reagents and reaction conditions: (a) (i) 1-iodopropane, K_2CO_3, acetone, reflux, 72 h, 84%; (ii) benzenesulfonyl chloride, TBAB, 50% NaOH, H_2O, toluene, 0–25 °C, 69 h, 97%; (b) Br_2, DMF, 25 °C, 7 h, 47%; (c) [2-(methylsulfonyl)phenyl]boronic acid, 1 M $NaHCO_3$, $Pd(PPh_3)_4$, DME, 25–85 °C, 15 min, 33%; (d) (i) 2 M NaOH, MeOH, 85 °C, 5 h, 69%; (ii) AcCl, NaOH, TBAHS, DCM, 25 °C, 13 h, 63%. Abbreviations: TBAB, tetra-*n*-butylammonium bromide; DMF, dimethylformamide; DME, 1,2-dimethoxyethane; TBAHS, tetrabutylammonium hydrogen sulfate.

intermediate **8** or **9**, respectively. Cyclization in the presence of hydrazine hydrate afforded hit compound **1b** and derivative **10** in moderate yields (Scheme 2).

Hit compound **1b** was then reacted with a variety of acid and sulfonyl chlorides, affording disubstituted (**11–18**) as well as monosubstituted dihydro-pyrazole derivatives (**19–22**) as indicated in Scheme 3. Two more derivatives were prepared: upon condensation of 1,2-dibromoethane with compound **1b** in the presence of K_2CO_3, derivative **23** was obtained. The reaction of **1b** with *p*-methoxybenzyl bromide in the presence of NaH afforded O-alkylated product **24** (Scheme 3).

DOI: 10.1021/acs.jmedchem.5b01757
J. Med. Chem. 2016, 59, 3087–3097

Scheme 2[a]

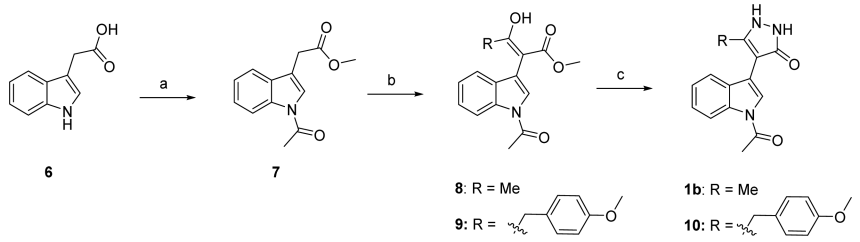

[a]Reagents and reaction conditions: (a) (i) MeOH, H_2SO_4, 25 °C, 1 h, 94%; (ii) Ac_2O, DMAP, Et_3N, THF, 25 °C, 17 h, 90%; (b) $(^iPr)_2NH$, *n*-BuLi, THF, −75 °C, 1 h, then, acetic anhydride or 4-methoxyphenylacetic anhydride, −78 °C, 2−4 h; (c) hydrazine hydrate, camphoric acid, EtOH, toluene, 93 °C, 30 min−1 h, 29−51% over two steps. Abbreviation: DMAP, 4-dimethylaminopyridine.

Scheme 3[a]

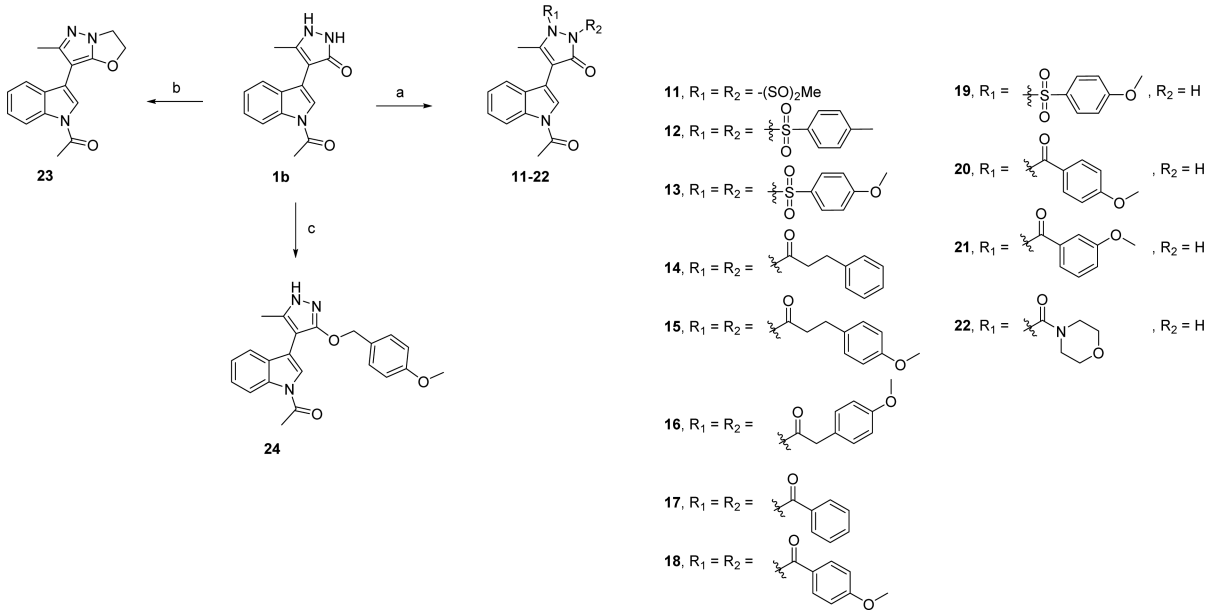

[a]Reagents and reaction conditions: (a) R-Cl, Et_3N, DCM, 0−25 °C, 5−12 h, 24−89%; (b) 1,2-dibromoethane, K_2CO_3, DMF, 80 °C, 7 h, 41%; (c) PMB-Br, NaH, TBAI, DMF, 0−25 °C, 1.5 h, 23%. Abbreviations: PMB, 4-methoxybenzyl ether; TBAI, tetrabutylammonium iodide.

Finally, we decided to incorporate the propoxy group at position 5 of the indole, for which a similar protocol was applied to 1*H*-indol-5-ol (**1**), delivering the final products **27** and **28** (Scheme 4).

*Synthesis of Derivatives of Compound **1g**.* The common intermediate for the synthesis of derivatives of ligand **1g** was obtained from the commercially available non-natural amino acid **29** in four steps with a 20% overall yield (Scheme 5). Condensation of intermediate **32** with diverse commercially available anilines afforded acetyl indole intermediates **33**−**38**, which were then acylated in the presence of diverse acid chlorides, affording compounds **39**−**46**. Four additional derivatives were prepared by cleaving the methoxy substituent in the presence of BBr_3 to produce phenol derivatives **47**−**50** (Scheme 5).

Biophysical Characterization. *Compound **1b** and Its Derivatives.* Compound **1b** was screened against a panel of 10 different bromodomains using a thermal shift assay (Table 1 and Table S2 in the Supporting Information). This initial screening revealed BRD9 bromodomain as a potential off target for compound **1b** with a shift in the melting temperature of 1.3 °C, which translated into a K_D of 5.3 μM, as measured by a competition binding assay,[55,56] and a ligand efficiency (LE) value of 0.38 kcal/mol per heavy atom. This result is in line with the recent work of Brennan and co-workers, who

Scheme 4[a]

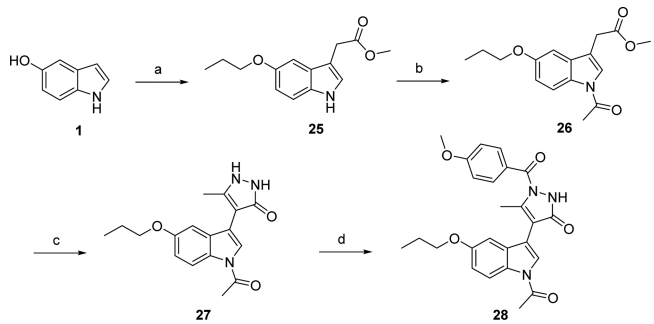

[a]Reagents and reaction conditions: (a) (i) 1-iodopropane, K_2CO_3, acetone, reflux, 72 h, 84%; (ii) $(COCl)_2$, Et_2O, 0 °C, then NaOMe in MeOH, −78 °C, 3 h; (iii) Pd/C, NaH_2PO_2, dioxane, H_2O, 25 °C, 12 h, 88% over two steps; (b) Ac_2O, DMAP, Et_3N, THF, 25 °C, 12 h, 42%; (c) (i) $(^iPr)_2NH$, *n*-BuLi, THF, −78 °C, 1 h, then, acetic anhydride, −78 °C, 4 h; (ii) hydrazine hydrate, camphoric acid, EtOH, toluene, reflux, 4 h, 18%; (d) 4-methoxybenzoyl chloride, Et_3N, DCM, 0−25 °C, 12 h, 19%.

DOI: 10.1021/acs.jmedchem.5b01757
J. Med. Chem. 2016, 59, 3087−3097

Scheme 5[a]

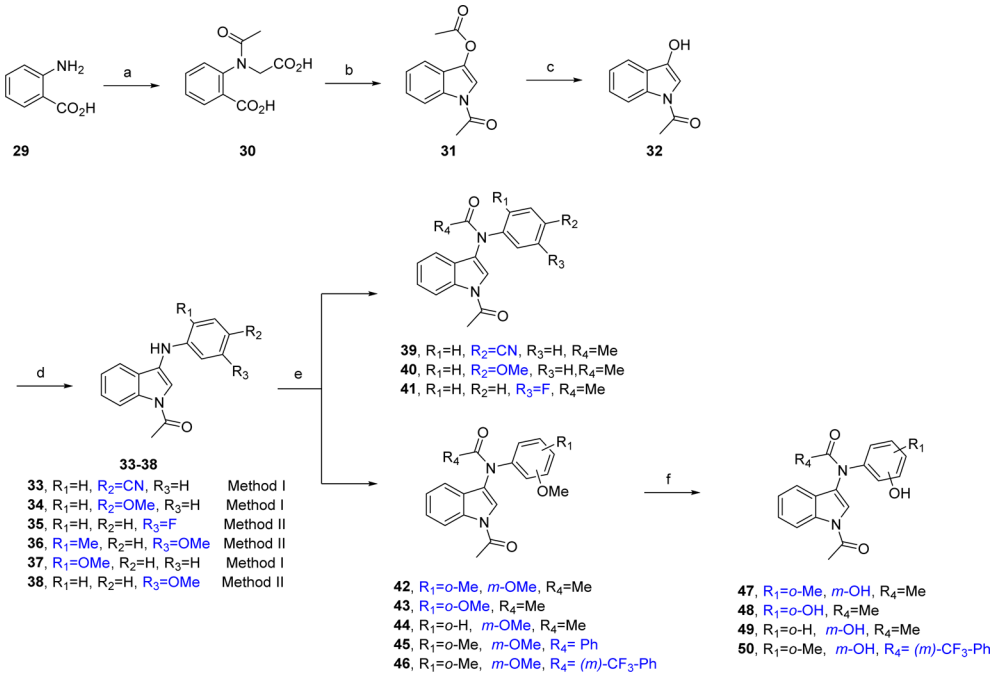

[a]Reagents and reaction conditions: (a) (i) chloroacetic acid, K_2CO_3, H_2O, 90 °C, 16 h; (ii) Ac_2O, 25 °C, 30 min, then 37% HCl for 12 h, 33% over two steps; (b) Ac_2O, Et_3N, reflux, 30 min, 89%; (c) Na_2SO_3, reflux, 2 h, 83%; (d) method I: aniline, AcOH, reflux, 1−8 h, 26−56%; method II: aniline, pTSA, toluene, reflux, 2.5−4 h, 50−52%; (e) for MeCOCl, toluene, reflux, 12 h, 36−78%; if R_4 = aryl, R_4COCl, toluene, Et_3N, DMAP, 100 °C, 1 h, 13−21%; (f) BBr_3, DCM, 0−25 °C, 1−12 h, 47−84%. Abbreviation: pTSA, *p*-toluenesulfonic acid.

developed BRD7 and BRD9 nanomolar potent indolizine derivatives starting from the BAZ2B inhibitor **1a**.[22] Importantly, no activity of compound **1b** was observed for the tested BET family members, BRD4(1) and BRD4(2) (see the Supporting Information).

Because of the involvement of the acetyl group of compound **1b** in hydrogen bonds with the conserved Asn1168 and Tyr1125 residues of CREBBP (Figure 3), we decided to maintain this moiety and introduce the main modifications at the dihydro-pyrazole ring to gain affinity for CREBBP.

On the outset, we decided to modulate the interactions of the solvent-exposed NH groups of the dihydro-pyrazole ring. To do so, mono- and disubstituted amide and sulfonamides that could establish new interactions with the surrounding amino acid residues, including the characteristic Leu1109 and Arg1173 residues in the CREBBP bromodomain and His42 and Phe44 in BRD9, were incorporated [compounds **11**−**22** (Table 1)]. The presence of methyl-substituted sulfonamides in compound **11** provided a K_D of 6.6 μM in CREBBP, which is a 3-fold binding affinity improvement with respect to the hit compound **1b** and corresponds to a LE value of 0.26 kcal/mol per heavy atom.

In an effort to form π-stacking interactions with Arg1173 in CREBBP,[11,38] and residues Phe43 and Phe44 in BRD9, aromatic substituents, some of them electron-rich, were incorporated (compounds **14**−**18**, **20**, and **21**). Compound **14** yielded the most active ligand toward BRD9 with a K_D of 3.5 μM. Interestingly, the presence of a *p*-methoxybenzoate substituent in compound **20** resulted in a 2-fold improvement of binding affinity with a thermal shift of 3.3 °C in CREBBP and a K_D of 9.3 μM. At the same time, compound **20** retained the activity toward BRD9 with a thermal shift of 5.1 °C and a K_D of 6.3 μM. The presence of a morpholine ring at the same position (derivative **22**) could only slightly improve the binding affinity for CREBBP with a K_D of 12 μM.

A dihydro-pyrazolo-oxazole ring was installed (compound **23**), which allowed us to revert the hydrogen bond donor capacity of the dihydro-pyrazole ring bearing two NH groups to a hydrogen bond acceptor-fused ring. Remarkably, compound **23** showed a K_D of 6.2 μM in CREBBP and retained the LE of the initial hit (0.34 kcal/mol per heavy atom), which makes it an attractive lead for further optimization. On the other hand, compound **24** exhibited a drop in the thermal shift, probably due to steric clashes of the *p*-methoxybenzyl group.

We then aimed to establish new interactions with the hydrophobic residues located on top of the binding site, Ile1122 and Leu1120 in CREBBP and Ala54 and Ile53 in BRD9, by substitution of the indole moiety at position 5 with a propoxy group (Table 1, compounds **27** and **28**), a modification that has proven to be successful in our previous work and in compound **1a**.[39,41] Unfortunately, the presence of the propoxy substituent retained an activity of ∼10 μM.

Importantly, with the exception of compounds **14** and **23**, all derivatives displayed ΔT_m values of <0.6 °C for BRD4(1), one of the most promiscuous bromodomains.[11,38,57]

*Compound **1g** and Its Derivatives.* Intrigued by the selectivity difference observed in the hit compound **1g** toward BAZ2B (Figure 2), we decided to examine its binding mode more closely. As we could not obtain crystals of the complex of compound **1g** with BAZ2B, several analogues were synthesized (Table 2), aiming not only to obtain a crystal structure of the complex but also to improve the binding affinity for BAZ2B. The chloroacetamide moiety was replaced by metabolically more stable amides in all derivatives to avoid covalent binding to the protein.

DOI: 10.1021/acs.jmedchem.5b01757
J. Med. Chem. 2016, 59, 3087−3097

Table 1. Evaluation of Compounds 10−24, 27, and 28 Derived from 1b

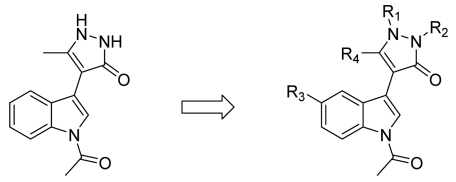

1b **10-24, 27, 28**

Cmpd	R_1	R_2	R_3	R_4	ΔT_m (°C)[a] CBP	EP300	BRD9	BRD4(1)	K_d (μM) [b] CBP	BRD9
1b	H	H	H	Me	0.3 (0.1)	0.4 (0.1)	1.3 (0.1)	−0.1 (0.1)	20.0	5.3
10	H	H	H		−0.1 (0.2)	−0.6 (0.2)	−0.8 (0.7)	−0.9 (0.4)	-	-
11	$-SO_2Me$	$-SO_2Me$	H	Me	2.2 (0.2)	2.7 (0.1)	1.0 (0.8)	0.6 (0.5)	6.6	
12			H	Me	1.4 (0.5)	−0.7 (0.7)	−0.5 (0.3)	−0.4 (0.5)	-	-
13			H	Me	1.5 (0.4)	0.0 (0.2)	−1.0 (0.7)	0.0 (0.3)	-	-
14			H	Me	2.8 (0.7)	1.0 (0.3)	2.8 (1.6)	1.2 (0.5)	17	3.5
15	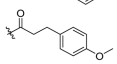	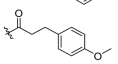	H	Me	−0.6 (0.1)	−0.3 (0.1)	0.2 (0.2)	−0.3 (0.1)	-	-
16	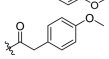	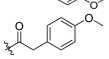	H	Me	−0.9 (0.1)	−0.3 (0.1)	0.3 (0.3)	0.1 (0.2)	-	-
17			H	Me	−0.2 (0.7)	0.0 (0.2)	−0.5 (0.7)	−0.9 (0.3)	-	-
18			H	Me	−0.5 (0.6)	0.0 (0.1)	-	−2.3 (0.5)	-	-
19		H	H	Me	−0.4 (0.2)	−0.4 (0.2)	0.8 (0.5)	−1.6 (0.3)	-	-
20		H	H	Me	3.3 (0.7)	5.3 (0.9)	5.1 (1.5)	0.2 (0.7)	9.3	6.3
21		H	H	Me	−0.6 (0.8)	1.0 (0.7)	-	−0.5 (0.4)	-	-
22		H	H	Me	1.4 (0.3)	2.5 (0.1)	−0.6 (0.7)	0.6 (0.3)	12	-
23		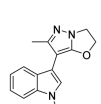			3.5 (0.2)	2.2 (0.4)	1.8 (1.0)	1.5 (0.4)	6.2	-
24		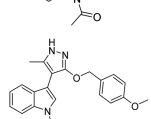			0.1 (0.1)	0.0 (0.1)	0.3 (0.3)	−0.3 (0.2)	-	-
27	H	H	OPr	Me	0.4 (0.2)	0.4 (0.1)	0.7 (0.1)	0.5 (0.3)	-	-
28		H	OPr	Me	-	2.7 (1.0)	-	−2.7 (1.2)	9.8	>50

[a]Median value of the shift in the melting temperature. The total number of measurements for each compound and bromodomain was between 7 and 24. Ligand and protein concentrations were 100 and 2 μM, respectively. Standard errors of the mean are given in parentheses. The similar thermal shift values measured with the CREBBP bromodomain and its paralogue, EP300, are consistent with the fact that identical residues are present in the acetyllysine binding site of both proteins. [b]K_d values were determined by a competition binding assay[55,56] in duplicate. Dose−response data and fitting curves can be found in the Supporting Information. Dashes indicate data not acquired.

The affinity of the synthesized derivatives **39**−**50** for BAZ2B was assessed by an AlphaScreen competition binding assay at a compound concentration of 50 μM. Compound **47**, bearing an *o*-methyl and *m*-hydroxy substituent at the benzene ring, showed a 54% reduction in the magnitude of the signal relative to the negative control DMSO in the AlphaScreen binding assay, which translated into a K_D of 23 μM and a LE value of 0.27 kcal/mol per heavy atom. Upon substitution of the acetyl substituent at R_4 with a *m*-CF_3-benzoate group, an IC_{50} value of 27 μM in the AlphaScreen assay and a K_D of 39 μM (BROMOscan) were measured for compound **50**.

Crystal structures of the most potent derivatives, **47** and **50**, in complex with BAZ2B were determined at 1.71 and 1.78 Å resolution, respectively. Compounds **47** and **50** (Figure 4A,B) have essentially identical binding modes in BAZ2B. As in the binding mode of hit **1b** in CREBBP (Figure 3), the *N*-acetyl substituent of the indole moiety of compounds **47** and **50** is engaged in hydrogen bonds with the side chain of the conserved Tyr1901 and Asn1944, where the hydrogen bond with Tyr1901 is bridged by a water molecule. An additional hydrogen bond is formed between the carbonyl group of the acetamide and the backbone NH of Asn1894 in the ZA loop.

DOI: 10.1021/acs.jmedchem.5b01757
J. Med. Chem. 2016, 59, 3087−3097

Table 2. Evaluation of Compounds 39−50 Derived from 1g

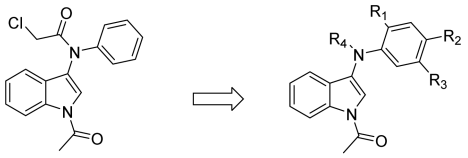

1g 39-50

Cmpd	R_1	R_2	R_3	R_4	K_d (μM)[a] BAZ2B	%Ctrl BAZ2B[b]
1g	H	H	H		>50	91.3
39	H	CN	H	Acetyl	-	99.7
40	H	OMe	H	Acetyl	-	73.5
41	H	H	F	Acetyl	-	91.4
42	Me	H	OMe	Acetyl	-	71.9
43	OMe	H	H	Acetyl	-	86.3
44	H	H	OMe	Acetyl	-	89.6
45	Me	H	OMe		-	77.5
46	Me	H	OMe		140	87.3
47	Me	H	OH	Acetyl	23	54.2
48	OH	H	H	Acetyl	-	88.4
49	H	H	OH	Acetyl	-	86.3
50	Me	H	OH		39	29.8 (IC_{50} = 27 μM)

[a] K_d values were determined by a competition binding assay[55,56] in duplicate. Dose−response data and fitting curves are in the Supporting Information. [b] Percentage of the measured signal (i.e., percentage binding of acetylated histone peptide to BAZ2B) relative to the negative control at a compound concentration of 50 μM. Lower values indicate stronger binding of the compounds. The AlphaScreen competition binding assay was performed at Reaction Biology. Dashes indicate data not acquired.

The *o*-methyl substituent of the phenol ring provides sufficient steric hindrance to block the conformation of compounds **47** and **50** with their hydroxyphenyl ring pointing toward Trp1887, which is the first residue of the WPF segment in BAZ2B. The additional trifluoromethylbenzoate of compound **50** points toward the solvent (Figure 4B), which explains the similar affinity for BAZ2B of compounds **47** and **50** (Table 2).

As mentioned above, the bromodomains of BRD9 and BRPF1/3 belong to the same subfamily. Aiming to obtain further structural information, we took advantage of the availability in our laboratory of crystals of the apo state of the bromodomain of BRPF1b that were soaked in a solution of compound **1b**. In this way, we determined the crystal structure of the complex of compound **1b** with BRPF1b at a resolution of 1.35 Å (PDB entry 5D7X). Interestingly, the size of the so-called gatekeeper residue, small (Val1174 in CREBBP) and large (Phe714 in BRPF1b), has a noticeable influence on the orientation of the indole moiety (Figure 4C). Furthermore, the presence of the bulkier Phe714 residue in the BRPF1b bromodomain has a strong effect on the orientation of the dihydro-pyrazole ring that is rotated by ∼180° in BRPF1b with respect to the complex with CREBBP. Despite these structural differences, compound **1b** has a very similar affinity for the bromodomains of CREBBP and BRPF1b with K_d values of 20 and 15 μM, respectively (see the Supporting Information).

The superposition of the X-ray structures of compound **1b** in CREBBP and BRPF1b with compound **47** in BAZ2B provides additional evidence of the influence of the gatekeeper residue for ligand binding (Figure 4, D). Interestingly, the 6-membered ring of the indole moiety of compound **47** is located between the indole of compound **1b** in BRPF1b and CREBBP because the gatekeeper residue in BAZ2B (Ile1950) is smaller than the one in BRPF1b (Phe714) and larger than that in CREBBP (Val1174). It is important to note that in these three crystal structures (viz., the **1b**/CREBBP, **1b**/BRPF1b, and **47**/BAZ2B complexes) there are no crystal contacts in the binding site that could affect the orientation of the acetyl indole scaffold. Moreover, the structure of BAZ2B is essentially identical in the complex with compounds **47** and **50**, and the same is observed for the structures of CREBBP in the complex with compound **1b** and a previously reported acetyl benzene ligand (PDB entry 4TQN) that differ only by a small rigid-body displacement of the ZA loop. It is also interesting to compare with the orientation of the scaffold of the BAZ2B inhibitor **1a**. The same progressive tilting of the indole emerges from the structural superposition of the complex of BAZ2B and the nanomolar inhibitor **1a** (PDB entry 4RVR)[41] with the crystal structures of the hit compound **1b** in CREBBP and BRPF1b (Figure 4E). Overall, these structural data suggest that acetyl indole mimics the acetylated lysine side chain in its rather unselective binding to bromodomains. In addition, the precise orientation of the indole double-ring system and the substituent at its position 3 are influenced by the size of the gatekeeper residue that is different in different bromodomains.

CONCLUSIONS

We have discovered *in silico* a series of small-molecule antagonists of the bromodomains of CREBBP and BAZ2B by docking ∼200 compounds containing an acetyl indole moiety, which we had identified by scaffold hopping from a potent BAZ2B ligand. Considering that only 14 compounds were tested *in vitro* (by a competition binding assay), the hit rates of the *in silico* screening based on scaffold hopping and docking are 50 and 29% for CREBBP and BAZ2B, respectively. One of the original hits (compound **1b**) has equilibrium dissociation constants of 20, 15, and 5.3 μM for CREBBP, BRPF1b, and BRD9, respectively. With a relatively small derivatization campaign (i.e., ∼30 derivatives), we were able to improve the affinity for CREBBP and BAZ2B and maintain the ligand efficiency (0.34 kcal/mol per heavy atom for both hit **1b** and derivative **23** in CREBBP) or even slightly improve it (from <0.26 kcal/mol for hit **1g** to 0.27 kcal/mol per heavy atom for compound **47** in BAZ2B). The crystal structures of three acetyl indole derivatives in complex with three different bromodomains confirm the binding mode predicted by docking with the acetyl oxygen of the ligand involved as a hydrogen bond acceptor in two hydrogen bonds with the conserved Asn side chain in the BC loop and a structural water that acts as bridge to the conserved Tyr of the ZA loop. Moreover, the X-ray structures show that the size of the gatekeeper side chain (Val1174, Ile1950, and Phe714 in the bromodomains of CREBBP, BAZ2B, and BRPF1b, respectively) influences the orientation of the indole moiety. This structural information can be used to further improve the selectivity for a single bromodomain target or a small subset of bromodomains sharing the same gatekeeper residue.

DOI: 10.1021/acs.jmedchem.5b01757
J. Med. Chem. 2016, 59, 3087−3097

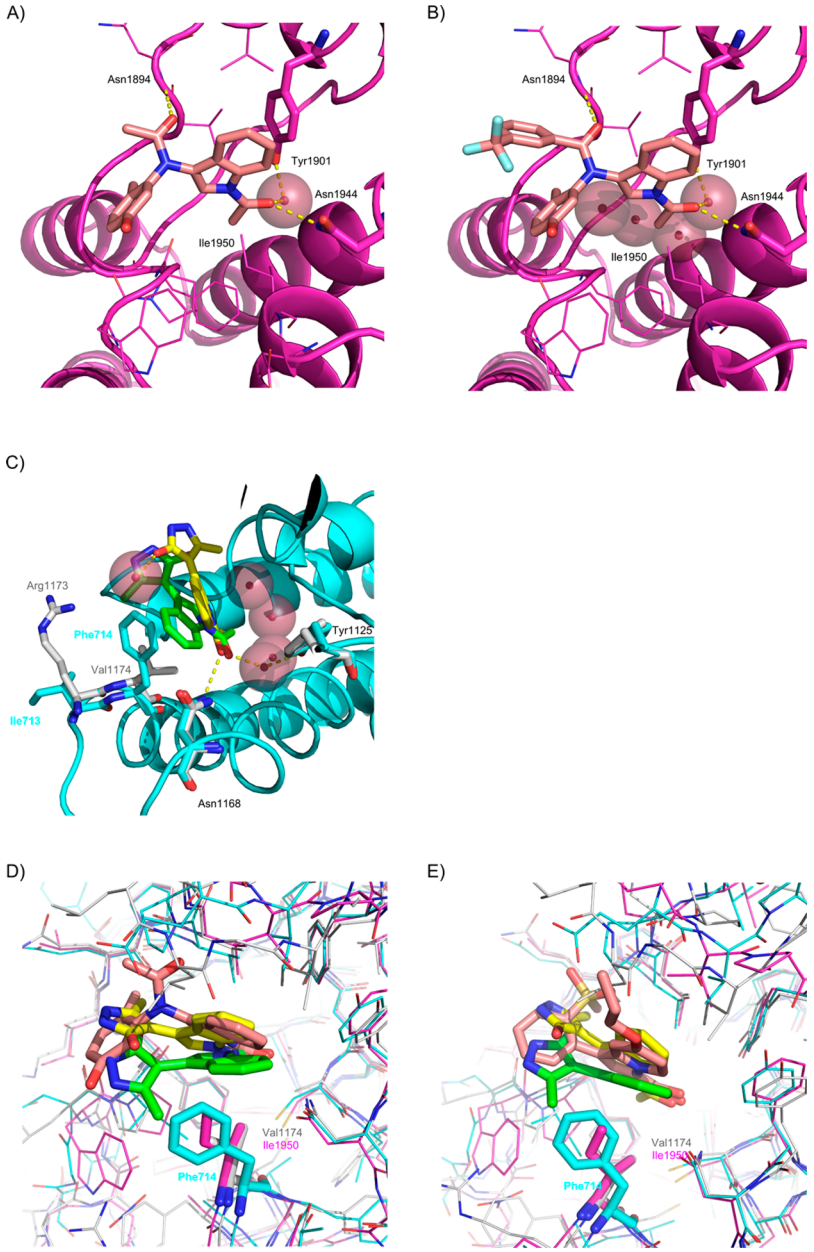

Figure 4. Crystal structures show the influence of the gatekeeper on the binding mode of the ligand. (A) Crystal structures of the BAZ2B bromodomain in complex with compound **47** (PDB entry 5E73). (B) Same as panel A for the complex with compound **50** (PDB entry 5E74). (C) Crystal structure of the complex of compound **1b** (yellow) and the BRPF1b bromodomain (blue) (PDB entry 5D7X) structurally superposed to the crystal structure with CREBBP (compound **1b** colored green and CREBBP side chains colored gray). (D) Superposition of the crystal structures of compound **47** (brown) in BAZ2B (pink) and compound **1b** (green and yellow), in CREBBP (gray) and BRPF1b (blue). The side chain of the gatekeeper is shown as cylinders with labels for the residue number. (E) Same as panel D for the BAZ2B inhibitor **1a** (brown) (PDB entry 4RVR). In all panels, hydrogen bonds are shown as yellow dashed lines and the crystallographic water molecules are represented by spheres.

EXPERIMENTAL SECTION

Scaffold Hopping. We have used an activity-oriented fingerprint that consists of (1) chemical features such as hybridization states and different types of hydrogen bonding donors and acceptors, (2) the two-dimensional topology index as a way to reflect the spatial arrangement of such features, and (3) three-dimensional shape descriptors (Figure S1 of the Supporting Information). A similarity coefficient is computed between two fingerprints ranging from 0 to 1, with 1 being the highest degree of similarity, where the two molecules are not necessarily identical. As such, scaffold hopping resembles pharmacophore mapping but distinguishes itself by using a molecular fingerprint.

Docking and Scoring. The genetic algorithm-based program for flexible ligand docking has been described in previous applications.[50−52] Approximately 20 docking poses for each compound were first minimized by the CHARMM program[58] and subsequently ranked by a transferable scoring function.[45,50−54]

Assays. Thermal shift measurements were taken as previously described.[39,49] Thermal shift assays detect, by a fluorescent dye, the increase in the thermal stability of a protein in the presence of a ligand.[59] BROMOscan technology is a competition experiment that uses an immobilized ligand and a DNA-tagged bromodomain protein.[55,56] Compounds that bind to the bromodomain of interest will prevent binding of the bromodomain to the immobilized ligand. The amount of bromodomain captured on the solid support is then quantified by qPCR, and dissociation constants are calculated.

DOI: 10.1021/acs.jmedchem.5b01757
J. Med. Chem. 2016, 59, 3087−3097

AlphaScreen assays consist of a donor bead that is able to transfer singlet oxygen to an acceptor bead that is in the proximity, and as a result, the acceptor bead emits a luminescent/fluorescent signal. In the presence of a bromodomain ligand, the donor/acceptor complex is disrupted, leading to a loss of singlet oxygen transfer and loss of the fluorescent signal. Further details about the assays can be found in the Supporting Information.

X-ray Crystallography. The His-tagged human bromodomains of CREBBP (residues 1081−1097), BRPF1b (residues 626−740), and BAZ2B (residues 1858−1972) were expressed in *Escherichia coli*. The purification procedures are reported in the Supporting Information. The inhibitors were soaked into apo crystals of the bromodomains of BRPF1b and BAZ2B, while the structure of the complex of compound **1b** and CREBBP was obtained by cocrystallization as described in the Supporting Information. Data collection and refinement statistics are listed in Table S1.

■ ASSOCIATED CONTENT

Supporting Information

The Supporting Information is available free of charge on the ACS Publications website at DOI: 10.1021/acs.jmedchem.5b01757.

General procedures for scaffold hopping, synthesis and characterization, biophysical and biological evaluation of final compounds, and X-ray crystal structure refinement data (PDF)
(CSV)

Accession Codes

The PDB entries for CREBBP and BRPF1b in complex with the hit compound **1b** are 4TS8 and 5D7X, respectively. Coordinates and structure factors for the BAZ2B bromodomain in complex with compounds **47** and **50** have been deposited in the PDB as entries 5E73 and 5E74, respectively.

■ AUTHOR INFORMATION

Corresponding Authors

*E-mail: caflisch@bioc.uzh.ch. Phone: +41 44 635 55 21.
*E-mail: cristina.nevado@chem.uzh.ch. Phone: +41 44 635 39 45.

Notes

The authors declare no competing financial interest.

■ ACKNOWLEDGMENTS

We thank Dr. Emilie Frugier and Dr. Dimitrios Spiliotopous for interesting discussions and help with the thermal shift assay. We thank Lisa Caflisch, Ursina Suter, and Cecilia Ferdenzi for protein purification and Dr. Alvaro Salvador and Anna Coppola for their efforts towards the synthesis of the hit compound **1b**. Nicholas Deerain is acknowledged for performing part of the thermal shift assays. We are grateful to the staff at PXI and PXIII beamlines, Swiss Light Source, Paul Scherrer Institute (Villigen, Switzerland), and at XDR1 beamline, ELETTRA Synchrotron Light Source (Trieste, Italy), for on-site assistance. This work was supported by the Swiss Cancer Society (Krebsliga, KFS-3098) and the Swiss National Science Foundation (315230_149897). We thank the Structural Genomics Consortium at University of Oxford for providing the plasmids of all the bromodomains but EP300 (provided by AddGene).

■ ABBREVIATIONS USED

BAZ2B, bromodomain adjacent to zinc finger domain 2B; BET, bromodomain and extra terminal domain; BRD2, -3, -4, -7, and -9, bromodomain containing 2, 3, 4, 7, and 9, respectively; BRD4(1), first/second bromodomain of BRD4; BRPF1b, bromodomain and PHD finger containing 1; CBP, CREB binding protein; CREBBP, CREB binding protein; DMAP, 4-dimethylaminopyridine; DME, 1,2-dimethoxyethane; DMF, dimethylformamide; DMSO, dimethyl sulfoxide; EP300, E1A binding protein p300; HAT, histone acetyltransferase; LE, ligand efficiency; NMC, NUT midline carcinoma; NUT, nuclear protein in testis; PHD, plant homeodomain; PMB, 4-methoxybenzyl ether; SWI/SNF, switch/sucrose nonfermentable; TBAB, tetra-*n*-butylammonium bromide; TBAHS, tetrabutylammonium hydrogen sulfate; TBAI, tetrabutylammonium iodide

■ REFERENCES

(1) Holliday, R. The inheritance of epigenetic defects. *Science* **1987**, *238*, 163−170.
(2) Kouzarides, T. Chromatin modifications and their function. *Cell* **2007**, *128*, 693−705.
(3) Flynn, E. M.; Huang, O. W.; Poy, F.; Oppikofer, M.; Bellon, S. F.; Tang, Y.; Cochran, A. G. A subset of human bromodomains recognizes butyryllysine and crotonyllysine histone peptide modifications. *Structure* **2015**, *23*, 1801−1814.
(4) Prinjha, R. K.; Witherington, J.; Lee, K. Place your BETs: the therapeutic potential of bromodomains. *Trends Pharmacol. Sci.* **2012**, *33*, 146−153.
(5) Müller, S.; Filippakopoulos, P.; Knapp, S. Bromodomains as therapeutic targets. *Expert Rev. Mol. Med.* **2011**, *13*, 1−21.
(6) Hewings, D. S.; Rooney, T. P. C.; Jennings, L. E.; Hay, D. A.; Schofield, C. J.; Brennan, P. E.; Knapp, S.; Conway, S. J. Progress in the development and application of small molecule inhibitors of bromodomain-acetyl-lysine interactions. *J. Med. Chem.* **2012**, *55*, 9393−9413.
(7) Filippakopoulos, P.; Knapp, S. Targeting bromodomains: epigenetic readers of lysine acetylation. *Nat. Rev. Drug Discovery* **2014**, *13*, 337−356.
(8) Brand, M.; Measures, A. M.; Wilson, B. G.; Cortopassi, W. A.; Alexander, R.; Höss, M.; Hewings, D. S.; Rooney, T. P. C.; Paton, R. S.; Conway, S. J. Small molecule inhibitors of bromodomain−acetyl-lysine interactions. *ACS Chem. Biol.* **2015**, *10*, 22−39.
(9) www.clinicaltrials.gov (accessed October 18, 2015).
(10) Jennings, L. E.; Measures, A. R.; Wilson, B. G.; Conway, S. J. Phenotypic screening and fragment-based approaches to the discovery of small-molecule bromodomain ligands. *Future Med. Chem.* **2014**, *6*, 179−204.
(11) Hay, D. A.; Fedorov, O.; Martin, S.; Singleton, D. C.; Tallant, C.; Wells, C.; Picaud, S.; Philpott, M.; Monteiro, O. P.; Rogers, C. M.; Conway, S. J.; Rooney, T. P. C.; Tumber, A.; Yapp, C.; Filippakopoulos, P.; Bunnage, M. E.; Müller, S.; Knapp, S.; Schofield, C. J.; Brennan, P. E. Discovery and optimization of small-molecule ligands for the CBP/p300 bromodomains. *J. Am. Chem. Soc.* **2014**, *136*, 9308−9319.
(12) Ait-Si-Ali, S.; Polesskaya, A.; Filleur, S.; Ferreira, R.; Duquet, A.; Robin, P.; Vervish, A.; Trouche, D.; Cabon, F.; Harel-Bellan, A. CBP/p300 histone acetyl-transferase activity is important for the G1/S transition. *Oncogene* **2000**, *19*, 2430−2437.
(13) Iyer, N. G.; Xian, J.; Chin, S. F.; Bannister, A. J.; Daigo, Y.; Aparicio, S.; Kouzarides, T.; Caldas, C. p300 is required for orderly G1/S transition in human cancer cells. *Oncogene* **2007**, *26*, 21−29.
(14) Mujtaba, S.; He, Y.; Zeng, L.; Yan, S.; Plotnikova, O.; Sachchidanand; Sanchez, R.; Zeleznik-Le, N. J.; Ronai, Z.; Zhou, M. M. Structural mechanism of the bromodomain of the coactivator CBP in p53 transcriptional activation. *Mol. Cell* **2004**, *13*, 251−263.
(15) Prives, C.; Hall, P. A. The p53 pathway. *J. Pathol.* **1999**, *187*, 112−126.

DOI: 10.1021/acs.jmedchem.5b01757
J. Med. Chem. 2016, 59, 3087−3097

(16) Coutts, A. S.; La Thangue, N. B. The p53 response: Emerging levels of co-factor complexity. *Biochem. Biophys. Res. Commun.* **2005**, *331*, 778−785.
(17) Alarcon-Vargas, D.; Ronai, Z. p53-Mdm2 - the affair that never ends. *Carcinogenesis* **2002**, *23*, 541−547.
(18) Wang, F.; Marshall, C. B.; Ikura, M. Transcriptional/epigenetic regulator CBP/p300 in tumorigenesis: structural and functional versatility in target recognition. *Cell. Mol. Life Sci.* **2013**, *70*, 3989−4008.
(19) Lavau, C.; Du, C. C.; Thirman, M.; Zeleznik-Le, N. Chromatin-related properties of CBP fused to MLL generate a myelodysplastic-like syndrome that evolves into myeloid leukemia. *EMBO J.* **2000**, *19*, 4655−4664.
(20) Pasqualucci, L.; Trifonov, V.; Fabbri, G.; Ma, J.; Rossi, D.; Chiarenza, A.; Wells, V. A.; Grunn, A.; Messina, M.; Elliot, O.; Chan, J.; Bhagat, G.; Chadburn, A.; Gaidano, G.; Mullighan, C. G.; Rabadan, R.; Dalla-Favera, R. Analysis of the coding genome of diffuse large B-cell lymphoma. *Nat. Genet.* **2011**, *43*, 830−837.
(21) Bedford, D. C.; Brindle, P. K. Is histone acetylation the most important physiological function for CBP and p300? *Aging* **2012**, *4*, 247−255.
(22) Hay, D. A.; Rogers, C. M.; Fedorov, O.; Tallant, C.; Martin, S.; Monteiro, O. P.; Müller, S.; Knapp, S.; Schofield, C. J.; Brennan, P. E. Design and synthesis of potent and selective inhibitors of BRD7 and BRD9 bromodomains. *MedChemComm* **2015**, *6*, 1381−1386.
(23) Middeljans, E.; Wan, X.; Jansen, P. W.; Sharma, V.; Stunnenberg, H. G.; Logie, C. SS18 Together with animal-specific factors defines human BAF-type SWI/SNF complexes. *PLoS One* **2012**, *7*, e33834.
(24) Kaeser, M. D.; Aslanian, A.; Dong, M. Q.; Yates, J. R.; Emerson, B. M. BRD7, a Novel PBAF-specific SWI/SNF subunit, is required for target gene activation and repression in embryonic stem cells. *J. Biol. Chem.* **2008**, *283*, 32254−32263.
(25) Tae, S.; Karkhanis, V.; Velasco, K.; Yaneva, M.; Erdjument-Bromage, H.; Tempst, P.; Sif, S. Bromodomain protein 7 interacts with PRMT5 and PRC2, and is involved in transcriptional repression of their target genes. *Nucleic Acids Res.* **2011**, *39*, 5424−5438.
(26) Kang, J. U.; Koo, S. H.; Kwon, K. C.; Park, J. W.; Kim, J. M. Gain at chromosomal region 5p15.33, containing TERT, is the most frequent genetic event in early stages of non-small cell lung cancer. *Cancer Genet. Cytogenet.* **2008**, *182*, 1−11.
(27) Scotto, L.; Narayan, G.; Nandula, S. V.; Subramaniyam, S.; Kaufmann, A. M.; Wright, J. D.; Pothuri, B.; Mansukhani, M.; Schneider, A.; Arias-Pulido, H.; Murty, V. V. Integrative genomics analysis of chromosome 5p gain in cervical cancer reveals target over-expressed genes, including drosha. *Mol. Cancer* **2008**, *7*, 58.
(28) Zhou, J.; Ma, J.; Zhang, B. C.; Li, X. L.; Shen, S. R.; Zhu, S. G.; Xiong, W.; Liu, H. Y.; Huang, H.; Zhou, M.; Li, G. Y. BRD7, a novel bromodomain gene, inhibits G1-S progression by transcriptionally regulating some important molecules involved in ras/MEK/ERK and Rb/E2F pathways. *J. Cell. Physiol.* **2004**, *200*, 89−98.
(29) Wu, W. J.; Hu, K. S.; Chen, D. L.; Zeng, Z. L.; Luo, H. Y.; Wang, F.; Wang, D. S.; Wang, Z. Q.; He, F.; Xu, R. H. Prognostic relevance of BRD7 expression in colorectal carcinoma. *Eur. J. Clin. Invest.* **2013**, *43*, 131−140.
(30) Park, Y. A.; Lee, J. W.; Kim, H. S.; Lee, Y. Y.; Kim, T. J.; Choi, C. H.; Choi, J. J.; Jeon, H. K.; Cho, Y. J.; Ryu, J. Y.; Kim, B. G.; Bae, D. S. Tumor suppressive effects of bromodomain-containing protein 7 (BRD7) in epithelial ovarian carcinoma. *Clin. Cancer Res.* **2014**, *20*, 565−575.
(31) Burrows, A. E.; Smogorzewska, A.; Elledge, S. J. Polybromo-associated BRG1-associated factor components BRD7 and BAF180 are critical regulators of p53 required for induction of replicative senescence. *Proc. Natl. Acad. Sci. U. S. A.* **2010**, *107*, 14280−14285.
(32) Drost, J.; Mantovani, F.; Tocco, F.; Elkon, R.; Comel, A.; Holstege, H.; Kerkhoven, R.; Jonkers, J.; Voorhoeve, P. M.; Agami, R.; Del Sal, G. BRD7 is a candidate tumour suppressor gene required for p53 function. *Nat. Cell Biol.* **2010**, *12*, 380−389.
(33) Mantovani, F.; Drost, J.; Voorhoeve, P. M.; Del Sal, G.; Agami, R. Gene regulation and tumor suppression by the bromodomain-containing protein BRD7. *Cell Cycle* **2010**, *9*, 2777−2781.
(34) Demont, E. H.; Bamborough, P.; Chung, C. W.; Craggs, P. D.; Fallon, D.; Gordon, L. J.; Grandi, P.; Hobbs, C. I.; Hussain, J.; Jones, E. J.; Le Gall, A.; Michon, A. M.; Mitchell, D. J.; Prinjha, R. K.; Roberts, A. D.; Sheppard, R. J.; Watson, R. J. 1,3-Dimethyl benzimidazolones are potent, selective inhibitors of the BRPF1 bromodomain. *ACS Med. Chem. Lett.* **2014**, *5*, 1190−1195.
(35) Palmer, W. S.; Poncet-Montange, G.; Liu, G.; Petrocchi, A.; Reyna, N.; Subramanian, G.; Theroff, J.; Yau, A.; Kost-Alimova, M.; Bardenhagen, J. P.; Leo, E.; Shepard, H. E.; Tieu, T. N.; Shi, X.; Zhan, Y.; Zhao, S.; Barton, M. C.; Draetta, G.; Toniatti, C.; Jones, P.; Geck Do, M.; Andersen, J. N. Structure-guided design of IACS-9571, a selective high-affinity dual TRIM24-BRPF1 bromodomain inhibitor. *J. Med. Chem.* **2016**, *59*, 1440−1454.
(36) Bennett, J.; Fedorov, O.; Tallant, C.; Monteiro, O.; Meier, J.; Gamble, V.; Savitsky, P.; Nunez-Alonso, G. A.; Haendler, B.; Rogers, C.; Brennan, P. E.; Müller, S.; Knapp, S. Discovery of a chemical tool inhibitor targeting the bromodomains of TRIM24 and BRPF. *J. Med. Chem.* **2016**, *59*, 1642−1647.
(37) Ferguson, F. M.; Fedorov, O.; Chaikuad, A.; Philpott, M.; Muniz, J. R. C.; Felletar, I.; von Delft, F.; Heightman, T.; Knapp, S.; Abell, C.; Ciulli, A. Targeting low-druggability bromodomains: fragment based screening and inhibitor design against the BAZ2B bromodomain. *J. Med. Chem.* **2013**, *56*, 10183−10187.
(38) Rooney, T. P. C.; Filippakopoulos, P.; Fedorov, O.; Picaud, S.; Cortopassi, W. A.; Hay, D. A.; Martin, S.; Tumber, A.; Rogers, C. M.; Philpott, M.; Wang, M. H.; Thompson, A. L.; Heightman, T. D.; Pryde, D. C.; Cook, A.; Paton, R. S.; Müller, S.; Knapp, S.; Brennan, P. E.; Conway, S. J. A series of potent CREBBP bromodomain ligands reveals an induced-fit pocket stabilized by a cation-pi interaction. *Angew. Chem., Int. Ed.* **2014**, *53*, 6126−6130.
(39) Unzue, A.; Xu, M.; Dong, J.; Wiedmer, L.; Spiliotopoulos, D.; Caflisch, A.; Nevado, C. Fragment-based design of selective nanomolar ligands of the CREBBP bromodomain. *J. Med. Chem.* **2016**, *59*, 1350−1356.
(40) Drouin, L.; McGrath, S.; Vidler, L. R.; Chaikuad, A.; Monteiro, O.; Tallant, C.; Philpott, M.; Rogers, C.; Fedorov, O.; Liu, M. J.; Akhtar, W.; Hayes, A.; Raynaud, F.; Müller, S.; Knapp, S.; Hoelder, S. Structure enabled design of BAZ2-ICR, a chemical probe targeting the bromodomains of BAZ2A and BAZ2B. *J. Med. Chem.* **2015**, *58*, 2553−2559.
(41) Chen, P.; Chaikuad, A.; Bamborough, P.; Bantscheff, M.; Bountra, C.; Chung, C.; Fedorov, O.; Grandi, P.; Jung, D.; Lesniak, R.; Lindon, M.; Müller, S.; Philpott, M.; Prinjha, R.; Rogers, C.; Selenski, C.; Tallant, C.; Werner, T.; Willson, T. M.; Knapp, S.; Drewry, D. H. Discovery and characterization of GSK2801, a selective chemical probe for the bromodomains BAZ2A and BAZ2B. *J. Med. Chem.* **2016**, *59*, 1410−1424.
(42) Clark, P. G. K.; Vieira, L. C. C.; Tallant, C.; Fedorov, O.; Singleton, D. C.; Rogers, C. M.; Monteiro, O. P.; Bennett, J. M.; Baronio, R.; Müller, S.; Daniels, D. L.; Mendez, J.; Knapp, S.; Brennan, P. E.; Dixon, D. J. LP99: Discovery and synthesis of the first selective BRD7/9 bromodomain inhibitor. *Angew. Chem., Int. Ed.* **2015**, *54*, 6217−6221.
(43) Theodoulou, N. H.; Bamborough, P.; Bannister, A. J.; Becher, I.; Bit, R. A.; Che, K. H.; Chung, C.-w.; Dittmann, A.; Drewes, G.; Drewry, D. H.; Gordon, L.; Grandi, P.; Leveridge, M.; Lindon, M.; Michon, A.-M.; Molnar, J.; Robson, S. C.; Tomkinson, N. C. O.; Kouzarides, T.; Prinjha, R. K.; Humphreys, P. G. Discovery of I-BRD9, a selective cell active chemical probe for bromodomain containing protein 9 inhibition. *J. Med. Chem.* **2016**, *59*, 1425−1439.
(44) Kolb, P.; Kipouros, C. B.; Huang, D. Z.; Caflisch, A. Structure-based tailoring of compound libraries for high-throughput screening: discovery of novel EphB4 kinase inhibitors. *Proteins: Struct., Funct., Genet.* **2008**, *73*, 11−18.
(45) Zhao, H.; Huang, D. Hydrogen bonding penalty upon ligand binding. *PLoS One* **2011**, *6*, e19923.

DOI: 10.1021/acs.jmedchem.5b01757
J. Med. Chem. 2016, 59, 3087−3097

(46) Unzue, A.; Lafleur, K.; Zhao, H.; Zhou, T.; Dong, J.; Kolb, P.; Liebl, J.; Zahler, S.; Caflisch, A.; Nevado, C. Three stories on Eph kinase inhibitors: from in silico discovery to in vivo validation. *Eur. J. Med. Chem.* **2016**, *112*, 347−366.
(47) Unzue, A.; Dong, J.; Lafleur, K.; Zhao, H. T.; Frugier, E.; Caflisch, A.; Nevado, C. Pyrrolo[3,2-b]quinoxaline derivatives as types I-1/2 and II Eph tyrosine kinase inhibitors: structure-based design, synthesis, and in vivo validation. *J. Med. Chem.* **2014**, *57*, 6834−6844.
(48) Lolli, G.; Caflisch, A. High-throughput fragment docking into the BAZ2B bromodomain: efficient in silico screening for X-ray crystallography. *ACS Chem. Biol.* **2016**, *11*, 800−807.
(49) Xu, M.; Unzue, A.; Dong, J.; Spiliotopoulos, D.; Nevado, C.; Caflisch, A. Discovery of CREBBP bromodomain inhibitors by high-throughput docking and hit optimization guided by molecular dynamics. *J. Med. Chem.* **2016**, *59*, 1340−1349.
(50) Zhao, H.; Caflisch, A. Discovery of ZAP70 inhibitors by high-throughput docking into a conformation of its kinase domain generated by molecular dynamics. *Bioorg. Med. Chem. Lett.* **2013**, *23*, 5721−5726.
(51) Zhao, H.; Caflisch, A. Discovery of dual ZAP70 and Syk kinases inhibitors by docking into a rare C-helix-out conformation of Syk. *Bioorg. Med. Chem. Lett.* **2014**, *24*, 1523−1527.
(52) Zhao, H.; Gartenmann, L.; Dong, J.; Spiliotopoulos, D.; Caflisch, A. Discovery of BRD4 bromodomain inhibitors by fragment-based high-throughput docking. *Bioorg. Med. Chem. Lett.* **2014**, *24*, 2493−2496.
(53) Zhao, H.; Huang, D.; Caflisch, A. Discovery of tyrosine kinase inhibitors by docking into an inactive kinase conformation generated by molecular dynamics. *ChemMedChem* **2012**, *7*, 1983−1990.
(54) Zhao, H. T.; Dong, J.; Lafleur, K.; Nevado, C.; Caflisch, A. Discovery of a novel chemotype of tyrosine kinase inhibitors by fragment-based docking and molecular dynamics. *ACS Med. Chem. Lett.* **2012**, *3*, 834−838.
(55) Fabian, M. A.; Biggs, W. H.; Treiber, D. K.; Atteridge, C. E.; Azimioara, M. D.; Benedetti, M. G.; Carter, T. A.; Ciceri, P.; Edeen, P. T.; Floyd, M.; Ford, J. M.; Galvin, M.; Gerlach, J. L.; Grotzfeld, R. M.; Herrgard, S.; Insko, D. E.; Insko, M. A.; Lai, A. G.; Lelias, J. M.; Mehta, S. A.; Milanov, Z. V.; Velasco, A. M.; Wodicka, L. M.; Patel, H. K.; Zarrinkar, P. P.; Lockhart, D. J. A small molecule-kinase interaction map for clinical kinase inhibitors. *Nat. Biotechnol.* **2005**, *23*, 329−336.
(56) Quinn, E.; Wodicka, L.; Ciceri, P.; Pallares, G.; Pickle, E.; Torrey, A.; Floyd, M.; Hunt, J.; Treiber, D. Abstract 4238: BROMOscan - a high throughput, quantitative ligand binding platform identifies best-in-class bromodomain inhibitors from a screen of mature compounds targeting other protein classes. *Cancer Res.* **2013**, *73*, 4238.
(57) Vidler, L. R.; Brown, N.; Knapp, S.; Hoelder, S. Druggability analysis and structural classification of bromodomain acetyl-lysine binding sites. *J. Med. Chem.* **2012**, *55*, 7346−7359.
(58) Brooks, B. R.; Brooks, C. L., III; Mackerell, A. D., Jr; Nilsson, L.; Petrella, R. J.; Roux, B.; Won, Y.; Archontis, G.; Bartels, C.; Boresch, S.; Caflisch, A.; Caves, L.; Cui, Q.; Dinner, A. R.; Feig, M.; Fischer, S.; Gao, J.; Hodoscek, M.; Im, W.; Kuczera, K.; Lazaridis, T.; Ma, J.; Ovchinnikov, V.; Paci, E.; Pastor, R. W.; Post, C. B.; Pu, J. Z.; Schaefer, M.; Tidor, B.; Venable, R. M.; Woodcock, H. L.; Wu, X.; Yang, W.; York, D. M.; Karplus, M. CHARMM: the biomolecular simulation program. *J. Comput. Chem.* **2009**, *30*, 1545−1614.
(59) Niesen, F. H.; Berglund, H.; Vedadi, M. The use of differential scanning fluorimetry to detect ligand interactions that promote protein stability. *Nat. Protoc.* **2007**, *2*, 2212−2221.

DOI: 10.1021/acs.jmedchem.5b01757
J. Med. Chem. 2016, 59, 3087−3097

Supporting Information

The "gatekeeper" residue influences the binding mode of acetyl indoles to bromodomains

Andrea Unzue,[a] Hongtao Zhao,[b] Graziano Lolli,[b] Jing Dong,[b] Jian Zhu,[b]

Melanie Zechner,[a] Aymeric Dolbois,[a] Amedeo Caflisch,*[b] Cristina Nevado*[a]

Department of Chemistry[a] and Department of Biochemistry[b] University of Zürich

Winterthurerstrasse 190, CH-8057 Zürich, Switzerland.

Table of contents

*To whom correspondence should be addressed. Phone: (41) 446353945. Fax: (41) 446353948.
E-mail: cristina.nevado@chem.uzh.ch, caflisch@bioc.uzh.ch

1. Computational methods

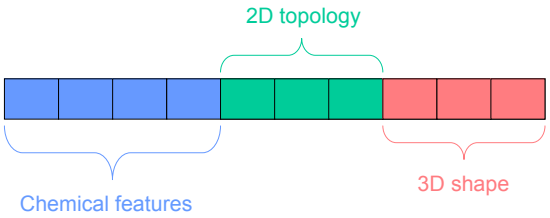

Figure S1. Scheme of the activity-oriented fingerprint (AoF), which consists of three sections: chemical features, 2D topology indices, and 3D shape descriptors. See below for detailed explanation.

Section A: Chemical features
1: number of heavy atoms divided by 2;
2: number of element phosphor
3: number of elements halogen (F + Cl + Br + I)
4: degrees of unsaturation
5: number of chemical rings
6: number of C.1
7: number of (N.ar + N.2)
8: number of (N.pl3 + N.am)
9: number of N.1
10: number of N.4
11: number of (O.3+S.3)
12: number of (O.2+S.2)
13: number of O.co2
14: number of S.o
15: number of S.o2
16: number of rotatable bonds.
*Atom types follow the definition of SYBYL atom types.

Section B: 2D topology
1: Randic first topology index divided by number of bonds scaled by a factor of 10
2: Randic second topology index divided by number of bonds scaled by a factor of 10

Section C: 3D shape
12 moments described in reference 1.

Similarity Index
In each section, a similarity index was computed between two molecules A and B by the following equation,[1]

$$simi = \frac{1}{1 + \frac{\sum_{i=1}^{n} | Ai - Bi |}{n}} \qquad (1)$$

The overall similarity index is the arithmetic mean of those from the three sections.

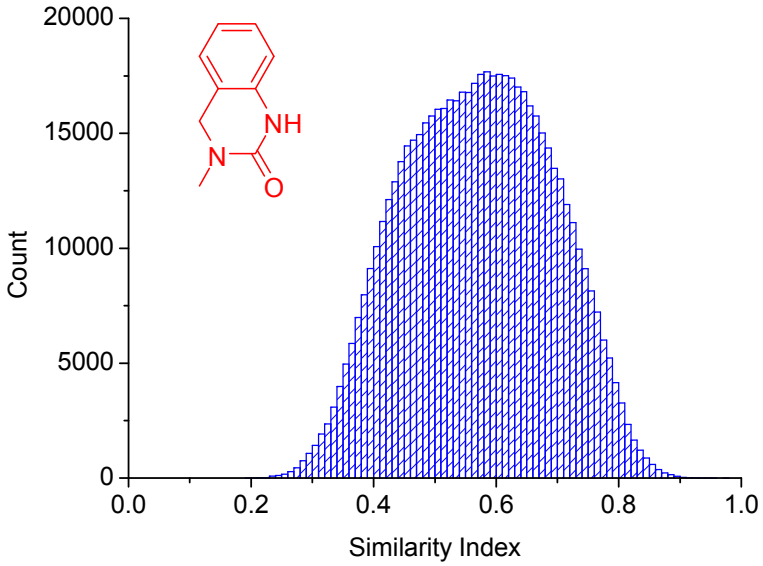

Figure S2. Distribution of similarity index between a query fragment and a 0.6 million fragments library. The 2D structure of the query molecule is shown in red.

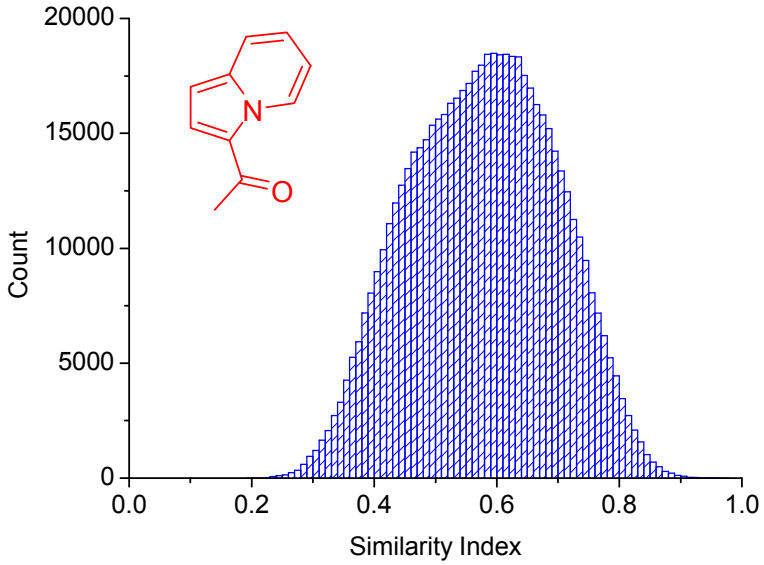

Figure S3. Distribution of similarity index between a query fragment and a 0.6 million fragments library. The 2D structure of the query molecule is shown in red.

2. Synthetic methods

All reactions, unless otherwise stated, were carried out under a nitrogen atmosphere using standard Schlenk-techniques. All reagents were used as received unless otherwise noted. Solvents were purchased in the best quality available, degassed by purging thoroughly with nitrogen and dried over activated molecular sieves of appropriate size. Alternatively, they were purged with argon and passed through alumina columns in a solvent purification system (Innovative Technology). Reactions were monitored by thin layer chromatography (TLC) using Merck TLC silica gel 60 F_{254}. Flash column

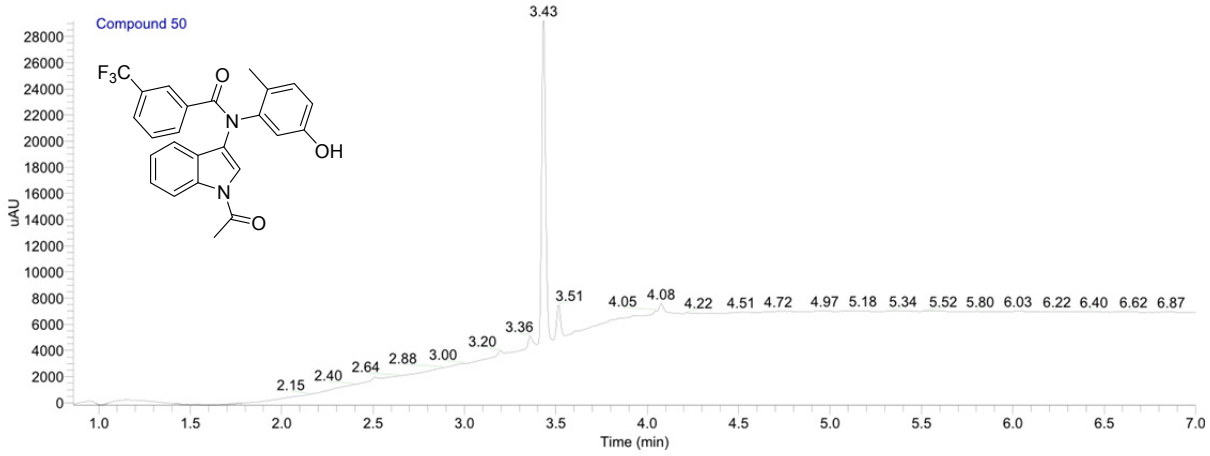

Apex RT	Start RT	End RT	Area	%Area	Height	%Height
3.43	3.4	3.48	36896.297	90.23	24638.591	90.13
3.51	3.49	3.55	3733.925	9.13	2540.89	9.3
3.61	3.59	3.63	260.667	0.64	155.749	0.57

References

1. Ballester, P. J.; Richards, W. G. Ultrafast shape recognition to search compound databases for similar molecular shapes. *J. Comput. Chem.* **2007**, *28*, 1711-1723.
2. Rap, J. M. R.; Venkatesham, U.; George, J.; Fernand, G.; Doppalapudi, S. R.; Madhavan, G. R.; Arumugam, N.; Ansari, M.; Murugavel, K.; Pradeep, J.; Allavuddeen, S.; Vijayaramalingam, K.; Prasad, H. S.; Raj, A. M.; Gnanavel, S.; Kottamalai, R.; Babu, N. M. P. S.; Kenchegowda, B. Y. Cyclic amide derivatives as inhibitors of 11-Beta-hydroxysteroid dehydrogenase and uses thereof *Connexios Life Sciences PVT. LTD.* **2013**, *WO2012IN00841 20121221*
3. Ryabova, S. Y.; Rastorgueva, N. A.; Lisitsa, E. A.; Alekseeva, L. M.; Granik, V. G. Synthesis and study of some properties of 1-aryl-2-oxo-1,2,3,6tetrahydro[1,4]diazepino[6,5-b]indole 4-oxides. *Russ. Chem. B+* **2003**, *52*, 1386-1398.
4. Cox, E. D.; Diaz-Arauzo, H.; Huang, Q.; Reddy, M. S.; Ma, C. R.; Harris, B.; McKernan, R.; Skolnick, P.; Cook, J. M. Synthesis and evaluation of analogues of the partial agonist 6-(propyloxy)-4-(methoxymethyl)-beta-carboline-3-carboxylic acid ethyl ester (6-PBC) and the full agonist 6-(benzyloxy)-4-(methoxymethyl)-beta-carboline-3-carboxylic acid ethyl ester (Zk 93423) at wild type and recombinant GABA(A) receptors. *J. Med. Chem.* **1998**, *41*, 2537-2552.
5. Davies, H. M. L.; Townsend, R. J. Catalytic asymmetric cyclopropanation of heteroaryldiazoacetates. *J. Org. Chem.* **2001**, *66*, 6595-6603.
6. Filippakopoulos, P.; Picaud, S.; Mangos, M.; Keates, T.; Lambert, J. P.; Barsyte-Lovejoy, D.; Felletar, I.; Volkmer, R.; Muller, S.; Pawson, T.; Gingras, A. C.; Arrowsmith, C. H.; Knapp, S. Histone recognition and large-scale structural analysis of the human bromodomain family. *Cell* **2012**, *149*, 214-231.
7. Kabsch, W. Automatic processing of rotation diffraction data from crystals of initially unknown symmetry and cell constants. *J. Appl. Crystallogr.* **1993**, *26*, 795-800.
8. Bailey, S. The Ccp4 suite - programs for protein crystallography. *Acta Crystallogr. D.* **1994**, *50*, 760-763.
9. Mccoy, A. J.; Grosse-Kunstleve, R. W.; Adams, P. D.; Winn, M. D.; Storoni, L. C.; Read, R. J. Phaser crystallographic software. *J. Appl. Crystallogr.* **2007**, *40*, 658-674.

10. Adams, P. D.; Grosse-Kunstleve, R. W.; Hung, L. W.; Ioerger, T. R.; McCoy, A. J.; Moriarty, N. W.; Read, R. J.; Sacchettini, J. C.; Sauter, N. K.; Terwilliger, T. C. PHENIX: building new software for automated crystallographic structure determination. *Acta Crystallogr. D.* **2002**, *58*, 1948-1954.
11. Evans, P. R.; Murshudov, G. N. How good are my data and what is the resolution? *Acta Crystallogr. D.* **2013**, *69*, 1204-1214.
12. Emsley, P.; Lohkamp, B.; Scott, W. G.; Cowtan, K. Features and development of Coot. *Acta Crystallogr. D.* **2010**, *66*, 486-501.
13. Filippakopoulos, P.; Qi, J.; Picaud, S.; Shen, Y.; Smith, W. B.; Fedorov, O.; Morse, E. M.; Keates, T.; Hickman, T. T.; Felletar, I.; Philpott, M.; Munro, S.; McKeown, M. R.; Wang, Y. C.; Christie, A. L.; West, N.; Cameron, M. J.; Schwartz, B.; Heightman, T. D.; La Thangue, N.; French, C. A.; Wiest, O.; Kung, A. L.; Knapp, S.; Bradner, J. E. Selective inhibition of BET bromodomains. *Nature* **2010**, *468*, 1067-1073.

Chapter 7

X-ray crystal structures and binding mode analysis of BRPF1 bromodomain complexed with ligand-efficient virtual screening hits

In chapter 2, we showed that several diverse chemotypes targeting BRPF1 were discovered by high-through virtual screening and validated by X-ray crystallography. Subsequent hit optimization work led to the discovery of two series of low micromolar selective BRPF1 inhibitors, which was described in chapter 3. Here, we present another virtual screening campaign carried out for a different fragment library which resulted in two novel ligand-efficient fragments targeting BRPF1 bromodomain.

The rigid-ligand docking campaign was performed with SEED [1,2]. A fragment-like library of 60000 compounds was assembled from a large panel of commercial vendors and academic collaborators. The crystal structure of BRPF1 in complex with a pan-bromodomain inhibitor Bromosporine (PDB code 5C7N) was used for docking. The conserved asparagine (Asn708) and conserved water molecules in the Kac pocket were defined as the binding site. The partial charges and van der Waals parameters for the atoms in the receptor and the small molecules were taken from the CHARMM36 all-atom force field [3,4] and the CHARMM general force field (CGenFF) [5], respectively. The SEED binding energy consists of van der Waals energy, and electrostatics energy which is evaluated in the continuum dielectric approximation. The values of the dielectric constant were set to be 2.0 and 78.5 for the volume occupied by solute and solvent, respectively.

The docked poses of fragments were ranked by a consensus scoring method to prioritize the total binding energy, the electrostatic contribution to the ligand binding and van der Waals interactions divided by the number of non-hydrogen atoms of ligand. The latter term favors small molecules with few non-hydrogen atoms. Three top-ranked fragments were selected after inspection of the novelty for further biochemical assays. All three fragments showed more than 50% inhibition activity at 500 μM concentration in the single dose BROMOscan assay. Next, DSPBP1004 and DSPBP1010 were analyzed by dose-response BROMOscan and AlphaScreen assays. DSPBP1004 displayed highly favorable ligand efficiencies of 0.53 and 0.48 in the BROMOscan assay (K_D = 24 uM) and AlphaScreen assay (IC50 = 60.2 μM), respectively (Table 1). Compound DSP1010 appeared to be slightly less potent as BRPF1 inhibitor, showing a K_D value of 74 μM in the BROMOscan assay (ligand efficiency is 0.33), while the IC_{50} value was not determined in the AlphaScreen assay.

Table 1. 2D chemical structure of screening hits for BRPF1and their biochemical assay data.

Cpd	2D structure	HAC[a]	BROMOscan % Ctrl[b]	BROMOscan K_D (μM) LE[c]	AlphaScreen IC_{50} (μM) LE[c]
DSPBP1004	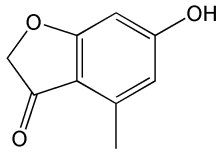	12	15 @500 μM	24 [0.53]	60.2 [0.48]
DSPBP1010	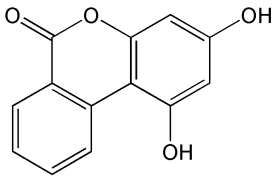	17	17 @330 μM	74 [0.33]	> 157 [< 0.31]
DSPBP1002	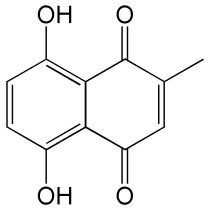	15	46 @500 μM	-	-

[a]Heavy atom count. [b]The single-dose value is the percentage of remaining binding of the competitor molecule with respect to DMSO solution at the compound concentration shown in μM; thus lower values indicate stronger binding of the compounds. [c]Ligand efficiency is calculated as LE = (1.4/HA) × pK_D.

In our previous fragment-based virtual screening campaigns for bromodomains BRPF1 [6] and CREBBP [7], the predicted docking pose of screening hits were validated by X-crystallography. Similarly, in this study, co-crystallization of the BRPF1 with ligand was performed to experimentally determine the binding mode.

The BRPF1 bromodomain was expressed and purified as an N-terminal GST fusion protein in *E.coli* as described previously [6]. It was co-crystallized with inhibitors by vapor diffusion in hanging drops at 277 K. Co-crystals of BRPF1 with compound DSPBP1004 and DSPBP1010 were grown by mixing protein sample at 23 mg/ml concentration with an equal volume of reservoir buffer of 0.1 M Bis-tris propane, pH 6.5, 0.15 M Sodium nitrate, 20% PEG3350.

Crystal datasets were collected at beamline X06SA of Swiss Light Source. Data reduction was performed with XDS [8] and scaled with Aimless [9]. Structures were solved by molecular replacement with Molrep [10] in CCP4 suite [11] using apo BRPF1 structure 4LC2 as staring model, further refined with PHENIX [12] and were manually built with COOT [13] for several rounds. The co-crystal of BRPF1/DSPBP1004 and BRPF1/DSPBP1010 were solved at resolutions of 1.65 and 1.70 angstrom, respectively. The data collection and refinement statistics are summarized in table 2.

Table 2. X-ray data collection and refinement statistics for complex structures of the BRPF1 bromodomain and two fragments identified by docking with SEED.

PDB ID	**5OWB**	**5OWE**
Compound	**DSPBP1004**	**DSPBP1010**
Data Collection		
space group	$P3_221$	$P3_221$
Cell dimensions a, b, c (Å)	60.43, 60.43, 63.47	60.53, 60.53, 63.68
Cell dimensions α, β, γ (°)	90.00,90.00, 120.00	90.00, 90.00, 120.00
resolution (Å)	40.38 - 1.65	27.33 - 1.70
unique observations*	16528(815)	15062 (794)
completeness*	99.8 (99.3)	98.9 (98.2)
redundancy*	19.3(17.0)	19.8 (20.9)
Rmerge*	0.068 (0.641)	0.050 (0.540)
CC (1/2)	0.999 (0.924)	0.998 (0.956)
I/σI*	26.7 (4.3)	31.1 (5.2)
Refinement		
R_{work}/R_{free}*	0.174(0.240)/0.204(0.264)	0.190(0.229)/0.213(0.272)
r.m.s deviations bond (Å)	0.007	0.007
r.m.s deviations angles (°)	0.831	0.666
Ramanchandran Favored	99.09	98.20
Ramanchandran Allowed	0.91	1.80
Ramanchandran Disallowed	0.00	0.00
* Statistics for the highest resolution shell is shown in parentheses.		

As seen from the co-crystal structure of BRPF1/DSPBP1004, the fragment locate at the Kac binding site sandwiched by van der Waals contacts with ZA-loop residues Val657, Pro658 and Val662 on one side of the pocket and Ile652, Phe653 and Phe714 on the opposite side (Figure 1A). The methyl group on the benzene locates deeply in the Kac site, forming van der Waals interactions with surrounding residues Ile652, Phe653 and Phe714. Extensive hydrogen

bonds formation upon fragment binding was also observed. The carbonyl group on the benzofuran core is involved in the hydrogen bond with the NH group of the conserved asparagine Asn708 as well as a water-bridged hydrogen bond to the Tyr665. The hydroxyl group on the benzene and the oxygen atom on the furan ring contact conserved and re-organized water molecules in the Kac site as hydrogen bond donor and receptor, respectively. Interestingly, a relatively weaker CH···O hydrogen bond interaction is observed between the backbone carbonyl group of Ile652 and a carbon atom on the benzene ring. The docked pose of DSPBP1004 shows that key hydrogen bond interactions with the Asn708 and the conserved water molecule bridging to Tyr665 are present by involving the carbonyl group on the furan ring as same as the crystal structure.

Compound DSPBP1010 is located at the hydrophobic Kac pocket in the co-crystal structure with BRPF1 in a similar way as DSPBP1004 (Figure 1B). The carbonyl group of the pyran ring hydrogen bonds to the Asn708 and Tyr665 via a conserved water molecule. In addition, the oxygen atom on the paran forms a hydrogen bond with Asn708 in a distance of 3.6 angstrom. The CH···O hydrogen bonding is observed between the carbonyl group of Ile652 and one of the carbon atoms of the benzene ring. The docked pose shows a flipped conformation of fragment as compared to the crystallographic pose, while the key hydrogen bond between carbonyl group on the pyran and the conserved water molecule is still maintained.

Despite the main hydrogen bond is predicted correctly, the docked pose of the two fragments shows different orientation as compared to the crystallographic pose, this might be due to the reorientation and rearrangement of water molecules in the Kac pocket. Another reason might be related with the protein receptor used for docking. It is also possible that both poses are populated with different weights in solution conditions. As previously reported, the loop regions of BRPF1 always undergo conformational changes upon binding of different ligands [6]. To investigate the discrepancy between the poses predicted by docking and in the the crystal structure, we suggest a molecular dynamics (MD) analysis of the binding mode. Multiple MD runs should be started from each of the docked pose and binding mode in the crystal structure to assess kinetic stability.

In this study, a fragment-based virtual screening by SEED followed by X-ray crystallography validation was carried out which led to the identification of two ligand-efficient BRPF1 inhibitors. To the best of our knowledge, these two fragments represent two novel chemotypes that have not reported as bromodomain inhibitors. The structural information of fragment binding revealed by X-ray crystallography analysis is helpful for further developing these fragment hits into potent BRPF1 inhibitors.

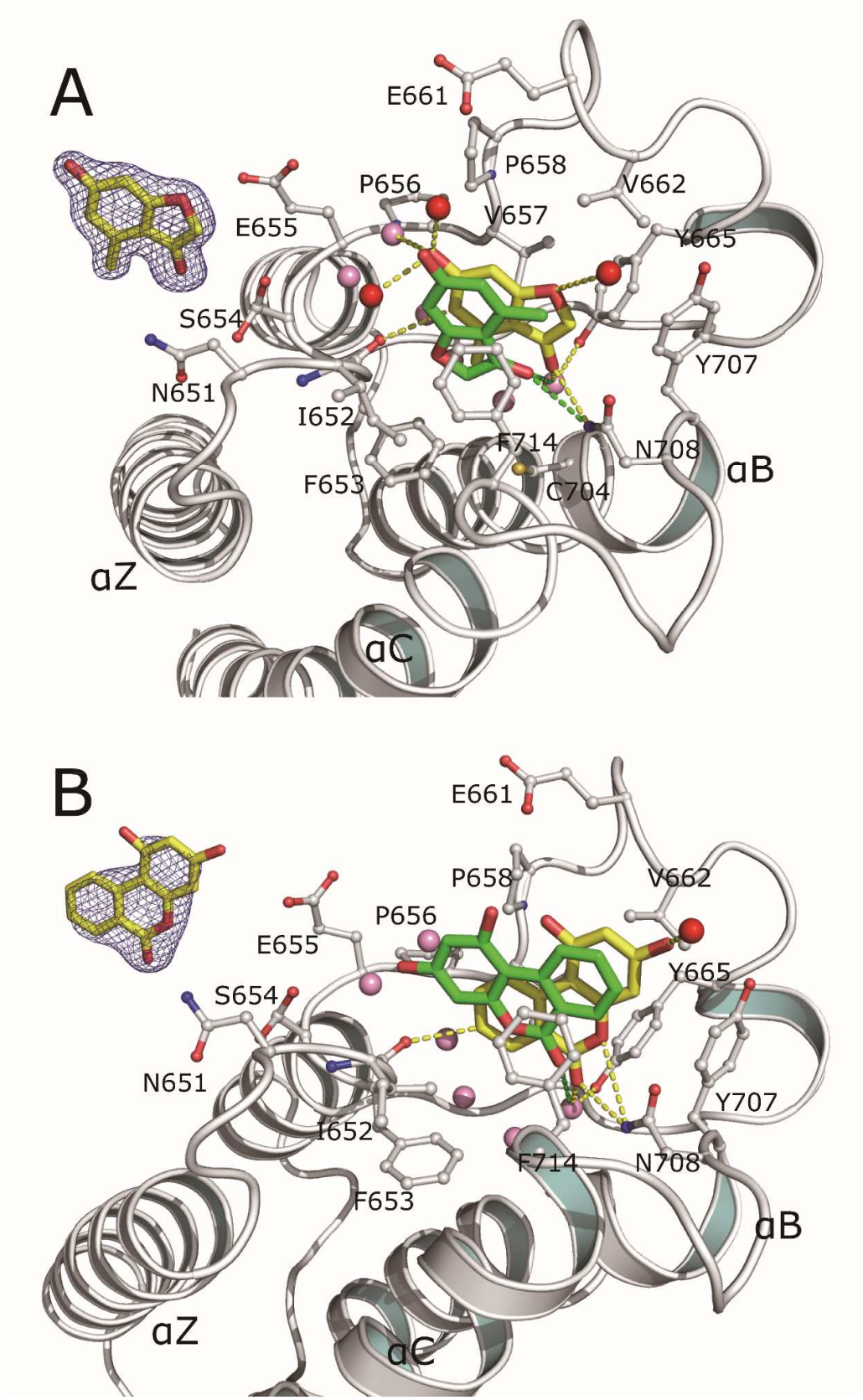
A
E661
P658
P656
V662
E655
V657
Y665
S654
Y707
N651
I652
F714
N708
αB
F653
C704
αZ
αC
B
E661
P658
V662
P656
E655
Y665
S654
N651
Y707
I652
F714
N708
F653
αB
αZ
αC

Figure 1. Comparison of the crystallographic pose (yellow) and docking pose (green) of DSPBP1004 (A) and DSPBP1010 (B). The conserved water molecules and other water molecules involved in ligand binding are shown as pink and red spheres, respectively, while hydrogen bonds are shown by dashed lines. The 2Fo – Fc electron density maps are shown in blue mesh at a contour level of 1.0 sigma. Note that in the predicted pose the fragments make the same hydrogen bonds with the conserved Asn708 and the water bridging to the conserved Tyr665 as in the crystal structure. The docked and crystal poses are related by a rotation of 180 degrees around axis that spans two oxygen atoms.

References

1. Majeux, N.; Scarsi, M.; Apostolakis, J.; Ehrhardt, C.; Caflisch, A., Exhaustive docking of molecular fragments with electrostatic solvation. *Proteins* **1999,** *37* (1), 88-105.
2. Majeux, N.; Scarsi, M.; Caflisch, A., Efficient electrostatic solvation model for protein-fragment docking. *Proteins* **2001,** *42* (2), 256-68.
3. MacKerell, A. D.; Bashford, D.; Bellott, M.; Dunbrack, R. L.; Evanseck, J. D.; Field, M. J.; Fischer, S.; Gao, J.; Guo, H.; Ha, S.; Joseph-McCarthy, D.; Kuchnir, L.; Kuczera, K.; Lau, F. T.; Mattos, C.; Michnick, S.; Ngo, T.; Nguyen, D. T.; Prodhom, B.; Reiher, W. E.; Roux, B.; Schlenkrich, M.; Smith, J. C.; Stote, R.; Straub, J.; Watanabe, M.; Wiorkiewicz-Kuczera, J.; Yin, D.; Karplus, M., All-atom empirical potential for molecular modeling and dynamics studies of proteins. *J Phys Chem B* **1998,** *102* (18), 3586-616.
4. MacKerell, A. D., Jr.; Feig, M.; Brooks, C. L., 3rd, Improved treatment of the protein backbone in empirical force fields. *J Am Chem Soc* **2004,** *126* (3), 698-9.
5. Vanommeslaeghe, K.; Hatcher, E.; Acharya, C.; Kundu, S.; Zhong, S.; Shim, J.; Darian, E.; Guvench, O.; Lopes, P.; Vorobyov, I.; Mackerell, A. D., Jr., CHARMM general force field: A force field for drug-like molecules compatible with the CHARMM all-atom additive biological force fields. *J Comput Chem* **2010,** *31* (4), 671-90.
6. Zhu, J.; Caflisch, A., Twenty Crystal Structures of Bromodomain and PHD Finger Containing Protein 1 (BRPF1)/Ligand Complexes Reveal Conserved Binding Motifs and Rare Interactions. *J Med Chem* **2016,** *59* (11), 5555-61.
7. Spiliotopoulos, D.; Zhu, J.; Wamhoff, E. C.; Deerain, N.; Marchand, J. R.; Aretz, J.; Rademacher, C.; Caflisch, A., Virtual screen to NMR (VS2NMR): Discovery of fragment hits for the CBP bromodomain. *Bioorg Med Chem Lett* **2017,** *27* (11), 2472-2478.

8. Kabsch, W., Integration, scaling, space-group assignment and post-refinement. *Acta Crystallogr D Biol Crystallogr* **2010,** *66* (Pt 2), 133-44.
9. Evans, P. R.; Murshudov, G. N., How good are my data and what is the resolution? *Acta Crystallogr D Biol Crystallogr* **2013,** *69* (Pt 7), 1204-14.
10. Vagin, A.; Teplyakov, A., Molecular replacement with MOLREP. *Acta Crystallogr D Biol Crystallogr* **2010,** *66* (Pt 1), 22-5.
11. Winn, M. D.; Ballard, C. C.; Cowtan, K. D.; Dodson, E. J.; Emsley, P.; Evans, P. R.; Keegan, R. M.; Krissinel, E. B.; Leslie, A. G.; McCoy, A.; McNicholas, S. J.; Murshudov, G. N.; Pannu, N. S.; Potterton, E. A.; Powell, H. R.; Read, R. J.; Vagin, A.; Wilson, K. S., Overview of the CCP4 suite and current developments. *Acta Crystallogr D Biol Crystallogr* **2011,** *67* (Pt 4), 235-42.
12. Adams, P. D.; Afonine, P. V.; Bunkoczi, G.; Chen, V. B.; Davis, I. W.; Echols, N.; Headd, J. J.; Hung, L. W.; Kapral, G. J.; Grosse-Kunstleve, R. W.; McCoy, A. J.; Moriarty, N. W.; Oeffner, R.; Read, R. J.; Richardson, D. C.; Richardson, J. S.; Terwilliger, T. C.; Zwart, P. H., PHENIX: a comprehensive Python-based system for macromolecular structure solution. *Acta Crystallogr D Biol Crystallogr* **2010,** *66* (Pt 2), 213-21.
13. Emsley, P.; Lohkamp, B.; Scott, W. G.; Cowtan, K., Features and development of Coot. *Acta Crystallogr D Biol Crystallogr* **2010,** *66* (Pt 4), 486-501.

Chapter 8

Conclusions

This thesis focuses on the application of fragment-based drug discovery approach in the identification of inhibitors targeting human bromodomain proteins with an emphasis of the use of X-ray crystallography in fragment-based drug design. Usually bromodomains can be recombinantly expressed and purified as stable single-domain constructs so that biophysical tools, such as NMR spectroscopy, X-ray crystallography and differential scanning fluorimetry (DSF) are suitable for the analysis of protein-ligand interactions for bromodomains.

In practice, the FBDD in our group commonly starts with fragment-based high throughput docking, which can efficiently filter out putative hits from a large library of rigid framents by binding energy ranking. Top-ranked fragments are then assayed for affinity biophysically and/or biochemically. In this thesis, we present in silico fragment screening studies for BRPF1 (Chapters 2 and 7) and CREBBP (Chapter 4) bromodomains. These docking campaigns successfully generated highly ligand-efficient fragment hits, and importantly, some screening hits provided chemical expansion vectors for optimization by medicinal chemistry. In these cases, the success ratio, i.e., ratio of binders versus purchased fragments are greater than 10%, according to the X-ray crystallography validation, which is significantly higher than the success rate (< 1%) of conventional high throughput screening.

This theis presents two stories of hit optimization by different ways. In the BRPF1 project (Chapter 3), using an integrative approach based on in silico docking, compoud searching by cheminformatics techniques and experimental validation, two series of low micromolar inhibitors that derive from initial fragment hits were discovered. The main idea of this approach is to use structural information of fragment binding to explore the commercial available chemical collections. One of the identified compounds exhibits 2-μM affinity for the BRPF1 bromodomain and more than 100-fold selectivity for BRPF1 over other tested bromodomains. These newly identified chemotypes provided interesting starting points for further development of BRPF1 chemical probes. It's worth mentioning that due to the high sequence similarity of bromodomain proteins, highly selective chemical probes are required to effectively prevent off-target effects. In a hit optimization effort for CREBBP (Chapter 5), in silico chemical coupling

alongside organic synthesis enabled the identification of a series of low nanomolar selective CREBBP inhibitors. In this study, fragment-based docking and structure-guided chemical synthesis were jointly used as an efficient way for hit expansion. Similar to the aforesaid work on BRPF1, the CREBBP hit-optimization campaign took full advantage of structural information obtained from high quality protein-ligand crystal structures. In Chapter 6, hit optimization was carried out by scaffold hopping followed by ligand docking, which led to the identification of acetyl indoles that target the bromodomains of CREBBP, BAZ2B and BRPF1. Analysis of crystal structures of these bromodomains with the same ligand revealed the importance of the so-called gatekeeper residue with respect to the binding of ligands, which provided useful information for development of selective bromodomain inhibitors.

Taken togethor, FBDD approach was applied in different ways for bromodomain drug development in our group. X-ray protein crystallography played a central role in these work, as high resolution complex crystal structures can clearly illustrate detailed protein-ligand interactions which is pivotal for hit optimization in FBDD. The combination of in silico and in vitro (mainly X-ray crystallography) methods described here could be employed for other drug discovery projects for epigenetic modules and even challenging therapeutic protein targets.

Acknowledgement

First and foremost, I have to thank my advisor Prof. Amedeo Caflisch for his supervision during my PhD study. The completion of this thesis would not have been possible without his guidance and support. I would also thank my committee members Prof. Raimund Dutzler and Prof. Martin Jinek for their helpful suggestions on my study.

I have to express my gratitude to all the Caflisch group members for their help in the past few years. I thank Dr. Jing Dong for his help in laboratory activities. I thank Dr. Min Xu, Lars Wiedmer, Dr. Andreas Vitalis and Dr. Jean-Rémy Marchand for teaching me to use certain computational tools at the beginning of my study. I thank Dr. Danzhi Huang and Dr. Hongtao Zhao for interesting discussions. My special thanks goes to Beat Blamann and Céline Stutz for their assitance in setting up crystallization trays. I also thank some Chinese friends who used to live in Zurich for sharing their life experiences.

This thesis is dedicated to memory of my beloved father Zemin Zhu and my grandfather Zhemin Yu, who passed away during my PhD study. I deeply miss them.

Finally, I must express my gratitude and appreciation to my mother Runshi Yu, my wife Chunxian Zhou and my daughter Siqi Zhu for their unfailing emotional support. I hope I can spend more time with them in the future.

List of publications

Zhu J, Caflisch A. Twenty crystal structures of bromodomain and PHD finger containing protein 1 (BRPF1)/ligand complexes reveal conserved binding motifs and rare interactions. . Journal of Medicinal Chemistry 2016; 59(11): 5555–5561.

Zhu J, Zhou CX, Caflisch A. Structure-based discovery of selective BRPF1 bromodomain inhibitors. European Journal of Medicinal Chemistry. European Journal of Medicinal Chemistry 2018;155: 337-352.

Spiliotopoulos D, **Zhu J**, Wamhoff EC, Deerain N, Marchand JR, Aretz J, Rademacher C, Caflisch A. Virtual screen to NMR (VS2NMR): Discovery of fragment hits for the CBP bromodomain. Bioorganic & Medicinal Chemistry Letters 2017; 27(11):2472-2478.

Batiste L, Unzue A, Dolbois A, Hassler F, Wang X, Deerain N, **Zhu J**, Spiliotopoulos D, Nevado C, Caflisch A. Chemical space expansion of bromofomain ligand sguided by in silico virtual couplings (Autocouple). ACS Central Science 2018, 4 (2): 180–188.

Unzue A, Zhao H, Lolli G, Dong J, **Zhu J**, Zechner M, Dolbois A, Caflisch A, Nevado C. The “gatekeeper” residue influences the mode of binding of acetyl indoles to bromodomains. Journal of Medicinal Chemistry 2016; 59(7): 3087-3097.

Curriculum vitae

Jian Zhu

Born on May 30, 1980 in Zhejiang, China

EDUCATION:

2014.4 – 2018.3 **PhD Student, Biochemistry**
Department of Biochemistry, University of Zurich
•Supervisor: Prof. Amedeo Caflisch

2012.2 - 2014.1 **Master in Bioengineering**
School of Life Sciences, Fudan University
•Supervisors: Professor Qiang Huang and Dr. Jun Wang
•Thesis: "Structural Basis for Inhibitor Selectivity of Phosphodiesterase 2"

1999.9 - 2003.6 **Bachelor in Biotechnology**
School of Life Sciences, Zhejiang University

EMPLOYMENT:

2011 - 2013 **Group Leader**
Shanghai Medicilon Inc.

2008 - 2010 **Scientist**
Shanghai Medicilon Inc.

2003 - 2007 **Research Assistant**
Institute of Infectious Diseases, Zhejiang University